The University of Nottingham

Nottingham Geospatial Institute

Precise Point Positioning (PPP): GPS vs. GLONASS and GPS+GLONASS with an alternative strategy for Tropospheric Zenith Total Delay (ZTD) Estimation

Jareer Jaber Mohammed

BSc Eng., MSc Eng.

Thesis submitted to the University of Nottingham for the degree of Doctor of Philosophy

2017

Abstract

Different Global Navigation Satellite System (GNSS) constellations are available these days. This has led to an increase in the number of satellites available for the user, and that presents different performance levels for the user requirements like accuracy and convergence time. However, these benefits come from different constellations that have different reference times and for some, different frequencies. At the same time, the Precise Point Positioning (PPP) has also been presented as being a position solution within a certain level of accuracy and precision. Therefore, it is important to investigate the potential benefits from the PPP with a view to using a single or multi-constellation. These investigations include accuracy, precision, and convergence time. In addition, it is important to look at the individual performance of these constellations regarding the above improvements. This will give a clear decision about adopting a single or multi-constellation. It will also provide an independent solution, for instance for the station coordinates and troposphere, and independent estimated station velocities, without additional cost. This research has been conducted in three stages.

Firstly, the research begins with an evaluation of the GPS and the GLONASS (GLO) constellation geometry using a new approach for computing the cumulative dilution of precision (DOP) rather than the conventional DOP which was found to be latitude-dependent. Then it investigates the achievable station coordinate accuracy from PPP scenarios for static positioning after choosing the most appropriate PPP strategy that needs to be followed. Furthermore, the effect of different precise products (satellite orbits and clocks) on the PPP solutions and the difference between those products has been covered. It has been proven that PPP solutions can reach the same precision as a Global Double-Difference (GDD) GPS solution. Most importantly, the PPP GLO is found to be capable of producing similar precision and accuracy when compared to PPP GPS as well as the GDD GPS solution.

Secondly, this research also investigates the conventional strategy (using a model for the hydrostatic component and estimating the wet component) for estimating the troposphere Zenith Total Delay (ZTD) from the PPP solutions with an evaluation of the obtained accuracy of the tropospheric ZTD from four tropospheric models. It also presents an alternative strategy (estimating both components using different mapping functions and different process noises) for estimating the tropospheric ZTD from the PPP that can give millimeters of ZTD accuracy without affecting the station coordinate estimation and without relying on any metrological data or models. Validations have been conducted for the new strategy using PPP GPS, PPP GLO and PPP GPS+GLO. Regional validation was conducted over seven consecutive days for seven weeks, using the Ordnance Survey of Great Britain (OSGB) stations in the UK, and long-term (over one year) validation was conducted using 22 stations from the OSGB. The regional and long-term validations have been conducted using three different final precise products (satellite orbits (SP3) and clocks (CLK)), which are the EMX, ESA and GFZ. A global validation using ~76 IGS stations was conducted over a different period. This was conducted in three stages, using the final EMX, final IGS and real-time IGS precise products. It was found that this approach can be used in *real-time* as well as in post processing without a significant difference between the results.

Finally, this research has investigated the potential of using the PPP GLO for crustal motion separate to using the PPP GPS. Consistent horizontal station rates were found between PPP GPS and GDD GPS solutions. It was also concluded that it should be possible to use the PPP GLO for crustal motion, as an independent and precise solution. However, there was a bias in the orientation components of the estimated horizontal station rates between the PPP GLO and both other solutions (PPP GPS and GDD GPS), which was concluded to be a system bias rather than a strategy bias.

Acknowledgments

First, I am grateful for my supervisors, Professor Terry Moore and Dr. Chris Hill, for their valuable comments and suggestions during the research period. Alison Mellor is also acknowledged for arranging the supervision meetings for the entire three years. Mr. Pekka Peltola is also acknowledged for changing the POINT software platform, which made the processing faster.

My deepest gratitude should go to my external examiner Professor Felix Norman Teferle, for his significant effort, valuable comments and feedback to improve the content and the shape of this thesis. Same gratitude should go to my internal examiner Dr. Richard M. Bingley for his comments and feedback on the submitted reports, the meetings for comparing the results, for the long time that he spent on the first submission of this thesis and for the time that he has spent with me following all the modifications and corrections. Their efforts have the major effect on thesis.

Also, I acknowledge the support of the UK Natural Environment Research Council (NERC) through its British Isles continuous GNSS Facility (BIGF) for providing Ordnance Survey of Great Britain GNSS observation data, as well as the BIGF solutions for station coordinates and the ZTD. The International GNSS Service (IGS) is also acknowledged for the availability of the GNSS observations, precise products and the tropospheric ZTD.

I will always thank my wife who has stood beside me and taken all of the responsibility for the family, and has left me free to spend all of my time studying.

I also acknowledge the financial support from my government in Iraq through the ministry of higher education and scientific research. The Iraqi cultural attaché is also acknowledged for their arrangement during the time of studying.

Paper published

MOHAMMED, J., MOORE, T., HILL, C., BINGLEY, R. M. & HANSEN, D. N. 2016. An assessment of static precise point positioning using GPS only, GLONASS only, and GPS plus GLONASS. Measurement, 88, 121-130.

Papers in preparation

- *Alternative Strategy for Estimating Zenith Tropospheric Delay from Precise Point Positioning*
- *An Assessment of the Precise Products on Static Precise Point Positioning using Multi-Constellation GNSS*
- Long Term Biases Between PPP GPS and GLO PPP and Their Effect on The Velocity Estimation
- A Modified Approach for Evaluating The Satellites Geometry
- The Effect of Weight Observation on The Accuracy and Convergence Time of Precise Point Positioning

Table of content

Abstract ---------- **ii**

Acknowledgments ---------- **iv**

Paper published ---------- **vi**

Papers in preparation ---------- **vi**

Table of content ---------- **vii**

List of Figures ---------- xiv

List of Tables ---------- xxiii

List of Abbreviations ---------- xxx

Chapter 1. Introduction ---------- **1**

1.1 Aims and objectives ---------- 3

1.2 Methodology ---------- 3

1.3 Contribution to knowledge ---------- 5

Chapter 2. Literature Review ---------- **7**

2.1 Precise Point Positioning Overview ---------- 8

2.2 PPP GPS, PPP GLO and PPP GPS+GLO ---------- 9

2.2.1 Accuracy ---------- 9

2.2.2 Convergence time ---------- 15

2.2.3 Coverage and availability ---------- 17

2.3 PPP for Troposphere Studies ---------- 18

2.4 PPP for Station Velocity and Crustal Motion Studies ---------- 27

2.5 PPP Ambiguity Resolution ---------- 35

2.6 Chapter Summary ---------- 41

Chapter 3. Precise Point Positioning ---------- **43**

3.1 Extended Kalman Filter ---------- 43

3.2 Observation Equations ---------- 44

3.3 PPP Errors, Biases and Corrections ---------- 46
3.3.1 Satellite orbits and clocks ---------- 46
3.3.2 Ionospheric Bias ---------- 47
3.3.3 Tropospheric bias ---------- 49
3.3.3.1 Tropospheric models ---------- 51
3.3.3.1.1 Saastamoinen ---------- 51
3.3.3.1.2 UNB3m ---------- 52
3.3.3.1.3 GPT ---------- 54
3.3.3.1.4 EGNOS ---------- 56
3.3.3.2 Mapping functions ---------- 57
3.3.3.3 Tropospheric gradient ---------- 59
3.3.3.4 Tropospheric Estimation Strategies ---------- 60
3.3.3.4.1 Derivation of the tropospheric components ---------- 60
3.3.3.4.2 Process noise ---------- 62
3.3.4 Site corrections ---------- 65
3.3.4.1 Ocean tide loading displacement ---------- 65
3.3.4.2 Solid Earth Tide Correction ---------- 66
3.3.4.3 Earth Orientation Parameters ---------- 67
3.3.5 Shapiro delay ---------- 67
3.3.6 Phase wind-up ---------- 68
3.3.7 Differential Code Biases ---------- 68
3.3.8 Antenna Phase Centre ---------- 68
3.3.9 Polar Tide Correction ---------- 68
3.4 Weighting functions ---------- 68
3.4.1 Elevation weighting ---------- 69
3.4.2 Signal to noise ratio ---------- 69
3.4.3 Extended Signal to noise ratio ---------- 69
3.4.4 Multipath elevation weighting ---------- 70
3.4.5 Residual-based weighting ---------- 71
3.4.6 Stochastic elevation weighting ---------- 71

3.4.7 Code only elevation weighting ---------- 72
3.4.8 Rtklib elevation weighting ---------- 72
3.5 Multipath ---------- 72
3.6 Cycle slips ---------- 73
3.7 Ambiguity Resolution ---------- 74
3.8 Chapter Summary ---------- 76

Chapter 4. POINT software as it was at the start of this research ---------- 77

4.1 POINT software ---------- 77
4.2 POINT software capabilities ---------- 80
4.3 Papers published using POINT software ---------- 81
4.4 Test results using POINT software ---------- 82
4.5 Chapter summary ---------- 83

Chapter 5. An Initial Comparison of Precise Point Positioning Results from GPS and GLONASS ---------- 85

5.1 Global Double Difference (GDD) Solutions Methodology ---------- 85
5.2 Precise Products' effect on GDD and PPP ---------- 87
5.3 Second Order Ionospheric Delay ---------- 89
5.4 GNSS Geometry analysis ---------- 92
5.4.1 The Cumulative Dilution Of Precision ---------- 92
5.4.2 Correlation between the station latitude and the cumulative DOP -- 94
5.5 The effect of observation weighting on the accuracy and the convergence time ---------- 96
5.6 Choosing an expanded dataset ---------- 98
5.7 Observables Performance ---------- 100
5.7.1 GLO observables ---------- 101
5.7.2 GPS observables ---------- 104
5.8 Convergence time analysis ---------- 107
5.9 Chapter Summary ---------- 110

Chapter 6. PPP single and multi-constellation station coordinate accuracy and precision analysis with precise products' assessment ---------- 111

6.1 Conventional PPP strategy and configuration ---------- 112

6.2 The Author's PPP strategy and configuration (including modification to POINT software) ---------- 112

6.3 Initial Experiments ---------- 116

6.3.1 Repeatability analysis ---------- 120

6.4 Experimental Results: Extended Investigation ---------- 122

6.4.1 Precision compared to the Global Double-Difference ---------- 122

6.4.2 Accuracy compared to the Global Double-Difference ---------- 127

6.5 Discussion of the results ---------- 130

6.6 Precise Products' Effects on Precise Point Positioning ---------- 135

6.6.1 Reference station time-base offsets ---------- 135

6.6.1.1 GPS ---------- 135

6.6.1.2 GLO ---------- 138

6.6.2 Satellite coordinates effects ---------- 141

6.6.2.1 Helmert transformation parameters among the products ---------- 144

6.7 Chapter Summary ---------- 154

Chapter 7. Tropospheric Analysis with an alternative strategy for estimating tropospheric Zenith Total Delay from Precise Point Positioning ---------- 157

7.1 Conventional tropospheric strategies used in PPP ---------- 158

7.1.1 Using a model for the tropospheric zenith total delay ---------- 158

7.1.2 Using a model for the hydrostatic component and estimating the wet component with the other unknowns ---------- 160

7.2 An alternative strategy for estimating tropospheric zenith total delay using PPP 164

7.2.1 Initial Test ---------- 166

7.2.2 The correlation between the estimated ZTD and other estimated states 167
7.3 Validating the alternative tropospheric strategy ---------- 171
7.3.1 PPP GPS validation ---------- 171
7.3.1.1 Seven consecutive days validation using PPP GPS ---------- 171
7.3.1.2 Regional Validation using PPP GPS ---------- 174
7.3.2 PPP GLO Validation ---------- 176
7.3.2.1 Seven consecutive days validation using PPP GLO ---------- 176
7.3.2.2 Regional Validation using PPP GLO ---------- 178
7.3.3 PPP GPS+GLO Validation ---------- 179
7.3.3.1 Seven consecutive days validation using PPP GPS+GLO ---------- 179
7.3.3.2 Regional Validation of the new strategy using PPP GPS+GLO ---------- 180
7.3.4 Long-term validation ---------- 182
7.3.5 Global IGS validation ---------- 185
7.3.5.1 Global IGS validation using final precise products ---------- 187
7.3.5.2 Global Validation using real-time Precise Products ---------- 188
7.3.5.3 Suitability for different variations ---------- 190
7.4 The effect of the initial values on the estimated tropospheric ZHD and ZWD 191
7.5 The correlation between estimated station height and tropospheric ZTD using PPP and Global Double-Difference ---------- 196
7.6 Additional PPP improvement when using the alternative tropospheric strategy 198
7.6.1 Convergence time ---------- 198
7.6.2 The improvement on one-year repeatability ---------- 200
7.7 Chapter summary ---------- 202
Chapter 8. Estimation of station velocity from PPP GPS, PPP GLO and PPP GPS+GLO ---------- 205
8.1 Datasets ---------- 205

8.2 Methodology ---------- 206
8.3 One-year Station Coordinates Repeatability Analysis ---------- 207
8.3.1 East Coordinate Component Repeatability ---------- 207
8.3.2 North Coordinate Component Repeatability ---------- 209
8.4 One-year estimated horizontal station rates ---------- 211
8.4.1 Precise Products effect on estimated horizontal station rates ------ 212
8.4.1.1 PPP GPS ---------- 213
8.4.1.2 PPP GLO ---------- 215
8.4.1.3 PPP GPS+GLO ---------- 217
8.4.2 System effects on estimated horizontal station rates ---------- 219
8.5 Differences in estimated horizontal station rates ---------- 221
8.6 Chapter Summary ---------- 228

Chapter 9. Conclusions and recommendations ---------- 229

9.1 PPP background and initial analyses ---------- 229
9.2 PPP station coordinate assessment ---------- 230
9.3 PPP tropospheric ZTD assessment, including an alternative tropospheric strategy 231
9.4 PPP station rate/velocity assessment ---------- 232
9.5 Conclusion summary ---------- 233
9.6 Recommendations for Future Work ---------- 234

References ---------- 235

Appendices ---------- 261

Appendix-A- Flow chart for automation of the POINT software via Matlab -- 262
Appendix-B- Station coordinates for 85 OSGB stations in the UK and 76 IGS stations ---------- 264
Appendix-C- Summary of the differences between EMX, ESA and GFZ analysis centre strategies ---------- 272

Appendix-D- Comparison of tropospheric ZTD from GDD GPS and PPP GPS, PPP GLO and PPP GPS+GLO for 56 OSGB stations over seven consecutive days (figure summary) ---------- 277

Appendix-E- Station coordinates and tropospheric ZTD differences between all PPP scenarios using EMX, ESA and GFZ precise products and GDD GPS for 85 OSGB stations in the UK over seven weeks and between PPP GPS (using real-time precise products) and the IGS near real time solutions for 76 IGS stations over 12 weeks ---------- 285

Appendix-F- Horizontal Station rate estimates (mm/yr) for 22 OSGB stations in the UK (table summary) ---------- 315

Appendix-G- Horizontal station rate estimates (mm/yr) for 22 OSGB stations in the UK (figures summary) ---------- 319

List of Figures

Figure 3-1 Signal refraction because of troposphere (Group, 2012) 50
Figure 3-2 Ocean tide loading correction for ALDB station on DOY 12, 2014 65
Figure 3-3 Solid Earth tide correction for ALDB station on DOY 12, 2014 67
Figure 4-1 POINT software Structure 79
Figure 5-1 The network used for the GDD solution on DOY 12, 2014 87
Figure 5-2 The 56 OSGB stations included in BIGF that were used 88
Figure 5-3 The RMS for 7 days in GPS week 1775 (DOY 12-18, 2014) for 56 OSGB stations, with and without 2nd order ionospheric correction 90
Figure 5-4 Kp values for 7 days in GPS week 1775 (DOY 12-18, 2014) 91
Figure 5-5 Dilution of Precision for ALDB (left) and AMER (right) over 24 hours, DOY 12, 2014 for three PPP solutions 92
Figure 5-6 The Cumulative DOP for PPP (GPS, GLO and GPS+GLO) solutions versus latitude 95
Figure 5-7 The mean of the 3D error and the 5 cm 3-D convergence time for 56 OSGB stations using eight weighting methods 97
Figure 5-8 The 85 OSGB stations chosen for the expanded 7 weeks dataset 100
Figure 5-9 RMS of the GLO code observation residuals for each station on all days 102
Figure 5-10 GLO mp1 and mp2 values for the stations that have higher RMS of observation residuals 103
Figure 5-11 RMS of the GPS code observation residuals for each station on all days 104
Figure 5-12 GPS mp1 and mp2 values for the stations that have higher RMS of observations residuals 105
Figure 5-13 The daily mean of mp1 and mp2 values for GPS and GLO 106
Figure 5-14 GPS mp1 and mp2 values for each station on each day 107
Figure 5-15 Convergence time comparison for PPP GPS, PPP GLO and PPP GPS+GLO scenarios 108

Figure 6-1 Daily station coordinate differences from the mean for one year for the ALDB station on 354 days 118
Figure 6-2 Daily station coordinate differences from the mean for one year for the AMER station on 350 days 119
Figure 6-3 Repeatability of the daily solution station coordinate estimates from the PPP (GPS, GLO and GPS+GLO) and GDD GPS for the ALDB station 121
Figure 6-4 Repeatability of the daily solution station coordinate estimates from the PPP (GPS, GLO and GPS+GLO) and GDD GPS for the AMER station 121
Figure 6-5 East, North and Plan RMS of the repeatabilities of the weekly solution station coordinate estimates from the PPP (GPS, GLO and GPS+GLO) and GDD for all stations considered 124
Figure 6-6 Up RMS of the repeatabilities of the weekly solution station coordinate estimates from the PPP (GPS, GLO and GPS+GLO) and GDD for all stations considered 126
Figure 6-7 East, North and Plan RMS of the differences between the weekly solution station coordinate estimates from the PPP (GPS, GLO and GPS+GLO) and the GDD GPS for all stations considered 128
Figure 6-8 Up RMS of the differences between the weekly solution station coordinate estimates from the PPP (GPS, GLO and GPS+GLO) and the GDD GPS for all stations considered 130
Figure 6-9 The mean differences of the PPP (GPS, GLO and GPS+GLO) solutions from the GDD GPS for East and North coordinate components and three precise products 131
Figure 6-10 Satellites availability (Left: GPS, Right: GLO) for ALDB station DOY 12, 2014 133
Figure 6-11 North biases relative to the GDD Solution for 85 OSGB stations in GPS week 1775 134

Figure 6-12 GPS satellite clock offset differences from the mean for the EMX, ESA and GFZ precise products (upper) and Receiver clock offset differences from the mean for EMX, ESA and GFZ for ALDB station on DOY 12, 2014 (lower) 136
Figure 6-13 GPS satellite clock offset differences from the mean for the EMX, ESA and GFZ precise products (upper) and Reciever clock offset differences from the mean for ALDB station with the EMX, ESA and GFZ precise products on DOY 14, 2014 (lower) 138
Figure 6-14 GLO satellite clock offset differences from the mean for the EMX, ESA and GFZ precise products (upper) and Reciever clock offset differences from the mean for ALDB station with the for EMX, ESA and GFZ precise products on DOY 12, 2014 (lower) 139
Figure 6-15 Reciever clock offset differences between GPS and GLO for ALDB station with EMX, ESA and GFZ precise products on DOY 12, 2014 140
Figure 6-16 Satellite Coordinate differences from the mean for the EMX, ESA and GFZ precise products on DOY 12, 2014 141
Figure 6-17 Precise Product effects on the estimated station coordinates from PPP GPS and PPP GLO for ALDB station on DOY 12, 2014 143
Figure 6-18 Precise Product effects on the estimated station coordinates from PPP GPS and PPP GLO for 56 OSGB stations on DOY 12-18, 2014 144
Figure 6-19 Daily Seven-parameter Helmert transformation parameters for GPS week 1775 between the EMX, ESA and GFZ precise product satellites coordinates and the mean of the three 145
Figure 6-20 The number of stations that were used for EMX, ESA and GFZ precise products on DOY 12-18, 2014 146
Figure 6-21 Per satellite seven parameters Helmert transformation parameters for GPS and GLO for EMX, ESA and GFZ precise products on DOY 12, 2014 148
Figure 6-22 EMX precise products station distribution (GPS only green; GPS+GLO red), on DOY 12, 2014 149

Figure 6-23 ESA precise products station distribution (GPS only green; GPS+GLO red, unknown: blue) on DOY 12, 2014 150
Figure 6-24 GFZ precise products station distribution (GPS only green; GPS+GLO red, unknown: blue) on DOY 12, 2014 150
Figure 6-25 Epoch-by-epoch seven parameter Helmert transformation parameters for the EMX, ESA and GFZ precise products on DOY 12-18, 2014..... 152
Figure 7-1 Comparison of modelled tropospheric ZTD from four tropospheric models with tropospheric ZTD estimated using GDD 159
Figure 7-2 Comparison of tropospheric ZTD from GDD GPS and PPP GPS using four tropospheric models of tropospheric ZHD and estimating tropospheric ZWD.. 163
Figure 7-3 Comparison of tropospheric ZTD using PPP GPS with the alternative tropospheric and GDD GPS strategy for three OSGB stations on DOY 12, 2014 167
Figure 7-4 The difference between the estimated phase receiver clock offsets for PPP GPS when using the alternative and the conventional tropospheric strategies 168
Figure 7-5 The difference between the estimated code receiver clock offsets for PPP GPS when using the alternative and the conventional tropospheric strategies 169
Figure 7-6 Comparison of phase residuals (top), ionosphere-free-ambiguities (middle) and widelane ambiguities (bottom) for PPP GPS when using the conventional tropospheric strategy (left) and the alternative tropospheric strategy (right). 170
Figure 7-7 Comparison of tropospheric ZTD from GDD GPS and PPP GPS for ASAP station over seven consecutive days 173
Figure 7-8 Comparison of tropospheric ZTD from GDD GPS and PPP GLO for ASAP station over seven consecutive days 177
Figure 7-9 Comparison of tropospheric ZTD from GDD GPS and PPP GPS+GLO for ASAP station over seven consecutive days 180
Figure 7-10 The mean statistics between the estimated tropospheric ZTD from PPP GPS PPP GLO and PPP GPS+GLO using three precise products (EMX (pink), ESA

(blue) and GFZ (green)) and the estimated tropospheric ZTD from GDD for 22 OSGB stations over one year 183
Figure 7-11 The RMS statistics between the estimated tropospheric ZTD from PPP GPS, PPP GLO and PPP GPS+GLO using three precise products(EMX (pink), ESA (blue) and GFZ (green)) and the estimated tropospheric ZTD from GDD GPS for 22 OSGB stations over one year 184
Figure 7-12 IGS stations' used for further validating the alternative tropospheric strategy 186
Figure 7-13 Comparison of tropospheric ZTD from GPS GDD and PPP GPS using final and real-time precise products at ALGO and WES2 IGS stations on DOY ,2014 190
Figure 7-14 Estimated tropospheric ZHD and ZWD starting from zero initial values for ASAP station over seven consecutive days 192
Figure 7-15 Estimated tropospheric ZHD and ZWD for DRUM, FARB, and KEYW stations on DOY 12, 2014, left axis: hydrostatic, right axis: wet 193
Figure 7-16 The effect of the initial values on the estimated tropospheric ZHD and ZWD for DRUM station on DOY 12, 2014 194
Figure 7-17 The effect of the initial value on the estimated tropospheric ZTD for DRUM station on DOY 12, 2014..... 195
Figure 7-18 The difference between estimated tropospheric ZTD and station heights from PPP GPS, PPP GLO and PPP GPS+GLO, and from GPS GDD for AMER, ALDB stations over one year (dtrop: red, dU: blue) 197
Figure 7-19 Improvements in the convergence time when using the alternative strategy for PPP GPS (top), PPP GLO (middle) and PPP GPS+GLO (bottom) ... 199
Figure 7-20 Comparison between the repeatability analysis when using a model for troposphere and by using the alternative tropospheric strategy (AMER Left, ALDB Right) 200

Figure 8-1 22 OSGB stations that were chosen for a one-year assessment of estimated station rates 206
Figure 8-2 Comparison of East coordinate component repeatability for GDD GPS and PPP GPS, PPP GLO and PPP GPS+GLO using EMX, ESA and GFZ precise products 208
Figure 8-3 Comparison of North coordinate component repeatability for GDD GPS and for PPP GPS, PPP GLO and PPP GPS+GLO using EMX, ESA and GFZ precise products 210
Figure 8-4 Example coordinate time series and station rate estimation for the East component 212
Figure 8-5 The difference between the estimated East station rate and the mean for PPP GPS with EMX, ESA and GFZ precise products 213
Figure 8-6 The difference between the estimated North station rate and the mean for PPP GPS with EMX, ESA and GFZ precise products 214
Figure 8-7 The difference between the estimated East station rate and the mean for PPP GLO with EMX, ESA and GFZ precise products 216
Figure 8-8 The difference between the estimated North station rate and the mean for PPP GLO with EMX, ESA and GFZ precise products 217
Figure 8-9 The difference between the estimated East station rate and the mean for PPP GPS+GLO with EMX, ESA and GFZ precise products 218
Figure 8-10 The difference between the estimated North station rate and the mean for PPP GPS+GLO with EMX, ESA and GFZ precise products 219
Figure 8-11 Comparison of Moving average East station coordinates for the PPP scenarios using the EMX, ESA and GFZ precise products for the APPL station. (Blue: PPP GPS, Red: PPP GLO, Green: PPP GPS+GLO) 220
Figure 8-12 Comparison of Moving average East coordinate components for the PPP scenarios using the EMX, ESA and GFZ precise products for the BLAP station. (Blue: PPP GPS, Red: PPP GLO, Green: PPP GPS+GLO) 221

Figure 8-13 Horizontal station Rate comparisons using EMX precise products 223
Figure 8-14 Horizontal station rate comparisons using ESA precise products 224
Figure 8-15 Horizontal station Rate comparisons using GFZ precise products 225
Figure 8-16 Comparison of the horizontal station rate orientations from PPP GPS and PPP GLO using the EMX, ESA and GFZ precise products 226
Figure 8-17 Comparison of horizontal station rate magnitudes from PPP GPS and PPP GLO using the EMX, ESA and GFZ precise products 227

Figure A- 1 Flow char for automated the POINT software in MATLAB 263

Figure D-1 Comparison of tropospheric ZTD from GDD GPS and PPP GPS, PPP GLO and PPP GPS+GLO for 56 OSGB stations over seven consecutive days..... 278
Figure D- 2 Comparison of tropospheric ZTD from GDD GPS and PPP GPS, PPP GLO and PPP GPS+GLO for 56 OSGB stations over seven consecutive days..... 279
Figure D- 3 Comparison of tropospheric ZTD from GDD GPS and PPP GPS, PPP GLO and PPP GPS+GLO for 56 OSGB stations over seven consecutive days..... 280
Figure D- 4 Comparison of tropospheric ZTD from GDD GPS and PPP GPS, PPP GLO and PPP GPS+GLO for 56 OSGB stations over seven consecutive days..... 281
Figure D- 5 Comparison of tropospheric ZTD from GDD GPS and PPP GPS, PPP GLO and PPP GPS+GLO for 56 OSGB stations over seven consecutive days..... 282
Figure D- 6 Comparison of tropospheric ZTD from GDD GPS and PPP GPS, PPP GLO and PPP GPS+GLO for 56 OSGB stations over seven consecutive days..... 283
Figure D- 7 Comparison of tropospheric ZTD from GDD GPS and PPP GPS, PPP GLO and PPP GPS+GLO for 56 OSGB stations over seven consecutive days..... 284

Figure G- 1 Coordinate time series and station rate estimation for the East component using EMX (left), ESA (middle) and GFZ (right) precise products for all PPP scenarios as well as GDD GPS 320
Figure G- 2 Coordinate time series and station rate estimation for the East component using EMX (left), ESA (middle) and GFZ (right) precise products for all PPP scenarios as well as GDD GPS 320
Figure G- 3 Coordinate time series and station rate estimation for the East component using EMX (left), ESA (middle) and GFZ (right) precise products for all PPP scenarios as well as GDD GPS 320
Figure G- 4 Coordinate time series and station rate estimation for the East component using EMX (left), ESA (middle) and GFZ (right) precise products for all PPP scenarios as well as GDD GPS 320
Figure G- 5 Coordinate time series and station rate estimation for the East component using EMX (left), ESA (middle) and GFZ (right) precise products for all PPP scenarios as well as GDD GPS 320
Figure G- 6 Coordinate time series and station rate estimation for the East component using EMX (left), ESA (middle) and GFZ (right) precise products for all PPP scenarios as well as GDD GPS 320
Figure G- 7 Coordinate time series and station rate estimation for the East component using EMX (left), ESA (middle) and GFZ (right) precise products for all PPP scenarios as well as GDD GPS 320
Figure G- 8 Coordinate time series and station rate estimation for the East component using EMX (left), ESA (middle) and GFZ (right) precise products for all PPP scenarios as well as GDD GPS 320
Figure G-9 Coordinate time series and station rate estimation for the North component using EMX (left), ESA (middle) and GFZ (right) precise products for all PPP scenarios as well as GDD GPS 320

Figure G- 10 Coordinate time series and station rate estimation for the North component using EMX (left), ESA (middle) and GFZ (right) precise products for all PPP scenarios as well as GDD GPS 320
Figure G- 11 Coordinate time series and station rate estimation for the North component using EMX (left), ESA (middle) and GFZ (right) precise products for all PPP scenarios as well as GDD GPS 320
Figure G- 12 Coordinate time series and station rate estimation for the North component using EMX (left), ESA (middle) and GFZ (right) precise products for all PPP scenarios as well as GDD GPS 320
Figure G- 13 Coordinate time series and station rate estimation for the North component using EMX (left), ESA (middle) and GFZ (right) precise products for all PPP scenarios as well as GDD GPS 320
Figure G- 14 Coordinate time series and station rate estimation for the North component using EMX (left), ESA (middle) and GFZ (right) precise products for all PPP scenarios as well as GDD GPS 320
Figure G- 15 Coordinate time series and station rate estimation for the North component using EMX (left), ESA (middle) and GFZ (right) precise products for all PPP scenarios as well as GDD GPS 320
Figure G- 16 Coordinate time series and station rate estimation for the North component using EMX (left), ESA (middle) and GFZ (right) precise products for all PPP scenarios as well as GDD GPS 320

List of Tables

Table 2-1 Comparison of GPS, GLONASS, Galileo and BeiDou((Hofmann-Wellenhof et al., 2007);(Bhatta, 2011);(BDS-OS-PS-2.0, 2013)) 7

Table 2-2 Summary of the biases in tropospheric delay models (Böhm et al., 2014) 23

Table 2-3 Summary of literature gaps and the suggested approaches for this research 42

Table 4-1 GPS Test station coordinates results using PPP GPS and PPP GPS+GLO with default settings in POINT 82

Table 5-1 The processing parameters for the Global Double-Difference solution..... 86

Table 5-2 Precise products' effect on the station coordinates from the PPP GPS solutions for the 56 OSGB stations 88

Table 5-3 The Cumulative DOP statistics for 57 OSGB stations from DOY 12-18, 2014 94

Table 5-4 The 14 OSGB Stations that are different from the majority of the 85 OSGB stations selected..... 98

Table 5-5 GPS week, doy range and number of the 85 OSGB stations selected that were available during that week 99

Table 5-6 Statistics of the observations residuals for the expanded 7-week dataset 100

Table 6-1 Configuration to be used for PPP processing 114

Table 6-2 Extended Kalman Filter configuration to be used for PPP processing..... 116

Table 7-1 Different PPP GPS and solutions for (DRUM, FARB and KEYW) using four models of tropospheric ZTD 160

Table 7-2 RMS of the daily differences between PPP GPS, PPP GLO, PPP GPS+GLO and GDD GPS station coordinates and tropospheric ZTD using four models of tropospheric ZHD while solving for the tropospheric ZWD 161

Table 7-3 Extended Kalman Filter configurations for the PPP using the alternative tropospheric strategy 165

Table 7-4 PPP GPS solution (three stations) using the alternative tropospheric strategy 166
Table 7-5 The difference between the estimated station coordinates and tropospheric ZTD from PPP GPS and GDD GPS for 56 OSGB staptions over seven consecutive days..... 173
Table 7-6 The difference between the estimated station coorldinates and tropospheric ZTD from PPP GPS using three precise products (EMX, ESA and GFZ) for 56 OSGB stations and GPS GDD over seven weeks..... 175
Table 7-7 The difference between the estimated station coordinates and tropospheric ZTD from PPP GLO and GDD GPS for 56 OSGB stations over seven consecutive days..... 177
Table 7-8 The difference between the estimated station coordinates and tropospheric ZTD from PPP GLO using three precise products (EMX, ESA and GFZ) and GDD GPS for 56 OSGB stations over seven weeks 178
Table 7-9 The difference between the estimated station coordinates and tropospheric ZTD from PPP GPS+GLO and GDD GPS for 56 OSGB stations over seven consecutive days 180
Table 7-10 The difference between the estimated station coordinates and the tropospheric ZTD from PPP GPS+GLO using three precise products (EMX, ESA and GFZ) and GDD GPS for 56 OSGB stations over seven weeks 181
Table 7-11 GPS week and the number of IGS stations considered in the analysis of each week 187
Table 7-12 RMS differences between the estimated station coordinates and tropospheric ZTD from the PPP GPS (using two different final precise products) and the IGS near real time and final solutions for IGS stations over 12 weeks 187
Table 7-13 RMS differences between the estimated station coordinates and tropospheric ZTD from the PPP GPS (using real-time precise products) and the IGS near real time and final solutions for IGS stations over 12 weeks 189

Table 7-14 PPP GPS, PPP GLO and PPP GPS +GLO tropospheric ZTD statistics for ALDB and AMER stations over one year 196

Table B- 1 Station coordinates for 85 stations in the UK 265
Table B- 2 Station coordinates for 85 stations in the UK 266
Table B- 3 Station coordinates for 85 stations in the UK 267
Table B- 4 Station coordinates for 85 stations in the UK 268
Table B- 5 Station coordinates for 76 IGS stations 269
Table B- 6 Station coordinates for 76 IGS stations 270
Table B- 7 Station coordinates for 76 IGS stations 271

Table C- 1 Summary of the differences between EMX, ESA and GFZ analysis centre strategies 273
Table C- 2 Summary of the differences between EMX, ESA and GFZ analysis centre strategies 274
Table C- 3 Summary of the differences between EMX, ESA and GFZ analysis centre strategies 275
Table C- 4 Summary of the differences between EMX, ESA and GFZ analysis centre strategies 276

Table E-1 The differences between the estimated station coordinates and tropospheric ZTD from GPS GDD and PPP GPS using EMX precise products for 85 OSGB stations over seven weeks 286
Table E-2 The differences between the estimated station coordinates and tropospheric ZTD from GPS GDD and PPP GPS using EMX precise products for 85 OSGB stations over seven weeks 287

Table E-3 The differences between the estimated station coordinates and tropospheric ZTD from GPS GDD and PPP GPS using EMX precise products for 85 OSGB stations over seven weeks 288
Table E-4 The differences between the estimated station coordinates and tropospheric ZTD from GPS GDD and PPP GPS using ESA precise products for 85 OSGB stations over seven weeks 289
Table E-5 The differences between the estimated station coordinates and tropospheric ZTD from GPS GDD and PPP GPS using ESA precise products for 85 OSGB stations over seven weeks 290
Table E-6 The differences between the estimated station coordinates and tropospheric ZTD from GPS GDD and PPP GPS using ESA precise products for 85 OSGB stations over seven weeks 291
Table E-7 The differences between the estimated station coordinates and tropospheric ZTD from GPS GDD and PPP GPS using GFZ precise products for 85 OSGB stations over seven weeks 292
Table E-8 The differences between the estimated station coordinates and tropospheric ZTD from GPS GDD and PPP GPS using GFZ precise products for 85 OSGB stations over seven weeks 293
Table E-9 The differences between the estimated station coordinates and tropospheric ZTD from GPS GDD and PPP GPS using GFZ precise products for 85 OSGB stations over seven weeks 294
Table E-10 The differences between the estimated station coordinates and tropospheric ZTD from GPS GDD and PPP GLO using EMX precise products for 85 OSGB stations over seven weeks 295
Table E-11 The differences between the estimated station coordinates and tropospheric ZTD from GPS GDD and PPP GLO using EMX precise products for 85 OSGB stations over seven weeks 296

Table E-12 The differences between the estimated station coordinates and tropospheric ZTD from GPS GDD and PPP GLO using EMX precise products for 85 OSGB stations over seven weeks 297
Table E-13 The differences between the estimated station coordinates and tropospheric ZTD from GPS GDD and PPP GLO using ESA precise products for 85 OSGB stations over seven weeks 298
Table E-14 The differences between the estimated station coordinates and tropospheric ZTD from GPS GDD and PPP GLO using ESA precise products for 85 OSGB stations over seven weeks 299
Table E-15 The differences between the estimated station coordinates and tropospheric ZTD from GPS GDD and PPP GLO using ESA precise products for 85 OSGB stations over seven weeks 300
Table E-16 The differences between the estimated station coordinates and tropospheric ZTD from GPS GDD and PPP GLO using GFZ precise products for 85 OSGB stations over seven weeks 301
Table E-17 The differences between the estimated station coordinates and tropospheric ZTD from GPS GDD and PPP GLO using GFZ precise products for 85 OSGB stations over seven weeks 302
Table E-18 The differences between the estimated station coordinates and tropospheric ZTD from GPS GDD and PPP GLO using GFZ precise products for 85 OSGB stations over seven weeks 303
Table E-19 The differences between the estimated station coordinates and tropospheric ZTD from GPS GDD and PPP GPS+GLO using EMX precise products for 85 OSGB stations over seven weeks 304
Table E-20 The differences between the estimated station coordinates and tropospheric ZTD from GPS GDD and PPP GPS+GLO using EMX precise products for 85 OSGB stations over seven weeks 305

Table E-21 The differences between the estimated station coordinates and tropospheric ZTD from GPS GDD and PPP GPS+GLO using EMX precise products for 85 OSGB stations over seven weeks 306
Table E-22 The differences between the estimated station coordinates and tropospheric ZTD from GPS GDD and PPP GPS+GLO using ESA precise products for 85 OSGB stations over seven weeks 307
Table E-23 The differences between the estimated station coordinates and tropospheric ZTD from GPS GDD and PPP GPS+GLO using ESA precise products for 85 OSGB stations over seven weeks 308
Table E-24 The differences between the estimated station coordinates and tropospheric ZTD from GPS GDD and PPP GPS+GLO using ESA precise products for 85 OSGB stations over seven weeks 309
Table E-25 The differences between the estimated station coordinates and tropospheric ZTD from GPS GDD and PPP GPS+GLO using GFZ precise products for 85 OSGB stations over seven weeks 310
Table E-26 The differences between the estimated station coordinates and tropospheric ZTD from GPS GDD and PPP GPS+GLO using GFZ precise products for 85 OSGB stations over seven weeks 311
Table E-27 The differences between the estimated station coordinates and tropospheric ZTD from GPS GDD and PPP GPS+GLO using GFZ precise products for 85 OSGB stations over seven weeks 312
Table E-28 The differences between the estimated station coordinates and tropospheric ZTD from IGS and PPP GPS (using real-time precise products) for 76 IGS stations over 12 weeks 313
Table E-29 The differences between the estimated station coordinates and tropospheric ZTD from IGS and PPP GPS (using real-time precise products) for 76 IGS stations over 12 weeks 314

Table F-1 Horizontal station rate estimates (mm/yr) for 22 OSGB stations in the UK using PPP with EMX precise products 316
Table F-2 Horizontal station rate estimates (mm/yr) for 22 OSGB stations in the UK using PPP with ESA precise products 317
Table F-3 Horizontal station rate estimates (mm/yr) for 22 OSGB stations in the UK using PPP with GFZ precise products 318

List of Abbreviations

ANTEX	Antenna Exchange Format
APPS	Automatic Precise Positioning Service
BNC	BKG Ntrip Client
BIGF	British Isles continuous GNSS Facility
BSW	Bernese GNSS Software
C/A	Coarse/Acquisition
CDMA	Code Division Multiple Access
CDOP	Cumulative Dilution Of Precision
CNES	Centre National d'Etudes Spatiales
CODE	Centre for Orbit Determination in Europe
CORS	Continuously Operating Reference Station
CSRS-PPP	Canadian Spatial Reference System Precise Point Positioning service
DCB	Differential-Code Biases
EGNOS	European Geostationary Navigation Overlay Service
EKF	Extended Kalman Filter
EOPs	Earth Orientation Parameter
ENU	East North Up
ESA	European Space Agency
FCB	Fractional Cycle Bias
FDMA	Frequency Division Multiple Access
FES	Finite Element Solution
GAPS	GPS Analysis and Positioning Software
GDD	Global Double-Difference
GDOP	Geometric Dilution of Precision
GFZ	GeoForschungsZentrum
GOA	GIPSY-OASIS

GLONASS	Globalnaya navigatsionnaya sputnikovaya sistema
GMF	Goblal Mapping Function
GNSS	Global Navigation Satellite System
GPS	Global Positioning System
GPT2	Global Pressure and Temperature 2 model
GPT2W	Global Pressure and Temperature 2 Wet model
HDOP	Horizontal Dilution of Precision
IERS	International Earth Rotation and Reference Frame Services
IGS	International GNSS Service
iNsight	Innovative Navigation using new GNSS Signals with Hybridised Technologies
ITRF	International Terrestrial Reference Frame
MWWL	Melbourn-Wubbena Wide Lane
NRCan	Natural Resources Canada
NWM	Numerical Weather Model
OSGB	Ordnance Survey of Great Britain
PDOP	Position Dilution Of Precision
PPP	Precise Point Positioning
RMS	Root mean square
TEC	Total Electron Content
TECR	Total Electron Content Residual
UNB3	University of New Brunswick 3 model
UNB3m	Modified University of New Brunswick 3 model
VMF	Vienna Mapping Function
ZHD	Zenith Hydrostatic Delay
ZTD	Zenith Total Delay
ZWD	Zenith Wet Delay

Chapter 1. Introduction

Precise Point Positioning (PPP) using the Global Positioning System (GPS) is widely used nowadays, and recent research studies have been attempting to give it wider recognition. This is because it has the advantages of absolute positioning without the need for reference receivers at the same time of observation. However, it has its limitations for relying on the availability and accuracy of particular precise products, the bias that need to be handled and the correction models that need to be applied. In addition, much research has suggested that solving of the ambiguities is the key to an accurate PPP, which is still challenging because of the fractional cycle biases from the satellites as well as the receiver. On the other hand, the obtained accuracy and precision from PPP in general can be assessed and compared to the Global Double-Difference (GDD).

Further, PPP GPS also suffers from long convergence times that are necessary to reach the required level of accuracy. Therefore, many pieces of research have pushed this down by including the GLONASS (GLO) observation data. Obviously, it is good to increase the number of observations from other constellations, but it may be better to adopt a new PPP solution that will be independent (i.e using PPP GLO for the same station).

Furthermore, each correction model for the PPP GPS should also be included in the PPP GLO, even though it has different frequencies. This needs to be done for assessing and investigating the possibility of using a PPP GLO solution as an independent solution rather than treating its data observation as assisting observations. Therefore, this will give a clear view of the constellation performance and the level of the accuracy that could be achieved.

On the other hand, one of the most important factors that affect the obtained accuracy from PPP is the tropospheric delay. Previous studies have primarily concentrated on one of two approaches to overcome the tropospheric delay by

adopting the conventional approach for the hydrostatic part (taken from a model) and estimating the wet delay, or by using numerical weather models alone or combined with tropospheric models. Even though this is the followed strategy for dealing with the delay until now, the accuracy for the estimated Zenith Total Delay (ZTD) is still within a ~5 cm level. Thus, an improved strategy is presented in this research for using the PPP not just as an accurate tool for determining station coordinates from both constellations, but also as an accurate tool for estimating the tropospheric ZTD.

Although the PPP has also been adopted as a tool for crustal motion, only PPP GPS has been used without the GLO or sometimes PPP GPS+GLO, without any evaluation for the potential use of the PPP GLO alone. Thus, this study investigates the potential of using the PPP GLO for geophysical applications as well as addressing long-term biases that will be faced. Additionally, an evaluation for the precise product's effect on long-term monitoring is also investigated.

Overall, this thesis can be outlined as follows: the next sections include the main aims and objectives of this research, the methodology followed for achieving that, and the author's opinion of its contribution to knowledge. Chapter 2 covers the literature review, and Chapter 3 includes the PPP errors, biases and corrections that were considered and the methods that were used for developing the optimal strategy that is to be followed. Chapter 4 presents the POINT software that was used for the processing, with its structure and the research papers that have previously used this software prior to this study. Chapter 5 includes an evaluation of the observables as well as the convergence time and a new approach for analysing the geometry. Chapter 6 contains an assessment of the precision and accuracy obtained from the PPP scenarios for station coordinates, as well as the evaluation of the precise product's effect on the solution. Chapter 7 includes an assessment of available tropospheric models as well as the currently used strategy for tropospheric ZTD estimation, along with details of an alternative strategy for tropospheric ZTD

estimation and its validation. Chapter 8 investigates the potential for using the PPP solutions for crustal motions, along with the effect of different final precise products on the reliability of the estimated components. Chapter 9 contains the conclusions and the recommendations for future research.

1.1 Aims and objectives

The overall aim is to investigate PPP accuracy and precision from a multi-constellation (the two fully operated constellations GPS and GLO). The specific aims and objectives are as follows:

1. Investigate the achievable precision and accuracy of station coordinates from the PPP compared to a reference Global Double-Difference (GDD) solution with an evaluation of the effect of different final precise products on the accuracy and precision as well as the differences between precise products.

2. Modification of the POINT software for using the PPP GLO solution as an accurate and precise independent solution to PPP GPS in static mode.

3. Investigating the available tropospheric models with an analysis for the achievable accuracy for estimating the tropospheric ZTD from PPP using the conventional strategy.
4. Developing an alternative approach for estimating the tropospheric ZTD from the PPP solutions with its validation in *real-time* and post-processing.
5. Testing the PPP solution, GPS as well as GLO, for station velocity estimation. The long-term goal being to figure out the possibility of using the PPP GLO as an independent solution to PPP GPS.

1.2 Methodology

The following methodology is considered for satisfying the above aims and objectives:

1. The appropriate strategy for the PPP will be found in terms of accuracy and convergence time, and based on weighting, using the second order ionospheric method, and the effect of PPP precise products. Also, the observables from both constellations will be assessed based on their residuals with their correlation with the receiver type and multipath on L_1 frequency (mp1) and multipath on L_2 frequency (mp2).
2. The PPP GLO will be implemented and tested with the same correction models adopted for the PPP GPS using POINT software, with implementations wherever it is needed for separating the PPP GLO solution as an independent solution. Implementation of the PPP GLO will be used as an independent tool based on the available frequencies from the GLO constellation. In addition, the obtained accuracy from the PPP GPS, PPP GLO and the PPP GPS+GLO will be assessed and compared to an independent 'truth' from a Global Double-Difference (GDD) solution. Further, precision analysis will be conducted for all the available solutions, including the 'truth' Global Double-Difference solution.
3. An investigation will be conducted for the available tropospheric models and the conventional tropospheric strategy. This is to account for the accuracy level of the estimated tropospheric ZTD from PPP.
4. An alternative tropospheric strategy will be developed for estimating the tropospheric ZTD from the PPP. The resulting differences will be compared to the estimated ZTD from an independent Global Double-Difference (GDD) solution.
5. A least squares implementation for station rate estimation from a one-year data set will be carried out in order to investigate the potential of using the PPP GLO solution for crustal motion. This needs to be done with an investigation of the precise product's effect on the long-term processing.

1.3 Contribution to knowledge

This study contributes to our knowledge by addressing the following important issues:

- Improving the PPP solution by choosing the most appropriate models, products and observation weighting methods with the PPP strategy to be followed for obtaining significant accuracy and precision.

- Presenting a new approach for evaluating a satellite's geometry.

- Using the PPP GLO as an independent solution to PPP GPS with an optimal strategy for obtaining station coordinates and an assessment of the achieved accuracy and precision.

- Developing an alternative approach for estimating the tropospheric Zenith Total Delay (ZTD) from various PPP scenarios with its validation using final precise products as well as *real-time* products. The finding of this an alternative approach will turn the PPP into an accurate tool for estimating the tropospheric ZTD as well as the station coordinates.

- Using the PPP GLO as an independent solution to PPP GPS for one-year station rate estimation with an evaluation of different final precise products.

Chapter 2. Literature Review

The use of Global Navigation Satellite Systems (GNSS) for navigation and surveying has increased over the last few decades. The GPS is now modernized to include new frequencies. The Russians' plans for GLONASS modernization will include Code Division Multiple Access (CDMA) as well as Frequency Division Multiple Access (FDMA). The European Union has begun work on their constellation Galileo. In addition, the Chinese have started to move their constellation BeiDou from a regional to a global constellation. The availability of four constellations in the future will give the flexibility to use more than 120 satellites in the sky. The increased number of the satellites will be reflected as an improvement in the availability and the coverage compared to using one constellation. However, different frequencies of various constellations will be obtained with different coordinate systems and at the same time, different time references are available for every constellation as is shown in Table 2-1 ((Hofmann-Wellenhof et al., 2007);(Bhatta, 2011);(BDS-OS-PS-2.0, 2013)). This will raise questions about which individual system should be used, and whether the combination of all of them, or some of them will improve the user's requirements or simply bring in different errors and bias from other constellations. Therefore, there is a need for exploring and investigating the use of using a multi-constellation GNSS.

Table 2-1 Comparison of GPS, GLONASS, Galileo and BeiDou((Hofmann-Wellenhof et al., 2007);(Bhatta, 2011);(BDS-OS-PS-2.0, 2013))

Parameters	GPS	GLONASS	Galileo	BeiDou (MEO)
Status	Fully operational	Fully operational	Under development	Under development
Orbital planes	6	3	3	3
No. of satellites(as originally planned)	21 operational + 3 spare	21 operational + 3 spare	27 operational + 3 spare	27 + 3 IGSO
Nominal Inclination(degrees)	55	64.8	56	55
Nominal Semi-major axis (km)	26,560	25,508	29,601	27,878
Orbit plane separation	60	120	120	120

Parameters	GPS	GLONASS	Galileo	BeiDou (MEO)
(degrees)				
Nominal Altitude above sea level (km)	20,200	19,100	23,222	21,528
Orbiting speed of satellite (m/s)	3,870	3,950	3,675	3,805
Orbital period	11 h 57 min 28 s	11 h 15 min 44 s	14 h 4 min	12 h 37 min 34.45 sw
Services	2	2	5	10
Master control station	1 active + backup in US	1 in Russia	2 in Europe	1 in China
Broadcast Ephemeris format	Keplerian elements of the orbit and its first derivative	Geocentric Cartesian coordinates and their derivatives	Keplerian elements of the orbit and its first derivative	Keplerian elements of the orbit and its first derivative
Broadcast Ephemeris data	Keplerian elements, correction coefficients	Position, velocity, acceleration vectors	Keplerian elements, correction coefficients	Keplerian elements, correction coefficients
Update rate of broadcast ephemeris	2 h	30 min	3 h	1h
Geodetic reference system	WGS84	PZ90	GTRF	Beijing 1954
Time system	GPS time, UTC (USNO)	GLONASS time, UTC (SU)	Galileo system time	BeiDou system time
Leap seconds	No	Yes	No	No
Signal separation	CDMA	FDMA	CDMA	CDMA
Frequencies bands	3 (L1, L2, L5)	3 (L1, L2, L3)	4+1(E1 or L1, E5a, E5b, E6 and L6)	6 (B1, B1-BOC, B 1-2, B2, B3 and L5)
Transmission time of almanac	12.5 min	2.5 min	10 min	12 min
Carrier frequencies [MHz]	L1:1575.42	L1: 1598.0625 - 1607.0625	L1/E1:1559-1591	B1:1561.098-1589.742
	L2:1227.60	L2:1242.9375-1251.6875	-	B2:1207.14
	-	L3:1198-1208	-	B3:1268.52
	L5:1176.45	-	E5:1164-1214	L5:1176.45
	-	-	E6:1260-1300	-
	-	-	L6:1544-1545	-
Code	Different for each satellite	Same for all satellites	Different for each satellite	Different for each satellite
Selective availability	Off	N/A	N/A	N/A
Anti-spoofing	On	N/A	N/A	N/A

2.1 Precise Point Positioning Overview

By using one a GNSS receiver, it is possible to obtain centimetre level of station coordinate accuracy using a method known as Precise Point Positioning (PPP) first introduced by Zumberge et al. (1997). This can be done by post-processing data,

estimating carrier-phase ambiguities and employing precise products (satellite orbit and clocks) using a combination of ionosphere-free measurements. PPP has also been developed to potentially provide daily station coordinate estimates with millimetres level of repeatability and accuracy for static positioning (Larson et al., 2004), as an alternative to the Global double-difference (GDD) technique.

2.2 PPP GPS, PPP GLO and PPP GPS+GLO

The focus of this research is on the two full constellations, the GPS and GLONASS (GLO), for PPP. Significant research efforts have already been made towards using and evaluating these constellations; as detailed in this section.

2.2.1 Accuracy

The significant factor that can be used to evaluate multi-constellations is the accuracy of the estimated parameters obtained from one constellation or a combination of different constellations.

Cai (2009) tested PPP GPS+GLO in static mode and found an improvement in terms of the obtained station coordinate accuracy from adding GLONASS to the GPS constellation. These improvements were 40% and 28% in East and North components respectively and 24% in the Up component. However, according to Cai and Gao (2013b), the accuracy will not be significantly improved if there are sufficient numbers of GPS satellites with a good geometry. In addition, Nik and Petovello (2010) found that the GLONASS constellation can be treated as a method of GPS augmentation to achieve more reliable accurate navigation solutions.

Jokinen et al. (2012c) also showed that PPP GPS+GLO will improve the station coordinate accuracy. Additionally, Jokinen et al. (2013b) found that including GLONASS with GPS reduced the average vertical and horizontal errors by 17% and 4%, respectively. Similarly, Reussner and Wanninger (2011) concluded that PPP GPS+GLO reduces the average horizontal error. However, Cai and Gao (2009) claimed that the accuracy obtained from PPP GPS with four GPS satellites is better than using

the same number of satellites in PPP GPS+GLO. That was due to the lower accuracy of the GLONASS satellite orbit and clock data and the influence of the system difference between the two constellations, whereas Zhang et al. (2008) indicated that using more constellations is better than using one constellation with the same number of satellites.

Zhao et al. (2013) used the BeiDou constellation (BDS) and found that PPP BDS can achieve an accuracy of better than 1cm in the horizontal and 3cm in the vertical in static mode, while in kinematic mode it can be within 1–2cm in the horizontal and 4–7cm in the vertical. They suggested that PPP BDS kinematic are generally better than PPP GPS for the selected location. Furthermore, PPP GPS+BDS is better than PPP GPS which had RMS values smaller than 1 cm in the horizontal and 3–4 cm in the vertical.

Cai and Gao (2013b) stated that PPP GPS+GLO will significantly improve the station coordinate error in all three components compared with those obtained using PPP GPS or PPP GLO. They also showed that the station coordinate error using PPP GLO is larger than the error using PPP GPS, stating the reason for that as being the smaller number of GLONASS satellites and the worse satellite geometry, or because of the lower accuracy of GLONASS precise products and the difficulty of resolving GLONASS ambiguities. In addition to that, Cai and Gao (2013a) investigated the use of PPP GLO on 15 globally distributed stations on three consecutive days (1-3 November 2011) and found that PPP GLO could reach an accuracy of 0.035, 0.054 and 0.086 m in the North, East and Up, respectively. Comparing that to the PPP GPS, this is still about 2 cm better as it was found to be 0.015, 0.031 and 0.077m when compared to the International GNSS Service (IGS) weekly solution. They also tried to use PPP GLO, but they only obtained less than decimetre accuracy. However, their results can be considered as unreliable for the PPP GPS and PPP GLO because they considered the receiver clock offset to be different between the GPS and GLONASS when it should have the same variation for the same receiver but with an offset with

respect to both constellations (unless there was an unmodelled error for one of the constellations or the processing parameters were not the same in both scenarios).

To benefit from using GLONASS to improve the satellite geometry, Jokinen et al. (2013d) showed that PPP GPS+GLO will improve satellite geometry and add more pierce points for tropospheric delay estimation, and for that reason, using GLONASS with the GPS was expected to improve the PPP accuracy. Horizontal, vertical and 3D station coordinate errors using PPP GPS+GLO were found to be reduced by 40%, 23.8%, and 31.7% respectively when compared to PPP GPS. Furthermore, better accuracy has been obtained from PPP GPS+GLO rather than PPP GPS in the kinematic mode as presented by Anquela et al. (2013). Also, Cai et al. (2013) used a single frequency PPP GPS+GLO and showed an improvement of 30% in comparison to the results from PPP GPS or PPP GLO.

Then, Tegedor et al. (2014) presented an analysis about the accuracy and availability of quad-constellation PPP daily solutions using the MGEX data sets and found that PPP GPS+GLO+GAL+BDS kinematic results show enhanced accuracy when using all four satellite systems together. However, the accuracy improvement is relatively small compared to the PPP GPS+GLO under good sky visibility, and the improvement only became more significant under reduced sky visibility conditions, where the increased number of satellites was more significant.

Separately, Hernandez-Pajares et al. (2014) showed that the higher order ionosphere delay impact on a PPP user is lower than the current uncertainties of the PPP solutions, after applying consistent precise products, from Analytical Centres who applied these corrections during the estimation of their precise products.

Li et al. (2014a) indicated that the precision of PPP BDS static and kinematic can reach centimetre level, and the precision of PPP GPS+BDS kinematic is improved significantly compared to that of PPP BDS or PPP GPS. This is comparable with Cai et al. (2015) who used three-hour static processing results to evaluate the performance

improvement of PPP GPS+GLO+GAL+BDS in a short time interval, based on 5 stations on 16 consecutive days. Since the precise coordinates of most stations are not available, they compared their estimated station coordinates with the Online Positioning User Service (OPUS) that was developed by the United States' National Geodetic Survey. They concluded that PPP GPS+BDS improved the station coordinate accuracy by 28%, 6% and 7% over PPP GPS in the three coordinate components, respectively. However, PPP GPS+GLO achieved slightly better performance than the PPP GPS+BDS. While, PPP GPS+GLO+BDS increased the accuracy of station coordinates which suggested that multi-constellation PPP has the potential to significantly improve the station coordinate accuracy. However, the improvement in station coordinate accuracy was not significant after adding Galileo due to its limited number of satellites at that time. Similarly, Li et al. (2015a) evaluated the improvement from PPP GPS+GLO+GAL+BDS in satellite visibility, spatial geometry, dilution of precision, convergence, accuracy, continuity and reliability in constrained environments, using 100 days' data of MGEX and BDS Experimental Tracking Network (BETN). They concluded that PPP GPS can achieve millimetres accuracy but after a long convergence time of several hours while PPP GLO was worse than PPP GPS especially in the Up component and PPP GPS+GLO+GAL+BDS improve the station coordinate accuracy by 37%, 21% and 34% for the East, North and Up components respectively comparing to PPP GPS. A similar PPP combination was used by Li et al. (2015c), but for real time, who processed ~120 stations using PPP GPS+GLO+GAL+BDS and found an improvement of 25% in the station coordinate accuracy comparing to PPP GPS and highlighted that some outliers in the PPP GPS solutions were removed when multi-GNSS observations were used.

To achieve centimetre level of accuracy from single frequency receivers , numerical results have showed that single-frequency PPP based on the GRoup And PHase Ionospheric Correction (GRAPHIC) (Montenbruck, 2003) can achieve centimetre-level accuracy in static mode and decimetre-level accuracy in kinematic

mode, which is several times better than the obtained results from that of ionospheric mitigation models (Sterle et al., 2015).

To investigate the effect of Inter System Bias (ISB) on PPP solutions Chen et al. (2015) presented an approach for assessing ISB, and proved that ISB parameters are not correlated with the estimated station coordinate parameters and can be assimilated into receiver clock offset as well as the estimated ambiguities, based on 1 year of data processed using PPP GPS+GLO for 53 IGS stations and 1 month of PPP GPS+BDS data for 15 IGS+MGEX stations. They found that the RMS of station coordinate differences between the two types of solutions (with and without ISB estimation) are parts of millimetre for daily static PPP. Considering the millimetre-level precision of current GNSS PPP solutions, these statistics demonstrated equivalent performance of the two solution types. This is different from Wang et al. (2015a), however, who suggested that the refinement of an ISB model may weaken the correlation between station coordinates and ISB estimates and finally enhance the PPP performance in the case of poor observation conditions. While, for the case of a sufficient number of satellites with fairly good geometry, the PPP performance is not seriously affected by ISB due to the low correlation between the ISB and the other estimated parameters.

Later, Song et al. (2016), proposed a new PPP strategy based on a sliding window (constraining the station coordinates to the previous day of the time series) to improve the station coordinate accuracy. Based on one station using both the traditional and new PPP strategy they showed that the new strategy can effectively improve station coordinate accuracy, especially for the Up component.

While many Web-based online services are available for providing station coordinate estimates, Ocalan et al. (2016) used PPP GPS+GLO for six hours of data in 2015 and compared the obtained results from the Bernese GNSS Software 5.2 (BSW) and GIPSY-OASIS v6.3 (GOA), as well as six other Web-based online services

(AUSPOS, OPUS, CSRS-PPP, APPS, GAPS, Trimble-RTX). They concluded that 1cm station coordinate accuracy could be achieved from Web-based online services, BSW and GOA. In addition, the PPP-solution of the Trimble-RTX service delivers a better station coordinate accuracy than the other Web-based services that use a PPP approach.

Separately, Liu et al. (2016a) proposed an alternative approach to multi-GNSS PPP GPS+GLO+GAL+BDS, which is an expansion on the proposed method by Zhang et al. (2011) for slant ionospheric delays estimation (using raw code and phase observations). Using one month of data in April 2015 from 32 IGS+MGEX stations they found that the monthly RMS values for most station coordinate accuracies were within 6.0 (East), 6.2 (North) and 9.3mm (Up) for static PPP and 21.0 (East), 22.0 (North) and 49.0mm (Up) for kinematic PPP.

The deformation and landslide can be also monitored using PPP where Capilla et al. (2016) showed PPP GPS+GLO can detect deformations of more than 5cm of magnitude. Also based on real-time precise products, Afifi and El-Rabbany (2016) compared PPP GPS+GAL+BDS with PPP GPS in between-satellite single-difference (BSD) mode, using Natural Resources Canada's GPSPace PPP software, at four stations and found that the precision of the station coordinates were improved by 25% in comparison with PPP GPS. While Abdi et al. (2017) found that PPP GPS+GLO+BDS enhanced the station coordinate accuracy by 5%, 8% and 6%, in the East, North, and Up components respectively compared to PPP GPS.

Lastly, Pan et al. (2017a) investigated the performance of single frequency PPP using GRAPHIC for PPP GPS+GLO+GAL+BDS at 47 MGEX stations based on seven consecutive days. They found that the accuracy of station coordinates were significantly improved comparing to PPP GPS or PPP GPS+GLO, and they concluded that PPP GPS and PPP BDS are comparable.

2.2.2 Convergence time

The other effective benefit that can be obtained from using multi-constellations rather than a single constellation in PPP is the convergence time for reaching the required accuracy for estimated parameters.

Cai and Gao (2007) indicated that an improvement in the station coordinate convergence time could be obtained even with adding a limited number of GLONASS satellites because it is dependent on the improvement in satellite geometry. In addition, Cai (2009) found from his work that adding GLONASS to the GPS reduced the convergence time in PPP GPS+GLO by 21% (East), 24% (North) and 19% (up) in static mode when compared to PPP GPS.

Alternatively, Martin et al. (2011) found no significant convergence improvements between PPP GPS and PPP GPS+GLO. The improvement in the mean time was only 3.1%, 12.5% and 2.1% for the North, East and Up components respectively, which from their point of view, is not a significant improvement.

Going further, Stosius et al. (2011) used simulated data for GPS, GLONASS and Galileo (GAL) to investigate the benefit of combining these three constellations. They showed that PPP GPS took 53 minutes to detect the Sumatra tsunami while using 18 satellites from the GPS, whereas PPP GPS+GLO+GAL reduced that time to 17 minutes. This can provide support for the idea of using a multi-constellation because it will lead to different satellites in different geometries. However, they did not present an evaluation for the individual constellations (i.e. PPP GLO and PPP GAL). Also Jokinen et al. (2012c) found that adding GLONASS to the GPS will reduce the convergence time of PPP GPS+GLO compared to PPP GPS in some cases. Whereas, a significant reduced time was obtained by Cai and Gao (2013b) from PPP GPS+GLO as a 30% improvement in the convergence time when compared to PPP GPS. On the other hand, Anquela et al. (2013) showed that PPP GPS+GLO did not always improve the convergence in static mode.

Further, Cai et al. (2015) found that PPP GPS+GLO+GAL+BDS will reduce the convergence time by 26% (East), 13% (North) and 14% (Up) comparing to PPP GPS. In addition, Li et al. (2015c) observed that the combined PPP GPS+BDS and PPP GPS+GLO significantly shorten the convergence time comparing to PPP GPS. Again, Li et al. (2015a) found that PPP GPS station coordinate accuracy can be better than 10cm and 5cm after 30min and 120min convergence time respectively. While millimetres accuracy can be achieved after the long convergence time of several hours and both PPP GPS+BDS and PPP GPS+GLO significantly shortened the convergence time compared to PPP GPS. Further, PPP GPS+GLO+GAL+BDS presented the fastest convergence and took several minutes to achieve an accuracy of better than 10 cm, less than 30 minutes to be better than 5 cm and a few hours to reach mm-level accuracy. Comparing to PPP GPS they found that PPP GPS+GLO+GAL+BDS gave the most important contribution of multi-GNSS to PPP convergence time by reducing it by 70%. Less improvement was found by Afifi and El-Rabbany (2016), however, who only obtained a 25% convergence time improvement when using PPP GPS+GAL+BDS comparing to PPP GPS.

There are also other parameters that could improve the convergence time for PPP. Abdi et al. (2017) suggested that the improvement in the PPP convergence time could be affected by several parameters. Firstly, ambiguity resolution of un-differenced phase observations (for instance, Ge et al. (2007), Mervart et al. (2008), Laurichesse et al. (2009), Collins et al. (2010), Geng et al. (2010a), Teunissen et al. (2010), Li et al. (2013b), Teunissen and Khodabandeh (2014) and Odijk et al. (2015)) could enhance the convergence time upon the float solution. Secondly, using real-time precise atmospheric correction models as in Li et al. (2013a) and Li et al. (2013b).

Lastly, increasing the degrees of freedom and improving satellite geometry are obtained by using observations from multiple-frequency or other GNSS systems beside GPS especially in the areas with GNSS signal blockage (Cai et al. (2015)), and consequently, the PPP convergence time can be further reduced significantly (for

instance Melgard et al. (2009), Yigit et al. (2013), Elsobeiey (2014) and Gao et al. (2016)).

2.2.3 Coverage and availability

In terms of coverage and availability, researchers showed a variety of opinions and analyses about the benefits of using multi-constellations.

Balaei et al. (2007) suggested that GPS and Galileo can be considered as alternatives to each other in the presence of different frequencies and their availability. However, Zhang et al. (2008) concluded that in terms of GDOP using three constellations (GPS, GLONASS and Galileo) is better than using them separately or with other combinations, even when the same number of satellites are used for different combinations, because satellites are from different orbits. Li et al. (2009) and Tolman et al. (2010) found that using a combination of GPS and GLONASS will be beneficial when there are only five GPS satellites available, and that GLONASS can be used as an assistant to the GPS constellation. In addition, Ji et al. (2010) presented the potential benefits from combining GPS, GLONASS and Galileo in different scenarios, using the GPS as a base for adding GLONASS and Galileo. These combinations were evaluated based on simulated data with a conclusion that significant improvements in availability, coverage and continuity would be seen in the best scenario of GPS, GLONASS and Galileo, rather than the other scenarios because the three constellations are in a different geometry. Furthermore, Yang et al. (2011b) concluded that adding BDS will improve GDOP by 50% for GPS, 29.5% for GPS+GAL, and 22.6% for GPS+GLO+GAL.

Further, Li et al. (2015a) observed that the North coordinate component is still the most accurate component in multi-constellation PPP solutions (may be caused by the satellite constellation geometry), and highlighted that the accuracy, reliability and availability of station coordinate accuracy will be improved significantly as compared to PPP GPS, when a combination of satellite systems was used.

While the availability and reliability of PPP GPS decrease dramatically as the elevation cutoff increases, Li et al. (2015c) observed that PPP GPS+GLO+GAL+BDS can provide precise station coordinate estimates continuously even up to 40° elevation cutoff (e.g. in urban canyons). Also that if 5 to 10 satellites can be used for PPP GPS the PDOP variation will be from 2 to 6, whereas in contrast, 22 to 30 satellites can be used for PPP GPS+GLO+GAL+BDS and the PDOP values will be stable and below 1.5. They also concluded that station coordinate time series from PPP GPS+GLO+GAL+BDS will be more stable than those from PPP GPS, with less fluctuations. Similarly, Cai et al. (2015) concluded that the multi-constellation PPP performance benefits from the increased number of satellites and improved satellite geometry.

Furthermore, Wang et al. (2015a) suggested that PPP GPS+GLO is better than PPP GPS, indicating that the station coordinate accuracy and reliability are significantly improved with the additional GLONASS satellites in the case of insufficient number of GPS satellites or poor geometry conditions. Lastly, Ocalan et al. (2016) suggested that the use of PPP GPS+GLO observations in post processing could be an advantage due to the increase of number of observations.

2.3 PPP for Troposphere Studies

The estimation of tropospheric zenith total delay (ZTD) and tropospheric integrated water vapour (IWV) from GPS observations, denominated as GPS meteorology, was initially proposed by Bevis et al. (1992). For troposphere studies, the tropospheric zenith wet delay (ZWD) can be obtained by simple subtraction from an estimated tropospheric ZTD of the tropospheric zenith hydrostatic delay (ZHD) computed by using pressure data, and a station's latitude and height above mean sea level (Saastamoinen, 1972). Tropospheric IWV can then be computed by converting the tropospheric ZWD using temperature data.

Following Bevis et al. (1992), extensive studies based on post processing were conducted, such as Rocken et al. (1993), Dodson et al. (1996) and Haase et al. (2003), and the relevant factors affecting the accuracy of the estimated tropospheric ZTD were evaluated in detail. For instance, the effect of ocean tide loading on the tropospheric delays was discussed in Dach and Dietrich (2000) based on simulated data, and Ge et al. (2002) derived a coefficient matrix for the GPS observables that maps the orbital parameter errors into tropospheric ZTD errors. Agreements at the level of 10-12 mm in tropospheric IWV from the comparison of ground-based GPS measurements with radiosonde and water vapour radiometers were found in Bevis et al. (1992), Rocken et al. (1995), Duan et al. (1996), Tregoning et al. (1998) and Haase et al. (2001).

Since then, there have been many studies in the literature on how to improve the performance of ground-based GPS tropospheric ZTD estimation, as detailed in this section.

Schueler et al. (2000b) computed wet delay process noise from tropospheric time-series analysis, rather than using the mean process noise, as 2-9 mm $\sqrt{h}$, depending on the location of the station. Schueler et al. (2000a) also used a numerical weather model with an interpolation procedure to compare the estimated tropospheric ZTD from that interpolation with the estimated tropospheric ZTD available from the IGS, and found an agreement of 1.7 cm.

Penna et al. (2001) highlighted that it is unlikely that the EGNOS tropospheric model alone will fully mitigate the tropospheric delay effects. Therefore, they made an assessment to compare the tropospheric ZTD with those obtained from the analysis of one year of Global Double-Difference (GDD) solutions published by Dodson et al. (2000). For five stations in the UK for one year, they found differences of less than 5 cm between 72% and 78% of the true, and less than 10 cm for between 96% and 99% of the time. In addition, they highlighted that the RTCA (1999) stipulated that

the user should be required to apply a correction for the tropospheric delay based upon a model with a residual error of less than 12 cm. They also concluded that the RMS errors ranged from 4.0 to 4.7 cm with the maximum errors ranging from 13.2 to 17.8 cm, and that the EGNOS model is expected to fail due to weather variations over short periods of hours and days.

The University of New Brunswick's tropospheric delay model (UNB3m) was presented as a modified UNB3 and tested by Leandro et al. (2006), based on ray-tracing analyses of 703,711 profiles from 223 stations in North America and its surrounding territory over the period from 1990 to 1996. They found that the predicted errors of the UNB3m had a mean value -0.5 cm and a standard deviation of 4.9 cm. They mentioned that the standard error was similar to the UNB3 model, but the reduction in the mean absolute error was 75%. However, this model prediction is similar during the day for the hydrostatic part because it relies on the day of the year rather than the day of the year and the time during the day.

The treatment of the tropospheric ZWD as a stochastic parameter with an update at every observation epoch in a Kalman filter was evaluated as a very useful tool to account for the high variability in the wet component of tropospheric delay, in the research of Pany et al. (2007). They showed that the a-priori value of the process noise variance of the tropospheric ZWD significantly affected the estimation, which means that this value should be determined properly. In addition, they mentioned that future investigation for the process noise variance of the tropospheric ZWD would be necessary.

Furthermore, Pace et al. (2010) presented a method for estimating residual fields by using a ground-based GPS network. They modelled the tropospheric ZHD as an exponential function of latitude while the tropospheric ZWD was estimated every 5 minutes with a stochastic model (random walk) and a constraint of 20 mm/($\sqrt{h}$)) and

made an interpolation to account for these residuals. They found that these residuals were of the order of 5-10 cm.

Rohm et al. (2014) used an a-priori model for the troposphere, as a Saastamoinen-based tropospheric ZHD (using GPT) mapped with the dry Global Mapping Function (GMF), and zenith delay corrections estimated based on the wet GMF, and found that the tropospheric ZTD error was below 15 mm from PPP GPS using the Bernese GPS Software (version 5.0).

Additionally, the Saastamoinen tropospheric model can be used to calculate the tropospheric ZTD based on the meteorological parameter values obtained from the UNB3m or the GPT model. The results from 125 IGS stations were presented by Li et al. (2012). They summarized the magnitude of the bias and the RMS errors of the tropospheric ZTD for: EGNOS model (bias: 2.0 cm, RMS: 5.4 cm), UNB3m model (bias 0.7 cm, RMS: 5 cm) and IGGtrop model (bias: -0.7, RMS: 4.0 cm). Their results showed that the new IGGtrop model provides the smallest bias and RMS errors. However, IGGtrop is not available in the public domain and still has an RMS of 4 cm level of uncertainty. They also suggested that increasing the number of the satellites would enhance the current techniques and Yang et al. (2011a) suggested that using future new GNSS signals will also enhance the current techniques.

There has also been an increasing amount of literature on numerical weather modelling (NWM) products, relying on meteorological data, which are widely used nowadays for estimating the tropospheric delay, meaning that GPS could also be an important source for numerical weather prediction (NWP) models (Kuo et al. (1996); Yang et al. (1999); Baker et al. (2001)). In this sense, Yang et al. (2013) presented a new approach for estimating the slant tropospheric delay from high-resolution NWM products. And found that the RMS of the differences between the tropospheric slant delay from the NWM and the reverse computed tropospheric slant delay from the PPP was 6 cm below 10°, < 3.5 cm above 15° and 2 cm above 30° elevation. While Yao et

al. (2013) established a global non-meteorological parameter tropospheric delay model GZTD (Global Zenith Tropospheric Delay) based on spherical harmonics using the global zenith tropospheric delay grid data provided by Global Geodetic System (GGOS) Atmosphere. They found that the accuracy of this model were a bias of 0.2 cm, and an RMS of 3.7 cm, and comparing to other tropospheric models were, UNB3m (bias: 3.4 cm, RMS: 6.0 cm), UNB4 (bias: 4.7 cm, RMS: 7.4 cm), UNB3 (bias: 4.0 cm, RMS: 7.0 cm) and EGNOS (bias: 4.5 cm, RMS: 6.9 cm). GZTD has also been compared to tropospheric ZTD time series from 385 IGS stations and its accuracy was found to be -0.2 cm and 4.24 cm for the mean an RMS respectively. Then, Chen et al. (2014) presented GPT2 model that could predict the tropospheric ZTD with an average uncertainty of about 2 cm under normal atmospheric conditions. Additionally, they highlighted that the significance of the GPT2 lays in its availability for use as a precise a-priori tropospheric delay, which could improve the efficiency of data processing. This model also was implemented to the BNC software, with a process noise of $3e^{-6}$ m /√s for the ZWD, and tested using 20 IGS stations by Yuan et al. (2014) who found that over 90% of the results were within 20 mm RMS.

Separately, Böhm et al. (2014) reported on three models RTCA (RTCA, 1999), the ESA model (Krueger et al., 2005) and GPT2 (Lagler et al., 2013). In addition, they proposed a new tropospheric delay model (GPT2w) which is based on gridded values of water vapour pressure, the water vapour decrease factor, and the weighted temperature. They found that regarding the tropospheric ZTD, the globally averaged bias is about 0.1 cm, and the RMS is about 3.6 cm. They also compared their model with the other three blind models. Their comparison with the other models is in Table 2-2.

Table 2-2 Summary of the biases in tropospheric delay models (Böhm et al., 2014)

Model	Mean bias (cm)	Mean RMS (cm)
RTCA-MOPS	-2.50	4.55
ESA	0.83	3.82
GPT2	-0.28	3.79
GPT2w	-0.02	3.61

Recently, Yao et al. (2016) presented a further developed version of GZTD (GZTD2) that takes into consideration the diurnal variations with a modified function for the model expansion and showed that, comparing to the IGS tropospheric products, GZTD2 has a mean and RMS of -0.3 cm and 3.9 cm respectively.

Several studies have also showed that the availability of real-time precise products can support near real-time tropospheric ZTD estimation, as in Rocken et al. (1997) , Gendt et al. (2001). While Gendt et al. (2004) demonstrated that the tropospheric ZTD using PPP, with Earth Parameter and Orbit determination System software (EPOS.P.V2), supported with hourly updated precise satellite orbits and clocks, gave comparable results to those from a GDD network solution, and that PPP showed a potential to become the standard technique for tropospheric ZTD estimation from ground based GNSS observations as shown by Karabatić et al. (2011) using the Bernese GPS Software (version 5.0).

Estimated tropospheric ZTD from GNSS have been suggested to serve and meet different requirements, e.g. numerical weather prediction (NWP) but also climate monitoring (Gutman and Benjamin (2001);Guerova et al. (2016)).

To support NWP nowcasting or severe weather event monitoring, Dousa and Vaclavovic (2014) developed real-time estimates, and processed 36 European and global stations for nine months (February-October, 2013) using G-Nut/Tefnut software. Their result were within 6-10 mm ZTD mean standard deviations which can fulfil the requirement for the operational NWP (i.e. 30mm ZTD). In the mean time, Li

et al. (2014b) developed a real-time GPS water vapour processing system based on a PPP GPS with ambiguity fixing, using real-time satellite orbit, clock, and phase delay corrections in EPOS-RT software. A conclusion drawn from 80 globally distributed IGS stations over 10 days was that no significant difference between PPP GPS float and fixed solutions remains after a sufficiently long time of convergence (e.g. several hours).

Separately, Ahmed et al. (2014) compared the results from three different softwares (BNC2.7, G-Nut/Tefnut and PPP-Wizard software), at 22 IGS stations, for a period of 31 days and found an agreement of 1-3 cm regarding bias and 1-4 cm with regard to standard deviation.

The Multi-GNSS Experiment (MGEX) project was lunched by the IGS (Rizos et al., 2013), and has brought great opportunities and challenges for the real-time determination of tropospheric ZTD to improve weather prediction and to enhance the real-time ZTD processing. Li et al. (2015b) developed a multi-GNSS model at the Helmholtz Centre Potsdam GFZ German Research Centre for Geosciences (GFZ) to exploit the potential of observations from the available GNSS based on PPP. Using Saastamoinen as an a-priori model for the tropospheric ZHD and estimated the tropospheric ZWD as a piecewise linear function from a ~110 station IGS MGEX and Chinese BeiDou (BDS) Experimental Tracking Network (BETN) they found that the tropospheric ZTD form PPP GLO is comparable with the one from PPP GPS with RMS values between them of 10.7 and 12.1 mm, and with mean biases of 2.9 and -3.1 mm respectively when compared to VLBI. They also concluded that the real-time multi-GNSS PPP can provide more accurate and reliable tropospheric ZTD/IWV estimates than single-system processing. The accuracy of real-time single-system ZTD was found to be about 10–20 mm and it can be significantly improved by several millimetres when multi-GNSS observations are processed simultaneously enabling outlier elimination in the combined GNSS solution.

With the increasing number of satellites in the BDS constellation, Lu et al. (2015) have developed a real-time tropospheric ZTD processing method that is based on PPP GPS and PPP BDS, and considered 40 MGEX stations over a half year, using Saastamoinen as an a-priori model and estimating the tropospheric ZWD as a random-walk, with fixed station coordinates and estimation of an inter-system bias as a constant using EPOS-RT software. They concluded that the estimated tropospheric ZTD from real-time PPP BDS agreed with the estimated tropospheric ZTD from PPP GPS with an RMS of 11-16 mm. They also found that tropospheric ZTD from PPP BDS was slightly less accurate than from PPP GPS and the best tropospheric ZTD accuracy in real-time was found with PPP GPS+BDS. Their findings agreed with Dousa et al. (2016) who suggested that there is a potential for advanced GNSS tropospheric products for meteorological applications and emphasized a synergy in GNSS and meteorological data and products. However, Douša (2009) suggested that the orbits error can be easily absorbed by the satellites clocks and the estimated ambiguities.

Separately, the European Centre for Medium-Range Weather Forecasts (ECMWF) analysis was introduced to provide an improved multi-GNSS combined PPP (GPS, GLONASS, Galileo and BDS) solution in post-processing mode by Lu et al. (2016) using EPOS-RT software, by developing a numerical weather model (NWM)-constrained PPP processing system. Two PPP scenarios were presented. Firstly, the PPP GPS as a standard mode using Saastamoinen for the a-priori tropospheric ZHD with an estimation of the tropospheric ZWD using 5mm/√hr process noise. Secondly, the NWM-constrained PPP using tropospheric ZHD, ZWD and three mapping function coefficients from ECMWF, following Zus et al. (2014b), which are then interpolated linearly to be applied in the multi-GNSS PPP with an estimation for the residual wet delay. Using 34 MGEX stations during September 2015, they found that their NWM-constrained PPP solution gave an improvement of 2.5, 12.1 and 18.7 % for the North, East and Up station coordinates respectively, when compared to the PPP GPS standard

solution. They also found that the performance of PPP benefited greatly from multi-GNSS when compared to PPP GPS in term of convergence time.

Another use of ECMWF analysis is VMF1, which is available with updated values every 6 hours. Bock et al. (2016) used it as an a-priori model for tropospheric ZHD and ZWD, with a correction to be estimated as random-walk (using the suggested parameters by Bosser et al. (2009) and Bock et al. (2013)) and 5 min resolution in PPP GPS for ~100 ground-based GPS receivers over the period from 1 September 2012 to 31 March 2013. They compared their obtained final tropospheric ZTD (using GIPSY-OASIS (GOA) II v6.2 software, with fixed ambiguities and final precise products) with the tropospheric ZTD estimated using a previous version of GIPSY/OASIS II, following the Byun and Bar-Sever (2009) strategy, and found mean differences of between −3 mm to +3 mm with standard deviation ranges from 4 to 8 mm.

More recently, Ding et al. (2017) suggested that the performance of real-time GNSS meteorology can be further improved by incorporating observations from multi-GNSS. They used a modified version of PPP with integer and Zero-difference Ambiguity Resolution Demonstrator (PPP-WIZARD) including GPS, GLONASS and Galileo, with fixed station coordinates and $5e^{-5}$m/√hr process noise for ZWD, to extract tropospheric ZTD from 20 IGS stations over 30 days and concluded that PPP GPS is better than PPP GLO for real-time tropospheric ZTD estimation. They noted that PPP GPS ambiguity resolution can improve the accuracy of tropospheric ZTD estimates and that an average accuracy about 8 mm in tropospheric ZTD can be achieved after an initialization process of approximately 8.5 min. They also found that PPP GPS+GLO was not a great improvement, and even made things worse for some stations, which could be correlated with the weighting strategy between the two constellations, which used standard deviations of 0.01m for GPS and GLO phase measurements, but used 1 and 10m respectively for GPS and GLO code measurements.

Lastly, Lu et al. (2017) developed a NWM-augmented PPP processing algorithm derived from short-range forecasts from the Global Forecast System of the National Centers for Environmental Prediction (NCEP) (Kanamitsu et al., 2002) provided with a horizontal resolution of 1° isobaric levels and the algorithm from Zus et al. (2014a). This was used to improve real-time PPP BDS using MGEX stations and they compared the accuracy of the tropospheric ZTD with the IGS final tropospheric ZTD. The tropospheric ZHD and ZWD from NCEP were used as a-priori values, with estimates of a residual wet delay. They showed that an improvement in the convergence time of up to 60% and 66.7% for the East and Up coordinate components respectively can be achieved when compared to a standard PPP solution (when only tropospheric zenith delays were estimated and no gradient parameters were considered). However, their station coordinate accuracies were 3.5, 2 and 8 cm for East, North and Up respectively. Whereas, for the tropospheric ZTD, the differences mainly ranged from -2.0 cm to 2.0 cm, with overall RMS values of the tropospheric ZTD differences from the IGS of about 1.5 cm and a mean value of about 1.1 cm.

Nowadays, many on-line PPP solutions are also available and include strategies for estimating the tropospheric delay. Four on-line PPP solutions, APPS (Automatic Precise Positioning Service), GAPS (GPS Analysis and Positioning Software), CSRS-PPP (Canadian Spatial Reference System Precise Point Positioning service) and magic-PPP were tested by Guo (2014) for evaluating the PPP estimated tropospheric ZTD in comparison to that estimated by the IGS. The results showed differences in the tropospheric ZTD estimation of less than 1-2 cm.

2.4 PPP for Station Velocity and Crustal Motion Studies

Station velocities for crustal motion studies can be computed using continuous long-term data. For many years, such station velocities have been estimated from Global Double-Difference (GDD) and PPP solutions, as one of the significant inputs to the terrestrial reference frame, which is defined by a number of stations' coordinates with their estimated velocities.

The earliest reported GPS results dealt mainly with experiments spanning a few days or weeks. These started in 1986 with Bock et al. (1986) who analysed of a 1 to 2 week period in the 'March 1985 experiment', followed by an examination of the repeatability of GPS measurements across a triangle in the Gulf of California, with observations spanned over 4 to 6 consecutive days. Later, in 1992, Shimada and Bock (1992) were the first to derive tectonic plate kinematics, with horizontal station velocities derived using 2 consecutive days from every week of GPS data for 17 months. This was arguably the first demonstration of the potential of GPS monitoring networks for obtaining temporally dense measurements of small horizontal and vertical crustal motions across plate boundary zones.

Following on from this, in 1995, four years of GPS data were used by Argus and Heflin (1995) to estimate tectonic plate motion, and they found that the estimated angular velocities differed significantly from the corresponding angular velocities in the global plate motion model NUVEL-1A. While, by 1997, Larson et al. (1997) showed that the estimated angular velocities derived from 38 sites using 204 days of GPS data spanning from January 1991 through to March 1996 agreed with the no net rotation NUVEL-1A model at 95% confidence level, as well as with absolute plate model prediction within 95% confidence, except for some differences in the poles of rotation and plate rates for the Pacific and Nazca plates.

Since 1997, the study of crustal motion, based on station velocities derived from routinely generated time series of daily station coordinates, has been made possible through the establishment of many networks of continuous GPS (CGPS) stations around the world. These studies of crustal motions can include not only plate tectonics, but also glacial isostatic adjustment, crustal deformation and earthquake dynamics (Segall and Davis, 1997), and by 2000, with an increase in the number of global CGPS stations available, such studies had evolved to the point where discrepancies began to appear between geodetic station velocities and those predicted by the geologic models as in Dixon et al. (2000) and Wdowinski et al. (2001).

However, it was soon realised that time series of daily station coordinates are affected by many factors that contribute to the error budget of the estimated station velocities, and Argus et al. (1999) also showed that an error in the global reference frame can significantly affect the time series produced from GPS observations. Another factor that could affect the results is seasonal signals, as presented by Blewitt and Lavallee (2002) who showed that station coordinates can show an annual variation with typical amplitude of 2mm for horizontal variation and there will be a bias in station velocities if less than 2.5 years of data are used to form time series. They recommended 2.5 years as a standard minimum data span for station velocity estimation for plate tectonics and/or global reference frame definition. In addition to this, Williams (2003a) showed that all non-modelled physical phenomena or neglected correlated noise content can generate processes that affect velocity uncertainty estimation. In the meantime, Williams (2003b) suggested that station velocity estimation can be biased if there are coordinate offsets in time series and that these can dominate velocity uncertainties if left uncorrected.

As time has gone on, the demand for higher and higher accuracy station velocities required for different geophysical applications has increased, leading to a re-focus on errors in station coordinate time series. For example: antenna phase centre model effects were studied by Cardellach et al. (2007) using simulated data; the mis-modelling of satellite orbits was studied by Griffiths and Ray (2009) and Steigenberger et al. (2009); atmospheric effects (loading and tropospheric delay) were studied by Tregoning and Watson (2009); station-dependent effects like monument instability were studied by King and Williams (2009); and near-field multipath was presented by King and Watson (2010).

Furthermore, due to different mechanisms, it was shown by Stewart et al. (2005) and Penna et al. (2007) that sub-daily residual (systematic) errors can remain in the estimated station coordinates and propagate into the time series. While King et al. (2008) showed that even after modelling for solid earth tides and ocean tide

loading displacements, substantial signals at sub-daily periods can remain in station coordinate time series, which propagate into annual and semi-annual periods in 24-hr solutions with median amplitudes of ~0.5mm, but can reach several millimetres in certain parts of the world.

All of the above could clearly lead to results that give an erroneous interpretation of geophysical signals such as tectonics, glacial isostatic adjustment, vertical motion of tide gauges or seasonal geophysical loading signals. Furthermore, such errors would degrade the GPS contribution to the ITRF definition (Altamimi et al., 2007).

With all of this in mind, there have been, and continue to be, many studies of crustal motion based purely on global double-difference (GDD), using softwares such as the Bernese (BSW) and GAMIT/GLOBK. However, there have also been an increasing number of studies based on PPP, using softwares such as GIPSY/OASIS II (GOA) and BSW, and several studies that have considered both GDD and PPP.

Nocquet and Calais (2003) used 65 CGPS stations to study the horizontal crustal motion in Western Europe based on station velocity estimates derived from using global double-difference (GDD) GPS and two softwares, BSW (version 4.2) and GAMIT/GLOBK (version 10.05), to present a combined methodology similar to that used for the definition of the ITRF (Altamimi et al., 2002). They concluded that the resulting velocity field is consistent at a continental scale but that the selection of the 'best' stations was necessary to ensure a reliable final velocity field.

At around the same time, Perez et al. (2003) presented the use of GOA for PPP GPS as a more straightforward and efficient method when compared to GDD GPS for station velocity estimation and crustal motion studies. Their case study was of the South American Plate, and they concluded that PPP GPS could feasibly be used for station velocity estimation. Also using GOA for PPP GPS, Khan (2005) looked at CGPS

stations in Denmark, Greenland and the USA and focused on the observed displacement caused by surface loading of the Earth at different frequencies.

To consider different strategies and different softwares for estimating station velocities, Calais et al. (2006) processed up to 12 years (1993-2005) of data from 450 CGPS stations using GOA for PPP GPS and using GAMIT/GLOBK for GDD GPS, and included solutions from IGS and the full definition of the ITRF2000. They concluded that their estimated station velocities agreed with plate motion models for stations in plate interiors. Separately, Teferle et al. (2007) assessed BSW PPP by comparing their station coordinate time series and found RMS statistics to be 3.0 (North), 4.9 (East) and 7.7mm (Up). Furthermore, Sella et al. (2007) used GOA for PPP GPS at 360 CGPS stations in Canada and USA and compared their estimated station velocities to several different glacial isostatic adjustment (GIA) models, showing significant discrepancies between the model predictions and the observed horizontal station velocities. Similarly, Teferle et al. (2009) presented multiple independent solutions using BSW for PPP GPS and their in-house GPS Analysis Software (GAS) for regional double-difference (RDD) GPS, and found that the apparent crustal motion signal follows the predicted motions of the ITRF2000 plate motion model with residual horizontal station velocities being generally smaller than 1mm/yr.

Kogan and Steblov (2008) used GAMIT/GLOBK for GDD GPS to process data from 192 globally distributed CGPS stations for the period from 1995 to 2007, then selected 71 of these to represent stable plate regions in Africa and in the Arctic region of North America. The same software and strategy having also been used for regional tectonics by McClusky et al. (2000) at 189 CGPS stations for the period from 1988 to 1997, which was an extension to the work of Reilinger et al. (1997).

Since that time, the use of GOA for PPP GPS has continued to grow. Simons et al. (2007) used GOA for PPP GPS at about ~100 stations in Southeast Asia region for the period from 1994 to 2004, and defined the station velocities and the boundaries of

the Sundaland block in ITRF2000. To understand the deformation in Mexico, station velocities were estimated by Marquez-Azua and DeMets (2009) using GOA for PPP GPS at 448 stations. They transformed the estimated station velocities to ITRF2005 (Altamimi et al., 2007) using daily parameter Helmert transformations from JPL and observed small differences between the newly measured velocities and the predicted velocities because of the time-correlated noise. Desai et al. (2011) used GOA for PPP GPS and reprocessed six stations in which a large 5.5 day feature had been found in the JPL GPS PPP time series. They used the same satellite orbit and clock products as the JPL GPS PPP time series, but with a different processing strategy which resulted in a significant reduction in the strength of the 5.5 day feature and suggested that this signal is both station dependent and probably related to parts of the PPP processing strategy rather than the satellite orbit and clock products or GOA itself. Then, Bos et al. (2012) used GOA for PPP GPS to produce station coordinate that were subsequently mapped into ITRF2008 (Altamimi et al., 2011), and presented a method for dealing with missing data and outlier removal from time series. Similarly, Satirapod et al. (2013) used GOA for PPP GPS on data for the period from 1998 to 2008, and found a significant diversion in the North component of the station velocity of 1.7mm/yr in the Southeast Asia region (Thailand) when compared to ITRF 2000 and ITRF2005. They also highlighted that when using GOA for PPP GPS it was possible to obtain millimetre-level station coordinate repeatability in the horizontal and centimetre in the vertical, for 24-hr observations. In the meantime, and using an updated version of GOA (Version 6.0) and JPL precise products, Liang et al. (2013) used PPP GPS for 750 GPS stations around the Tibetan Plateau for the period from 1999 to 2009 to obtain daily loosely constrained station coordinates, followed by performing a joint adjustment to obtain their coordinate time series and optimum estimations of velocity in ITRF2008 using the Quasi-Observation Combination Analysis (QOCA) software of JPL (Dong et al. (1998),(2006)). They concluded that their 3D velocity field offers better kinematic constraints for understanding the dynamics of present-day uplift and growth of that plateau. Wang (2013) used GOA for PPP GPS

with Single Receiver Phase Ambiguity (PPP-SRPA) in the application of landslide monitoring, and Park et al. (2013a) used GOA for PPP GPS to calculate the crustal movements of Antarctica based on 8.5 years of data for 7 stations. Park et al. (2013b) then analysed 7 IGS stations between 2004 and 2012 using GOA for PPP GPS and validated their estimated station velocities by comparing with other models of tectonic motions. Further, Bogusz and Klos (2015) used GOA for PPP GPS at 180 IGS stations, and Wang et al. (2015b) used GOA for PPP GPS for long-term landslide monitoring. Then, Yu and Wang (2016) used GOA for PPP GPS and data up to the end of 2014 to summarise the current GPS geodetic infrastructure in the Gulf of Mexico (GOM) region, and establish a stable Gulf of Mexico reference frame (SGOMRF14).

At around the same time, Sidorov and Teferle (2015) considered station coordinate time series derived from PPP GPS as implemented in two softwares, BSW (version 5.2) and the Navigation Package for Earth Observation Satellites version 3.3.1 (NAPEOS). From their results, they suggested that antenna calibration differences propagate directly into station coordinate estimates, affecting both sub-daily and daily results and yielding periodic variations. They also confirmed that small differences between individual and type mean antenna/radome calibrations propagate into station coordinate time series and may be partly responsible for spurious signals with draconitic frequency and its harmonics.

More recently, the use of GOA for PPP GPS has been used alongside other softwares that are based on GDD. Alinia et al. (2017) used BSW GDD to process five years of data for 14 CGPS stations in Ontario and Quebec, Canada, for the period from 2008 to 2012, with data for 55 stations that had been processed using GOA PPP GPS (Blewitt, 2014) to estimate horizontal and vertical station velocities. They found that the pattern of horizontal deformation is not well explained in the North component because there were some biases in the horizontal station velocities. Such biases in both magnitude and directional components, have also been seen the in Antarctica and North America regions where the GIA signals are significant (King et al., 2015).

Then, Mustafar et al. (2017) used GOA (version 6.1.2) PPP GPS on two sets of GPS data; the first covering the period from 1999 to 2004, used to determine the continuous Sundaland tectonic plate motion, and the second covering the period from 2009 to 2011, used to investigate the current deformations of North Borneo. However, they also used GOA for a sort-of double difference (the same software configuration except that fixed coordinates were employed for a base station and satellite orbits and clocks were estimated through short baseline methods) to investigate horizontal and vertical station velocities. They found that the differences in horizontal velocity estimates between PPP GPS and these double difference solutions were below 1 mm/year, with the differences being larger in the longitudinal direction.

Separately, there are various online GNSS processing services that allow users to submit their own GNSS data and potentially obtain high quality results. Holden et al. (2017) processed 10 years GPS data (collected between day of year (DOY) 52–62 in the year 2000, DOY 39–47 in year 2005, DOY 58–71 in year 2007, and DOY 30–50 in year 2011) using the Jet Propulsion Laboratory Automated Precise Positioning Service (APPS) online service and derived station velocities from the obtained station coordinates. They found small differences observed when comparing to the estimated horizontal station velocities from the Bernese GPS Software (version 5.0) for GDD GPS. They also suggested that the APPS station velocities were reliable in the horizontal and that less reliability can be placed on the vertical as derived from the APPS height solutions, as in some cases the uncertainty of the vertical station velocities were significantly larger than their magnitude.

While, He et al. (2017) investigated several aspects of time series analysis by considering a set of 72 time series and applying different noise models. Their conclusion was that GOA for PPP GPS and GAMIT/GLOBK for GDD GPS produce very similar results in terms of daily station coordinate time series; however, when combining both solutions the WRMS is slightly better than for the individual solutions. Whereas in terms of station velocity differences between the combined and individual

solutions, these were found to be about 0.1 mm/yr, which agreed with other published comparisons (e.g. Khan and Knudsen (2012) who compared the differences between GOA PPP GPS and the Bernese GPS Software (version 5.0) GDD).

At the same time, Amiri-Simkooei et al. (2017) focussed on the possible improvements to GOA for PPP GPS, following the use of improved models of antenna phase centre variations and solar radiation pressure in JPL's reanalysed precise products. Considering 89 and 66 GPS stations for a period of 7 to 21 years, they found that the use of these reanalysed precise products leads to spatial correlations that are reduced on average by a factor of 1.25, while the white and flicker noise amplitudes for all coordinate components are reduced by 29–56%.

Lastly, Abraha et al. (2017) assessed the nature of periodic signals in station coordinate time series based on the use of the Bernese GNSS Software (version 5.2) for PPP GPS, PPP GLO and PPP GPS+GLO, from the combined IGS and four of its Analysis Centres (ACs). They concluded that a reduction of 52% for the horizontal and 36% for the vertical were achieved for the fortnightly signal from the PPP GPS+GLO solution compared to the PPP GPS solution, and that the source of most of the powers of the draconitic and fortnightly signals are satellite-induced with a non-zero contribution of site-specific errors. They also concluded that PPP has the potential to equal the accuracy of GDD.

2.5 PPP Ambiguity Resolution

The code observable represents an absolute value of the distance between the receiver and a satellite. While a more precise solution is the carrier phase observable which represents an ambiguous value of the distance because the exact integer number of cycles between the satellite and the receiver at lock on is not known and must be estimated as part of a positioning solution. Such estimates are then either left as real numbers leading to a so-called float solution or resolved as integer numbers leading to a so-called fixed solution.

Two well-known options for integer ambiguity resolution are integer bootstrapping (IBS) (Blewitt, 1989) and integer least-squares (ILS) (Teunissen, 2001). In terms of IBS, a very efficient implementation of this scheme is given by the least-squares ambiguity decorrelation adjustment (LAMBDA) which is optimal in the sense of maximizing the probability of correct ambiguity resolution (Teunissen, 1995). Whereas, for ILS, this corresponds to the maximum likelihood solution in the Gaussian case based on a search for the closest lattice point (Agrell et al., 2002).

In any case, consideration also has to be given to the case where the process of integer ambiguity resolution is not successful, as the wrongly fixed ambiguities may lead to severe biases in the state estimates. For that reason, ambiguity validation is a related and important issue. Different tests can be used to decide, whether or not to accept the integer solution. In order to increase the probability of correct ambiguity resolution and increase the average number of resolved ambiguities compared to Integer Aperture estimators (Teunissen, 2003) with a fixed failure rate, e.g. to shorten the time to first fix, partial ambiguity resolution (PAR) is a useful tool (Brack and Gunther (2014); Odijk et al. (2014)). Brack (2014) divided the available algorithms for PAR proposed into two groups: purely model-driven approaches based on the bootstrapping success rate (Teunissen (1999);Khanafseh and Pervan (2010); Odijk et al. (2014)), and algorithms that are data-driven (Dai et al. (2007); Parkins (2011); Verhagen et al. (2011);

Around the same time as the IBS and ILS were developed, Gabor and Nerem (1999) proposed a theoretical approach for single receiver ambiguity resolution based on the use of the Fraction Cycle Bias (FCB), that does not depend on the integer term, but would first need an estimation of the FCB in a Between Satellite Difference (BSD) mode, which is efficient and practical. Then, Gabor and Nerem (2000) proposed the algorithm and concept of fixing the ambiguity of a single receiver.

Since then, as the accuracy of satellite orbit and clock corrections improved to enable the use of PPP, techniques for integer ambiguity fixing in PPP have been subject to much research and have significantly improved in recent years. These techniques can roughly be divided into those where the FCBs of the wide-lane and narrow-lane biases are available to the PPP user (Ge et al. (2007); Geng et al. (2011a)), or as those where the satellite phase biases are merged with the satellite clock corrections (Collins et al. (2010); Laurichesse et al. (2009)). Clearly, it is crucial that the user's PPP strategy considers which technique is being used as they involve different precise products, as suggested by Håkansson et al. (2016).

Ge et al. (2007) proposed a FCB method to achieve ambiguity-fixed PPP solutions. They emphasized that the single-difference ambiguities of a certain satellite pair must have a similar fractional part because they come from double difference ambiguities close to an integer. They also showed that FCBs can be estimated by single-difference observations from a reference station network, and that these estimated FCBs could then be used to eliminate the satellite FCBs at a single-difference level in a PPP solution. According to Ge et al. (2007), in practice, the narrow-lane FCBs need to be supplied to the user at least every 15 minutes.

Separately, the integer clock (IRC) and decoupled clock model methods were proposed by Laurichesse et al. (2008) and Collins et al. (2010) respectively, for use with fixed undifferenced ambiguities. In these two methods, the clock biases of the satellite and the receiver are utilized to absorb the satellite and receiver FCBs respectively. The integer nature of the ambiguity can then be restored so that ambiguity fixing is possible in a PPP solution.

Geng et al. (2010b) analysed and compared the FCB and IRC methods for fixing ambiguities in PPP and proved their equivalence. However, it was pointed out that since the FCB products of Ge et al. (2007) are based on the BSD mode, the PPP user

would need to use the same mode, and they obtained 27% improvement in the repeatability of the East coordinate component.

Geng et al. (2010b) and Laurichesse (2011) both then demonstrated that it is possible to resolve the ambiguities in PPP GPS through the inclusion of FCBs, but that it will require a long period (30 to 60 minutes) to obtain a fixed solution. Moreover, because of frequency division multiple access (FDMA), fixing GLONASS ambiguities based on BSD in PPP GPS+GLO requires the ambiguity of the reference satellite. Also, Geng et al. (2011b) studied the technical factors that affect the rapidity of both the Wide-lane ambiguity resolution and the stabilization of narrow-lane-UPD estimates, and investigated the narrow-lane ambiguity resolution in real-time PPP GPS, and concluded that ambiguity-fixed solutions with centimetre-level station coordinate accuracy can be achieved with a few tens of minutes. They used the Positioning And Navigation Data Analyst (PANDA) software (Li et al., 2008).

To overcome the fact that a single-difference model is employed to determine the FCBs, whereas PPP based on an undifferenced model is preferable (and the undifferenced model is more suitable for the ideal of fixing GLONASS ambiguities), Li and Zhang (2012) proposed introducing the FCB of a specific station as the datum to solve the rank defect of the equations and enable undifferenced FCB estimation. In this method, the common-view satellites of adjacent stations are used to calculate the initial FCB of the receiver and satellites at all stations, which are then treated as the datum. However, this approach assumes that the single-difference integer ambiguity can be accurately fixed, while in practice, 100% ambiguity fixing is challenging due to the influence of various factors and any errors in this ambiguity fixing will then affect the FCB estimation.

For testing the effect of multi-GNSS on PPP GPS ambiguity fixing, Jokinen et al. (2013c) used PPP GPS+GLO to produce a float solution, followed by the resolution of the GPS ambiguities only, and proved that including the GLONASS measurements

could reduce the time for the GPS ambiguity resolution but only by approximately 5% using POINT software with CNES biases and precise products. Furthermore, Nadarajah and Teunissen (2013) used simulated data for three constellations; GPS, Galileo and BeiDou and supported the idea of using the three systems together to give the best possibility to resolve ambiguities rather than using them separately, and Odolinski et al. (2013) suggested that ambiguity resolution will be improved when using GPS and BeiDou constellations. Capilla et al. (2016) used PPP GPS+GLO, with ambiguity resolution based on the IRC method conducted for GPS, while ambiguities were kept as real values for GLONASS, and concluded that it is better to use PPP GPS+GLO, since GLONASS adds robustness to the solution, and that recovering fixed phase ambiguities is very useful because it can compensate losses of convergence in the observations and improves the accuracy of the solution. Similarly, Pan et al. (2017b) used PPP GPS+GLO+BDS to improve the performance of ambiguity float and ambiguity fixed PPP. Ambiguity resolution based on the FCB method was conducted for GPS, while ambiguities were kept as real values for GLONASS (it is still considered difficult to fix GLONASS ambiguity because of the FDMA scheme) and BDS (since the precise products of satellite orbit and clock of BDS were poorer than GPS and the precise correction of BDS satellite antenna phase centre offsets (PCO) and phase centre variation (PCV) were still unknown). They concluded that the fixed solution is better than the float in term of convergence time.

Most recently, many studies have published initial results about GLONASS and BDS ambiguity resolution (AR) for PPP. However, those studies about GLONASS ambiguity resolution for PPP need some special conditions, such as external ionosphere products (Geng et al., 2016) (DD with GPS and GLO fixed), common receivers (Liu et al., 2016b), or long converge time (Banville, 2016). The work by Liu et al. (2016c) and Pan et al. (2016) have also demonstrated that it is possible to perform BDS FCB estimation and BDS ambiguity resolution for PPP. However, the accuracy of the BDS FCBs is poorer than that of GPS FCBs and the BDS ambiguity

resolution for PPP needs more convergence time. The effect of including triple-frequency was also considered by Gu et al. (2015) for ambiguity-fixed PPP solutions based on BDS data, using PANDA software. They concluded that the impact of additional signals is almost negligible when only a float solution involved, but fixing Extended Wide-Lane (EWL) and Wide-lane (WL) together, as opposed to the single ambiguity fixing, improved the PPP accuracy.

Since 2015, the FCB and IRC methods for fixing ambiguities in PPP are being used more routinely. Li et al. (2015c) mentioned that GFZ, as one of the IGS real-time data analysis centres, is operationally running its Earth Parameter and Orbit determination System Real-Time (EPOS-RT) software for providing GPS satellite orbits and clocks, and FCBs, as uncalibrated phase delays (UPDs), as part of the IGS real-time PPP service (Li et al. (2013c), Li et al. (2013d)). Similarly, Capilla et al. (2016) have developed versions of the libraries of the CNES PPP client demonstrator, using the IRC method, with integer and zero-difference ambiguity resolution (Laurichesse and Privat, 2015).

Lastly, Yi et al. (2017) presented an improvement on the FCB estimation method proposed by Gabor and Nerem (1999) based on transforming the trigonometric function into a linear function using the Taylor series expansion. They highlighted that an equation without integer ambiguity will be obtained, which is suitable for estimating undifferenced FCBs (and is different from the previous method because it does not require single-difference ambiguity fixing).

2.6 Chapter Summary

To conclude, to the best of the author's knowledge, no report has so far been found using PPP GLO as an independent solution to PPP GPS or PPP GPS+GLO.

It could be concluded from the above sections that there is a need to make a clear decision about implementing PPP GLO and what improvements will be obtained. Dealing with the combinations of these constellations requires a full understanding for the coordinate systems and time systems of each constellation separately. Moreover, there are biases affecting each constellation individually that need attention and work to evaluate or treat them to reach the optimal combination from them.

It could also be concluded from the tropospheric delay part that there is clear scope for improving tropospheric ZTD estimation beyond the current use of models for tropospheric ZHD combined with an estimation of tropospheric ZWD.

It could also be concluded that although PPP GPS is already being widely used for station velocity estimation, and PPP GPS+GLO is also used for station velocity estimation by some researchers, PPP GLO is not used so far.

Thus, there is a need to cover these gaps by investigating the achievable accuracy from PPP GPS, PPP GLO and PPP GPS+GLO in terms of station coordinates and tropospheric ZTD, and station velocities.

The research presented in this thesis, therefore, attempts to address various aspects that have been discussed in the previous sections, and Table 2-3 summarizes these aspects.

Table 2-3 Summary of literature gaps and the suggested approaches for this research

Topic	Literature (conventional and current)	This research
Geometry	PDOP and HDOP	Cumulative DOP and its correlation with latitude Chapter 5
PPP station coordinates	Centimetre level of accuracy and precision based on PPP GPS and PPP GPS+GLO	General improvements for PPP to reach millimetre level of accuracy and precision by adopting an implementation of PPP GLO to be as accurate and precise as PPP GPS and PPP GPS+GLO Chapter 6
PPP Troposphere	~5cm level of accuracy by using a model of tropospheric ZHD and solving for tropospheric ZWD in order to compute tropospheric ZTD based on PPP GPS or PPP GPS+GLO	Implementing an alternative strategy for estimating tropospheric ZTD from PPP, with significant accuracy (to also work in real-time and offer improvement to the convergence time), and implementation of PPP GLO to be as accurate as PPP GPS and PPP GPS+GLO Chapter 7
PPP station rates /velocities	Based on PPP GPS or PPP GPS+GLO	Testing PPP GLO for station rate/velocity estimation as an independent tool to PPP GPS and in preference to PPP GPS+GLO Chapter 8
Products		Studies of short- and long-term effects on accuracy and precision of station coordinates, tropospheric ZTD and station rates/velocities. Chapter 6,Chapter 7 and Chapter 8

Chapter 3. Precise Point Positioning

Precise Point Positioning (PPP) represents an undifferenced solution, compared to the simple double-difference (base and rover) solution or a Global Double-Difference (GDD) solution. Therefore, the errors that affect the signal path, as well as the satellite and receiver parts, need to be taken into account when processing PPP solutions. Thus, this chapter includes details of the corrections models or methods that will be used in this research as the basis of the PPP processing strategy.

3.1 Extended Kalman Filter

The Extended Kalman Filter (EKF) as presented in Feng et al. (2008) was used as the core tool for the data processing with the POINT software (Chapter 4). The observation vector *Z(t)* corresponds to the difference between the observed and the predicted ionosphere-free measurements, where t is the current time epoch. The predicted measurements are calculated based on the current station coordinates, satellite coordinates, and error estimates. The EKF prediction step is described by equations (3.1) and (3.2)

$$x^{-}(t) = \emptyset * x^{+}(t-1) \tag{3.1}$$

$$P^{-}(t) = \emptyset * P^{+}(t-1) * \emptyset^{T} + Q \tag{3.2}$$

Where $\boldsymbol{x^{-}(t)}$ is the predicted state vector, $\boldsymbol{x^{+}(t-1)}$ the state vector estimated based on the measurements from the previous epoch, $\emptyset$ the state transition matrix, $\boldsymbol{P^{-}(t)}$ the predicted state vector variance/covariance matrix, $\boldsymbol{P^{+}(t-1)}$ the state vector variance/covariance estimated based on the measurements from the previous epoch and $\boldsymbol{Q}$ the variance/covariance matrix of the system noise (Abdel-Salam, 2005).

The EKF update step is described by equations (3.3), (3.4) and (3.5)

$$x^{+}(t) = x^{-}(t) + K(t) * [Z(t) - H(t) * x^{-}(t)] \tag{3.3}$$

$$P^{+}(t) = [I - K(t) * H(t)] * P^{-}(t) \quad (3.4)$$

$$K(t) = P^{-}(t) * H^{T}(t) * [H(t) * P^{-}(t) * H^{T}(t) + R(t)]^{-1} \quad (3.5)$$

Where K(t) is the Kalman gain, Z(t) is the observation vector, H(t) is the design matrix and R(t) is the measurement noise matrix. The design matrix represents the relation between the measurements and EKF states. For example, it shows the relation between the code and phase measurements and the station coordinates.

3.2 Observation Equations

Undifferenced measurements are used for each PPP daily solution, with the general observation equations for code and phase being as follows (Hofmann-Wellenhof et al., 2007):

For pseudo-range using C/A-Code on L_1:

$$C_1^i = e^i + c\delta_r - c\delta^i + \frac{I^i}{f_1^2} + \frac{S^i}{f_1^3} + T^i + M_{C1}^i + Q_{C1}^i + bias_{C1} - bias_{C1}^i \quad (3.6)$$

For pseudo-range using P-code on L_1,L_2:

$$P_F^i = e^i + c\delta_r - c\delta^i + \frac{I^i}{f_F^2} + \frac{S^i}{f_F^3} + T^i + M_{PF}^i + Q_{PF}^i + bias_{P,F} - bias_{P,F}^i \quad (3.7)$$

For carrier phase

$$L_F^i = e^i + c\delta_r - c\delta^i - \frac{I^i}{f_F^2} - \frac{S^i}{f_F^3} + T^i + m_F^i + q_F^i + \lambda_F\left(N_F^i + B_F - B_F^i\right) \quad (3.8)$$

Where:

i is the satellite index;

F represents the index of the GNSS frequency - for GPS satellites *F* = 1 (GPS L1) and *F* = 2 (GPS L2), while for GLO satellites *F* = 1 (GLO L1) and *F* = 2 (GLO L2) with

$$f_{k\,L1} = f_{0L1} + k\Delta f_{L1} \quad (3.9)$$

$$f_{k\,L2} = f_{0L2} + k\Delta f_{L2} \tag{3.10}$$

Where *k* represents the frequency channel; f_{0L1} = 1602 MHz for the GLONASS L_1 band; Δf_{L1} = 562.5 kHz frequency separation between GLONASS carriers in the L_1 band; f_{0L2} = 1246 MHz for the GLONASS L2 band; Δf_{L2} = 437.5 kHz frequency separation between GLONASS carriers in the L2 band.

e^i represents the geometric distance from the receiver to the satellite;

$c\delta_r$ is the receiver clock offset;

$c\delta^i$ is the satellite clock offset;

I^i is the first-order ionospheric bias term;

S^i is the second-order ionospheric bias term;

f_F is the GNSS frequency in Hz;

T^i is the tropospheric bias;

M_{PF}^i is the multipath error for P code measurements on the frequency *F*;

M_{C1}^i is the multipath error for C/A code measurements on L_1;

m_F^i is the multipath error for carrier-phase measurements on the frequency *F*;

Q_{PF}^i is the noise for the P code measurements on the frequency *F*;

Q_{C1}^i is the noise for C/A code measurements on L_1;

q_F^i is the noise for the carrier-phase measurements on the frequency *F*;

$bias_{C1}$ is the receiver code bias for C/A code measurements on L_1;

$bias_{C1}^i$ is the satellite code bias for C/A code measurements on L_1;

$bias_{P,F}$ is the receiver code bias for P code measurements on the frequency *F*;

$bias^{i}_{P,F}$ is the satellite code bias for P code measurements on the frequency *F*;

λ_F is the wavelength on the frequency *F*;

N^i_F is the carrier phase ambiguity term on the frequency *F*;

B_F is the receiver fractional cycle bias (FCB) on the frequency *F*;

B^i_F is a satellite fractional cycle bias (FCB) on the frequency *F*.

3.3 PPP Errors, Biases and Corrections

3.3.1 Satellite orbits and clocks

The accuracy of broadcast products (satellite orbits) is not adequate for the PPP solution because they are within the range of 1.1 m (Warren and Raquet, 2003). The broadcast ephemerides is necessary for the PPP GLO but only because it contains the frequency offset. Therefore, various organizations have produced precise products for the satellite orbits and clock (as satellite coordinates and satellite clock offsets). These products are application dependent. For instance, the IGS final precise products used in post-processing are the combination of several organizations' products; they are the weighted mean of all the agencies that contribute. There are also real-time products, which are transmitted to real-time users via different communication tools. Additionally, there are other precise products for helping PPP users in terms of ambiguity resolution, e.g. Centre National d'Etudes Spatiales (CNES) precise products which account for the fractional cycle bias by adding them to the satellite clock offsets. In this case, users need to apply the same strategy that the organization has used when these products were produced to be compatible. For instance, with the CNES precise products, users should implement PPP based on the between satellites difference (BSD) rather than undifferenced in order to cancel out the receiver clock offset which has a receiver fractional cycle bias.

Therefore, it is important to choose suitable products for PPP. In this study, the products to be used are usually the final precise products for the highest accuracy, as shown in Section 5.1, unless otherwise stated.

3.3.2 Ionospheric Bias

The ionosphere is located approximately between 70 km and 1000 km above the surface of the earth (Kaplan and Hegarty, 2005). The gas molecules in the ionospheric region are ionised by ultraviolet rays from the sun. This causes a release of free electrons, which induces delays in the code measurements and advances in the carrier phase measurements.

The magnitude of the ionospheric delay depends on the electron density and the frequency of the GNSS signal. Therefore, the refractive index will provide a measure of the impact of the ionosphere on the GNSS measurements. For the carrier phase observations, the phase refractive index (n_p) can be defined as:

$$n_p = 1 + \frac{I_1}{f^2} + \frac{I_2}{f^3} + \frac{I_3}{f^4} \dots \dots \quad (3.11)$$

While for the code observations, the group refractive index (n_g) can be defined as:

$$n_g = 1 - \frac{I_1}{f^2} + \frac{2I_2}{f^3} + \frac{3I_3}{f^4} \dots \dots \quad (3.12)$$

Where I_1 is the first order ionospheric delay term, I_2 is the second order ionosphere delay term, I_3 is the third order ionospheric delay term and f is the frequency of the GNSS signal. Using the ionosphere-free combination will remove the first order ionospheric delay $\frac{I_1}{f^2}$. The ionosphere-free combination for the code observable is (Dach et al., 2007):

$$P_3 = \frac{1}{f_1^2 - f_2^2} \left(f_1^2 P_1 - f_2^2 P_2\right) \tag{3.13}$$

While the ionosphere-free combination for the carrier phase observable is (ibid):

$$L_3 = \frac{1}{f_1^2 - f_2^2} \left(f_1^2 L_1 - f_2^2 L_2\right) \tag{3.14}$$

Where P_3 and L_3 refer to the ionosphere-free code and the ionosphere-free phase combination respectively; P_1 and P_2 refer to the P-code measurements; L_1 and L_2 refer to the phase measurements; and f_1 and f_2 refers to the frequencies.

The magnitude of the first-order ionospheric delay is typically between 1 and 50 m (Kedar et al., 2003) while in the period of extreme solar activity it can be as large as 150m. Employing the ionosphere-free can mitigate 99.9% of the ionospheric delay by eliminating the first-order ionospheric bias (Hofmann-Wellenhof et al., 2007). While the second- and third-order effects are typically ~0–2cm, and ~0–2mm at zenith, respectively, depending on the time of day, day of year, the solar cycle, the relative geometry of the magnetic field and the line of sight (Bassiri and Hajj, 1993).

The impact of the higher-order ionospheric bias on accurate positioning was studied by Kedar et al. (2003) under high-ionization conditions, i.e. solar maximum scenario (2000-2002). One of their main conclusions was that a global southward displacement of several millimetres was detected in the station coordinates. Later, Fritsche et al. (2005) suggested that there will be a correlation between station height and tropospheric ZTD that might force the troposphere parameters to absorb the effect of higher order ionospheric terms on station height, while Steigenberger et al. (2006) considered the adjustment of additional parameters such as satellite orbits and Earth rotation parameters in a reprocessing strategy and showed that not only the station coordinates are affected by this bias but also the estimated satellite orbits can be affected by this bias and can cause centimetre level errors. Also Hernandez-Pajares

et al. (2007) suggested that the most important aspect of the higher order ionospheric effect will appear for satellite clocks and it can be greater than 1cm depending on the geographical location. They also found, based on the period studied in their work, that the impact on station coordinates was smaller than 1 mm and presented a model for correcting the second-order ionospheric bias which is based on taking into account the interaction of the ionosphere with the Earth's magnetic field.

Triple frequency measurements can eliminate the second-order ionospheric bias when employing the measurement combination that will eliminate the first and the second order ionospheric errors (Hoque and Jakowski, 2008). However, using the triple frequency combination for eliminating the second-order ionospheric bias is still not currently possible because only half of GPS satellites are broadcasting on three frequencies.

This research implements the ionosphere-free combination for dual frequency with an evaluation for the performance of correcting the second order ionospheric bias in section 5.3.

3.3.3 Tropospheric bias

The velocity of the electromagnetic wave depends on the refractive index n, of the medium, which is defined by:

$$n = \frac{c}{v} \tag{3.15}$$

where *c* is the speed of light in vacuum and *v* is the speed of light in the medium. When the signal hits the troposphere at a non-normal angle, then the ray path will bend according to Snell's law:

$$n_{inc} * \sin(\theta_{inc}) = n_{trans} * \sin(\theta_{trans}) \tag{3.16}$$

where n_{inc} and n_{trans} are the refractive indices of the incident and transmitted medium; see Figure 3-1.

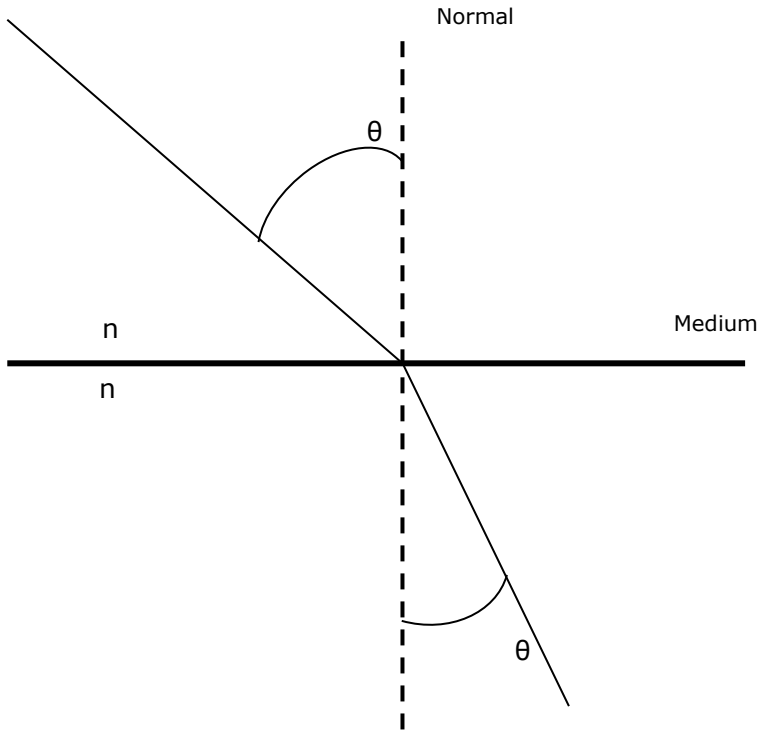


Figure 3-1 Signal refraction because of troposphere (Group, 2012)

As the refractive index increases when descending towards the horizon, i.e. when the elevation angle of the satellite decrease, the atmosphere becomes denser, and the ray gradually bends more intensively. The troposphere is a non-dispersive medium for the frequency below 30 GHz (Huang, 2007). That means the refractive indices are independent of the signal frequency, such that the code and phase propagate in the tropospheric layers at the same speed. Thus, they are both delayed by the same amount of tropospheric bias. The magnitude of this bias depends on the temperature, the relative humidity and the pressure along the signal path, and for low elevation satellites, the relatively longer path of the signal within the troposphere results in a correspondingly larger tropospheric bias. It could be about 2.4 m for a satellite at the zenith, and as large as 25 m at an elevation angle of 5 degrees (Kaplan and Hegarty, 2005). As the troposphere is a non-dispersive medium, a combination of multiple frequency observations is no longer applicable to remove the tropospheric

bias. Thus, it has to be modelled, for which purpose it is usually divided into two components. The first component is the hydrostatic delay d_h which contains ~90% of the total tropospheric bias and can be modelled to within an accuracy of a few mm at the zenith (Bevis et al., 1992). The second component is the wet delay, which contains ~10% of the total tropospheric bias but is harder to model because of the uncertainties and the dynamics in the distribution of water vapour in the atmosphere.

3.3.3.1 Tropospheric models

A wide variety of mathematical models of tropospheric delay have been developed. The tropospheric models investigated and used in this research include Saastamoinen, UNB3m, GPT and EGNOS as detailed in the following sub-sections.:

3.3.3.1.1 Saastamoinen

The Saastamoinen model is one of the most commonly used tropospheric delay models for calculating the hydrostatic (and wet) delay based on meteorological parameters (Saastamoinen, 1973).

The tropospheric zenith total delay D_t^z from the Saastamoinen model is as follows (Kleijer, 2004):

$$D_t^z = 10^{-6} k_1 \frac{R_d}{g_m}\left[P_0 + \left(\frac{k_3}{k_1(\lambda + 1 - \beta R_d/g_m)T_0} + \frac{k_2'}{k_1(\lambda+1)}\right)e_0\right] \qquad (3.17)$$

β and λ are place and time dependent. In the work of Saastamoinen (1972), the following constants were used:

k_1 = 77.624 K mbar^{-1}, k_2 = 64.7 K mbar^{-1}, Rd = 287.04 m^{2}s^{-2}K^{-1}, g_m = 9.784 m s^{-2}, k'$_2$ = k_2 −0.622 k_1 K mbar^{-1}, β = 0.0062 K m^{-1}, k_3 = 371900 K^2 mbar^{-1}, λ = 3

Substituting these values in (3.17), the tropospheric Zenith total delay D_t^z will be:

$$D_t^z = 0.002277\left[P_0 + \left(\frac{1255}{T_0} + 0.05\right)e_0\right] \quad (3.18)$$

Where P_0 is pressure in mbar, e_0 is water-vapour pressure, T_0 is temperature in [K] and D_t^z is in metres.

In practice the wet component that is related to water-vapour pressure and temperature is hard to model accurately, and it is normal practice to only consider the hydrostatic component in equation (3.18) using standard pressure and temperature (SPT) and hence obtain tropospheric zenith hydrostatic delay (ZHD).

3.3.3.1.2 UNB3m

UNB3m is a modified version of University of New Brunswick's (UNB3) neutral atmosphere model. It was created by altering a parameter's values in the UNB3 look-up table and the associated UNB3 algorithms. In this model, the wet component prediction was carried out using relative humidity to be converted subsequently to the partial water vapour pressure then used in the tropospheric ZTD computation (Leandro et al., 2006).

In the UNB3 model delay, the tropospheric zenith hydrostatic delay $\boldsymbol{d_h^z}$ can be computed according to:

$$d_h^z = \frac{10^{-6}k_1 R}{g_m}.P_0.\left(1 - \frac{\beta H}{T_0}\right)^{\frac{g}{R\beta}} \quad (3.19)$$

And the tropospheric zenith non-hydrostatic delay d_{nh}^z can be computed as:

$$d_{nh}^z = \frac{10^{-6}(T_m k_2' + k_3)R}{g_m\lambda' - \beta R}.\frac{e_0}{T_0}.\left(1 - \frac{\beta H}{T_0}\right)^{\frac{\lambda' g}{R\beta}-1} \quad (3.20)$$

Where *H* is the orthometric height in m;

R is the gas constant for hydrostatic air (287.054 J kg^{-1} K^{-1});

gm is the acceleration of gravity at the atmospheric column centroid in m s^{-2}

T_m is the mean temperature of water vapour in K and

can be computed from:

$$T_m = T\left(1 - \frac{\beta R}{g_m \lambda'}\right) \tag{3.21}$$

Where $\lambda' = \lambda + 1\ (unitless)$

and $T_0\ ,\ P_0\ ,\ e_0\ ,\ \beta\ and\ \lambda$ are the meteorological parameters of temperature, pressure, water vapour, place and time computed according to:

$$Avg_{\emptyset} = \begin{cases} \text{Avg}_{15}\ , \text{if}\ \emptyset \leq 15 \\ \text{Avg}_{75}\ , \text{if}\ \emptyset \geq 75 \\ \text{Avg}_{\text{i}} + \dfrac{(\text{Avg}_{\text{i+1}} - \text{Avg}_{\text{i}})}{15}.(\emptyset - \text{Lat}_{\text{i}}), \text{if}\ 1\,5 < \emptyset < 75 \end{cases} \tag{3.22}$$

Where $\emptyset$ is the latitude in degrees; $Avg_{\emptyset}$ is the annual computed average, *i* is the index of the nearest lower tabled latitude and *Lat* stands for latitude from a provided table.

In a similar manner, the annual amplitude can be computed as:

$$Amp_{\emptyset} = \begin{cases} \text{Amp}_{15}\ , \text{if}\ \emptyset \leq 15 \\ \text{Amp}_{75}\ , \text{if}\ \emptyset \geq 75 \\ \text{Amp}_{\text{i}} + \dfrac{(\text{Amp}_{\text{i+1}} - \text{Amp}_{\text{i}})}{15}.(\emptyset - \text{Lat}_{\text{i}}), \text{if}\ 15 < \emptyset < 75 \end{cases} \tag{3.23}$$

Where the $Amp_{\emptyset}$ stands for the computed amplitude.

After the average and the amplitude are calculated for the given latitude, the parameter values can be estimated for the desired day of year (DOY) according to:

$$X_{\emptyset,doy} = Avg_{\emptyset} - Amp_{\emptyset}\,.\cos\left((doy - 28) * \frac{2\pi}{365.25}\right) \tag{3.24}$$

Where $X_{\emptyset,doy}$ represents the computed meteorological parameter for the required latitude and doy is the day of the year.

Finally, the tropospheric slant total delay d_t can be computed according to:

$$d_t = m_h \, d_h^z + m_{nh} \, d_{nh}^z \tag{3.25}$$

where m_h and m_{nh} are hydrostatic and non-hydrostatic mapping functions, respectively (see section 3.3.3.2) .

For the UNB3m tropospheric model, the same procedure should be adopted except that it starts with the relative humidity, which is first transformed into water vapour pressure (Leandro et al., 2006).

Following the International Earth Rotation and Reference Frame Services (IERS) conventions, the transformation is as follows:

$$e_0 = \frac{RH}{100} \cdot e_s \cdot f_w \tag{3.26}$$

where the saturation vapour pressure, e_s, can be computed as:

$$e_s = 0.01 \cdot \exp(1.2378847 * 10^{-5} T_0^2 - 1.9121 * 10^{-2} T_0^2 + 33.93711047 - 6.3431645 * 10^3 T_0^{-1}) \tag{3.27}$$

moreover, the enhancement factor, f_w, can be determined as follows:

$$f_w = 1.00062 + 3.14 * 10^{-6} P_0 + 5.6 * 10^{-7} (T_0 - 273.15)^2 \tag{3.28}$$

Once the water vapour pressure is computed, the delays can be estimated according to equations (3.19), (3.20) and (3.25) (Leandro et al., 2006).

3.3.3.1.3 GPT

A model of global pressure and temperature (GPT) model was presented by Boehm et al. (2007). This model is an empirical model used to estimate the

temperature and pressure anywhere on the Earth's surface. Compared with the UNB3m model, this model does not provide the relative humidity information.

For each profile, the pressure and temperature values are determined for the Earth's surface by interpolating exponentially and linearly, respectively. The pressure values p on the Earth's surface at height h are then reduced to p_r at mean sea level (MSL) h_r as follows:

$$p = p_r(1 - 0.000226(h - h_r))^{5.225} \tag{3.29}$$

While, a linear decrease of temperature T with height is assumed:

$$\frac{dT}{dh} = -0.0065^0\ C/m_r \tag{3.30}$$

There are 36 monthly mean values of the pressure and temperature at MSL. The mean values for the two series and the annual amplitudes, namely a_0 and A respectively, are estimated with the phase offset fixed to January 28, where doy is the day of year:

$$a = a_0 - A \cdot \cos\left((doy - 28) * \frac{2\pi}{365.25}\right) \tag{3.31}$$

a_0 can be computed as follows:

$$a_0 = \sum_{n=0}^{9} \sum_{m=}^{n} P_{nm}(\sin\varphi) \cdot [A_{nm}\cos(m\lambda) + B_{nm}\sin(m\lambda)] \tag{3.32}$$

Where P_{nm} are the Legendre polynomials, φ and λ are latitude and longitude, A_{nm} and B_{nm} are the coefficients for degree n and order m which are determined within a least-squares adjustment.

These values are then used to calculate the a-priori tropospheric hydrostatic delay using equation (3.17).

3.3.3.1.4EGNOS

Another commonly used model is the EGNOS tropospheric model (RTCA, 1996). In this the tropospheric delay is calculated based on the total pressure, temperature, water vapour pressure, temperature lapse rate, water vapour lapse rate and height of the receiver above the mean sea level.

The tropospheric zenith hydrostatic delay d_{dry} and zenith wet delay d_{wet} are computed as follows (Penna et al., 2001):

$$d_{dry} = z_{dry}\left[1 - \frac{\beta H}{T}\right]^{\frac{g}{Rd\beta}} \tag{3.33}$$

$$z_{dry} = \frac{10^{-6} k_1 R_d P}{g_m} \tag{3.34}$$

$$d_{wet} = z_{wet}\left[1 - \frac{\beta H}{T}\right]^{\frac{(\lambda+1)g}{Rd\beta}-1} \tag{3.35}$$

$$z_{wet} = \frac{10^{-6} k_2 R_d P}{g_m(\lambda+1) - \beta R_d} * \frac{e}{T} \tag{3.36}$$

Where:

k_1 = 77.604K/mbar; P is the pressure at mean sea level (mbar); g_m =9.784 m/s^2;

k_2 = 382000 k^2/mbar; e is the water vapour pressure at mean sea level (mbar);

g = 9.80665 m/s^2; H is the height of the receiver above mean sea level (m);

T is the temperature at mean sea level (K); β is the temperature lapse rate (K/m); R_d is the gas constant 287.054 J/kg/K; λ is the water vapour-lapse rate (dimensionless); $z_{hydrostatic}$ is the zenith 'hydrostatic' delay at mean sea level; z_{wet} is the zenith 'wet' delay at mean sea level.

This model also requires a table for summarizing some coefficients in the case where there is no meteorological data. Using the table each meteorological parameter value can be computed as:

$$\xi(\emptyset, D) = \xi_0(\emptyset) - \Delta\xi(\emptyset) * \cos\left[\frac{2\pi(D - D_{min})}{365.25}\right] \quad (3.37)$$

where: φ is the receiver's latitude; *D* is the day-of-year (starting with 1 January); D_{min} = 28 for northern latitudes; D_{min} = 211 for southern latitudes; ξ and $\Delta\xi$ are the average and seasonal variation respectively for the particular parameter at the receiver's latitude (Penna et al., 2001).

3.3.3.2 Mapping functions

The mapping function is a mathematical expression for describing how the slant tropospheric delay varies with respect to the receiver-to-satellite elevation angle. A variety of different mapping functions have been proposed in the past. Bisnath et al. (1997) considered fifteen mapping functions for studying the effect on tropospheric delay. The conclusion that they obtained is that nearly all mapping functions could provide sub-centimetre accuracy for elevation angles above 15 degrees whereas for very low elevation angles, Lanyi, Herring, Ifadis and Niell mapping functions were among the best. The Neill Mapping function (NMF) is given below (Niell, 1996):

For the hydrostatic component:

$$mapping\ function\ dry\ (e) = \frac{1 + \frac{a}{1+\frac{b}{1+c}}}{\sin e + \frac{a}{\sin e + \frac{b}{\sin e + c}}} + \left[\frac{1}{\sin e} - \left(\frac{1 + \frac{a_{ht}}{1+\frac{b_{ht}}{1+c_{ht}}}}{\sin e + \frac{a_{ht}}{\sin e + \frac{b_{ht}}{\sin e + c_{ht}}}}\right)\right] \quad (3.38)$$

This mapping function used the DOY = 28 as the adopted phase for the northern hemisphere and DOY 211 for the southern hemisphere. Linear interpolation is needed

to produce the parameters a, b and c. The height correction a_{ht} , b_{ht} and c_{ht} were determined by a least squares fit to the height correction at nine elevation angles. For a_{wet} , b_{wet} and c_{wet} an interpolation in latitude for each parameter is required because no temporal dependence is included in the wet component.

Moreover, for the wet component:

$$mapping\ function\ wet(e) = \frac{1 + \frac{a_{wet}}{1+\frac{b_{wet}}{1+c_{wet}}}}{\sin e\ + \frac{a_{wet}}{\sin e + \frac{b_{wet}}{\sin e + c_{wet}}}} \tag{3.39}$$

$$mapping\ function\ (e) = \frac{1 + \frac{a}{1+\frac{b}{1+c}}}{\sin e\ + \frac{a}{\sin e + \frac{b}{\sin e + c}}} \tag{3.40}$$

Mendes (1998) analysed some mapping functions by comparing radiosonde profiles from 50 stations distributed worldwide (32,467 benchmark values). The conclusion was that the models that meet the high standards of modern space geodetic data analysis were Ifadis, Lanyi, MTT, and NMF. Furtheremore, he found that for an elevation angle of above 15 degrees, the models Lanyi, MTT, and NMF yield identical mean biases and the best total error performance, while Sakidin et al. (2009) suggested that Ifadis and NMF are superior mapping functions at lower elevation angles. In the mean time, in 2004 the Vienna Mapping Functions (VMF) were first presented by Boehm and Schuh (2004) and are based on direct ray-tracing through numerical weather models (NWM). Two years later, an updated version of VMF was also introduced by Boehm et al. (2006b) based on new coefficients and called VMF1. The Global Mapping Function (GMF) was then presented by Boehm et al. (2006a) based on data from the global ECMWF numerical weather model where its coffecients were obtained from an expansion of VMF1. Although the VMF, VMF1 and GMF are updated versions, in this research NMF was used as a mapping function that could be used consistently in all tests based on the POINT software.

3.3.3.3 Tropospheric gradient

To improve the tropospheric delay estimation, the azimuthal inhomogeneity can be taken into account by including the gradient of the tropospheric delay (MacMillan (1995);Chen and Herring (1997);Bar-Sever et al. (1998);Meindl et al. (2004)):

$$d_{trop} = m(\varepsilon)_h * d_h + m(\varepsilon)_w * d_w + m(\varepsilon)_{azi} * (G_N \cos\emptyset + G_E \sin\emptyset) \quad (3.41)$$

Where d_{trop} is the tropospheric slant total delay, $m(\varepsilon)_h$ is the hydrostatic mapping function, d_h is the tropospheric zenith hydrostatic delay, $m(\varepsilon)_w$ is the wet mapping function, d_w is the tropospheric zenith wet delay, ε is the satellite elevation angle, the subscript azi represents the gradient, G_N is the tropospheric gradient to the north, G_E is the tropospheric gradient to the east and Φ is the azimuthal angle of the satellite.

The tropospheric gradient parameters allow for taking into account the azimuthal variations of tropospheric refraction. For achieving high-accuracy results, it is important to use more observations, which means low elevation angles below 15 degrees (10 degrees is used in this research). The other reason to use lower elevation angles is to reduce the correlation between the estimated station height and the tropospheric delay estimation.

These variations can be taken into account by estimating so-called tropospheric gradient parameters. One model is commonly used for the tropospheric gradient; this model corresponds to a tilting of the tropospheric mapping functions. The Chen troposphere gradient mapping function is used according to the equation below (Zhang and Gao, 2001):

$$gradient\ mapping\ function\ (m(\varepsilon)_{azi}) = \frac{1}{sin\,\varepsilon \tan\varepsilon + 0.0032} \quad (3.42)$$

3.3.3.4 Tropospheric Estimation Strategies

3.3.3.4.1 Derivation of the tropospheric components

All of the tropospheric models that can be used for providing the tropospheric zenith hydrostatic delay (ZHD) or tropospheric wet delay (ZWD) rely on previous measured data. Hence, these models cannot account for real weather variations and thus, cannot provide highly accurate estimates of the tropospheric delay components. In addition, none of the tropospheric models account for the diurnal variations of the troposphere. For example, they assume that the pressure is stable for a particular day of year, and it will be steady for the same day from one year to another. The assumption that the hydrostatic component will not change during the day is likely to be flawed. However, the accuracy of all tropospheric zenith total delay (ZTD) results obtained from using tropospheric models have been shown to be within the range of centimeters, and those within the range of <1 cm have a standard deviation of about 5 cm (UNB3m bias, 0.7 cm; RMS, 5.0 cm).

The PPP can be extended from a tool for producing station coordinates to also be a tool for estimating the tropospheric ZTD. To achieve that, there is a need to consider the strategy used for tropospheric delay estimation, from PPP, in static and in *real-time* situations. In this research, the focus is on obtaining tropospheric ZTD, and with no a-priori models of the tropospheric ZHD and ZWD but a simple assumption of 2.2m and 0.1m for a-priori tropospheric ZHD and ZWD respectively. This can be justified because the tropospheric ZTD is the input to NWM for meteorology and real-time PPP services may not want to use VMF1 as this would require more information to be passed via the communications satellite.

The conventional strategy is to use tropospheric ZHD from a model and then solve for the tropospheric ZWD to give the tropospheric ZTD. In this research an alternative strategy is proposed to deal with both tropospheric components (the

hydrostatic and the wet) as unknown states rather than using the hydrostatic part as an input from a model.

It is known that the tropospheric delay relates to the used mapping function, which explains how the tropospheric delay varies relative to the satellite elevation angle. Therefore, for estimating the tropospheric delay, a design matrix needs to be formulated. The design matrix should contain the partial derivatives for each required unknown.

In the conventional strategy, as it is known that the required tropospheric delay for each station is the tropospheric ZTD, the tropospheric slant hydrostatic delay for every satellite at every epoch will be represented by the tropospheric ZHD multiplied by the chosen mapping function. Therefore, the final unknown to be estimated is the tropospheric ZWD with the partial derivative represented as the selected mapping function.

In the alternative strategy proposed for estimating the tropospheric ZTD, it is assumed that it is possible to estimate the zenith tropospheric delay ZTD as a summation of two estimated unknowns: the tropospheric ZHD as well as the tropospheric ZWD. The idea behind this is that the tropospheric ZHD is not the same for every epoch during the day, as is assumed by tropospheric models. Instead, as the tropospheric ZHD is a function of pressure over the station, it is unlikely for that delay to be stable over 24 hours. In addition, the tropospheric ZHD from a model does not reflect the real values for that day. This is because it is computed from previous data, and even though those values came from long-term data, they will not necessarily reflect the real values on a particular day.

The alternative strategy being presented here is to estimate both tropospheric components as unknowns. By releasing the hydrostatic component to be unknown in the processing rather than being an input value, the estimated tropospheric ZHD will

then have the same ability as the tropospheric ZWD to vary during the day, with the wet component also treated as unknowns.

The tropospheric delay is then represented as:

$$d_{trop} = m(\varepsilon)_h * d_h + m(\varepsilon)_w * d_w \quad (3.43)$$

For estimating this value, the dry mapping function will be used as a partial derivative for the hydrostatic component as is seen below:

$$\frac{\partial d_{trop}}{\partial d_h} = m(\varepsilon)_h \quad (3.44)$$

And the wet mapping function will be used for the wet component as is shown below:

$$\frac{\partial d_{trop}}{\partial d_w} = m(\varepsilon)_w \quad (3.45)$$

Some mapping functions have one value for each component, while others do not produce dual mapping functions. Therefore, it is important to choose a mapping function that can provide two different values to decorrelate the hydrostatic component and the wet component. However, as the difference between the dry mapping function and the wet mapping function can be tiny depending on the used mapping function, it can take a long time to converge to a reasonable value. To overcome this issue, the Extended Kalman filter (EKF) is used with a defined process noise as follows.

3.3.3.4.2 Process noise

The process noise represents how the state of the system changes over time. However, as it is not known when the exact behaviour of the state has to be changed, there is a need to model it as a random process.

Low process noise for a specific state will keep the state significantly unchanged and high process noise will allow the state to change rapidly.

To allow the estimation process to properly reflect the characteristics of the two components of the troposphere, the process noise for the two components has to be chosen carefully. In general, the hydrostatic component is relatively stable and predictable, whereas the wet component is more variable and less predictable, since it depends on the distribution of water vapour in the atmosphere. A higher process noise for the wet component, therefore, allows the value to change rapidly in response to real physical changes.

In the alternative strategy being presented here, since the wet and dry mapping functions, and the partials used to estimate the components, are similar it is not expected that the estimation process will determine separate reliable values for the tropospheric ZHD and Tropospheric ZWD, but it is expected that the sum of these two will reflect the tropospheric ZTD accurately. Therefore, the process noise and the initial values have to be chosen quite carefully in order to provide a balanced and optimal performance from the processing.

To replicate the conventional strategy for dealing with the tropospheric delay, when a model is used for the tropospheric ZHD and the tropospheric ZWD is estimated, the hydrostatic component will be treated as a known value. If the value is being fed and treated as a known value, then no process noise for this will be entered into the process noise matrix and no unknown requirements will be initialized for that, as the unknown requirements (the initial value, the standard deviation of the initial value and the process noise for the state) are initialized only for a state that was declared as unknown for the EKF. In this case, the only partial that has to be put in the design matrix will be the partial derivative with respect to the wet component. In this scenario, the tropospheric ZWD will be the in-charge component for this and the partial derivatives will be the wet mapping function for that specific satellite on that

specific epoch. As a result any errors in the hydrostatic component will then be absorbed by other components (receiver clock offset, ambiguities and the tropospheric ZWD) where the wet mapping function is the only part dealing with the tropospheric delay. With the alternative strategy, it allows the tropospheric ZHD to vary rather than expecting the tropospheric ZWD to absorb any un-mitigated tropospheric ZHD. However, although the resultant tropospheric ZTD will be physically meaningful, the separate tropospheric ZHD and ZWD may not be.

For the conventional strategy, a proper process noise for the wet component still needs to be chosen and many researchers have proposed different values for this process noise, normally based on empirical studies where an acceptable behaviour was obtained from the variation of the tropospheric ZTD when compared to Global Double Difference (GDD).

For the alternative strategy, the tropospheric delay is being split into two components; the hydrostatic and the wet. Thus, what remains for the alternative strategy is to introduce a process noise for the hydrostatic component. Following the literature and considering tropospheric models, it can be agreed that although the hydrostatic component changes, it does not have a dramatic change during the day compared to the wet delay. Therefore, values for the process noises were chosen empirically as 1e-5 m/√sec and 3e-5 m/√sec for the hydrostatic and wet components, respectively. The outcome of this is that, the hydrostatic component is treated more as datum for the tropospheric ZTD and the wet component more as the variations of the tropospheric ZTD. Thus, the tropospheric ZTD should have a good consistency with the tropospheric ZTD from the GDD, but the tropospheric ZWD and the tropospheric ZHD may not.

3.3.4 Site corrections

3.3.4.1 Ocean tide loading displacement

The deformation of the seafloor and coastal land from the redistribution of the ocean water that takes place during the ocean tide is referred to as ocean tide loading. Ocean tides are caused by the Moon and Sun. Many researchers have indicated that the ocean tidal loading effects can be up to several centimetres in magnitude (Penna et al., 2008). According to Kouba (2009) this correction should be taken into account unless the station is far (>1000 km) from the nearest coastline. For this, a FES (Finite Element Solution) tide model, called FES2004, will be used in this research and the particular coefficients for each location will be the ones provided by the Onsala Space Observatory. The type of the vertical and horizontal displacements was chosen, and the format of the file used was the BLQ. Figure 3-2 is an example of the displacement for Aldeburgh (ALDB) station from the Ordnance Survey of Great Britain (OSGB) on DOY 12, 2014.

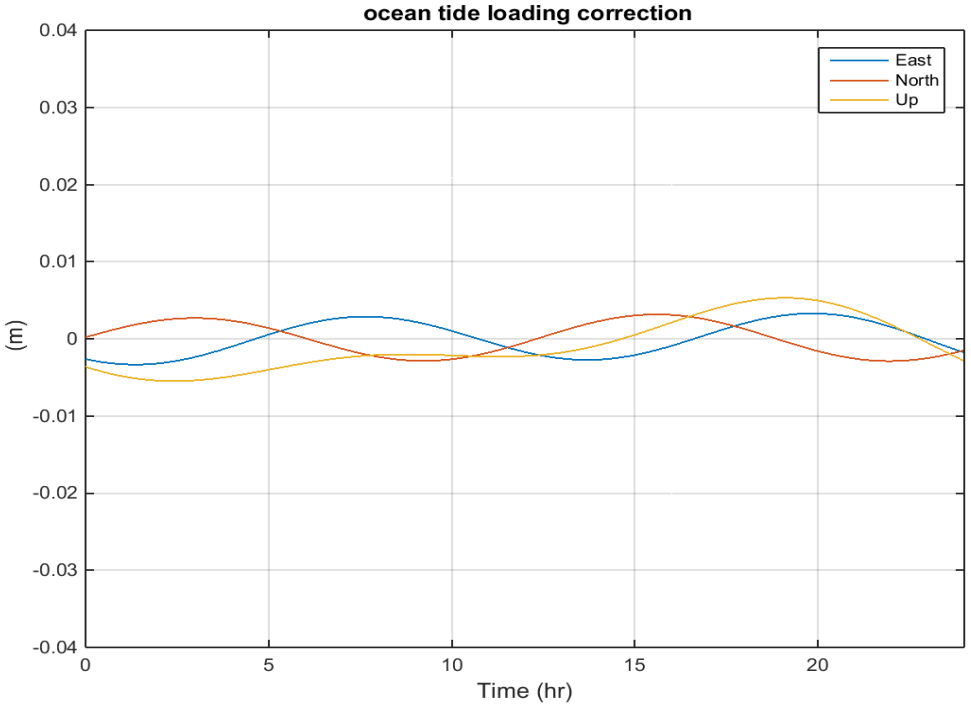


Figure 3-2 Ocean tide loading correction for ALDB station on DOY 12, 2014

3.3.4.2 Solid Earth Tide Correction

Station coordinate variation due to solid Earth tides occur due to gravitational attraction forces produced by external bodies, mainly the Sun and the Moon. These gravitational forces cause a decimetre diurnal level variation in the Earth's crust (Abdel-Salam, 2005). Such solid earth tides produce vertical and horizontal displacements that can be expressed by a harmonic expansion. The suggested solid earth tide correction $\hat{r}$ is as follows (Kouba, 2009):

$$\Delta\vec{r} = \sum_{j=2}^{3} \frac{GM_j\, r^4}{GM\, R_j^3} \left\{ \left[3l_2(\widehat{R}_j.\hat{r})\right]\widehat{R}_j + \left[3\left(\frac{h_2}{2} - l_2\right)\left(\widehat{R}_j.\hat{r}\right)^2 - \frac{h_2}{2}\right]\hat{r} \right\} + \left[-0.025\, m.sin(\emptyset).cos(\emptyset).sin\left(\theta_g + \lambda\right)\right].\hat{r} \quad (3.46)$$

Where GM and GM_j are the gravitational parameter of the Earth, the Moon (j = 2) and the Sun (j = 3); $\hat{r}$ and $\widehat{R}_j$ are the geocentric unit vector of the user location, the Moon (j = 2), and the Sun (j = 3); l_2 and h_2 are the nominal second degree Love and Sheba dimensionless numbers; $\emptyset$, λ and θ_g are the site latitude and longitude, and the Greenwich Mean Sidereal.

In this research, solid earth tides were modelled according to McCarthy and Petit (2004) and Heroux and Kouba (2001), as shown in Figure 3-3 for ALDB station on DOY 12, 2014.

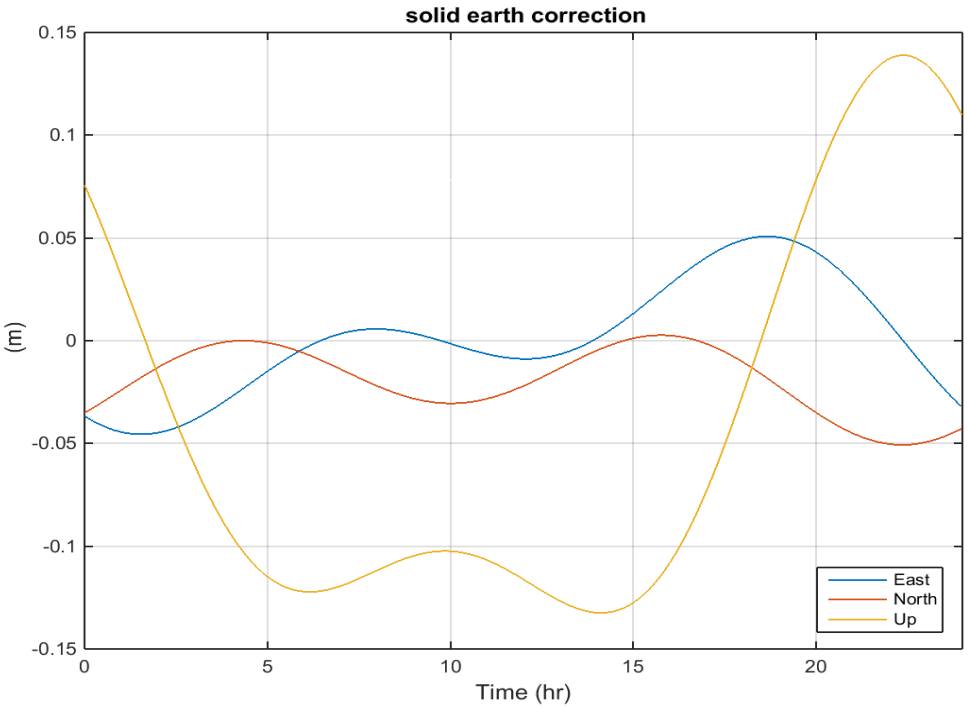


Figure 3-3 Solid Earth tide correction for ALDB station on DOY 12, 2014

3.3.4.3 Earth Orientation Parameters

Earth Orientation Parameters (EOPs) are used to describe the three quantificational movements of the Earth's rotation. The first is the change of the Earth's axis direction relative to the space, the second is the change of the Earth's axis direction relative to the Earth itself and the third is the velocity change of the axial rotation of the Earth (Yibin, 2006). In this research, correction for these parameters was applied using the position file produced by the NAIF (2014), which contains the orientation of the Earth as a function of time for a given interval and EOP files provided by the IERS.

3.3.5 Shapiro delay

As the signal propagation delay is affected by space-time curvature produced by the gravitational field, the geometric range should be corrected according to this effect, and this was applied in this research according to Ashby (2003).

3.3.6 Phase wind-up

This effect is for the carrier phase measurements only. It occurs due to the electromagnetic nature of the circular waves. This correction depends on the relative orientation of the satellite and receiver antenna and the direction of the line of sight (Wu et al., 1993).

3.3.7 Differential Code Biases

Because of using P and C code measurements in the processing, C_1/P_1 and C_2/P_2 differential Code Biases (DCB) need to be corrected. The corrections provided by The Centre for Orbit Determination in European (CODE) downloaded from ftp://ftp.unibe.ch/aiub/CODE/ were applied in this research (Dach et al., 2015).

3.3.8 Antenna Phase Centre

Receiver and satellite antenna phase centre offsets and variations need to be corrected using the Antenna Exchange format (ANTEX) provided by IGS. The ANTEX file that is compatible with the precise ephemeris header was downloaded from the IGS website and used in this research (Schmid et al., 2007).

3.3.9 Polar Tide Correction

The polar tide effect, which is the rotational deformation due to the Earth's mean pole motion needs to be considered for PPP processing. That deformation is due to Sun and Moon attraction causing periodical station position displacement. This correction was applied in this research according to Kouba (2009).

3.4 Weighting functions

In PPP, Some observations will be contaminated with some unmodeled errors, and such errors cannot be removed from the solution because they are not known. Therefore, some method for down-weighting these particular observations can be used to reduce the effect of these unmodeled errors. The observation weighting methods that will be considered in this research are as follows (note: the noise_std is the measurement noise that was chosen for the observable in the EKF).

3.4.1 Elevation weighting

This method depends only on the satellite elevation angle. Where the highest elevation satellites will have the greater weight, and this will be decreased as the satellites go down to the horizon (Black and Eisner, 1984).

$$weight = noise_std * \frac{1.001}{\sqrt{(0.002001 + \sin(elevation)^{2})}} \quad (3.47)$$

3.4.2 Signal to noise ratio

Signal to noise ratio (SNR) refers to the ratio of the signal power to the noise power in a specific bandwidth and can also be used as a weighting function for the observable (Langley, 1997):

$$\sigma L1, L2(m) = \sqrt{\frac{B}{c/n_0}} . \frac{\lambda}{2\pi} \quad (3.48)$$

Where B is the carrier tracking loop bandwidth (Hz), λ is the wavelength of the carrier (m) and c/n_0 is the carrier to noise density expressed as a ratio ($= 10^{\frac{c/n_0}{10}}$ for C/N_0 expressed in dB-Hz). This equation gives a nominal value for the L_1 carrier phase noise of 0.2 mm for a 2 Hz bandwidth loop and a C/N_0 value of 45dB-Hz.

3.4.3 Extended Signal to noise ratio

Wieser and Brunner (2014) presented an extended method for considering signal to noise ratio, based on robust estimation, and a combination of the information inherent in both the signal to noise ratio and the residual of the double-difference phase observation, in order to model random errors and signal distortion effects. This is seen as follows.

For the phase observable:

$$weight\ L_i = 2 * \sqrt{0.244 * 10^{\frac{-SNR}{10}}} \quad (3.49)$$

For the code observable:

$$weight\ P_i = 300 * \sqrt{0.244 * 10^{\frac{-SNR}{10}}} \tag{3.50}$$

3.4.4 Multipath elevation weighting

The multipath effect can degrade the performance of the observable. Therefore, it is also possible to down-weight the observable depending on the expected multipath. Equation (3.51) calculates the expected ionosphere-free code multipath by differencing the ionosphere-free code and ionospheric-free carrier from each other to give a value that can be an approximation for the expected multipath affecting that observable (Estey and Meertens, 1999).

$$\begin{aligned} &calculated\ multipath \\ &= \left(\frac{f_1^2}{f_1^2 - f_2^2} * \mathrm{PR}_1 \ - \frac{f_2^2}{f_1^2 - f_2^2} * \mathrm{PR}_2\right) \\ &- \left(\frac{f_1^2}{f_1^2 - f_2^2} * \emptyset_1 * \lambda_1 \ - \frac{f_2^2}{f_1^2 - f_2^2} * \emptyset_2 * \lambda_2\right. \\ &\left. - \text{ ionospheric free ambiguity} * \lambda_1\right) \end{aligned} \tag{3.51}$$

If the multipath is greater than zero, then this explains the situation that the observables from this satellite are affected. Therefore, this value could be divided as equation (3.52) to be transformed to a weighting value for the observable of a satellite for that specific epoch:

$$tmp\ weight = \sqrt{\frac{calulated\ multipath^2}{\left(\frac{f_1^2}{f_1^2 - f_2^2}\right)^2 + \left(\frac{f_2^2}{f_1^2 - f_2^2}\right)^2}} \tag{3.52}$$

$$weight = tmp\ weight + 0.25 \tag{3.53}$$

However, even though this method can be very useful for down-weighting observations that are expected to be contaminated by multipath, it is also affected by the cycle slips and the ionosphere-free ambiguity, which needs, in the first tracking of the satellites, time to converge to a certain value.

3.4.5 Residual-based weighting

In the adjustment sense, the residuals will contain any unmodeled errors, and they are available for balancing the equation of the 'observed minus computed' vector. In addition, these residuals could contain any imperfection from the models that have been used during the adjustment process. Therefore, these residuals reflect the behaviour of the observables, and thus can be used as a weighting for the observables. This means that the observable that has higher residuals will be given a small weight, while the higher weighting will be given to the observable that has lower residuals, depending on the magnitude of the residuals. In this research, thresholds have been chosen as 5 cm for the carrier and 100 m for the code ionosphere free observable.

3.4.6 Stochastic elevation weighting

This method can be used for weighting the observations, and was presented by Elsobeiey and El-Rabbany (2010). It is relies on empirical factors chosen based on the standard deviation of the observation and satellite elevation angle. They also conclude that the best fit model is an exponentioal decay function and agree with Xiang Jin and de Jong (2009), as follows:

$$C_1, P_1 weight = \left(0.1773 + 0.9232 * e^{-0.0945*(elevation\ angle)}\right) \tag{3.54}$$

$$P_2 weight = \left(0.1983 + 0.722 * e^{-0.1183*(elevation\ angle)}\right) \tag{3.55}$$

$$C_2 weight = \left(0.2188 + 1.4488 * e^{-0.1655*(elevation\ angle)}\right) \quad (3.56)$$

$$L_1, L_2 = noise_std \quad (3.57)$$

3.4.7 Code only elevation weighting

This method was presented by Black and Eisner (1984) for weighting the code observation only.

$$weighted\ code = noise_std * \frac{\left(1 + 0.5 * \left(\frac{1.001}{\sqrt{0.002001 + (\sin(elevation\ angle))^2}}\right)\right)}{1.5} \quad (3.58)$$

$$wighted\ carrier = noise_std \quad (3.59)$$

3.4.8 Rtklib elevation weighting

This method is an empirical method that was developed as part of the RTKLib software and implemented and tested in POINT software (TAKASU, 2014).

$$base_std = 0.003 + \frac{0.003}{\sin(elevation\ angle)} \quad (3.60)$$

$$GPS \text{ code weight} \quad C_1 = P_1 = C_2 = base_std * 100 \quad (3.61)$$

$$GPS \text{ carrier weight} \quad L_i = \frac{base_std}{\lambda_i} \quad (3.62)$$

$$GLONASS \text{ code weight} \quad C_1 = P_1 = C_2 = base\ std * 100 * 20 \quad (3.63)$$

$$GLONASS\ carrier\ weight \quad L_i = \frac{3 * base\ std}{\lambda_i} \quad (3.64)$$

3.5 Multipath

Multipath reflections are one of the important error sources in GNSS because they cannot be removed from the observation by using a model. The multipath reflection depends mainly on the antenna environment as well as the antenna and measurement type. The mp1 and mp2 values that are produced by TEQC are computed as(Estey and Meertens, 1999):

$$mp1 = PR_1 - \left(\left(\frac{f_1^2 + f_2^2}{f_1^2 - f_2^2}\right) * \emptyset_1 * \lambda_1 + \left(\frac{2 * f_2^2}{f_1^2 - f_2^2}\right) * \emptyset_2 * \lambda_2\right) \quad (3.65)$$

$$mp2 = PR_2 - \left(\left(\frac{2 * f_1^2}{f_1^2 - f_2^2}\right) * \emptyset_1 * \lambda_1 + \left(\frac{f_1^2 + f_2^2}{f_1^2 - f_2^2}\right) * \emptyset_2 * \lambda_2\right) \quad (3.66)$$

The mp_1 and mp_2 in equations (3.65) and (3.66) are the values of the RMS moving average values of the multipath combinations of mp1 and mp2 in metres. They compute the moving average for every satellite followed by the RMS for every satellite. Moreover, the extracted final value that is used for quality checking of the mp1 and mp2 is the weighted mean of the computed RMS. The used weight is the number of the observation for every satellite (Estey and Wier, 2014).

3.6 Cycle slips

The detection and correction of the cycle slips are carried out before any parameters estimation. In this research, using the POINT software, this is based on detecting the change in the ionospheric Total Electron Content Rate (TECR) as shown below (Liu, 2011):

$$TECR_{current} = \left(\frac{f_1^2 * \{(\lambda_1 * L_1 - \lambda_2 * L_2) - (\lambda_1 * N_1 - \lambda_2 * N_2)\}}{40.3 * 10^{16} * (gamma_v - 1)}\right) \quad (3.67)$$

$$TECR_{change} = \frac{TEC_{current} - TEC_{prev}}{rinex\ data\ rate} \quad (3.68)$$

And by using Melbourne-Wubbena (MW) ambiguities:

$$b_{WL}^i = \frac{\frac{f_1 L_1^i - f_1 L_2^i}{f_1 - f_2} - \frac{f_1 P_1^i - f_1 P_2^i}{f_1 + f_2}}{\lambda_{WL}} \quad (3.69)$$

Then the change in the MW ambiguity between two epochs (k, k-1) will be

$$[\lambda_1 \Delta N_1(k) - \lambda_2 \Delta N_2(k)] = \quad (3.70)$$

$$\frac{40.3*10^{16}*(gamma_v-1)*rinex\ data\ rate*TECR_{change}}{f_1^2} - [\lambda_1 *$$

$$\{L_1^k - L_1^{k-1}\}] + +[\lambda_1 * \{L_2^k - L_2^{k-1}\}]$$

And this will be equivalent to the MW (Widelane) ambiguities' difference between the current and previous epoch.

$$[\lambda_1 \Delta N_1(k) - \lambda_2 \Delta N_2(k)] = b_{WL}^i(k-1) - b_{WL}^i(k) \tag{3.71}$$

Where:

T is the current epoch; *Δt* is the time difference between the current and previous epoch; *TECR* is the total electron content rate; b_{WL}^i is the float MWWL ambiguity.

If there are no cycle slips, then both TECR and MWWL differences between epochs are small. The MWWL gives reliable results unless the cycle slip has the same magnitude both in L_1 and L_2. *TECR* gives reliable results unless a special cycle slip combination such as (L_1=*77N,* L_2=*60N*) occurred. Therefore, both *TECR* and *MWWL* difference tests are used together to provide better cycle slip detection.

If cycle slips have been detected, then a correction model is used from Banville and Langley (2009). The magnitude of the cycle slip on the L_1 and L_2 measurements is estimated and corrected based on the change of the geometry dependent widelane ambiguity and *TECR* between the current and previous epoch. In this case, the geometry dependent widelane is used for cycle slip correction instead of MWWL because it has a smaller multipath and noise error. Accordingly, the cycle slips are validated by checking the TECR and geometry dependent widelane difference between the current and previous epoch.

3.7 Ambiguity Resolution

For ambiguity resolution in PPP, i.e. accurate fixing of the undifferenced ambiguity to an integer, the fractional cycle biases from the satellite and the receiver

part need to be known. Different methods have been introduced to estimate those biases from a global network for the satellite part while the user takes care of their receiver part. To estimate those biases (the satellite part), the processing software has to be capable of generating precise products (satellite orbit and clocks) as well as the fractional cycle biases from the satellite. Ambiguity resolution has not been attempt in this research because the POINT software (which is the tool used for this research) is not capable of generating these fractional cycle biases, and because the focus is on daily (24 hour) PPP solutions in static mode for which a float solution is considered to be acceptable.

3.8 Chapter Summary

The PPP represents an undifferenced solution, which means there are no cancelled errors or biases, which means there is a need for taking into account and modelling every expected error and bias. This chapter was presented to summarize the models used for PPP processing in this research. Starting from the EKF equations that have been used for the adjustment part, this chapter then discussed the errors, biases and corrections that have to be corrected from the satellites part, for ionospheric biases, and for tropospheric biases. Further, it includes details of the models that have been applied in this research for the site part (Ocean Tide Loading displacement, Solid Earth Tide loading, Earth Orientation Parameters), along with corrections for Shapiro delay, phase wind-up, Differential Code bias, Antenna phase centre, and Polar Tide. This chapter has therefore, presented the tools for obtaining an optimal strategy for the PPP. It has also described the various tropospheric models that will be evaluated as well as giving a description of an alternative strategy for estimating tropospheric ZTD, along with the factors that have to be taken into account for this alternative strategy, which are the process noise evaluation and its effect on the estimated unknown parameters. It also covers the investigated weighting function that will be tested in this research as well as describing the *mp1* and *mp2* values that will be used, and the cycle slip detection and correction methods applied.

Chapter 4. POINT software as it was at the start of this research

Many GPS or GNSS processing software packages are available these days. Some of those could be classified as scientific software e.g. the Bernese GNSS Software developed at the Astronomical Institute of the University of Bern (AIUB), GIPSY-OASIS (GAO) developed by NASA Jet Propulsion Laboratory (JPL), PANDA (Positioning And Navigation Data Analyst) software developed originally by Wuhan University. While some of them are open source software e.g., RTKLIB, gLAB, and there is also other commercial software that is available, e.g. Grafnav. Many of those software packages are capable of producing a PPP solution. However, there is a gradual increase for universities to implement their own software, e.g University Of Nottingham has developed a software package named POINT, for GPS/INS applications. This chapter briefly shows the overall structure of the POINT software, along with details of the research papers that had been published before the start of using the software in this research.

4.1 POINT software

This software was first developed in 2008 as part of the iNsight project (www.insight-gnss.org). It is written in C and C++ programming languages. There are two options for controlling the software by using a command line or a control file. The use of the control file is the option that was followed in this research. It contains different scenarios for processing from PPP to a simple double-difference (DD) scenario (base and rover). Since the DD is not a part of this research, no further investigation will be done for the DD. In addition, some multi-constellations had also ben programmed in this software, namely GPS and GPS+GLONASS, and part of the Galileo constellation is partially implemented. The POINT software was used in this research for processing all PPP scenarios because it will give the ability for editing and modifying the source code in order to evaluate different scenarios for the PPP with

multi-constellations. Figure 4-1 is the general structure for the POINT software and highlights the parts relevant to the PPP.

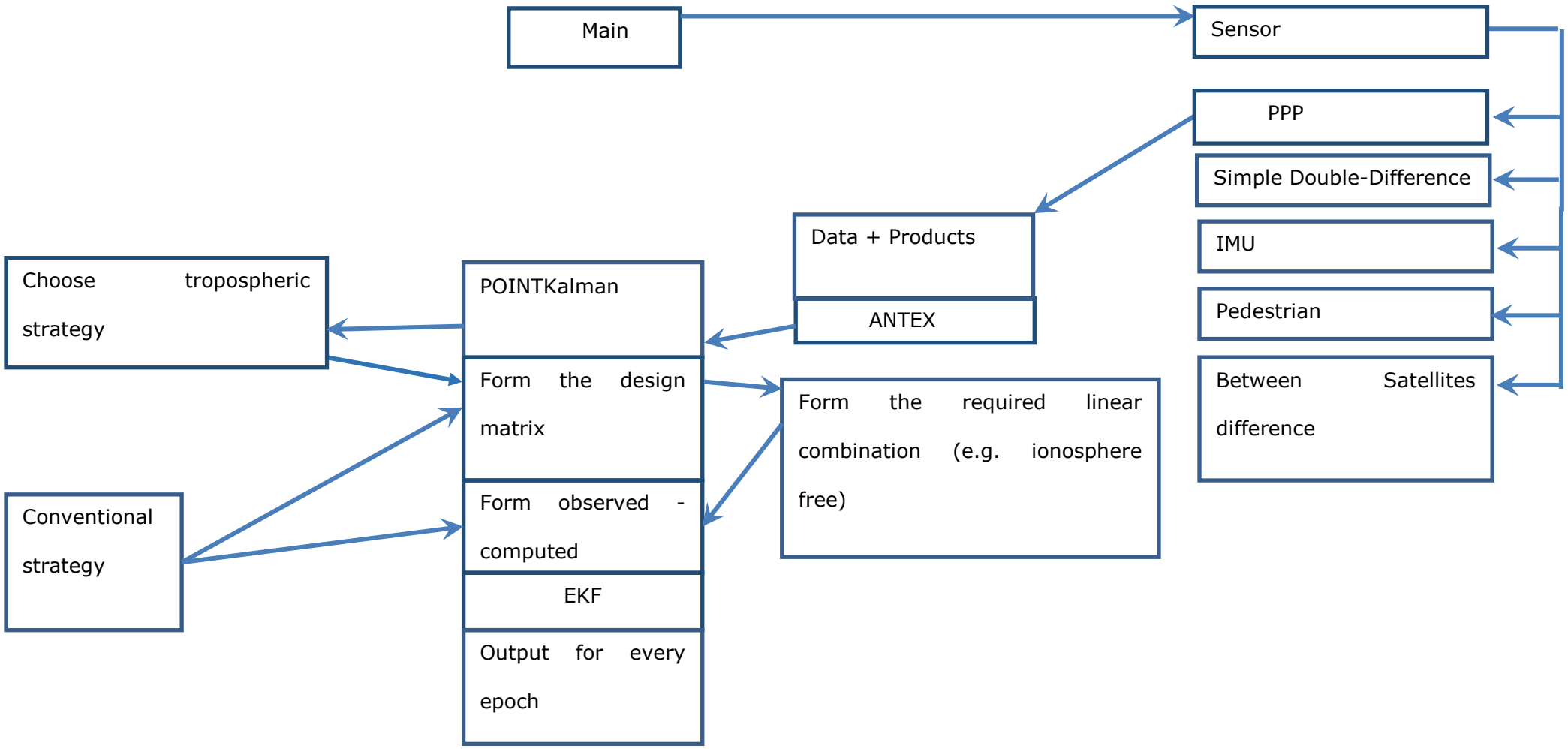


Figure 4-1 POINT software Structure

4.2 POINT software capabilities

At the start of this research, the POINT software was designed to provide different capabilities such as:

- PPP GPS or PPP GPS+GLO processing: This has a direct support for NovAtel and u-blox format files as well as RINEX files.
- Using EKF for data processing.
- It also contained different tropospheric models namely SAASTAMOINEN, EGNOS, GPT and UNB3m as presented in Saastamoinen (1973), RTCA (1996) and_ENREF_82 Leandro et al. (2006), and Boehm et al. (2007), respectively and an option for choosing from them.
- Furthermore, two mapping functions are available. They are NMF (Niell, 1996) and GMF (Boehm et al., 2006a). Although the POINT software allows NWF or GMF to be used with each of the models presented, some mapping functions are matched to a model (i.e GMF is matched to GPT) and, therefore, should not be used with other models.
- Another important part, which is an ionosphere-free combination, was also programmed, depending on the dual-frequency receiver.
- Method for cycle slips detection and correction.
- IMU integration with GPS.
- Differential pseudorange and phase processing: (single or dual frequency) using simple double-difference with one station as a base and one station as a rover.
- Options for the Least-square AMBiguity Decorrlation Adjustment (LAMBDA) (Teunissen et al., 1995).
- Extended Kalman filter smoothing for the GPS forward and reverse filter combined, using a smoothing algorithm for improving performance using post-processing.

4.3 Papers published using POINT software

From the initial start of the Innovative Navigation using new GNSS SIGnals with Hybridised Technologies (INSIGHT) project, research papers that have used the POINT software in their processing so far are listed as follows:

- Feng et al. (2008) used the POINT software to propose a new carrier phase–based integrity monitoring algorithm for high precision using Kalman filter. This was done using a short baseline Double-Difference (DD). Ochieng et al. (2008) used the POINT software to propose a new carrier phase–based integrity monitoring algorithm for high precision using the Kalman filter. This was done using a short baseline DD.
- Jokinen et al. (2012a) used the POINT software for analysing the impact of using University of Nottingham's Numerical Weather Modelling (NWM) based tropospheric corrections on float and fixed ambiguity Precise Point Positioning (PPP).
- Jokinen et al. (2012b) used the POINT software for fixing the ambiguity for PPP using the CNES products. They also used it to monitor the integrity of PPP by implementing and testing the Imperial College Carrier-phase Receiver Autonomous Integrity Monitoring (ICRAIM).
- Jokinen et al. (2013a) used the POINT software for presenting the state-of-the-art PPP method using the GPS and GLONASS measurements to estimate the float position solution before attempting to resolve the GPS integer ambiguities. They also used the ICRAIM method for detecting and excluding GPS base-satellite failures.
- Yang et al. (2013) used the POINT software for testing and evaluating the NWM method and its effect on the convergence time and the positioning accuracy for the PPP.

After investigating and exploring the POINT software, a test for real data was done at the start of this research with the PPP as shown in the next section.

4.4 Test results using POINT software

Although the POINT software had been used for some publications with good results, a test was done using the POINT software to see the level of accuracy of station coordinates. Ten stations from the Ordnance Survey of Great Britain (OSGB) on DOY 231, 2013 were used for this test. The test was conducted using the PPP GPS and PPP GPS+GLO with the available and default options of the POINT software. The test results are summarized for the 3D error compared to a Global Double Difference (GDD) reference solution from British Isles continuous GNSS Facility (BIGF) in Table 4-1.

Table 4-1 GPS Test station coordinates results using PPP GPS and PPP GPS+GLO with default settings in POINT

Point	3D(m) GPS	3D(m) GPS+GLO
CLAW	0.031	0.079
HOOB	0.034	0.019
KEYW	0.062	0.012
LEED	0.069	0.035
LEEK	0.036	0.048
LICF	0.054	0.019
LINO	0.055	0.071
PETE	0.055	0.012
SWAN	0.042	0.037
WELL	0.033	0.037

The test results presented in Table 4-1 were produced using the default settings and configuration without any modification of the current software. The author has since done numerous implementations and modifications as part of this research. One important aspect of this was the automation of the POINT software via MATLAB (see Appendix-A). Further details of the author's adoption and development of the POINT software are presented in Chapter 6.

4.5 Chapter summary

The POINT software is available at the Nottingham Geospatial Institute (NGI). This chapter presented a general description of the software. In addition, it presented the capabilities of the software. Moreover, the published research papers that have used POINT in their processing are also presented.

In addition to the description part of the POINT software, a test was performed using 10 stations from the OSGB. The test was done with PPP GPS and PPP GPS+GLO using the default settings of the software and without any modification from the author.

All PPP results in this research presented in Chapter 6, 7 and 8 were processed using the POINT software following the author's improvements and modifications, as well some as bug fixing.

Chapter 5. An Initial Comparison of Precise Point Positioning Results from GPS and GLONASS

To consider the quality of any PPP solution, there is a need for a truth value that is independent of but comparable with the PPP solution. In this chapter, a Global Double-Difference (GDD) solution will be presented as the reference value for the evaluation. In addition, one week of analysed data are presented for checking the effect of precise products on the PPP and GDD solutions. The effect of applying a second-order ionospheric delay will also be presented as well as the effect of using different weighting methods on the accuracy and the convergence time. This chapter also presents a new approach for the geometry analysis.

It is also important to analyse the factors that are considered to be a quality indication. Thus, the observable performance, the receiver type effect, the geometry effect and the achievable convergence time for a specific level of difference from the '*truth*' value will be presented and analysed in this chapter using 7 weeks worth of dataset.

5.1 Global Double Difference (GDD) Solutions Methodology

All of the global Double Difference (GDD) solutions presented in this research are GPS daily solution that were processed using the Bernese GNSS Software (version 5.2) (Dach et al., 2015). These daily solutions were created by the NERC British Isles continuous GNSS Facility (BIGF) from a re-processing and re-analysis of daily data from 1997 to 2014. The processing strategy for the GDD GPS daily solutions is summarized in Table 5-1 below.

Table 5-1 The processing parameters for the Global Double-Difference solution

Software	The Bernese GNSS Software version 5.2 (Dach et al., 2015)
Precise Products (satellite coordinates and satellite clock offsets)	C13 (CODE repro2/repro_2013) re-analyzed satellite orbit and earth orientation parameter products
Satellite and receiver antenna phase center offsets and variations	I08.ATX models for antenna phase center variations
Troposphere	a-priori modeling of troposphere effects using VMF1G and estimation using zenith path delay and gradient parameters
Ionosphere	mitigation of the first- and higher-order (second- and third-order and ray bending) ionospheric effects
Solid earth tides, Ocean tidal loading, and Atmospheric tidal loading	Applied
Carrier phase ambiguities	Fixed ambiguity

A total of approximately 150 continuous GNSS stations (CGNSS) in the British Isles, including 100+ that are part of the Ordnance Survey of Great Britain (OSGB) national network, were included in the processing along with some 200+ IGS stations, as illustrated in Figure 5-1.

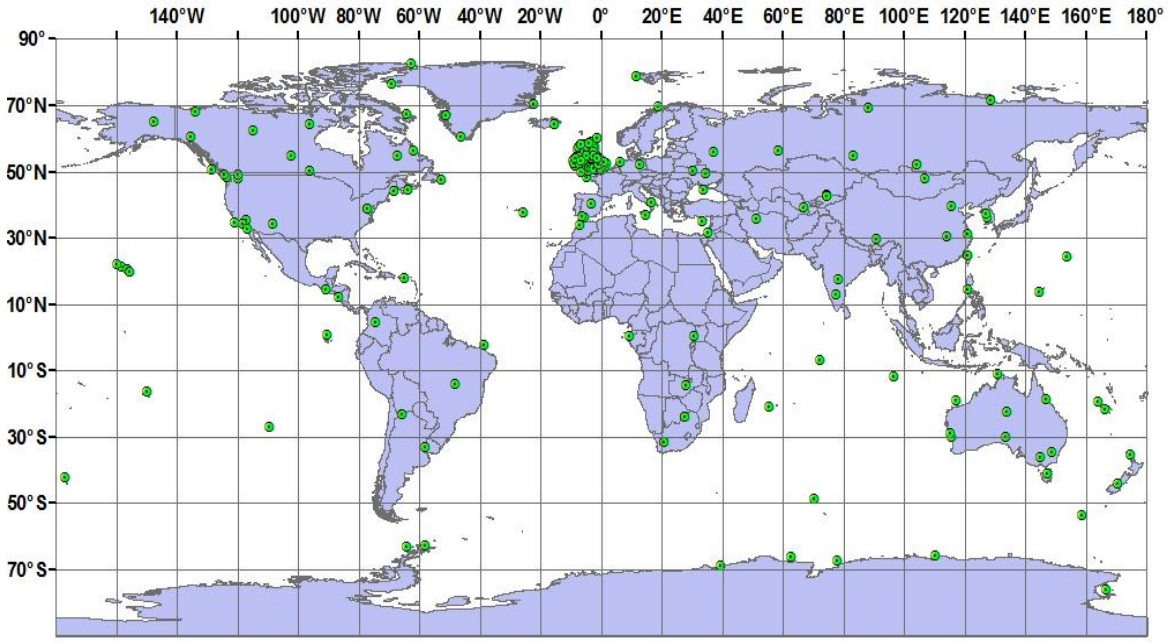


Figure 5-1 The network used for the GDD solution on DOY 12, 2014

5.2 Precise Products' effect on GDD and PPP

The PPP is highly dependent on the precise products (satellite coordinates and clock) that are used. Different products from various organizations are available. In this chapter, two products have been tested; those from Natural Resources Canada (EMX) and CODE products from the Centre of Orbit Determination in Europe (CODE) where there final precise products are used as input, for satellite coordinates and satellite clock corrections. This test is for checking the effect of different strategies (PPP, GDD) using the same precise products. EMX precise products were chosen due to their availability of GLO as well as GPS while CODE precise products were chosen as these were used for the GDD solution from BIGF (2014). This is because one part of the processing strategy for the GDD is to use the precise products, and they are CODE products that are compatible with the Bernese GNSS Software (version 5.2). A test was done for 56 OSGB CGNSS stations shown in Figure 5-2 for seven individual days from DOY 12-18, 2014 using CODE and EMX prercise products (SP3, CLK) for the PPP GPS scenario. Then the estimated station coordinates from the PPP were compared

with those from GDD. The dX, dY and dZ were converted to dE, dN and dU using the formula of Vincenty (2013) and the results are summarized in Table 5-2

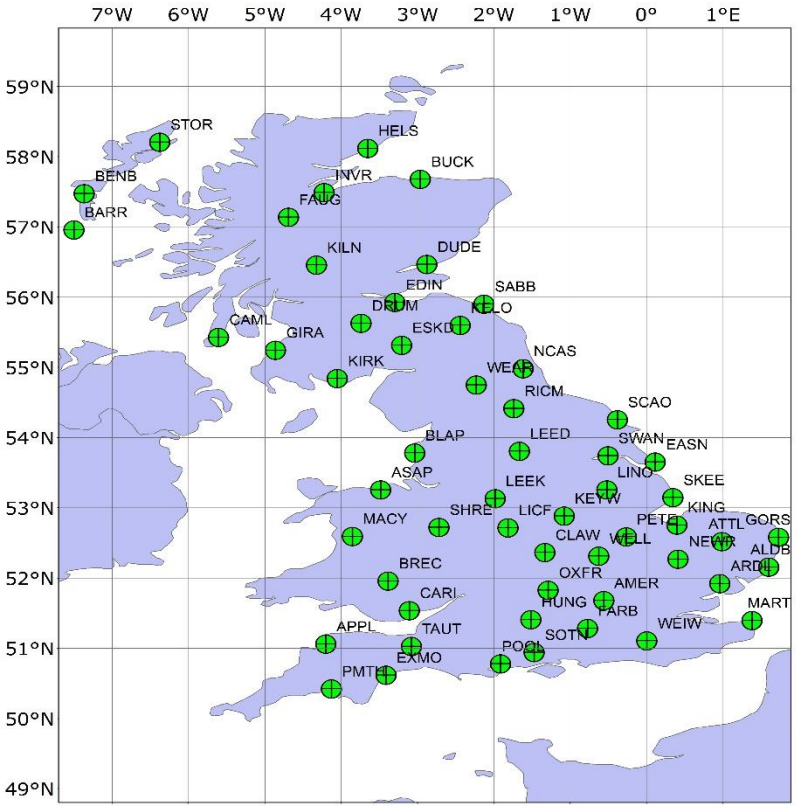


Figure 5-2 The 56 OSGB stations included in BIGF that were used

Table 5-2 Precise products' effect on the station coordinates from the PPP GPS solutions for the 56 OSGB stations

Component	Average (mm)	STD (mm)	RMS (mm)	Products
dE	-1.48	3.80	4.07	EMX
	-0.90	3.04	3.17	CODE
dN	2.13	1.89	2.85	EMX
	0.43	1.91	1.96	CODE
dU	3.57	5.98	6.96	EMX
	10.35	6.76	12.36	CODE
3D	7.55	4.02	8.55	EMX
	11.43	6.00	12.91	CODE

It can be seen from Table 5-2 that the PPP GPS results using CODE precise products are slightly more consistent in the East and North coordinate components than when using the EMX products, regarding the average difference and the RMS of the differences. The Up component, however, is better in the case of using EMX precise products rather than using CODE and as a result the 3D mean and the 3D RMS is also better in the case of using EMX precise products. Thus, EMX precise products were in further initial tests and investigations that were conducted. Another reason for using the EMX products is their availability of GLO, while the CODE organization then only treated GLO clocks as "*experimental and were used only internally*", and the fact that they are available for 5 min intervals (Ochsenbein, 2015). There are two other precise products that are used for producing the IGS final precise products for the GPS and GLO and they are from the European Space Agency (ESA) and German Research Centre for Geosciences (GFZ). All of these precise products (EMX, ESA and GFZ) will be investigated significantly in Chapter 6.

5.3 Second Order Ionospheric Delay

The effect of the second-order ionospheric delay on the station coordinates was also tested. It was conducted for the same 56 OSGB stations and the same duration but using the second-order ionosphere correction method proposed by Hernandez-Pajares et al. (2007). The results are summarized based on the RMS daily variation of the station coordinates as seen in Figure 5-3, with and without using the second-order ionospheric correction.

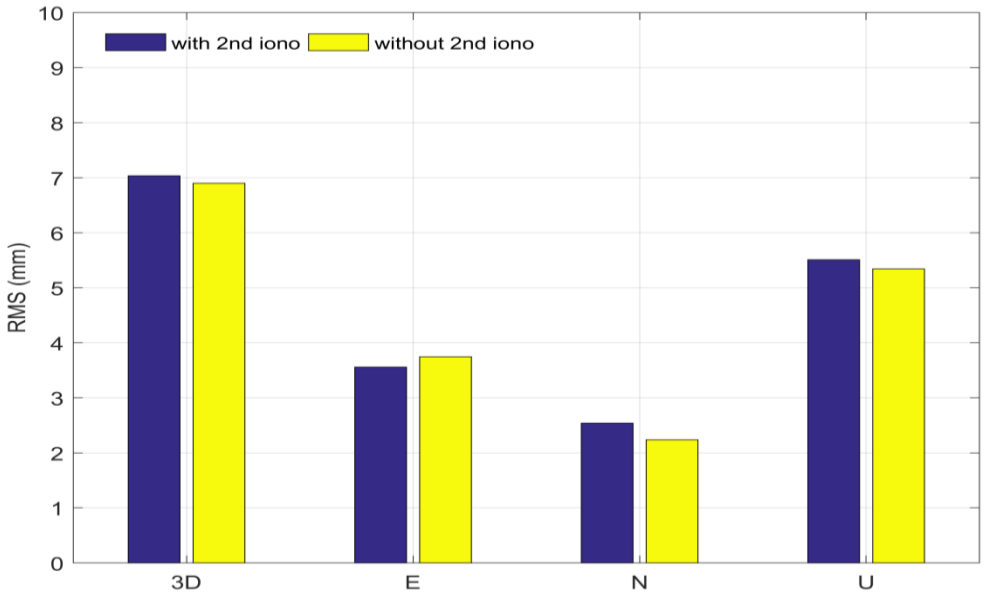


Figure 5-3 The RMS for 7 days in GPS week 1775 (DOY 12-18, 2014) for 56 OSGB stations, with and without 2nd order ionospheric correction

Athough the curent understanding is that corrections for higher order ionospheric delay have to be implemented for the highest precision and accuracy of result, for instance, Kedar et al. (2003), Fritsche et al. (2005), Steigenberger et al. (2006) and Hernandez-Pajares et al. (2007) (as introduced in section 3.3.2), this test could be considered as a limited test as it may be that this one-week of data was when the solar activity was minimal. This level of activity can be reflected in the planetary indices (Kp) values which are one of the most common indices used to indicate the severity of global magnetic disturbances. Kp values are derived from ground-based magnetic field measurements and range from 0-9. According to Wing et al. (2005), a typical 'quiet' day will have Kp values less than 3, while Kp values between 3 and 5 correspond to a moderately disturbed field, and Kp values of 6 or greater occur during a major magnetic storm. Whereas, according to the National Oceanic and Atmospheric Administration (NOAA) scales, Kp values of less than 5 are considered as 'Minor' (G 1 on the scale), while Kp values of 6 are considered as 'Moderate' (G 2 on the scale), Kp values of 7 are considered as 'Strong' (G 3 on the scale), Kp values of 8 are considered as 'Severe' (G 4 on the scale), and Kp values of

9 are considered as 'Extreme' (G 5 on the scale). Figure 5-4 summarises the Kp values for the period from 12 to 18 of January 2014, provided on a three-hour basis by NOAA and downloaded from ftp://ftp.ngdc.noaa.gov/STP/GEOMAGNETIC_DATA/INDICES/KP_AP/2014.

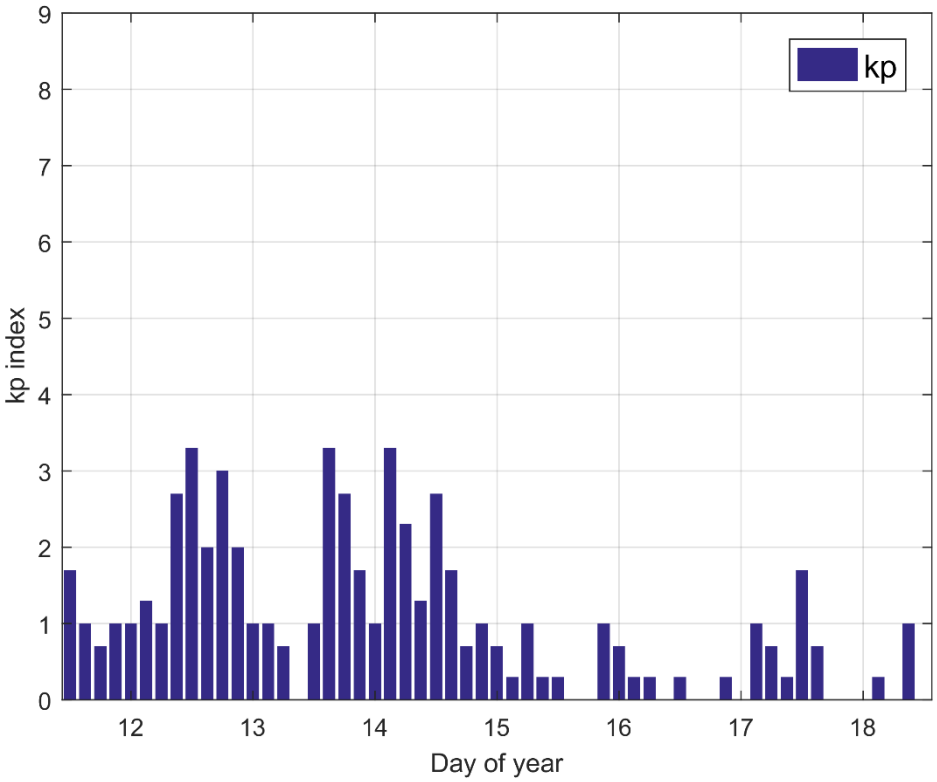


Figure 5-4 Kp values for 7 days in GPS week 1775 (DOY 12-18, 2014)

Considering Figure 5-4, it is clear that this one-week of data was actually when the solar activity was minimal, as the values of Kp are all below 5, and mostly below 2. Thus, considering the analysis and the Kp values, no clear decision could be made for the PPP processing about adopting the correction for the second-order ionospheric delay because the difference between applying this correction and not applying it are within parts of a millimetre, an accuracy which is beyond the scope of this research. Thus, all future results will be presented without applying the second-order ionospheric correction.

5.4 GNSS Geometry analysis

5.4.1 The Cumulative Dilution Of Precision

One of the important factors for evaluating and assessing the quality of a GNSS constellation is the chosen geometry for that constellation, as the GPS and GLO constellations are different in their number of satellites in orbit and the inclination of the orbits as well as the separated angles between the satellites in the same orbit. The dilution of precision DOP can be used to evaluate a GNSS constellation and is usually computed for every epoch as the trace of the first, second and third elements of the diagonal matrix from the normal matrix. Figure 5-5 shows the HDOP, VDOP and PDOP for two OSGB stations (ALDB and AMER) for 24 hours of DOY 12, 2014 extracted for three scenarios of PPP GPS, PPP GLO and PPP GPS+GLO solutions.

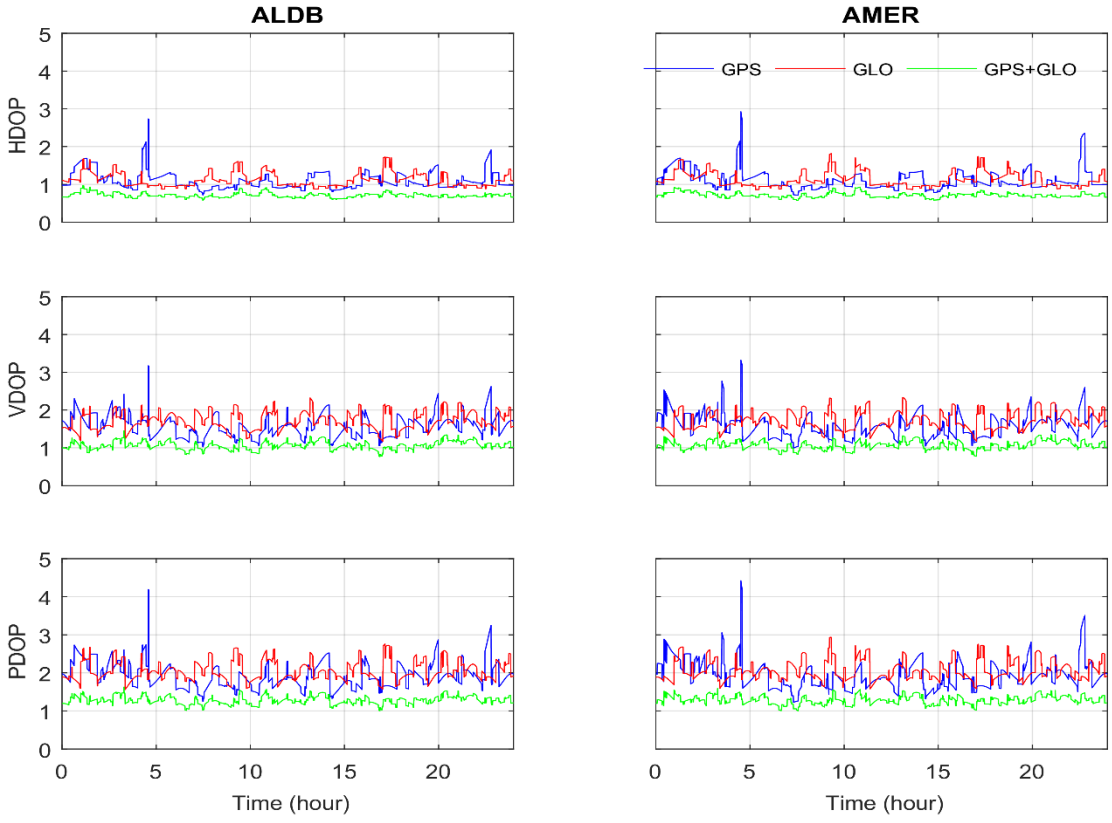


Figure 5-5 Dilution of Precision for ALDB (left) and AMER (right) over 24 hours, DOY 12, 2014 for three PPP solutions

Clearly, this strategy of computing the DOP does not reflect the total actual geometry for the constellation because the computed DOP for every epoch will be affected by the availability of the precise products. If the precise products are not available for a certain epoch, the resultant value of the DOP will be high because of the reduced number of the satellites and hence, worse geometry. It is also evident that any excluded satellites, because of residual checking or any other excluding strategy, will decrease the number of satellites, and this will be reflected in the computed DOP.

Therefore, instead of using the conventional DOP, a new approach is proposed here to compute the cumulative DOP from the normal matrix over the period of the test, using equations (5.1), (5.2) and (5.3).

$$N^{-1} = (\sum A^t A)^{-1} \tag{5.1}$$

$$\begin{bmatrix} \delta X^2 & \cdots & \\ \vdots & \ddots & \vdots \\ & \cdots & \delta t^2 \end{bmatrix} \tag{5.2}$$

$$\text{3D geometry} = \sqrt{\delta X^2 + \delta Y^2 + \delta Z^2} \tag{5.3}$$

This approach will be less sensitive to the unavailability of the precise products or satellites for certain epochs because it will be the summation of the DOP over the period of the observations (24 hours in this research, which mean 2,880 epochs for 30 sec data rate) from the normal matrix.

However, as the POINT software's core is the Extended Kalman Filter (EKF), the matrix $(A^t A)$ cannot be inverted because it has many zeros. Therefore, a least square implementation for the pseudorange observations was developed by the author inside the POINT software to formulate the normal matrix for every single epoch and to output them just for the geometry analysis. This was done by using another script (written by the author) in MATLAB software to overcome the failure of inverting the normal matrix. In addition, it was done to ensure that the geometry analysis will not

affect the obtained solution from the EKF, and also that the analysis itself will be independent of the solution.

Applying this approach produces one value for each station for the whole period of observation (i.e. 24 hours). Table 5-3 summarizes the mean value of the cumulative DOP for 57 OSGB stations from DOY 12-18, 2014 for different PPP scenarios (GPS, GLO and GPS +GLO).

Table 5-3 The Cumulative DOP statistics for 57 OSGB stations from DOY 12-18, 2014

Constellation	GPS	GLO	GPS+GLO
AVERAGE	0.0303	0.0323	0.0221
STDEV	0.0004	0.0003	0.0002
MAX	0.0327	0.0344	0.0236
MIN	0.0299	0.0320	0.0219
RANGE	0.0027	0.0024	0.0018

It is evident from Table 5-3 that the cumulative DOP for the GPS is better than the GLO because of the higher number of the satellites. This is also apparent when looking at the GPS+GLO solution where it is better than both of the individual constellations. This supports the theory that increasing the number of satellites will improve the geometry. In this case, the improvement will be because the user will obtain a greater number of observations from the satellites that have different inclination angles. In addition, the observations will come from satellites that have been distributed differently in their orbit plane and are moving differently from one constellation to another.

5.4.2 Correlation between the station latitude and the cumulative DOP

From the cumulative analysis, it was found that there is a correlation between the cumulative DOP, as computed in Section 5.4.1, and the latitude of the station. This correlation could not be computed or investigated using the conventional DOP

from the single epoch. It is important, however, to take a further step in investigating this cumulative DOP over a different region and explore how this can be affected by the changing of the latitude. Figure 5-6 shows the correlation between the computed cumulative DOP and the latitude of the 56 OS GB stations in Cartesian form.

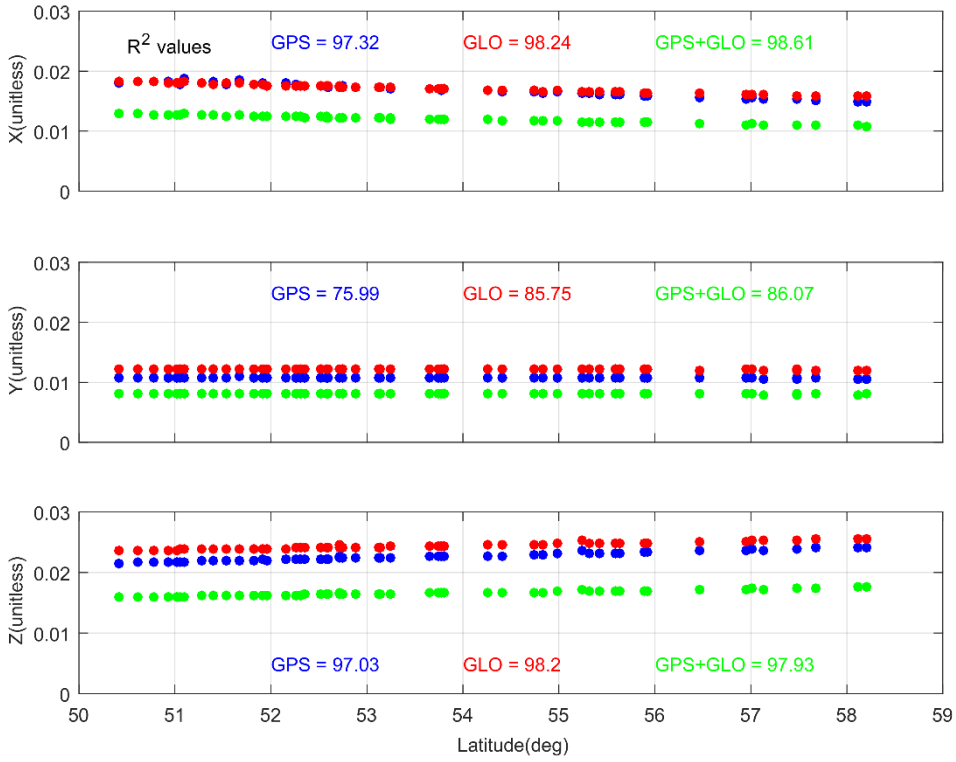


Figure 5-6 The Cumulative DOP for PPP (GPS, GLO and GPS+GLO) solutions versus latitude

For the chosen region, it can be seen that the GPS+GLO scenario will be better in all coordinate components and this is due to increasing number of the satellites. For the GPS and GLO scenarios, it can be concluded that both constellations have a similar performance for the X Cartesian component because the movement of both constellations are relatively perpendicular to the X direction. Moreover, this will be slightly improved when the latitude is increased. In the Y direction, it is evident from the figure that GPS has a better cumulative DOP than GLO. While For the Z direction, all the scenarios will be degraded with increasing latitude, due to the degradation of

the satellite's availability towards the north as well as the decrease in the strength shape of the distributed satellites.

5.5 The effect of observation weighting on the accuracy and the convergence time

Many authors have used different methods for weighting the observations, as described in Section 3.4. The use of a weighting function was proposed to eliminate or reduce the influence of specific unmitigated errors and biases in the measurements. Therefore, it is important to evaluate those methods depending on real observations to obtain a better performance from the PPP solutions. For that reason, the same datasets from Section 5.2 were used for assessing different observation-weighting methods. They were processed using PPP GPS with a similar configuration for every session, except for the changing of the specified weighting method. The results are summarized in Figure 5-7, based on the 3-D error and the 5-cm 3-D convergence time.

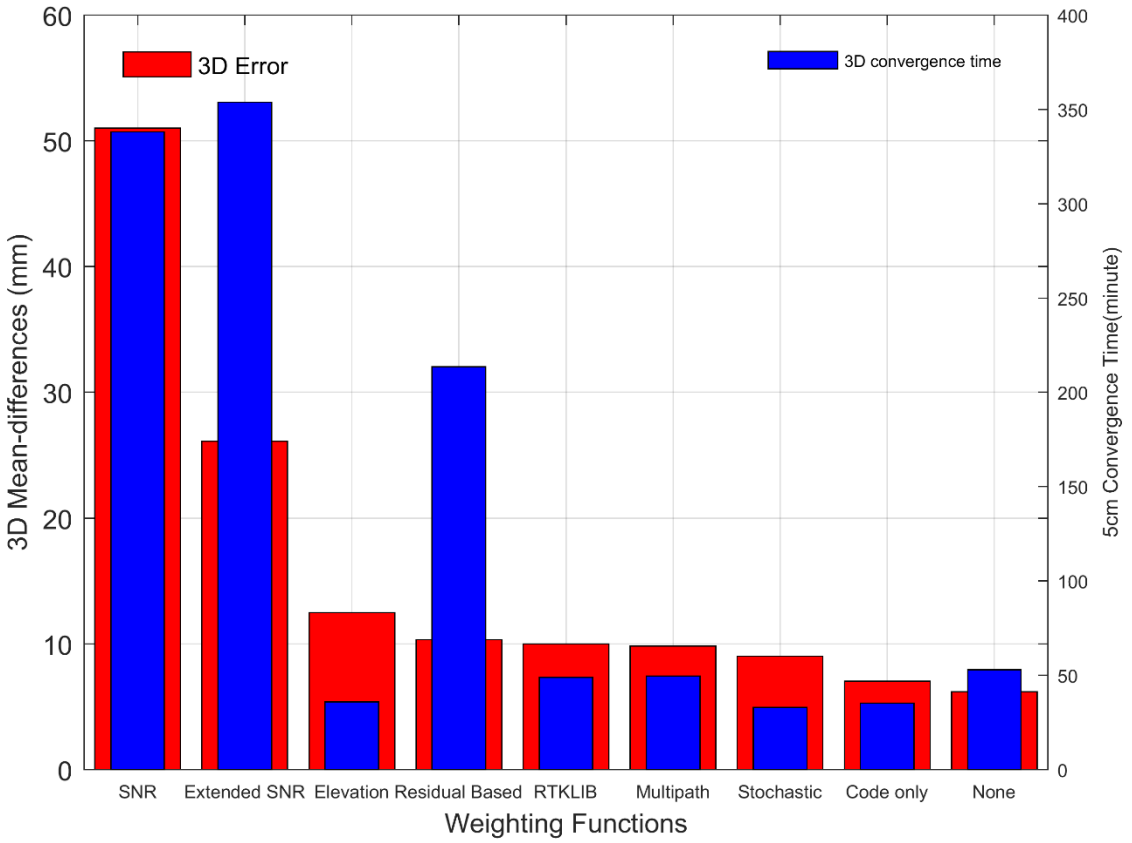


Figure 5-7 The mean of the 3D error and the 5 cm 3-D convergence time for 56 OSGB stations using eight weighting methods

Figure 5-7 represents the average convergence time for the 3D error to go below 5 cm, and the average of the final 3D error when compared to the GDD solution for the chosen dataset. It can be seen that the SNR, extended SNR, and residual based methods are worst, while the other five methods behaved much better. Of these five methods, the elevation stochastic and code only methods have a good performance in terms of the 3D error (12.5, 9.0 and 7.5 mm respectively), and also have the lowest convergence times of 35.8, 33 and 35.3 min respectively, which suggests that those methods are the most appropriate weighting methods to be used for the PPP processing.

However, in a test conducted without applying any weight, the 3D error was even better at 6.2 mm, while the convergence was worse at 52.9 min. Hence, without using weight was adopted in this research for three reasons:

Firstly, it is the method that gave the best 3D error. Secondly, the used dataset is based on stations located in good environments, which minimize effects such as multipath. Thirdly, it was considered better to see the performance of the constellations without down-weighting any observations.

5.6 Choosing an expanded dataset

The data set was then expanded in time, to cover different days, and in space in order to further investigate the variation of the PPP solutions on different days and in different areas. The chosen stations were based on a condition that they should have continued operation for the specific GPS weeks selected, and another condition was the availability of the GDD solution.

All the 85 OSGB stations selected, with their approximate coordinates, are listed in Appendix-B. The reason for choosing the OSGB stations was the homogeneity of these stations where the majority of these stations had the same receiver type (LEICA GRX1200+GNSS) that can provide GPS+GLONASS observations with the same firmware 8.2 and the same antenna (LEIR25 LEIT), except the 14 stations listed in Table 5-4.

Table 5-4 The 14 OSGB Stations that are different from the majority of the 85 OSGB stations selected

Point	Receiver type	Receiver firmware	Antenna type
STRA	TRIMBLE NETR9	4.62	TRM55971.00 NONE
SHOE	TRIMBLE NETR5	4.15	TRM55971.00 NONE
TEDD	LEICA GRX1200+GNSS	8.2	LEIAT504GG NONE
APPL	LEICA GRX1200+GNSS	7.81	LEIAR25 LEIT
LCAR	LEICA GRX1200+GNSS	7.81	LEIAR25 LEIT
LINO	LEICA GRX1200+GNSS	7.81	LEIAR25 LEIT
MART	LEICA GRX1200+GNSS	7.81	LEIAR25 LEIT

OXFR	LEICA GRX1200+GNSS	7.81	LEIAR25 LEIT
PRAE	LEICA GRX1200+GNSS	7.81	LEIAR25 LEIT
SCIL	LEICA GRX1200+GNSS	7.81	LEIAR25 LEIT
SKEE	LEICA GRX1200+GNSS	7.81	LEIAR25 LEIT
SOTN	LEICA GRX1200+GNSS	7.81	LEIAR25 LEIT
WELL	LEICA GRX1200+GNSS	7.81	LEIAR25 LEIT
BARR	LEICA GRX1200+GNSS	8.2	LEIAR25 NONE

The GPS week and the number of the stations that were available for that week are summarised in Table 5-5 with their locations spread over the UK in Figure 5-8.

Table 5-5 GPS week, doy range and number of the 85 OSGB stations selected that were available during that week

GPS week	doy range	No. of Stations
1775	12 - 18	56
1776	19 - 25	85
1777	26 - 32	79
1778	33 - 39	74
1783	68 - 74	74
1784	75 - 81	76
1785	82 - 88	79

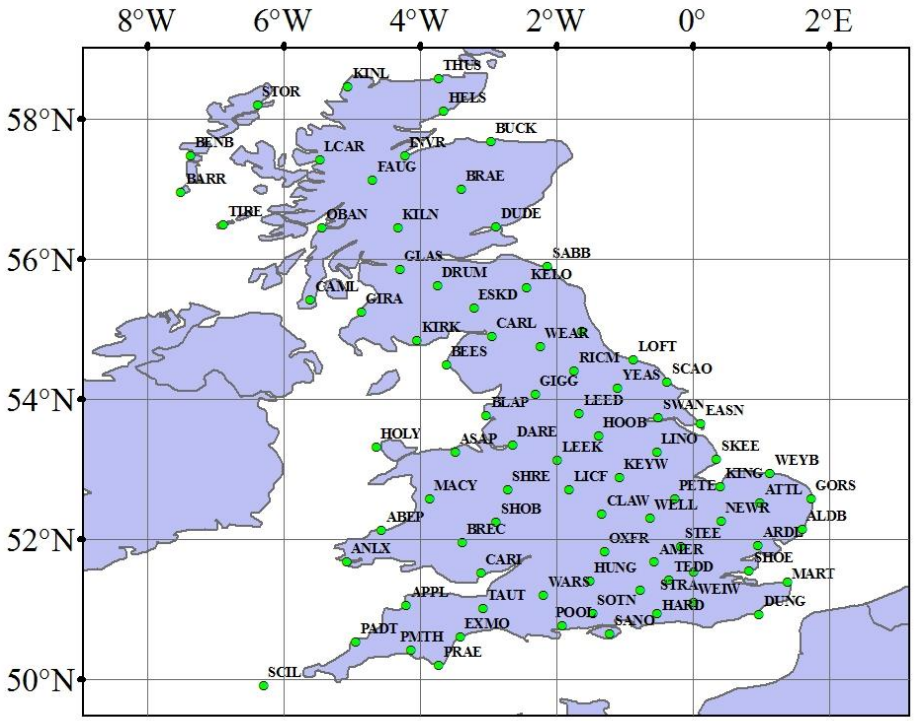


Figure 5-8 The 85 OSGB stations chosen for the expanded 7 weeks dataset

The results are analysed and presented in the following sections, in terms of observable performance as well as convergence. The full analysis of the station coordinate accuracy and precision will be conducted in Chapter 6.

5.7 Observables Performance

As a part of the investigation of the multi-constellation PPP, it is important to investigate the performance of the observables from the GPS and GLO constellation. To achieve this, the ionosphere-free, code and phase residuals were analysed. The RMS of the observables residuals was computed for each station from the dataset in Section 5.6 and then the average and other statistics were calculated and summarized in Table 5-6.

Table 5-6 Statistics of the observations residuals for the expanded 7-week dataset

Constellation	Code (m)		Phase (cycle)	
	GPS	GLO	GPS	GLO
AVERAGE	1.162	1.301	0.038	0.043

STDEV	0.158	0.267	0.006	0.009
MAX	1.863	2.313	0.135	0.276
MIN	0.890	0.726	0.026	0.029
RANGE	0.973	1.587	0.109	0.248

It can be seen from Table 5-6 that the GPS code is slightly better than the GLO code. However, the phase was found to be almost the same for the GPS and GLO, which could suggests means that if there is any degradation in the results, it mainly comes from the code observable in the GLO case.

However, this conclusion is coming from the overall statistics and does not reflect the actual performance of each station with a specific constellation. Therefore, it is important to see if this RMS is stable for all stations, or, if there are specific stations that have a particular behaviour for a specific constellation, depending on the equipment type and the surrounding environment. For investigating that, the observables were analysed separately for GLO and GPS.

5.7.1 GLO observables

For investigating the behaviour of each station on each day, the RMS of the observation residuals have been drawn for each station and each day on a horizontal axis (see Figure 5-9). This means that the horizontal axis of the drawing below represents 49 days, and every day contains the RMS that was computed for each station processed during that day.

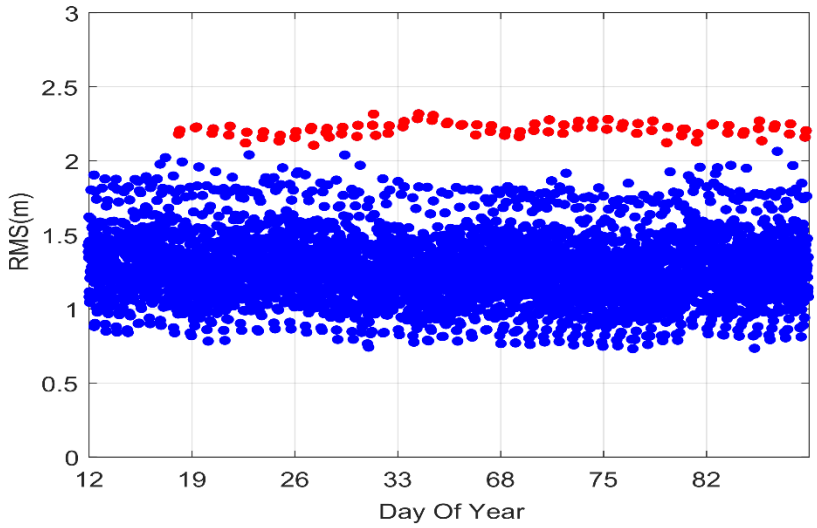


Figure 5-9 RMS of the GLO code observation residuals for each station on all days

It is evident from Figure 5-9 that there are three stations (marked as red, while the remaining stations are marked as blue) that have a continually higher RMS for the GLO code. These three stations are STRA, SHOE and ABEP. The first and second stations (STRA and SHOE) have a Trimble receiver type that is different from the majority of the other stations, which have a Leica receiver type, and could give an indication of the performance of the receiver type with the GLO observable.

Additionally, the first and second stations (STRA and SHOE) have the same antenna type (TRM55971.00) that is different from other stations, which have antenna type, and which gave a better performance for the GLO code.

The difference in the RMS between the two stations (STRA and SHOE) was ~ 4 cm, which suggests that both stations are quite similar with the small difference in the RMS possibly due to receiver firmware as it was noticed that on all days, the RMS was found to be higher in STRA (which had a 4.62 firmware) than SHOE (which had a 4.15 firmware).

The third station that had a higher RMS is ABEP. This has the same receiver type, receiver firmware and antenna type as the majority of the other stations, which

minimizes the possibility that the degradation is due to the used equipment, and suggests that the reason could be site multipath. Therefore, mp1 and mp2 values were computed as explained in Section 3.5. Figure 5-10 contains the mp1 and mp2 values for the stations (STRA, SHOE and ABEP) that have a higher RMS as well as the remaining five stations that were the next highest in terms of RMS.

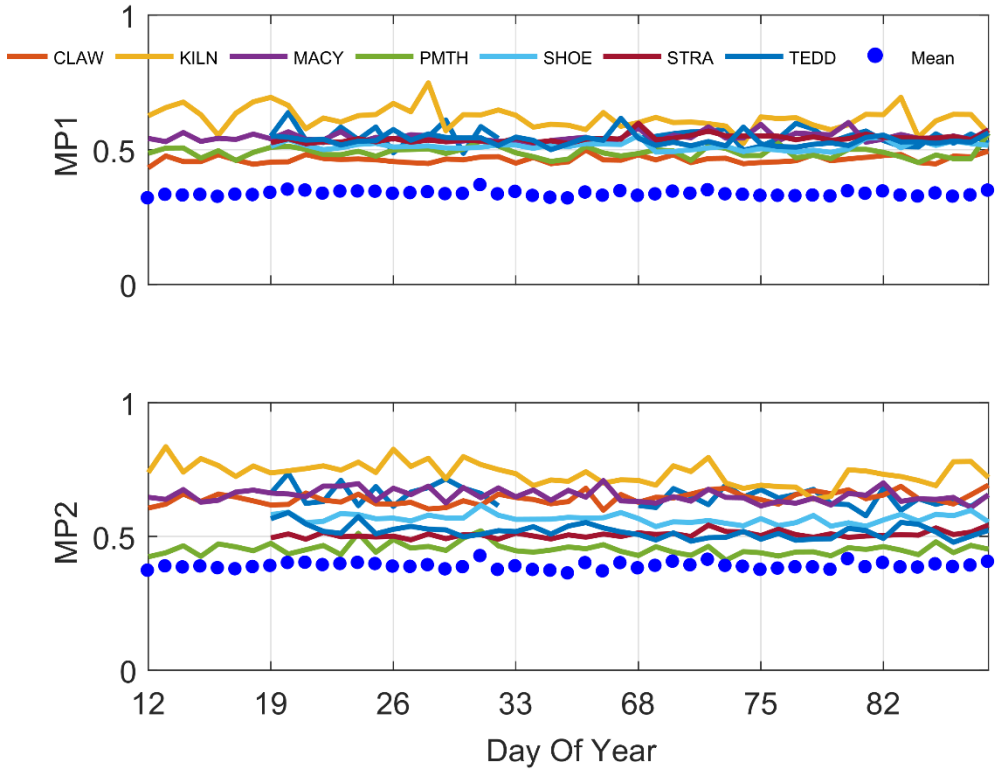


Figure 5-10 GLO mp1 and mp2 values for the stations that have higher RMS of observation residuals

In Figure 5-10, the mp1 and mp2 values of the eight stations with higher RMS were compared to the mean mp1 and mp2 values for all stations. From Figure 5-10, it can be seen that the mp1 value is generally lower than the mp2 value, which gives an indication that the GLO code on L_1 is less noisy than the GLO code on L_2. A comparison with the mean also confirms that all eight stations are above the mean and can be flagged as potential high multipath sites.

5.7.2 GPS observables

For the GPS ionosphere-free code observable, five stations were counted to have continually higher RMS for the GPS code observable (see Figure 5-11).

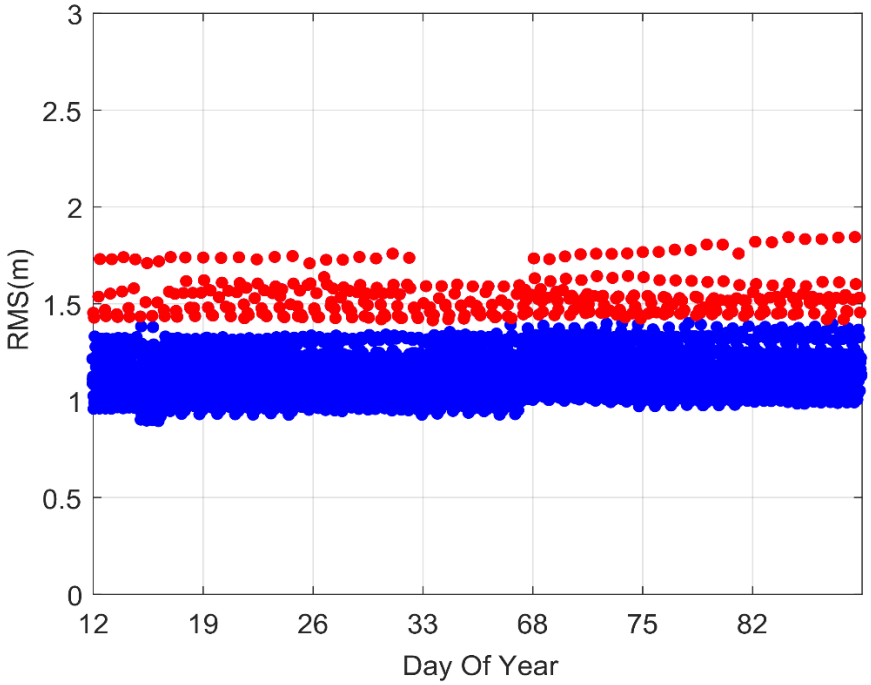


Figure 5-11 RMS of the GPS code observation residuals for each station on all days

Those five stations (marked as red, while the remaining stations are marked as blue) were ABEP, KILN, MACY, STRA and TEDD stations. What is noticeable is that the station STRA that had a Trimble receiver has a high continuous RMS for the GPS code observable as well as the GLO observable. Conversely station SHOE is not observed to have a high RMS for the GPS code observable, even when it has the same receiver type.

The mp1 and mp2 values have also been computed for each station, along with the mean for all stations, similar to the GLO case, and the eight stations with the highest RMS are shown in Figure 5-12, where it is clear that they also have mp1 and mp2 values that are above the mean and can be flagged as potential high multipath sites. A comparison of Figure 5-10 and 5-11 shows that six stations are present for

both GLO and GPS (ABEP, VLAW, KILN, MACY, STRA and TEDD) with two on GLO only (PMTH and SHOE) and two on GPS only (OBAN and TEDD).

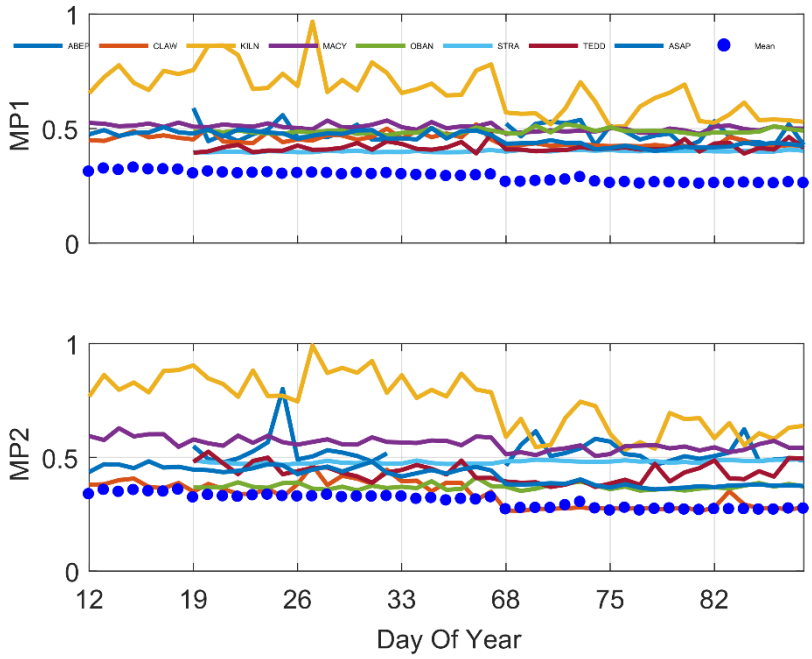


Figure 5-12 GPS mp1 and mp2 values for the stations that have higher RMS of observations residuals

In addition to the above individual stations and how their daily mp1 and mp2 changed, comparison of Figure 5-9 and 5-11 show that the mp1 and mp2 are also different for the GLO and GPS constellations. To illustrate this, Figure 5-13 shows the mean mp1 and mp2 values for all stations on each day for the GLO and GPS constellations.

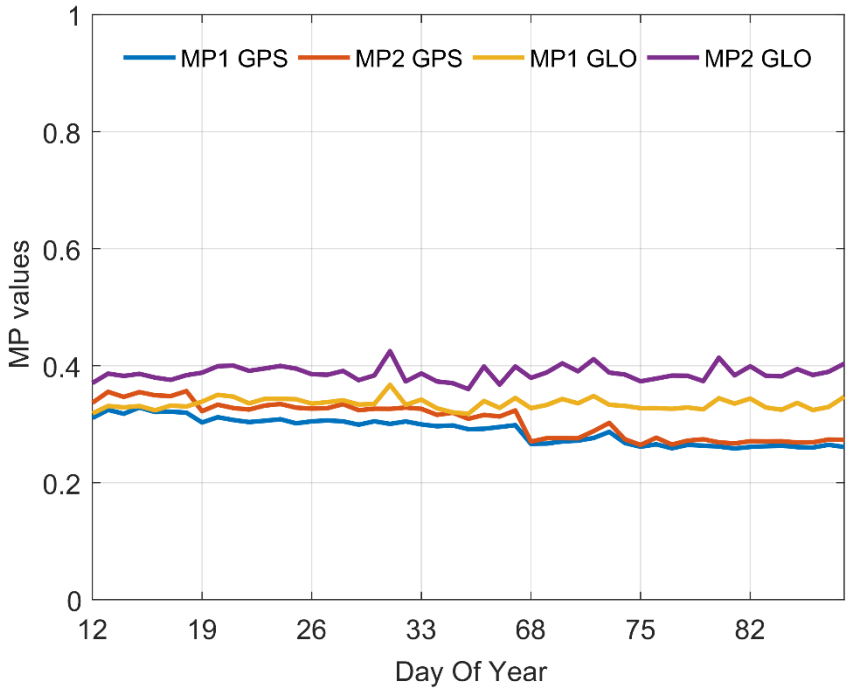


Figure 5-13 The daily mean of mp1 and mp2 values for GPS and GLO

It can be seen that GLO mp2 has the highest values for all days while the best value for all days is the GPS mp1 value. The code on L_1 is clearly a less sensitive observable for both constellations, and the GPS C/A code on L_1 less susceptible to multipath, while the GLO code on L_2 is most susceptible to multipath.

It can also be seen from Figures 5-12 and 5-13 that there is a decrease in the mean mp1 and mp2 values for GPS between the first four weeks (doys 12 to 39) and the last three weeks (doys 68 to 88) of the chosen dataset. To check if the reason for that is station-specific or constellation-specific, Figure 5-14 represents the mp1 and mp2 values for each station on each day.

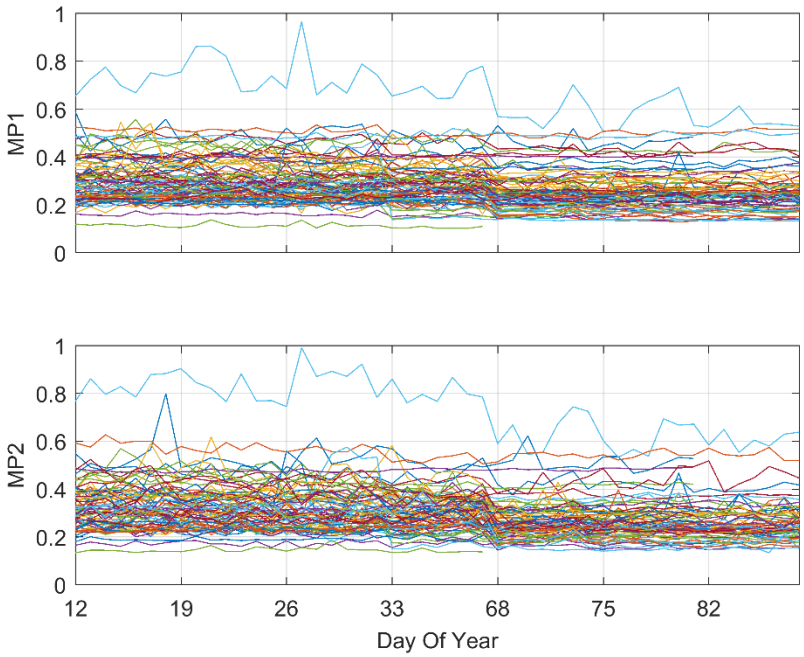


Figure 5-14 GPS mp1 and mp2 values for each station on each day

It can be seen from Figure 5-14 that the decrease in the mp1 and mp2 values for GPS appears to be present at the majority of stations, which suggests that it is a constellation-specific effect rather than a station-specific effect. This improvement in mp1 and mp2 values can be attributed to the fact that there was a de-activation of satellite PRN06 (SVN 036) in the period between the first four weeks (doys 12 to 39) and the last three weeks (doys 68 to 88) of the chosen dataset as, according to ftp://ftp.unibe.ch/aiub/BSWUSER52/GEN/SATELLIT.I01_out_of_service, this satellite, which was launched on 16/01/1994, was de-activated on 04/03/2014 (doy 63).

5.8 Convergence time analysis

The convergence time for the PPP is another important aspect when evaluating the performance of a PPP solution. It is the time required for convergence to a required level of accuracy. The convergence time was examined based on three categories of 20, 10 and 5 cm required level of accuracy. It was assessed based on the individual coordinate components as well as in 3D. The results are summarized in Figure 5-15 for the data set from Section 5.6.

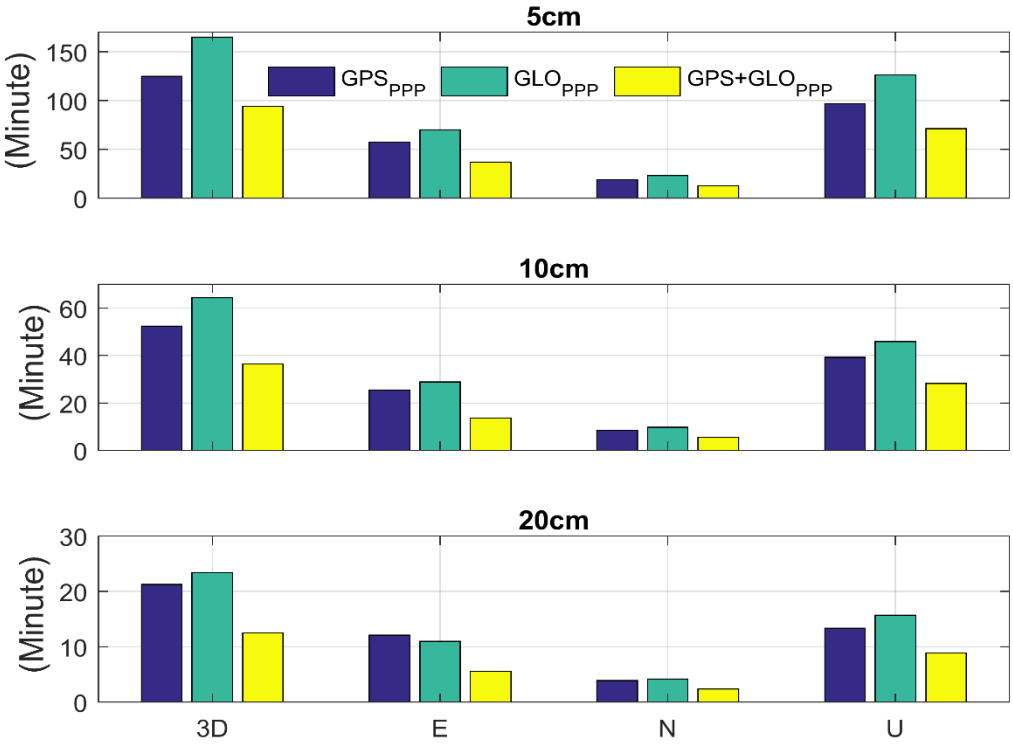


Figure 5-15 Convergence time comparison for PPP GPS, PPP GLO and PPP GPS+GLO scenarios

It can be seen from Figure 5-15 that PPP GPS+GLO provides the best convergence time for all coordinate components and all categories, while PPP GLO is slightly worse than PPP GPS. This significant improvement is coming from the increasing number of the satellites, which will increase the number of observation equations during a single epoch. Therefore, those observations will strengthen the normal matrix with relatively the same unknowns. Additionally, this was reflected in the improved geometry as explained in Section 5.4.

However, this improvement in the convergence time has a relation also with the observable weight as was shown in Section 5.5, as the weight for the observations may cause the EKF to converge quickly but to a solution far from the truth-value.

Considering the differences in the convergence time between the PPP GPS and PPP GLO, it can be seen that the 3D convergence time in all cases (20, 10 and 5 cm) is better for PPP GPS rather than PPP GLO. This difference in the 3D convergence time

of the PPP GLO mainly came from the Up component, and could be because the GLO orbit inclination angle is more than the GPS orbit inclination angle, which means that the Up component is more correlated with the tropospheric zenith total delay (ZTD) that is estimated when using PPP. The North component convergence time strongly agreed in both PPP GPS and PPP GLO, and it is less than the East component in all cases.

Overall, PPP GPS+GLO improved the 3D convergence time by 41.3%, 30.5% and 24.5% for 20,10 and 5 cm respectively. While PPP GPS is found to be better than PPP GLO by 10.2%, 22.8% and 30.1% for 20,10 and 5 cm respectively.

5.9 Chapter Summary

This chapter presented an alternative approach for evaluating the constellation geometry. This alternative is based on the cumulative DOP rather than the simple DOP, and it was found that the cumulative DOP varies as a function of the station latitude, but this approach will not be affected by any missing data during a day and can be used for evaluation of the geometry of the future satellites constellation.

The effect of weighting functions on the convergence time and station coordinate accuracy was also investigated based on two factors; convergence time to achieve 5 cm accuracy and the 3D error. It was found that, without using the weight function gave the best performance, and it was concluded that it is better to follow this approach for evaluating the observables as well as the constellations.

This chapter then went on to analyse observable performance at 85 OSGB stations for an extended 7-week data set. It was found that only a few stations exhibited abnormal behaviour in terms of the RMS of their observation residuals and that most of these also exhibited high mp1 and mp2 values, suggesting potential high multipath sites.

A convergence time analysis has also been presented which was found to be different for the constellation type and different between the coordinate components. The convergence time was found to be slightly better for PPP GPS than for PPP GLO, but that PPP GPS+GLO was the best overall.

Chapter 6. PPP single and multi-constellation station coordinate accuracy and precision analysis with precise products' assessment

Part of this chapter has been published as:

MOHAMMED, J., MOORE, T., HILL, C., BINGLEY, R. M. & HANSEN, D. N. 2016. An assessment of static precise point positioning using GPS only, GLONASS only, and GPS plus GLONASS. Measurement, 88, 121-130.

Different GNSS constellations are available these days. This has led to an increase in the number of satellites available for the user, and the potential for improvements in the accuracy and precision of daily solutions for static positioning, which are significant factors when evaluating the use of multi-constellations as one constellation or as a combination. At the same time, the Precise Point Positioning (PPP) technique has also been developed to provide daily solutions. Following the restoration of the GLONASS (GLO) constellation to a similar level as the GPS constellation, much research has been carried out on the PPP using the GPS only (PPP GPS) and the PPP when using the GPS plus GLONASS (PPP GPS+GLO), i.e. using GLONASS as an aid to the GPS.

This chapter will investigate the achievable accuracy and precision from PPP daily solutions when using the PPP GPS, PPP GLO and PPP GPS+GLO for static positioning following an optimum strategy. As part of the assessment, comparisons with Global Double-Difference (GDD) GPS daily solutions are presented. It is important here to mention that the results are presented in a progressive manner, with progressively expanded data sets used in initial tests and then for the final test.

In addition, this chapter also assess the effect of different precise products' (satellite orbits (SP3) and clock (CLK)) for PPP scenarios.

6.1 Conventional PPP strategy and configuration

The conventional PPP strategy from other research papers has been to apply a strategy consistent with applied for creating the precise products used, as well as considering weighting methods, which will affect the results.

In general, in the POINT software, the standard deviation of GPS code measurements was set to 100 times the GPS phase measurements. While, for GLO phase measurements the standard deviation was set at three times the GPS carrier-phase measurements, and for GLO code measurements the standard deviation was set at 20 times the GPS code measurements. The reasons given for significantly downweighting GLO code-phase measurements against GPS code-phase measurements in (Jokinen et al., 2013c) is that there were no separate code and carrier-phase satellite clock corrections for GLONASS and there can be inter-channel code-biases in GLONASS code-phase measurements. The result being that the standard deviations were set to: 0.02m for GPS phase measurements; 2.00m for GPS code measurements; 0.06m for GLO phase measurements; and 40.00m for GLO code measurements.

6.2 The Author's PPP strategy and configuration (including modification to POINT software)

One of the primary contributions of this research was the implementations that were done by the author for the POINT software. In addition, a significant amount of other implementation work and bug fixes was completed as a part of the research which had led to the creation of an optimal strategy to achieve the high accuracy PPP results in this research.

Since January 2014, the author has based his research study on the POINT software and significantly improved it. These improvements mainly include:

- Splitting the PPP GLO constellation to work independently from the PPP GPS, starting from input reading and processing through to the output solutions files.
- Implementation of cycle slip detection and correction for the PPP GLO constellation and correcting the previous implementation for cycle slip detection and correction.
- Implementation the decoupled clock for the PPP GLO.
- Different bugs have been resolved that were related to the observed minus computed implementation.
- Correcting the implementation of the CNES bias correction inside the POINT software.
- RINEX modification in the case of excluding some satellites or constellations which leave spaces in the RINEX file, and the software stop.
- Implementation of the least square normal matrix for the geometry analysis and outputting the normal matrix for computing the cumulative DOP.
- Separating the receiver clock offsets estimation to be from the Extended Kalman filter (EKF) rather than using it from the least squares implementation.
- Implementation of corrections for atmospheric tidal loading with the capability of interpolating the available atmospheric tide loading to produce an interpolated value instead of using a model.

Note that algorithm design and program development are an important contribution of this research. Furthermore, testing single and multi-constellation PPPs, it is important to use similar configurations as well as similar precise products.

Another significant difference between the author's PPP strategy and those used previously in the POINT software is that there was no downweighting of the GLONASS

code-phase measurements against GPS code-phase measurements. Instead, the standard deviation of both GPS and GLONASS code measurements was set to 200 times the respective GPS and GLONASS phase measurements. While, for GLO phase measurements the standard deviation was set to the same as the GPS carrier-phase measurements, and for GLO code measurements the standard deviation was set to the same as the GPS code measurements. The result being that the standard deviations were set to: 0.01m for GPS phase measurements, not the previously used 0.02m; 2.00m for GPS code measurements, as was previously used; 0.01m for GLO phase measurements, not the previously used 0.06m; and 2.00m for GLO code measurements, not the previously used 40.00m. The reason for this was to better evaluate the actual performance of both constellations for station coordinate estimates.

The configuration that was used is as shown in Table 6-1:

Table 6-1 Configuration to be used for PPP processing

Setting	Comment
Ambiguities	Float for GPS and GLO
Cycle slips	Applied, Section 3.6
Ionospheric bias	Ionosphere free combination; (for GLO it will be applied for each satellite based on the specified frequency extracted from the broadcast ephemerides). Section 3.3.2
Tropospheric bias	Using the Saastamoinen model for the hydrostatic delay and estimating the wet delay as an unknown. Section 3.3.3.1.1
Mapping functions	Niell mapping functions: dry for the hydrostatic delay and wet for the wet delay.
Tropospheric gradient	Tropospheric gradient E, N estimated. Section 3.3.3.3
Tropospheric gradient model	Chen model
Ocean tide loading	Applied according to Section 3.3.4.1

Setting	Comment
Solid earth tide	Applied according to Section 3.3.4.2
Pole Tide Loading	Applied according to Section 3.3.9
Shapiro Delay	Applied according to Section 3.3.5
Phase wind up	Applied according to Section 3.3.6
DCB	Applied according to Section 3.3.7
Weighting	No weighting functions had been used after the assessment of all available weighting functions (Section 5.5), and this applied for both GPS and GLONASS, meaning that equal weight for both constellations.
Second order ionosphere	No 2nd order ionospheric correction had been used after the assessment of the available method (5.3).
Precise Products	EMX for the initial validation, and EMX, ESA GFZ for the extended experiment.
Receiver clock offset	Two clocks were estimated, code receiver clock offset and carrier receiver clock offset, for both constellations.
Antenna Phase centre correction	Applied using the ANTEX08 file from IGS depending on the GPS week, to be compatible with the products.
Earth Rotation Parameters	Applied according to using IERS, Section 3.3.4.3

Bear in mind that although there are two mapping functions inside the POINT software, namely NMF (Niell, 1996) and GMF (Boehm et al., 2006a), and the software allows using either NMF or GMF mapping functions, GMF are matched and can only be used with GPT model. For that reason NMF and not GMF was used as the mapping function in this research.

It is important for the EKF to set the state statistics the processing. After investigation, the author suggests the following state properties to be followed for the PPP in static mode.

Table 6-2 Extended Kalman Filter configuration to be used for PPP processing

State	Initial value	Initial standard deviation	Process noise standard deviation
X	Based on a least squares solution	1000 m	0.000001 $\frac{m}{\sqrt{s}}$ the X component
Y	Based on a least squares solution	1000 m	0.000001 $\frac{m}{\sqrt{s}}$ the Y component
Z	Based on least squares solution	1000 m	0.000001 $\frac{m}{\sqrt{s}}$ the Z component
Receiver clock error	Based on EKF	1000 m	100 $\frac{m}{\sqrt{s}}$
Tropospheric wet delay	0.1	0.1 m	$3*10^{-5}$ $\frac{m}{\sqrt{s}}$
Troposphere gradient G_N	0	0.001 m	$3.1667 * 10^{-6}$ $\frac{m}{\sqrt{s}}$
Troposphere gradient G_E	0	0.001 m	$3.1667 * 10^{-6}$ $\frac{m}{\sqrt{s}}$
Carrier phase ambiguities	Based on the estimated range	1000 cycles	0

6.3 Initial Experiments

For testing the stability of the PPP solutions, as well as the stability of the precise products and software used, an investigation was carried out by choosing two stations that have continuous records. This was done because sometimes there were missing data when the updating process of the receiver firmware, or faults, caused that data to be missing. This was achieved by looking at the RINEX files from the OSGB stations, and if the station had 24 hours of records, it is considered as a continuous station for that day, bearing in mind that missing data for less than one hour is not considered as a condition. Two OSGB stations were found to be continuous for one year (2014), i.e. Amersham (AMER) and Aldeburgh (ALDB) with 350 and 354 days, respectively.

PPP solutions were created for these two stations for each day following the strategy presented in Table 6-1 and Table 6-2. Firstly, the precision was analysed by comparing the daily PPP GPS station coordinates to the mean for the year. In addition to the PPP GPS, PPP GLO and PPP GPS+GLO were also tested for the same two stations, over the same period, and by comparing to their mean for the year.

The Global Double-Difference (GDD) GPS solutions, from section 5.1, for the same period were also compared to its mean for the year. Figure 6-1 and Figure 6-2 summarize the differences between the daily solution and the one-year mean solution (dE, dN, dU) for each scenario (PPP GPS, PPP GLO, PPP GPS+GLO and GDD GPS) for ALDB and AMER stations, respectively.

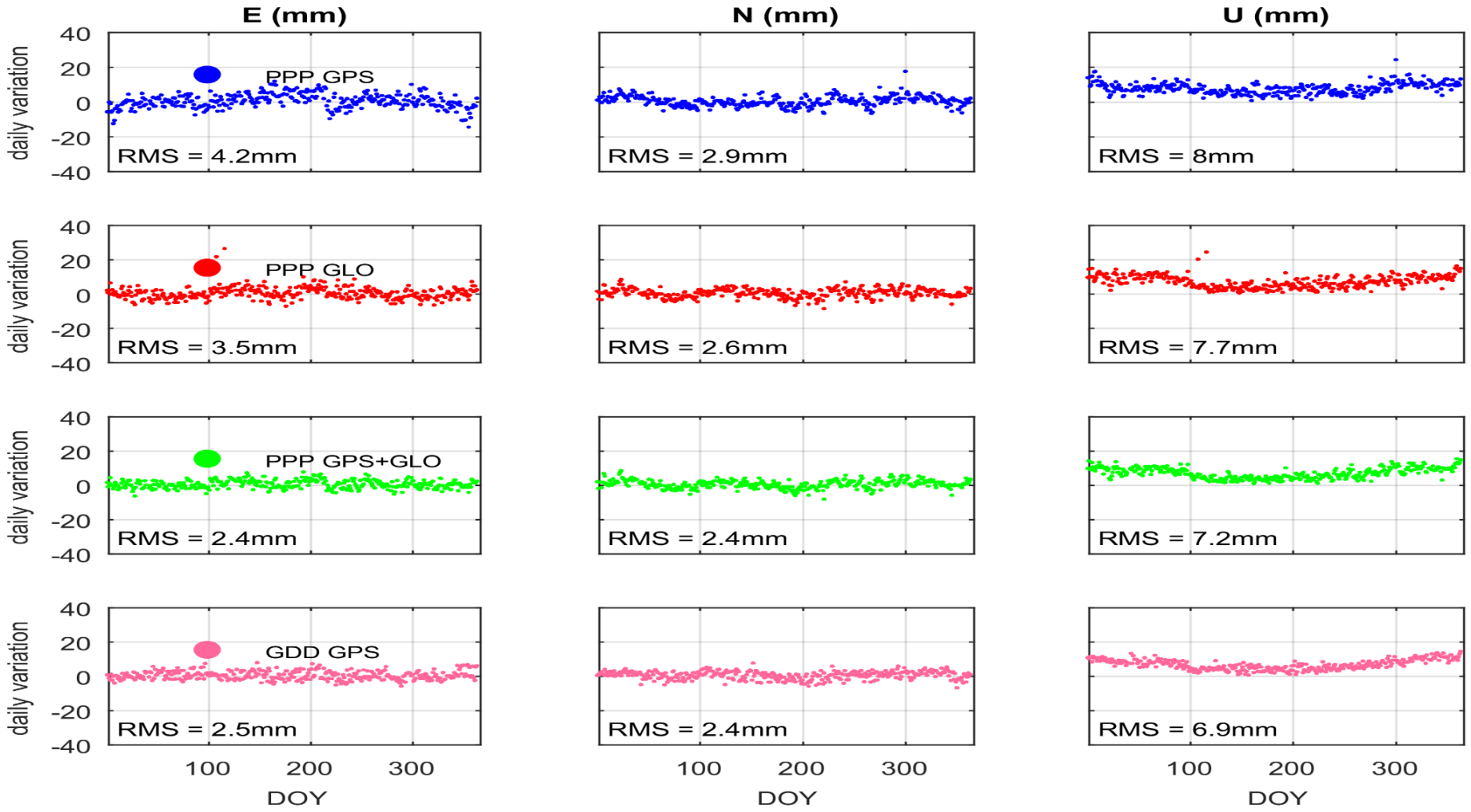


Figure 6-1 Daily station coordinate differences from the mean for one year for the ALDB station on 354 days

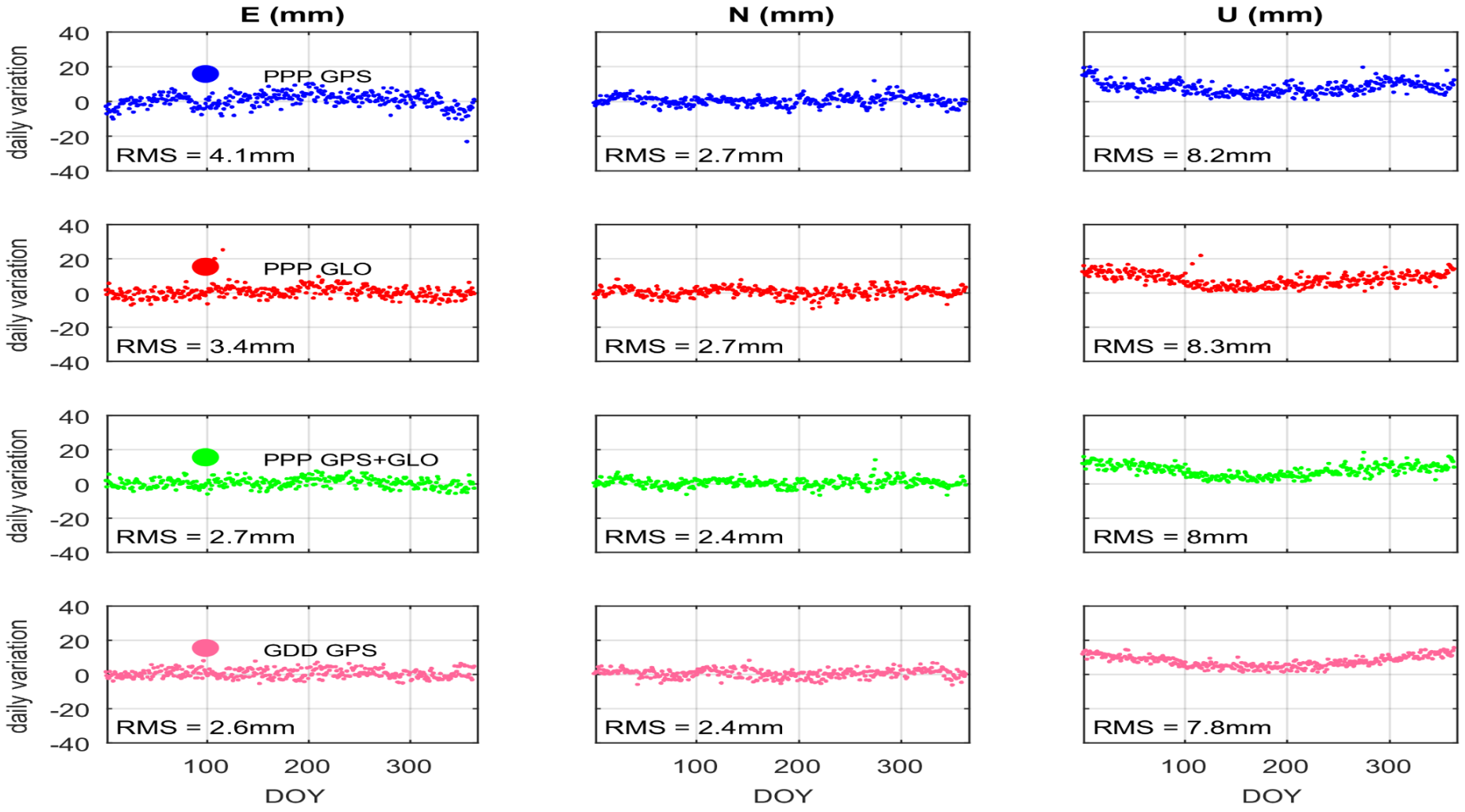


Figure 6-2 Daily station coordinate differences from the mean for one year for the AMER station on 350 days

Both figures show the stability of the daily solutions as well as the used precise products for all scenarios, i.e. the PPP (GPS, GLO and GPS+GLO) and the GDD GPS. Therefore, it is important to consider how to evaluate the level of precision from these different scenarios.

6.3.1 Repeatability analysis

A realistic measure of precision for the station coordinates was computed based on the daily repeatability. That is, the weighted quadratic averaged error which is given by equation (6.1) (Blewitt, 1989):

$$REP = \sqrt{\left(\frac{n}{n-1} * \frac{\sum_{i=1}^{n} \frac{(R_i - R_m)^2}{\sigma_i^2}}{\sum_{i=1}^{n} \frac{1}{\sigma_i^2}} \right)} \tag{6.1}$$

Where n is the number of days processed. R_i is the daily solution estimated station coordinate component for day "i"; σ_i is the standard error of the daily solution estimated station coordinate component for day "i". R_m is the mean of the daily solution estimated station coordinate component, considered as the average of the year from each of the PPP (GPS, GLO, GPS+GLO) solutions and the GDD GPS solution.

Bar charts representing the repeatability of the daily solution station coordinate estimates as individual coordinate components (East, North, and Up) for the ALDB and AMER stations are presented in Figure 6-3 and Figure 6-4, respectively.

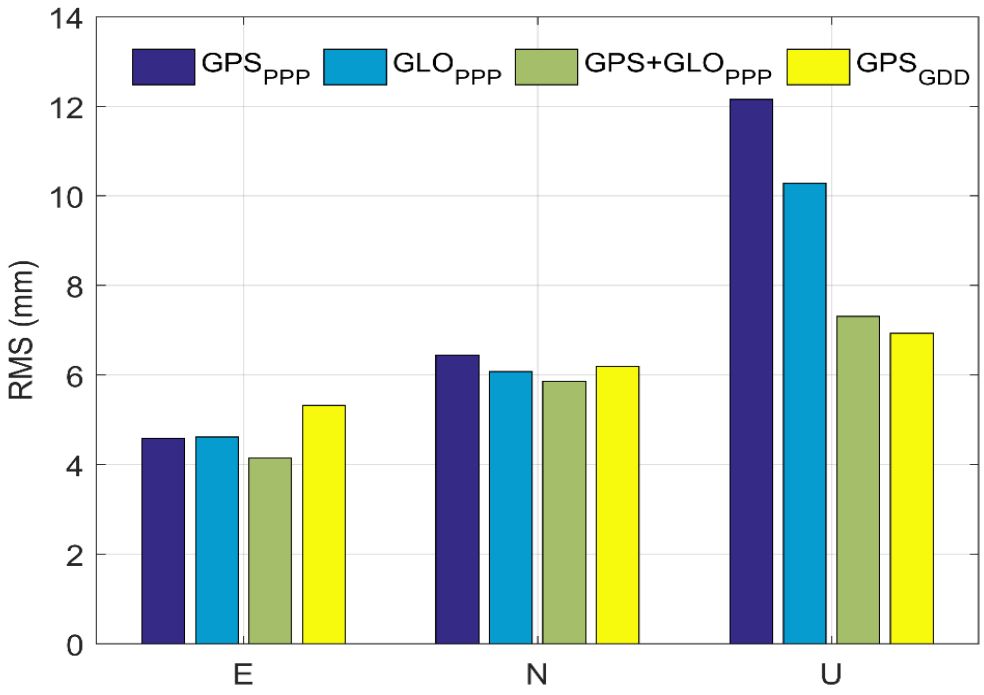


Figure 6-3 Repeatability of the daily solution station coordinate estimates from the PPP (GPS, GLO and GPS+GLO) and GDD GPS for the ALDB station

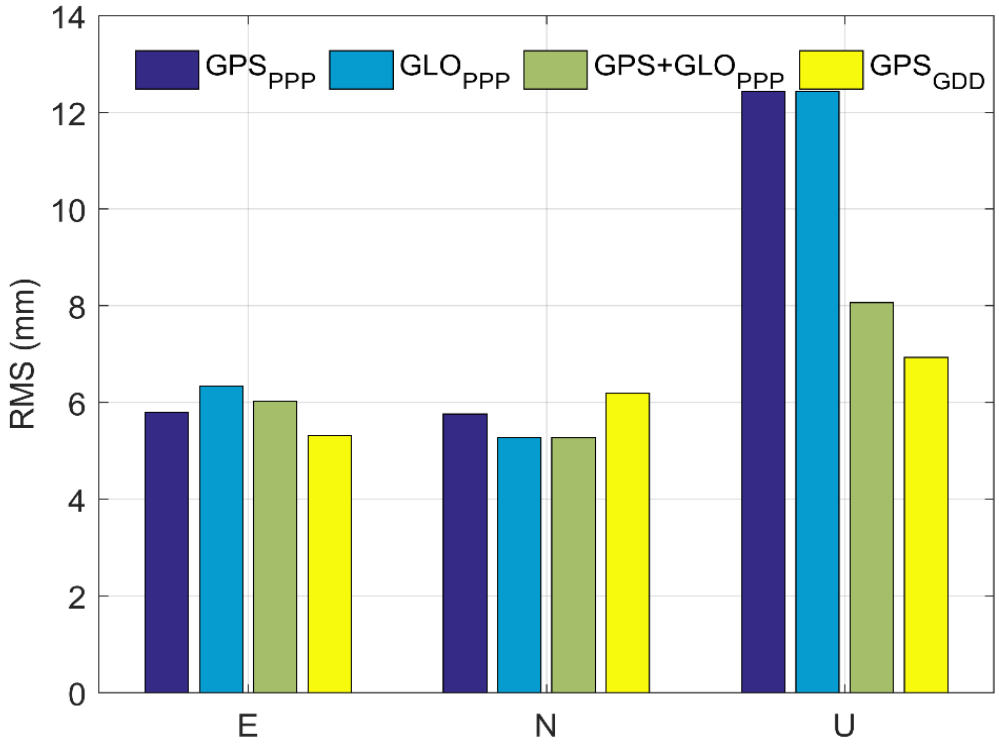


Figure 6-4 Repeatability of the daily solution station coordinate estimates from the PPP (GPS, GLO and GPS+GLO) and GDD GPS for the AMER station

It can be seen from Figure 6-3 and Figure 6-4, that the PPP GPS, PPP GLO and the PPP GPS+GLO have similar repeatabilities to the GDD GPS in the East and North coordinate components. It can also be seen that the PPP GPS+GLO has similar repeatability in the Up component as the GDD GPS, whereas PPP GPS and PPP GLO are slightly worse. Furthermore, it is clear that the PPP GLO has similar repeatabilities to the PPP GPS in all coordinate components.

The level of repeatability of GDD GPS can be explained as the GDD is based on a network of different receiver types and different antenna types which may affect the repeatability. While the PPP repeatabilities are strongly dependent on the availability of highly accurate models for systematic biases (Teferle et al., 2007), and the quality of the precise products.

These results are comparable with the results of Satirapod et al. (2013), who obtained millimetre-level station coordinate repeatabilities in the horizontal and centimetre-level in the vertical using GOA for PPP GPS (as introduced in section 2.2.1).

6.4 Experimental Results: Extended Investigation

Following the promising results for two stations, it was considered important to check multiple days with multiple stations. To generalize the assessment, an extended investigation was carried out using the dataset from section 5.6 processed as PPP GPS, PPP GLO and PPP GPS+GLO. The reason for using the same data is to assess each single station with the same environment at the same time. The processing strategy that was used for the PPP is the same as in Section 6.2, except that the precise products were expanded to include three alternative products, EMX, ESA and GFZ.

6.4.1 Precision compared to the Global Double-Difference

The analysis regarding repeatability followed a similar approach to the analysis used in the initial investigation but, in some instances, also considered weekly solution

station coordinate estimates as opposed to daily solution station coordinate estimates for the stations mentioned in Table 5-5 with their relevant GPS week. In these instances, for each of the three PPP (GPS, GLO and GPS+GLO) daily solutions and the GDD GPS daily solutions, the mean of the daily solution station coordinate estimates for each of the seven weeks were calculated. The weekly solution station coordinate estimates for each week were then subtracted from the overall average to create weekly station coordinate differences in terms of the East, North and Up components. Following this, it was possible to use the weekly station coordinate differences to calculate the repeatability of the weekly solution station coordinate estimates in terms of the East, North and Up components.

A bar chart representing the RMS of the repeatabilities of the weekly solution station coordinate estimates from the PPP (GPS, GLO and GPS+GLO) and the GDD GPS as individual coordinate components (East, North, and Plan) is shown in Figure 6-5 and Up in Figure 6-6, for all of the OSGB stations, considered.

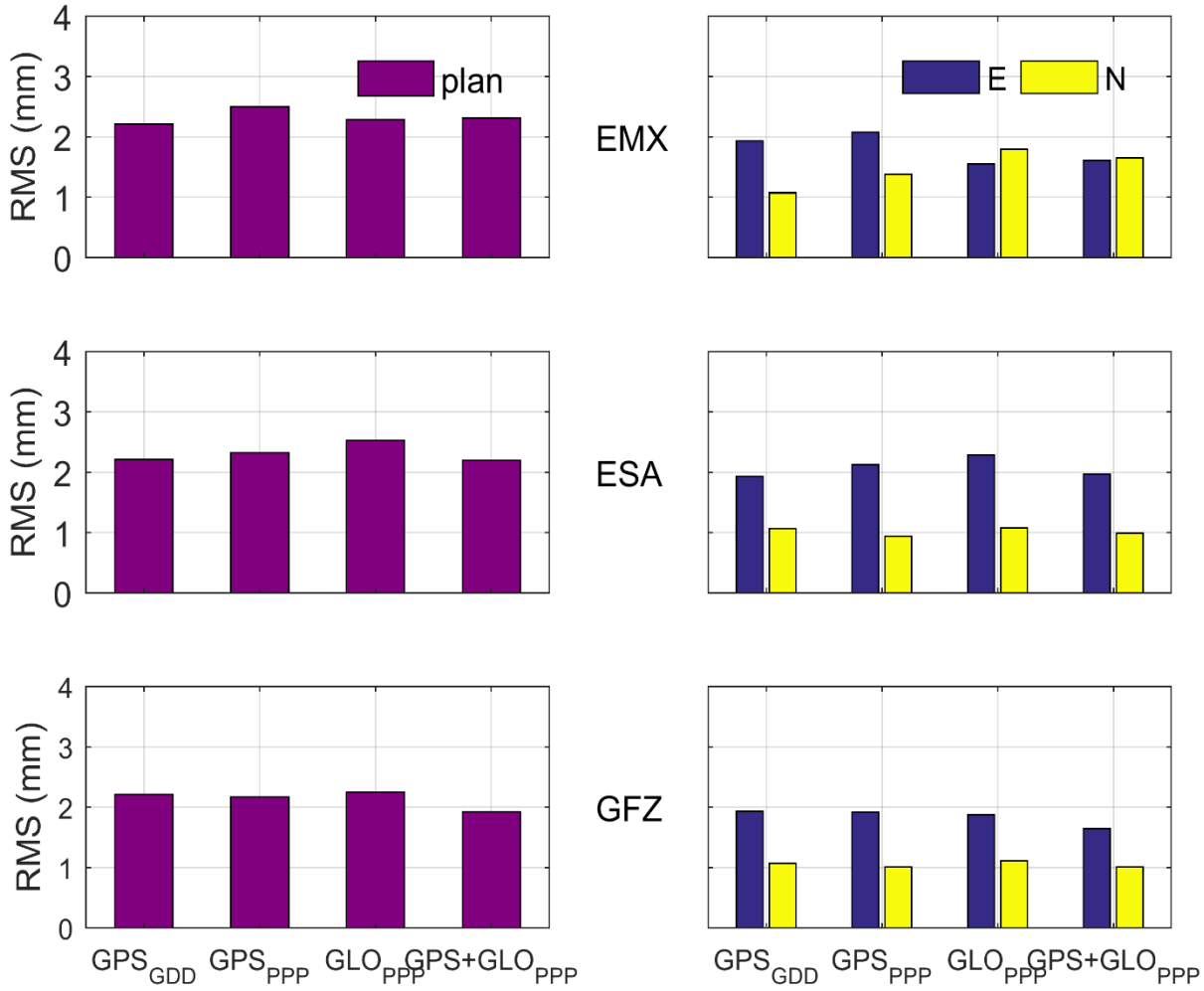


Figure 6-5 East, North and Plan RMS of the repeatabilities of the weekly solution station coordinate estimates from the PPP (GPS, GLO and GPS+GLO) and GDD for all stations considered

Considering Figure 6-5 and looking at the individual coorindate components, the two precise products that have a similar performance for the North and East components are ESA and GFZ. The North component in ESA and GFZ has an almost similar value and similar stability over time. Whereas, the East component has a lower performance as it is approximately twice the values of the North. This confirms what has been published by Li et al. (2015a) who observed that the North component is still the most accurate in PPP solutions because of the satellite constellation geometry, while for PPP GPS+GLO similar results were found by Wang et al. (2015a) who suggested that PPP GPS+GLO is better than PPP GPS, indicating that the station

coordinate accuracy and reliability are significantly improved with additional GLONASS satellites. However they also suggested that the improvement will only be in the case of insufficient number of GPS satellites or poor geometry conditions. While these results show an improvement, despite the fact that there is not an insufficient number of satellites or poor geometry, the reason for that is as mentioned by Ocalan et al. (2016) in that simply increasing the number of observations could be an advantage in PPP post processing. In addition these results (Figure 6-5) are comparable to Ge et al. (2007) who obtained average repeatabilities of 3.3mm (East) and 2.7mm (North) for a PPP float solution, but also saw an improvement in the East component by 27% when fixing the ambiguity (as introduced in section 2.2.1).

Regarding the Up component, the values are almost the same for all PPP scenarios as well as all of the used precise products, except the PPP GLO when using the GFZ products (see Figure 6-6).

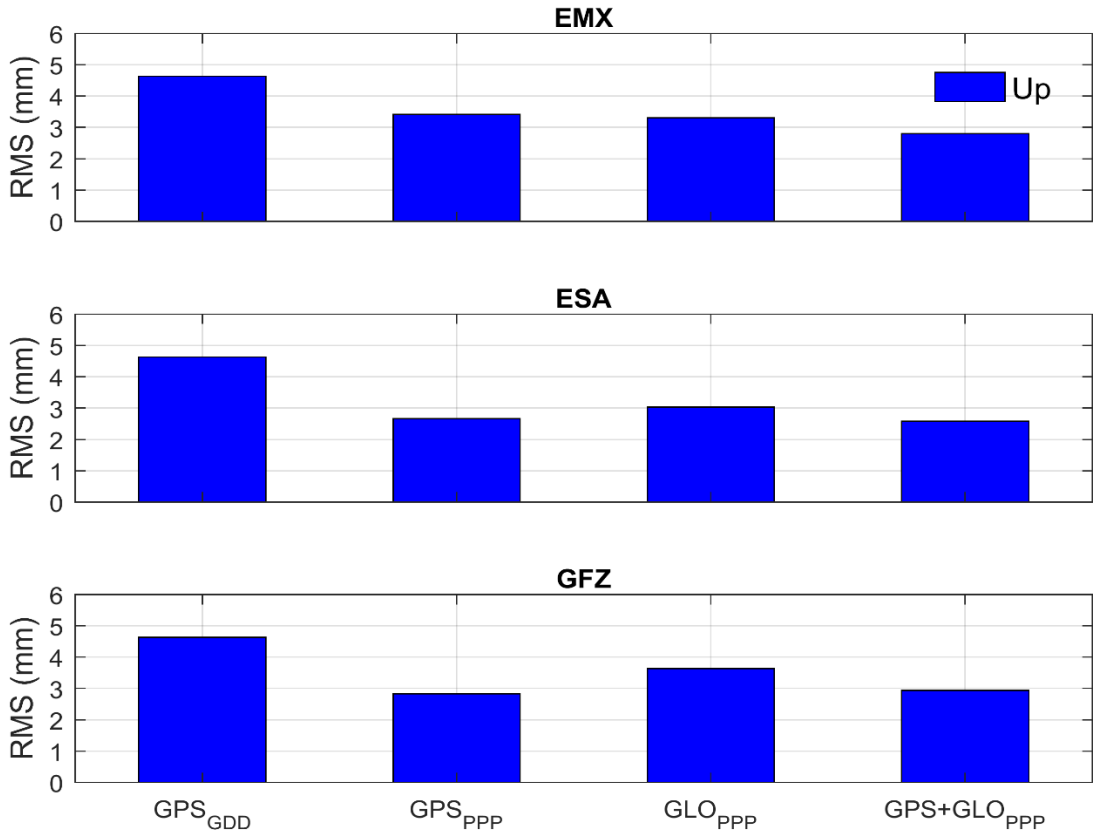


Figure 6-6 Up RMS of the repeatabilities of the weekly solution station coordinate estimates from the PPP (GPS, GLO and GPS+GLO) and GDD for all stations considered

As can be seen from Figure 6-6, when comparing precise products, the Up component repeatability varies in parts of a milimetre. These results are slightly better than Mustafar et al. (2017), who obtained 5.6mm repeatability for the Up component using GIPSY-OASIS software for PPP GPS. Furthermore, there is potential for more improvement in the repeatability of the Up component in the future by applying the higher-order ionospheric correction, which was proven to improve the station coordinate estimates as suggested by Kedar et al. (2003), Fritsche et al. (2005), Steigenberger et al. (2006) and Hernandez-Pajares et al. (2007) (as introduced in section 3.3.2).

Considering the PPP GPS and PPP GLO, it can be seen that the repeatabilities are the same within sub-millimetres, which provides an indication of the potential for

using the PPP GLO as an independent solution to the PPP GPS, rather than simply using GLONASS to aid the GPS (PPP GPS+GLO).

6.4.2 Accuracy compared to the Global Double-Difference

In addition to repeatability, it is also possible to estimate any differences between the weekly solution station coordinate estimates from PPP (GPS, GLO and GPS+GLO) and the weekly solution station coordinate estimates from GDD GPS. In this regard, measures of accuracy are obtained if the weekly solution coordinate estimates from the GDD, which are independent of the weekly solution station coordinate estimates from the PPP, are assumed to represent the most probable values.

A bar chart representing the RMS of the differences between the weekly solution station coordinate estimates from the PPP (GPS, GLO and GPS+GLO) and the weekly station solution coordinate estimates from the GDD as East, North and plan components is shown in Figure 6-7, and Up component in Figure 6-8, for all of the OSGB stations considered.

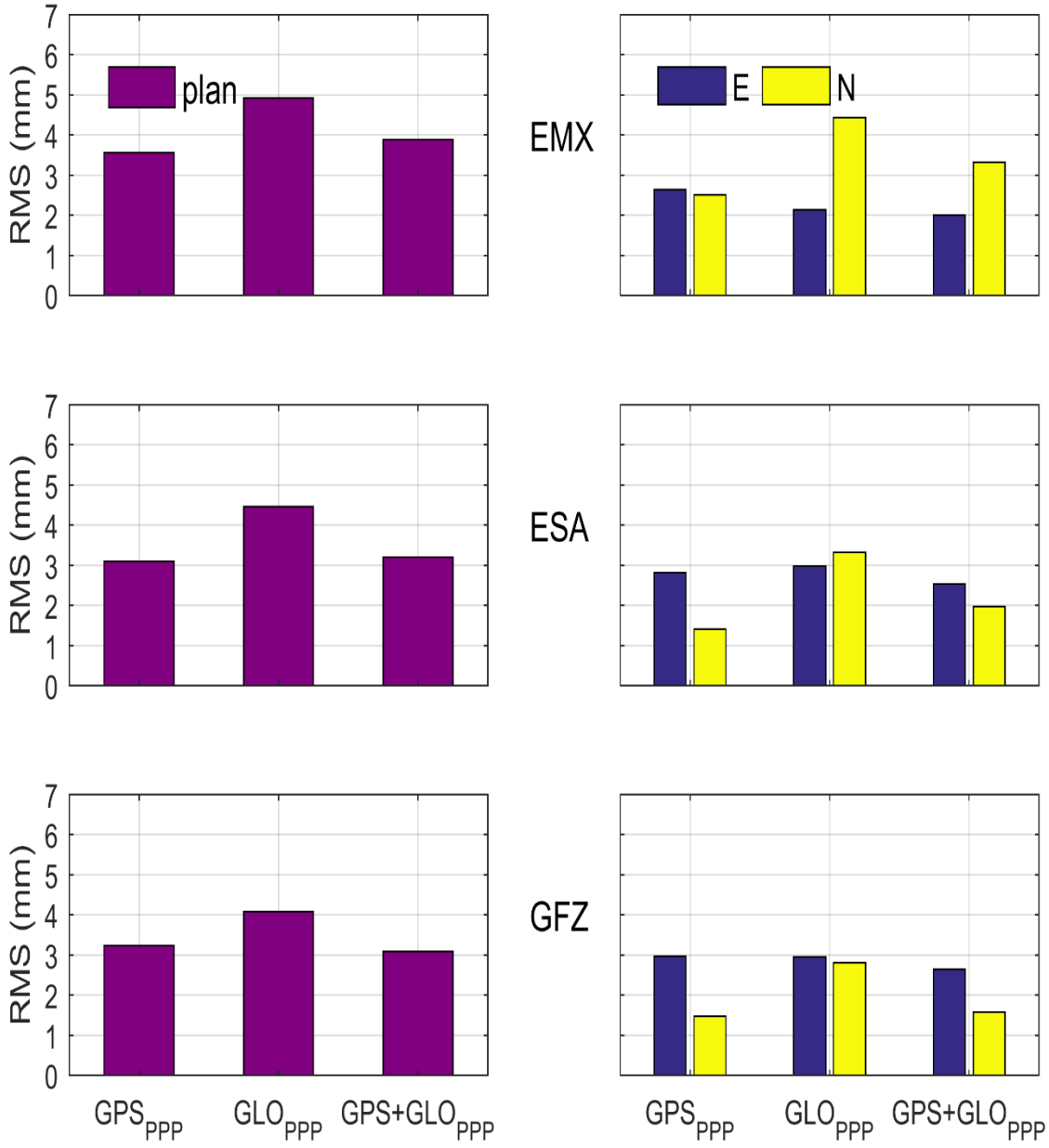


Figure 6-7 East, North and Plan RMS of the differences between the weekly solution station coordinate estimates from the PPP (GPS, GLO and GPS+GLO) and the GDD GPS for all stations considered

The PPP GPS and PPP GPS+GLO results in Figure 6-7 are similar to or slightly better than Liu et al. (2016a), who obtained monthly RMS values of station coordinate accuracies within ~6.0mm. Considering that these results are using 24-hr with fully operational GPS and GLONASS constellations, these results also confirm the

conclusions of Cai and Gao (2013b) that the accuracy will not be significantly improved if there are sufficient numbers of GPS satellites with good geometry. However, at this level of accuracy it is important to say that the horizontal accuracy from all PPP scenarios could be treated as the same because there are no significant differences between them.

Additionally, although these results are for a PPP float solution, there is potential for the accuracy of these results to be further improved by fixing the ambiguity as suggested by Ge et al. (2007) who found that the RMS for the East component in a float solution is reduced from 4.1 to 2.8mm by ambiguity fixing in PPP (as introduced in section 2.2.1).

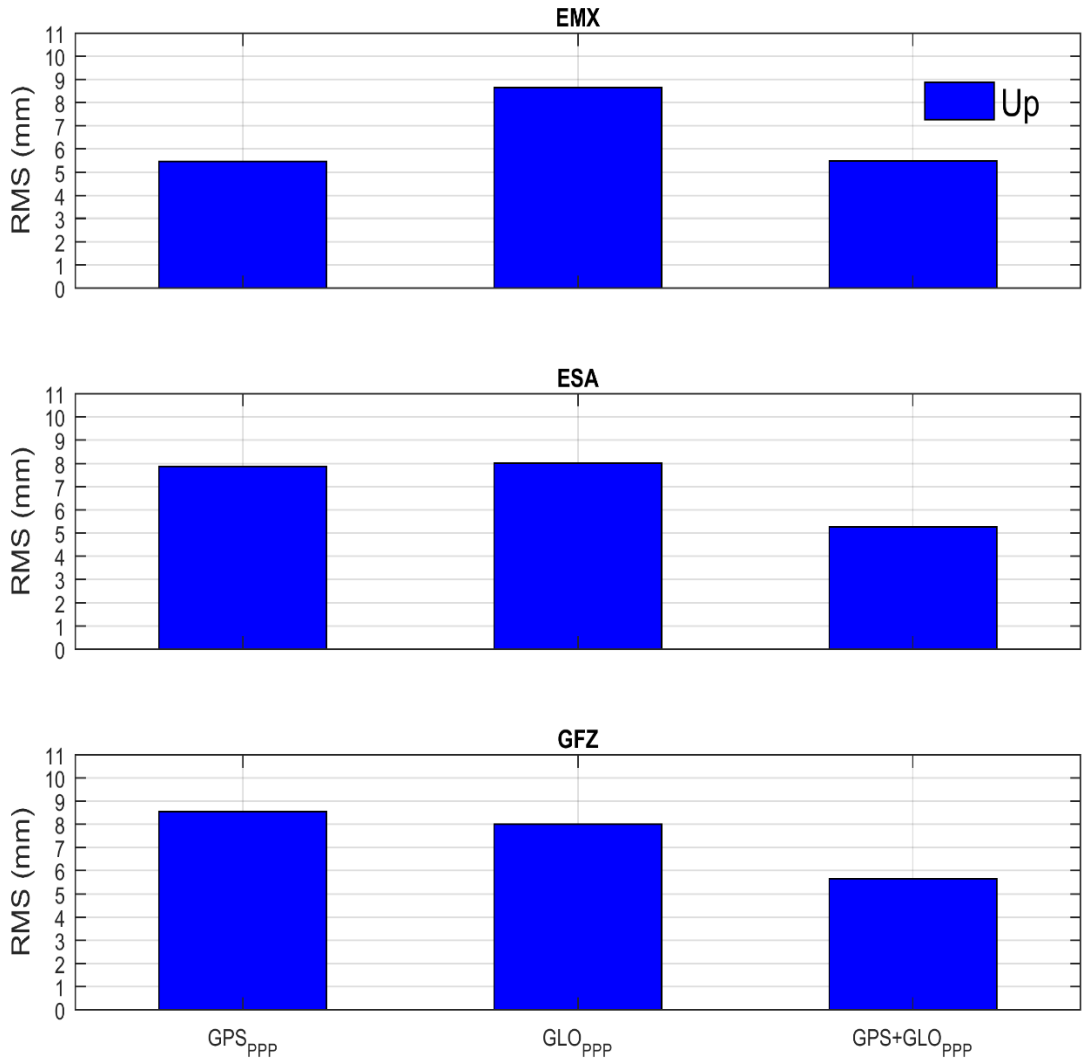


Figure 6-8 Up RMS of the differences between the weekly solution station coordinate estimates from the PPP (GPS, GLO and GPS+GLO) and the GDD GPS for all stations considered

The PPP GPS and PPP GPS+GLO results in Figure 7-8 are similar to Liu et al. (2016a), who obtained monthly RMS values of station coordinate accuracies within 9.0mm (as introduced in section 2.2.1).

6.5 Discussion of the results

Regarding the PPP GPS and PPP GLO, it can be seen from Figure 6-5 and Figure 6-6 that the precision differences are within a sub-millimetre. This gives first evidence of the potential for using of the PPP GLO solution as a precise independent solution.

The precision of the GDD GPS is also found to be different from the PPP single and multi-constellation within parts of a millimetre. The precision of the GDD GPS height is worse than the precision of the PPP (GPS, GLO, GPS+GLO) height. This might be because of different receivers and antenna type that formulate the GDD network.

In the case of the solution from the GDD GPS representing the most probable value, the differences between the PPP solutions from the GDD GPS solution were calculated for all days at all stations. Sometimes these differences are positive and sometimes they are negative. For the mean for each coordinate component of all stations and all days, see Figure 6-9.

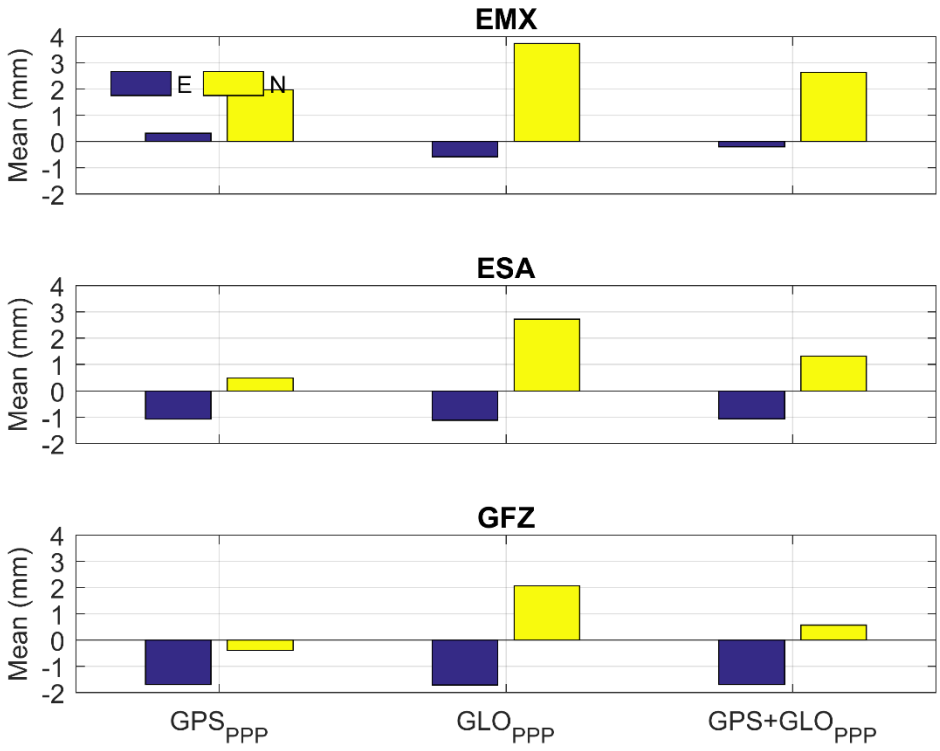


Figure 6-9 The mean differences of the PPP (GPS, GLO and GPS+GLO) solutions from the GDD GPS for East and North coordinate components and three precise products

For both ESA and GFZ precise products there is a bias for the East component and they are almost the same for different PPP scenarios. However, the differences are still a part of one millimetre. The noticeable change in the accuracy results from

the precision results is found in the North component, that is far then from the North components from the GDD GPS. This is not a degradation for the North component, but it is a difference between the two strategies of the GDD and the PPP.

No matter what precise products are being used, a bias will be observed in the North component in which it is higher than the computation from the GDD GPS. As has been noted before, this bias is the effect of the satellites' geometry. Looking at the PPP GPS bias, it is greater in the PPP GPS with EMX precise products because of their strategy of constraining their solution to the IGS, while the ESA and GFZ strategies adjust the station coordinates relative to a-priori values from selected IGS stations (see Appendix-C which summarises the differences between the 'acn' files from EMX, ESA and GFZ; although these differences come from their 'acn' files, accessed on 1/7/2015, it is assumed according to the IGS website (ftp://ftp.igs.org/pub/center/analysis/) that this what they used for producing the precise products). Whereas for the PPP GPS with ESA and GFZ precise products, it is not significant enough to be analysed, however, the PPP GLO is significant in the North component.

It is evident from Figure 6-9 that there is a bias between the PPP (GPS, GLO and GPS+GLO) solutions and GDD GPS solutions as well as between individual PPP solutions because they vary from the GDD GPS solution.

The North component causes the biggest bias in the horizontal. This could be because of the baseline and the distributed stations in the global network that were used for the GDD GPS solution. This means that the estimated North component from the PPP is to the north of the estimated North component from the GDD for a particular station.

The PPP solutions rely only on the satellite coordinates and clocks, which means that it represents the absolute position from the satellites. While the GDD GPS solution represents the solution from the satellites, but is also be affected by the

stations that form the global network. Considering the dataset in Section 5.6, and the global network presented for DOY 12, 2014 (Figure 5-1), this has 97 global stations to the south of the lowest latitude OSGB station (SCIL, lat = 49.9) and 19 global stations to the north of the highest latitude OSGB station (KIRW, lat = 58.9). This inhomogeneous network geometry could result in the GDD GPS solution being shifted from the PPP GPS solution. Furthermore, as the PPP GLO represents an entirely independent solution from both the PPP GPS as well as the GDD GPS solutions, the fact that the North bias in the PPP GLO is higher than the North bias from the PPP GPS, could be an effect of the different inclination angles which is reflected in the increased availability of the GLO constellation to the north when compared to GPS (see Figure 6-10). Another reason for that could be the reference frame because there were only a limited number of stations with GPS+GLO observations, which mean GPS precise products will be more closely aligned to the reference frame than GLO precise products at that moment in time.

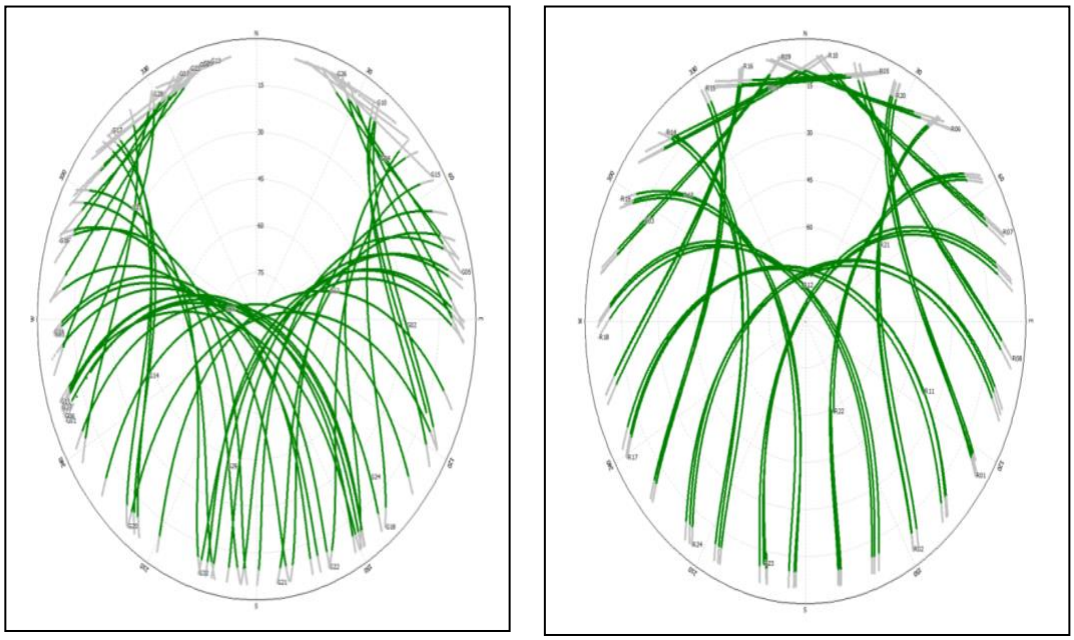


Figure 6-10 Satellites availability (Left: GPS, Right: GLO) for ALDB station DOY 12, 2014

However, the PPP GPS+GLO North component will balance between the PPP GPS that has an effect from the missing satellites to the north and the PPP GLO.

The differences between the mean weekly solution of the PPP GPS, PPP GLO and PPP GPS+GLO subtracted from the mean weekly solution from GDD GPS; for all 85 OSGB station in GPS week 1776 as shown in Figure 6-11.

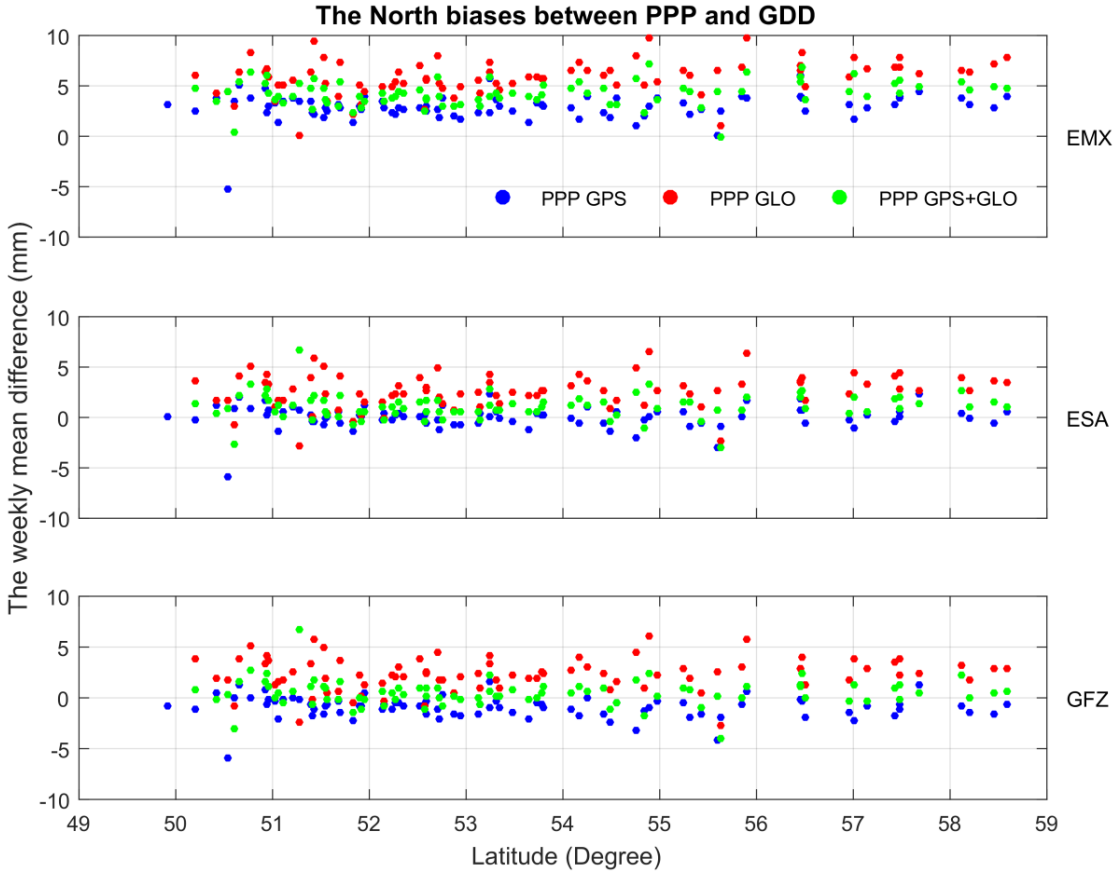


Figure 6-11 North biases relative to the GDD Solution for 85 OSGB stations in GPS week 1775

It is evident from Figure 6-11, that all PPP scenarios' have almost the same shape and that there is no relationship with the increase of the OSGB station latitude.

The Up component bias will be investigated and explained in detail with its correlation with the troposphere in Section 7.5.

6.6 Precise Products' Effects on Precise Point Positioning

The PPP is highly dependent on the precise products that have to be used. Three final precise products from three different ACs were introduced in 6.4 and their differences on the evaluating parameters (accuracy and precision) were found to be millimetres. However, it is important to investigate their effect on other estimated parameters, and it is important to see if there is a constant or continuous difference between these products. Therefore, the products' effect on the estimated receiver clock offsets were investigated, followed by an investigation of the differences between the satellite coordinates.

6.6.1 Reference station time-base offsets

The PPP is relying on the satellite clock offsets, however, a time component that is estimated is the receiver clock offsets, and many unmodeled errors or biases can be absorbed in these estimated receiver clock offsets.

6.6.1.1 GPS

Starting with the satellite clock, and more specifically with the GPS constellation, all the ACs produced precise products of GPS satellite clock offsets. To look at the actual estimated satellite clock offset by different AC, Figure 6-12 is an example for GPS PRN 5 and 7 on DOY 12, 2014 from the three ACs (EMX, ESA and GFZ) represented as the difference from the mean (See Appendix–C for the summary of the differences between these ACs strategies).

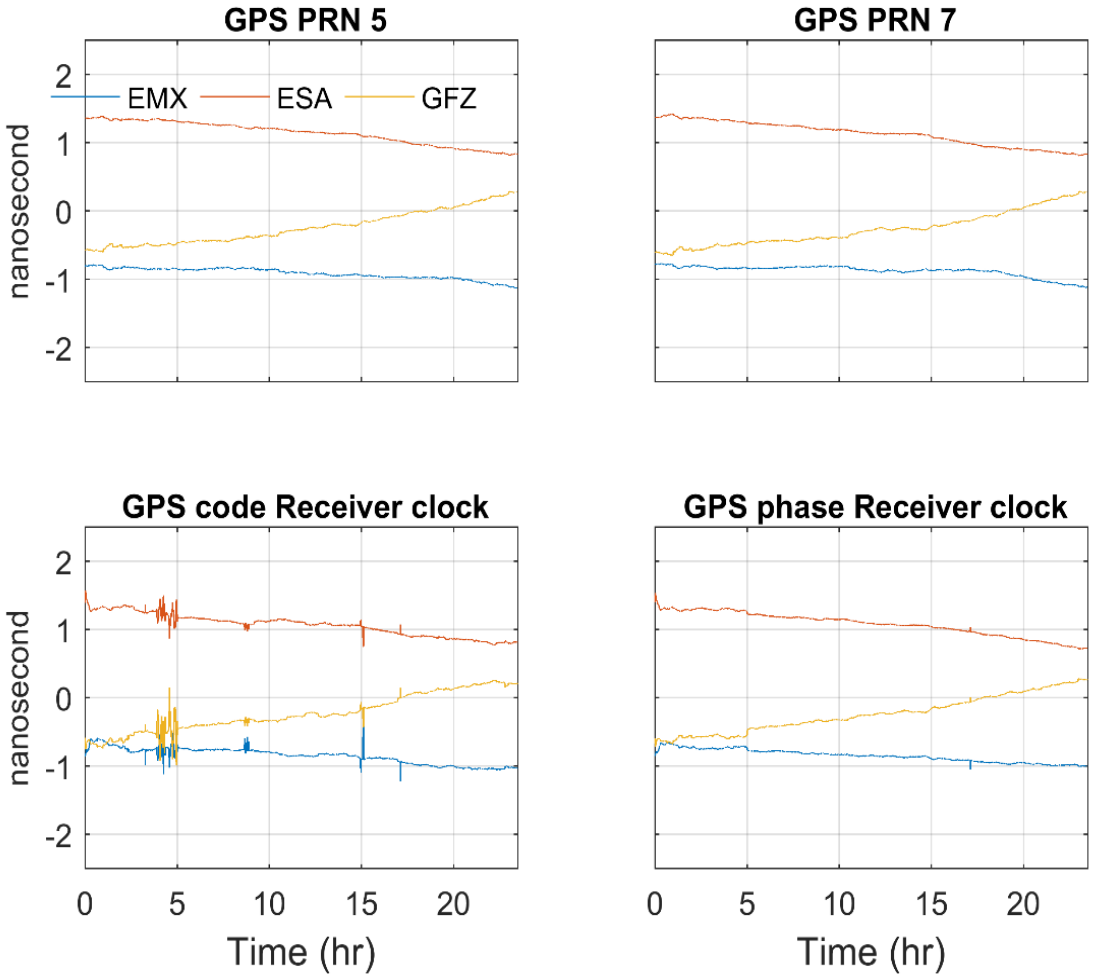


Figure 6-12 GPS satellite clock offset differences from the mean for the EMX, ESA and GFZ precise products (upper) and Receiver clock offset differences from the mean for EMX, ESA and GFZ for ALDB station on DOY 12, 2014 (lower)

It is clear from Figure 6-12 that the precise satellite clocks from different ACs are not the same, where every nanosecond multiplied by the speed of light will represent around 30 cm in the range. These ACs have different strategies for producing their precise products. However, all ACs are following the same strategy for the time referencing, meaning that one reference station from the IGS network for that day will be chosen and time will be fixed relative to a reference epoch. Even though this reference station has an external frequency, it can have a drift or offset from the true GPS time as can be seen from Figure 6-12. Hence, the selection of reference station will have an effect that will be propagated to the estimated satellite

clock offsets, where it is noticed that this offset is then almost the same for all satellites.

Any propagated time offset in the satellite clock offsets will affect the PPP solution. More specifically, it will affect the responsible parameter for balancing the time, namely the receiver clock offset, which will absorb the combination of the ACs propagated time offset from all satellites at a specific epoch. This means that if too tight a constraint is made on the receiver clock offset(s), then it will lose the ability to absorb the propagated time offset which will result in an effect on other estimated parameters from PPP. Figure 6-12, is an example of the difference from the mean between the estimated receiver clock offsets for both the code and phase and clearly shows that the receiver clock offset did absorb the propagated time offset in this case.

Here it is worth mentioning that the propagated offset is not a constant over different days, because it is changeable depending on the chosen reference station. In addition, it can be different from one AC to another even when they have used the same reference station. For example, Figure 6-13 represents similar differences from the mean for DOY 14, 2014 with the same satellites and station as in Figure 6-12. The reference stations were YELL, YELL and ALGO, for DOY 12, 2014 and YELL, CEBR and WSRT for DOY 14, 2014, for EMX, ESA and GFZ, respectively.

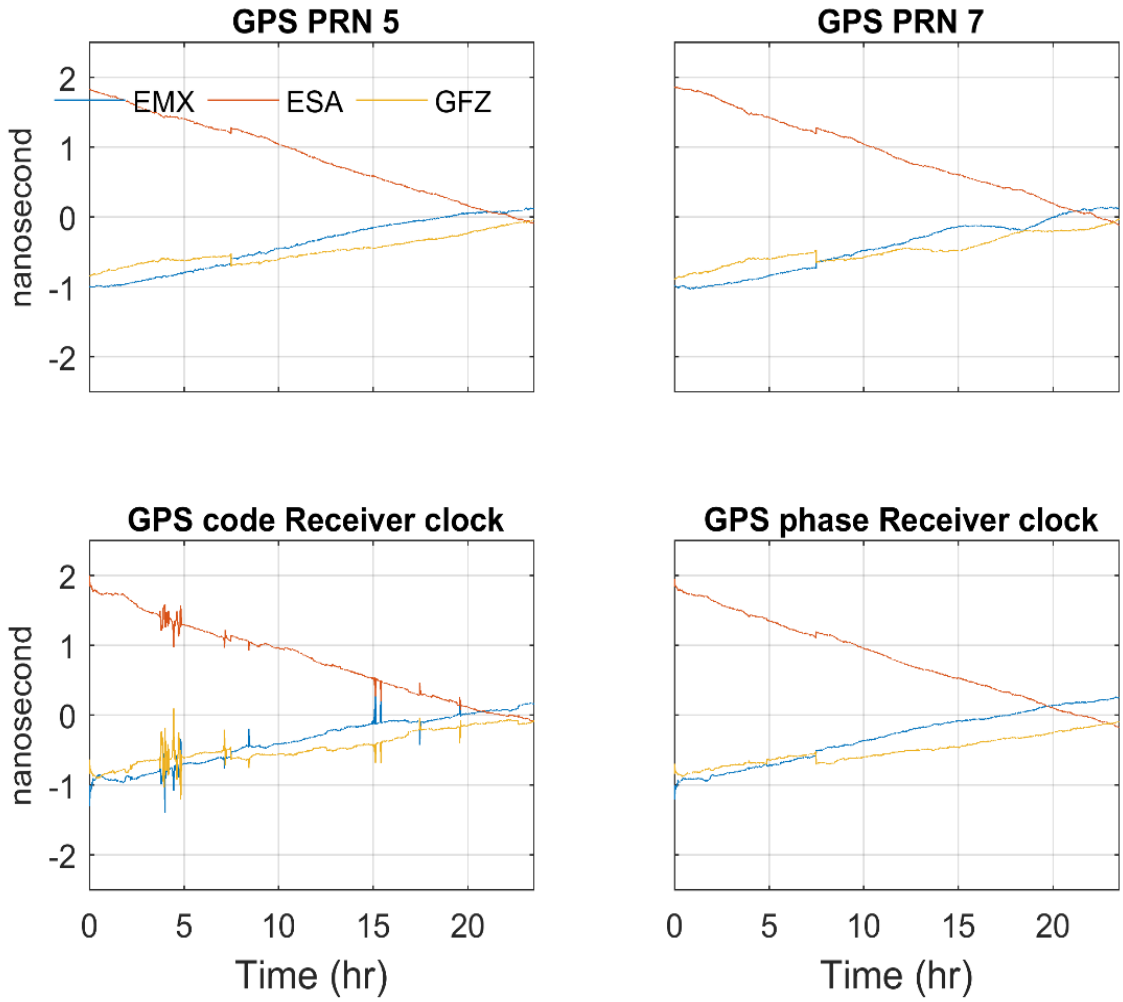


Figure 6-13 GPS satellite clock offset differences from the mean for the EMX, ESA and GFZ precise products (upper) and Reciever clock offset differences from the mean for ALDB station with the EMX, ESA and GFZ precise products on DOY 14, 2014 (lower)

6.6.1.2 GLO

The resultant offsets based on the GLO satellites clock offset is not the same for the GLO constellation. Figure 6-14 shows an example for GLO satellites no. 1 and 2 for DOY 12, 2014 and the receiver clock offsets from the PPP GLO solution for the same station used for the PPP GPS.

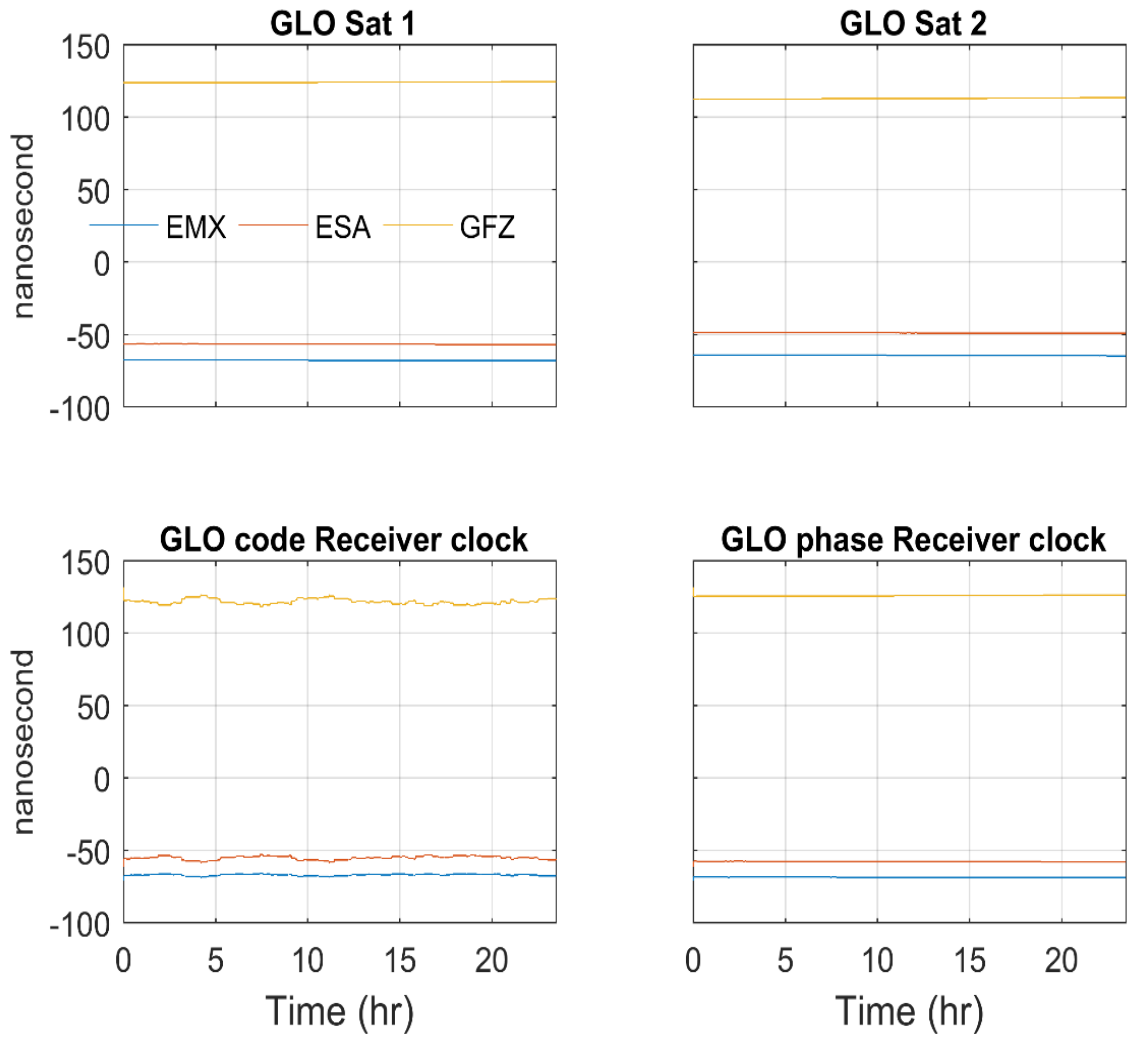


Figure 6-14 GLO satellite clock offset differences from the mean for the EMX, ESA and GFZ precise products (upper) and Reciever clock offset differences from the mean for ALDB station with the for EMX, ESA and GFZ precise products on DOY 12, 2014 (lower)

From Figure 6-14, it can be seen that the satellite clock and receiver clock offsets are much higher for GLO than for GPS. Cai and Gao (2008) claimed that the difference between the receiver clock offsets for the GPS and GLO represent the time difference between the two systems. However, this assumption is not entirely accurate (as introduced in section 2.2.1). To see why, there is a need to look at the difference between the receiver clock offsets for the same station. In the presented strategy two different clocks, one phase and the other a code, were estimated for every constellation.

Figure 6-15 represents the difference between the estimated receiver clock offsets for GPS and GLO, using all three precise products (EMX, ESA and GFZ).

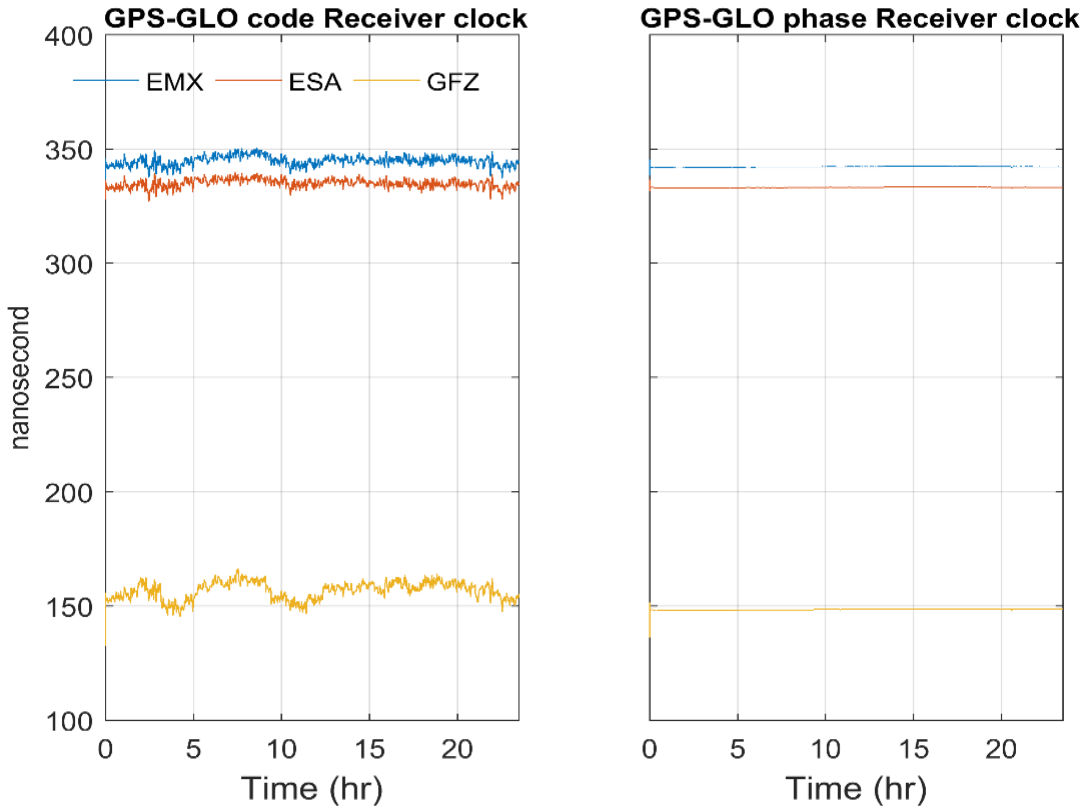


Figure 6-15 Reciever clock offset differences between GPS and GLO for ALDB station with EMX, ESA and GFZ precise products on DOY 12, 2014

If the assumption from Cai and Gao (2008) was correct, the differences between the estimated receiver clocks would be similar for all product types. Clearly, the differences are not the same, as they are contaminated by the AC-dependent propagated time offset as well as by the system time difference. Another opinion from Douša (2009) was that the satellite orbit error can be easily absorbed by the satellite clocks and the estimated ambiguities (as introduced in section 2.3).

It is also evident that the code clock has a higher variation and this is because of the noise in the code as well as the differential code biases (DCBs).

6.6.2 Satellite coordinates effects

Each AC uses a different strategy for estimating the satellite coordinates, e.g. different reference networks, different tropospheric models and tropospheric strategy, as well as possibly using different versions of IERS standards (see Appendix-C for the differences between EMX, ESA and GFZ strategies). In addition, there are different reference networks (number of stations and geometries) used by the three different ACs, and different reference networks (number of stations and geometries) used by each individual AC for GPS and GLO, which are the main reason for the differences in the precise products.

Therefore, it is important to investigate the level of the differences in the estimated satellite coordinates. Figure 6-16 represents the difference from the mean for the satellite's Cartesian coordinates, DOY 12, 2014.

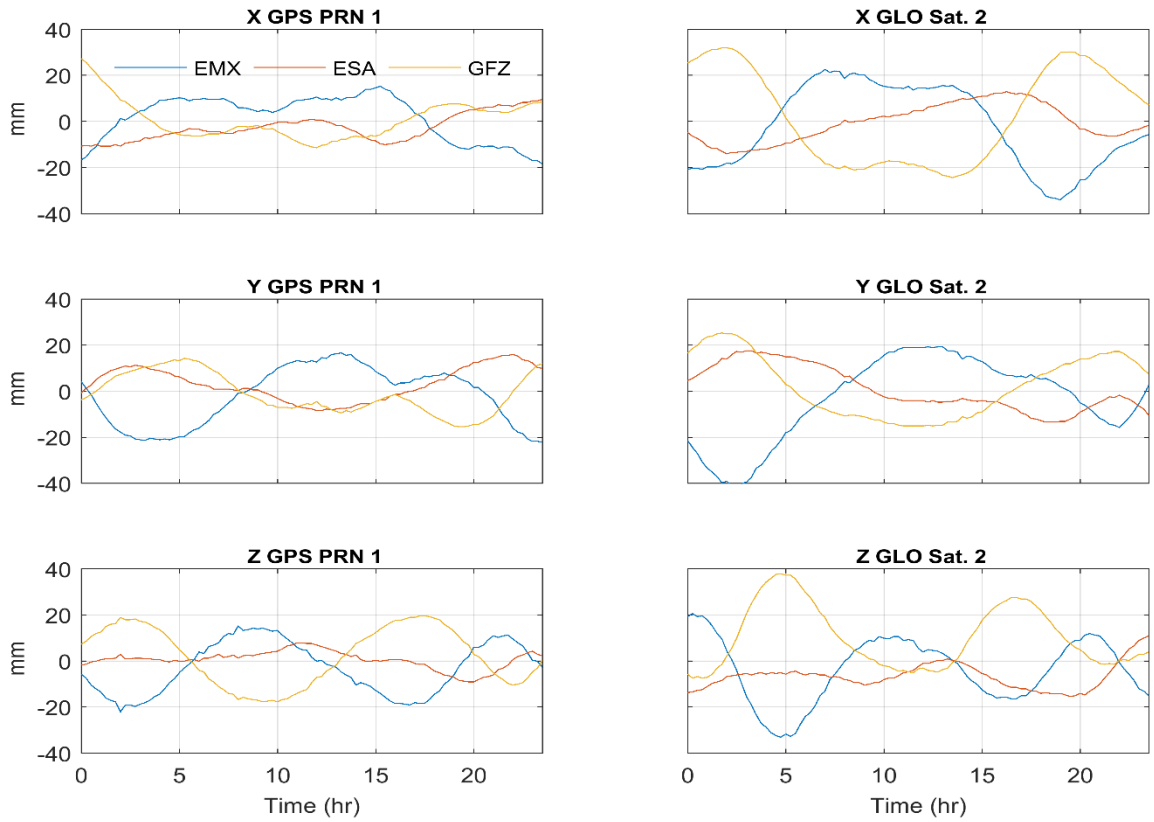


Figure 6-16 Satellite Coordinate differences from the mean for the EMX, ESA and GFZ precise products on DOY 12, 2014

In this respect, Douša (2009) suggested that the ambiguities represent a huge number of parameters and are highly capable of compensating for a part of the satellite coordinate errors. The ambiguities can be resolved into integers, in a network solution, which is usually performed one step before the final adjustment by different ACs. Such resolved ambiguities are then back-substituted, while the remaining unresolved ambiguities are estimated as real values simultaneously with all other parameters. However, in both cases, they could compensate for a significant part of the satellite coordinate errors. It is rather difficult to estimate their 'absorption' capabilities, but it could be assumed that a small part of the error will remain unabsorbed and will stay in the satellite coordinates.

For the PPP solution, the satellite coordinates (SP3 files) represent fundamental parameters because they are the responsible parameters for defining the reference frame. The use of the SP3 files from a specific AC, will give a different solution because the satellite coordinates have to be implemented in the design matrix, with respect to the station coordinates, as known values. Therefore, any differences or small errors between the used coordinates and the *'truth'* value will theoretically be propagated into the station coordinates, as in:

$$\frac{((X \pm error)^s - X_r)}{\rho}, \quad \frac{((Y \pm error)^s - Y_r)}{\rho} \quad , \frac{((Z \pm error)^s - Z_r)}{\rho}$$

Even though the differences between the satellite coordinates from different ACs can be at the centimetre level, the station coordinate will usually only be affected at the millimetre level, because of the adjustment done using the EKF, and the position being in static mode in this research.

Consequently, the effect of using different products from different ACs on the station coordinates can be seen in Figure 6-17, which represents the differences between the estimated Cartesian coordinates using the three ACs precise products and the mean solution of those three for the PPP GPS and PPP GLO of the ALDB station on DOY 12, 2014.

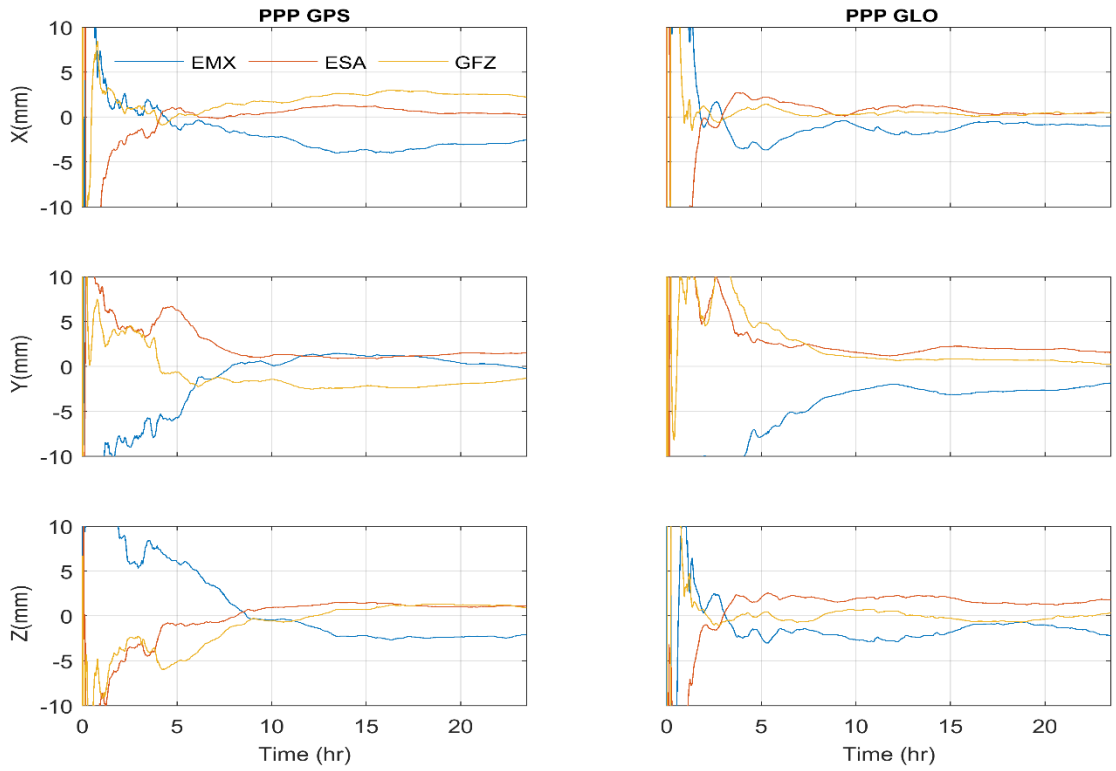


Figure 6-17 Precise Product effects on the estimated station coordinates from PPP GPS and PPP GLO for ALDB station on DOY 12, 2014

In this case, the processing strategy is the same for all PPP scenarios, except for the precise product types. This means that the differences between these solutions come from the precise products and more specifically, from the different satellites coordinates.

To cover a longer term, the differences from the mean solution of the PPP for seven individual days through DOY 12-18, 2014 (GPS week 1775) for the dataset in Table 5-5 were computed and are presented in Figure 6-18.

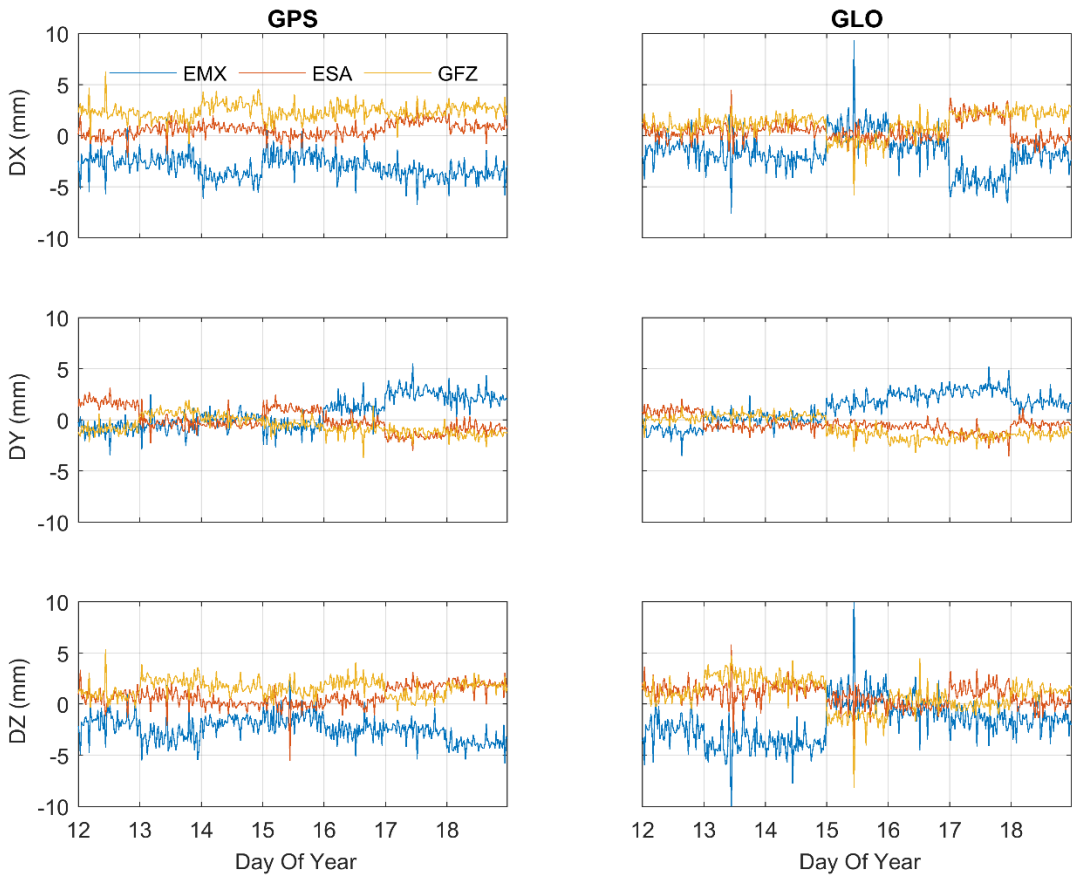


Figure 6-18 Precise Product effects on the estimated station coordinates from PPP GPS and PPP GLO for 56 OSGB stations on DOY 12-18, 2014

It is evident from Figure 6-18 that the differences are not stable over several days, and vary between ACs, but at similar level. Hence, it would be useful to investigate the differences between the satellite coordinates instead of investigating their impact on the station coordinates from the PPP solution.

6.6.2.1 Helmert transformation parameters among the products

One way of trying to understand the differences between satellite coordinates from different ACs is by investigating if there are stable or meaningful transformation parameters.

For that reason, a seven-parameter Helmert transformation was used, and was computed using three different approaches (coded in an automated Matlab script developed by the author):

1. Daily transformation parameters

The seven parameters were first computed for the satellite coordinates in the three precise products (EMX, ESA and GFZ) and their means. This was done for DOY 12-18, 2014 (GPS week 1775) and the computed parameters are summarized in Figure 6-19. Bear in mind that the rotation and the scale have been multiplied by 27,000 km, which is the approximate altitude of the satellites from the centre of the Earth.

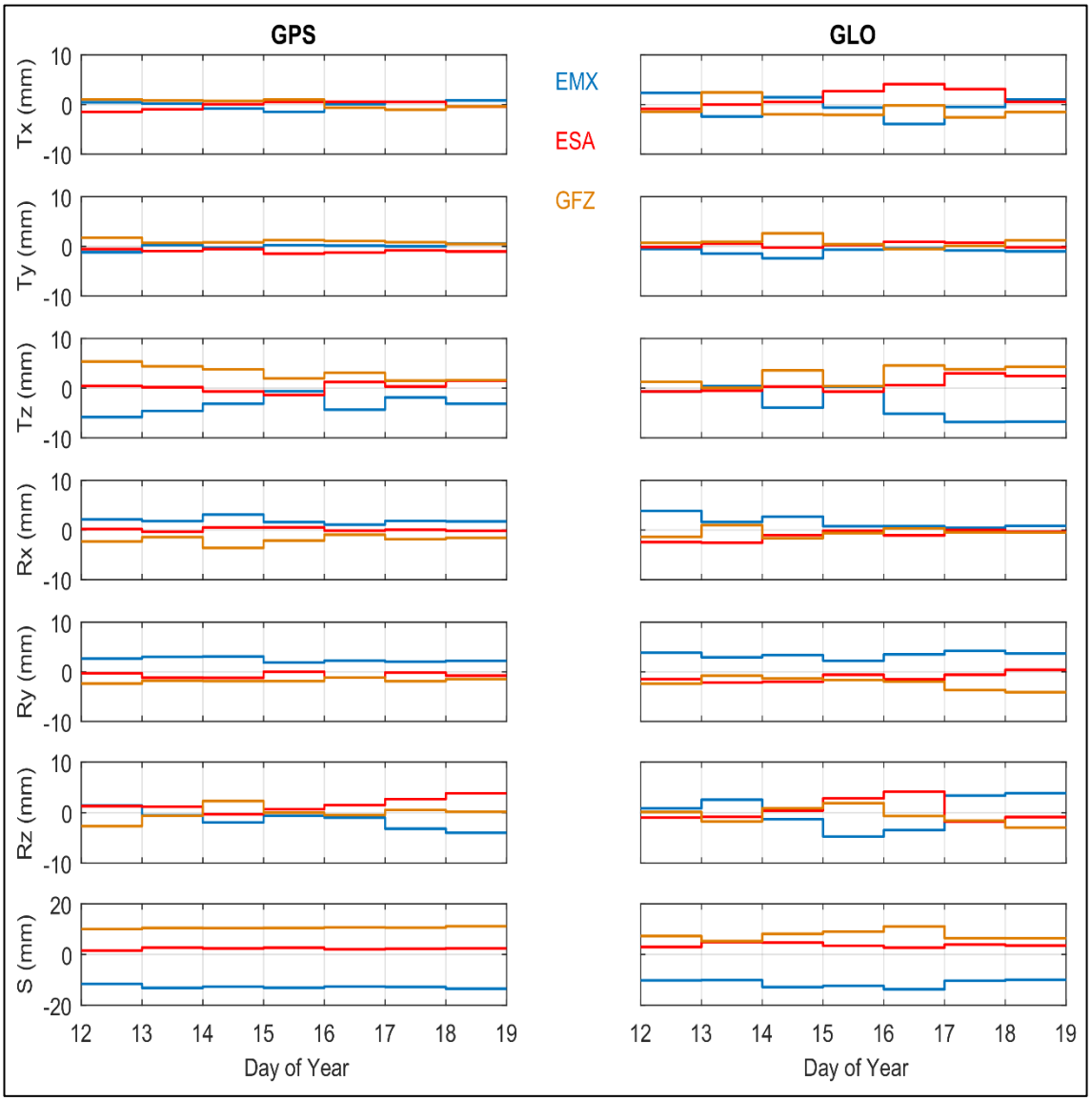


Figure 6-19 Daily Seven-parameter Helmert transformation parameters for GPS week 1775 between the EMX, ESA and GFZ precise product satellites coordinates and the mean of the three

From Figure 6-19, it is clear that there are translation, rotation and scale parameters between the precise products and the mean. These mainly come from the chosen network, whereby each AC has chosen different stations to form their precise products. The geometry of the selected network will then affect the estimated satellite coordinates; which will then affect the PPP station coordinates. Figure 6-20, summarizes the number of stations that were used for producing the precise products by each AC on DOY 12-18, 2014.

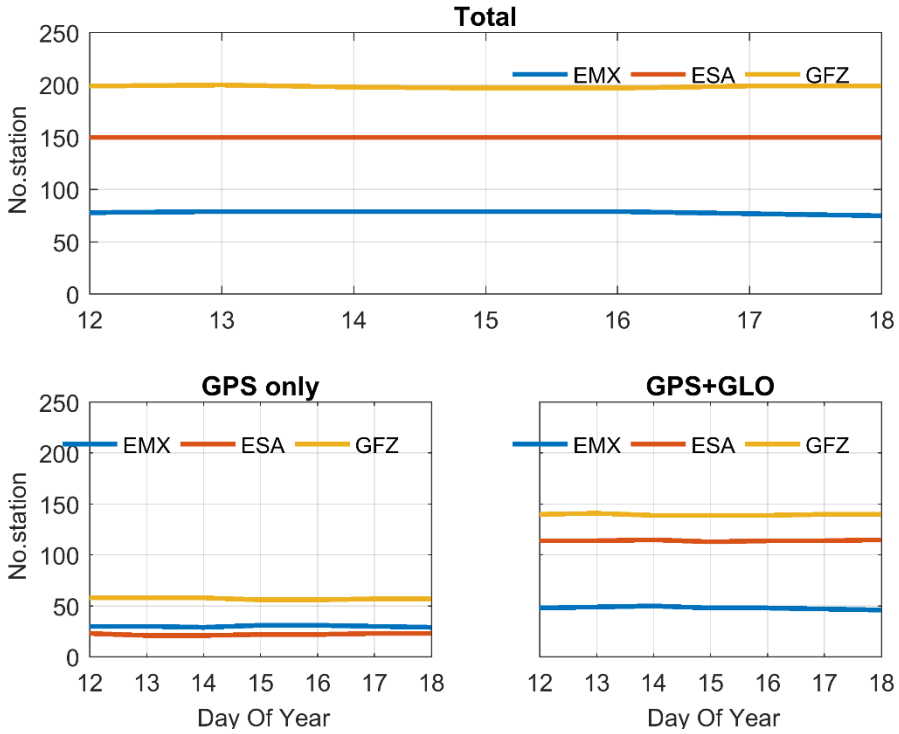


Figure 6-20 The number of stations that were used for EMX, ESA and GFZ precise products on DOY 12-18, 2014

It is clear that ESA AC used the same number of stations for their processing; however, they are not the same stations for all days. Whereas, EMX and GFZ used an inconsistant number of stations. The consistent number of stations used by ESA has implications on the long-term repeatability, as will be shown in Chapter 8.

It is also worth mentioning that the number of the stations from the three ACs appears to have a correlation with the scale parameter in Figure 6-19.

2. Per satellite transformation parameters

The seven transformation parameters were then computed for each satellite over one day, to see if the reason for the differences is because of bad satellites. The results are summarized in Figure 6-21 which represents the transformation parameters, as three translation parameters (DX, DY, and DZ), three rotation parameters (RX, RY, and RZ) and a scale parameter (S), between the three ACs and the mean of them per satellite (where each line represents one satellite).

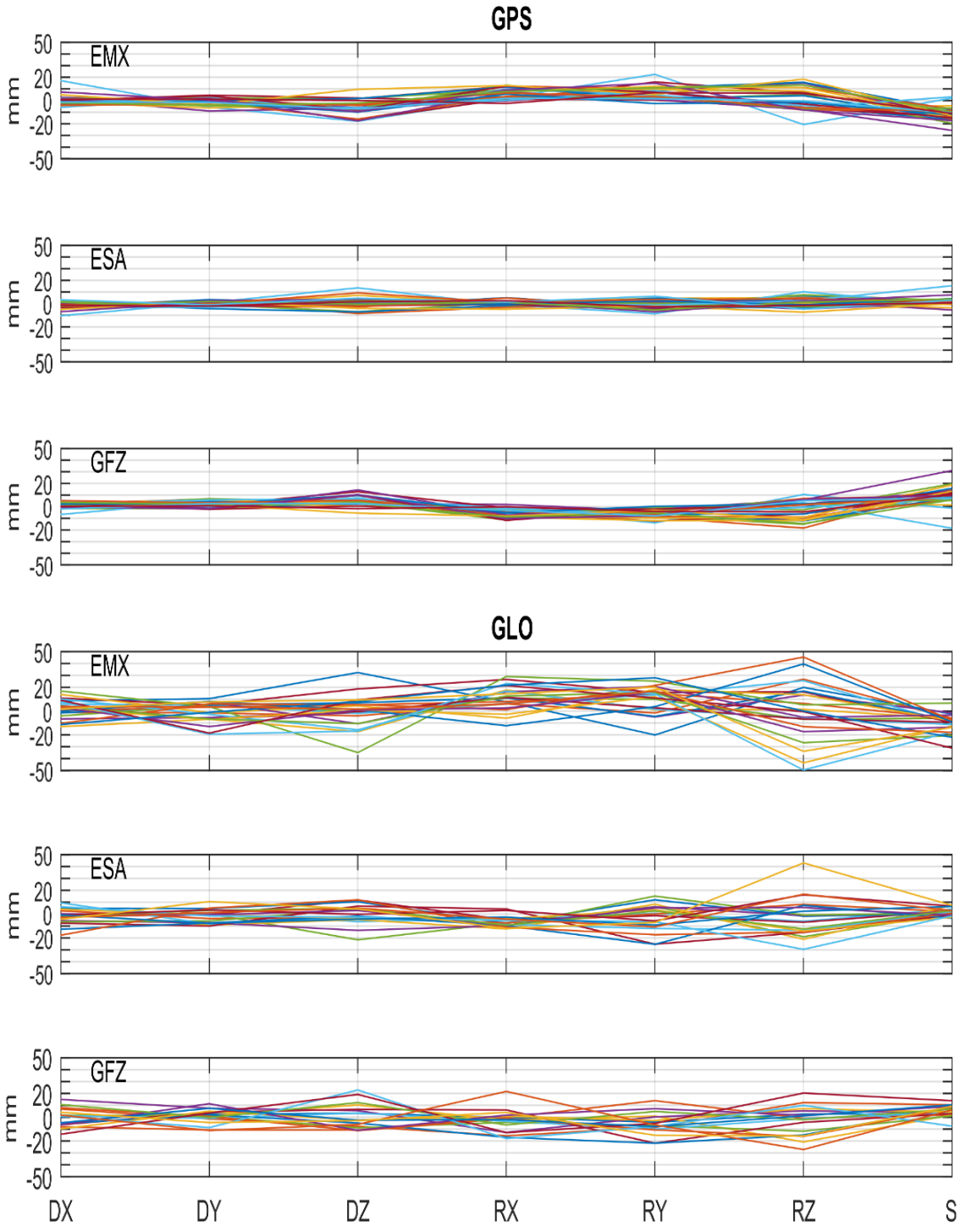


Figure 6-21 Per satellite seven parameters Helmert transformation parameters for GPS and GLO for EMX, ESA and GFZ precise products on DOY 12, 2014

For the GPS, it can be concluded from Figure 6-21 that the scale component has the biggest difference ACs which could be due to using different tropospheric and

ionospheric strategies between those ACs. The other parameters have almost similar performance, except the DZ and RZ because of the limited satellites at the North Pole.

Compared to the GPS parameters, the GLO transformation parameters seem to have less consistency among the three ACs, suggesting that the precise products for GPS are more stable than for GLO. The geometry of the AC's network and the number of GPS or GPS+GLO stations could also be factors for precise products quality. These differ among various ACs as shown in Figure 6-22, Figure 6-23 and Figure 6-24 for EMX, ESA and GFZ, respectively, using SNX files from IGS websites and the stations log files.

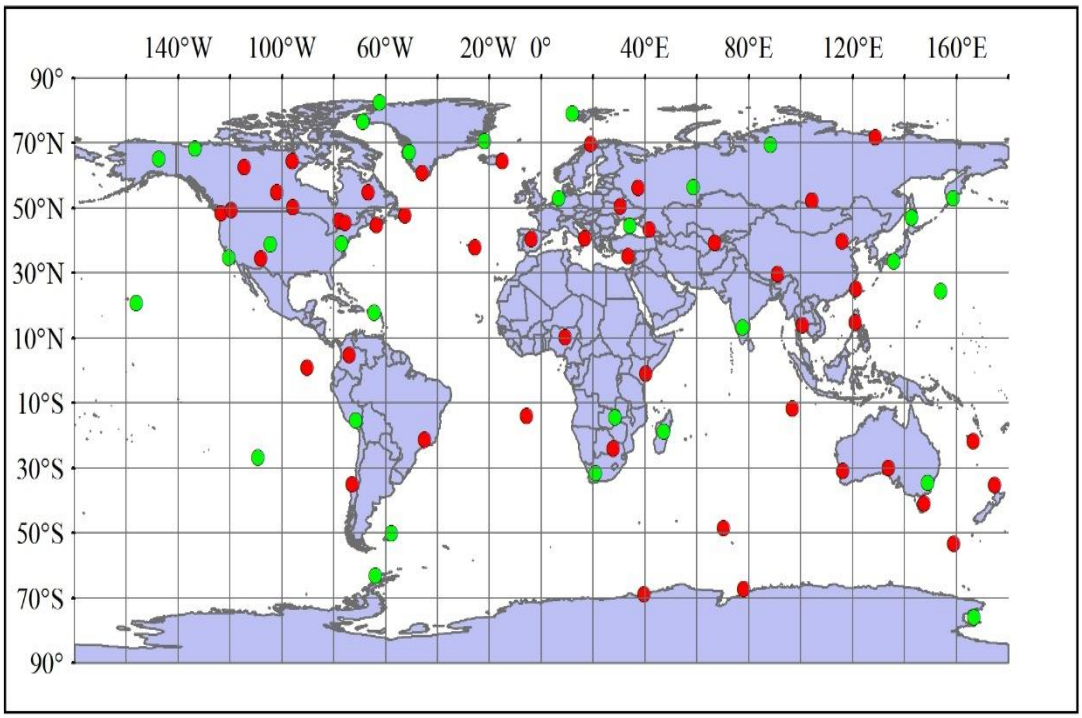


Figure 6-22 EMX precise products station distribution (GPS only green; GPS+GLO red), on DOY 12, 2014

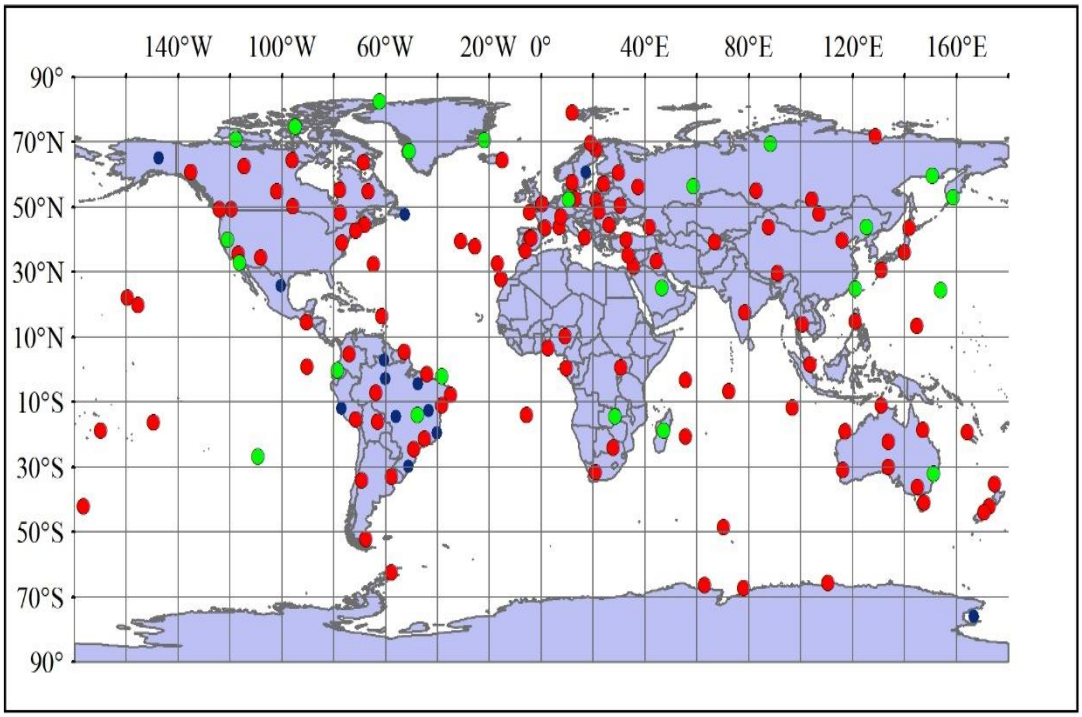


Figure 6-23 ESA precise products station distribution (GPS only green; GPS+GLO red, unknown: blue) on DOY 12, 2014

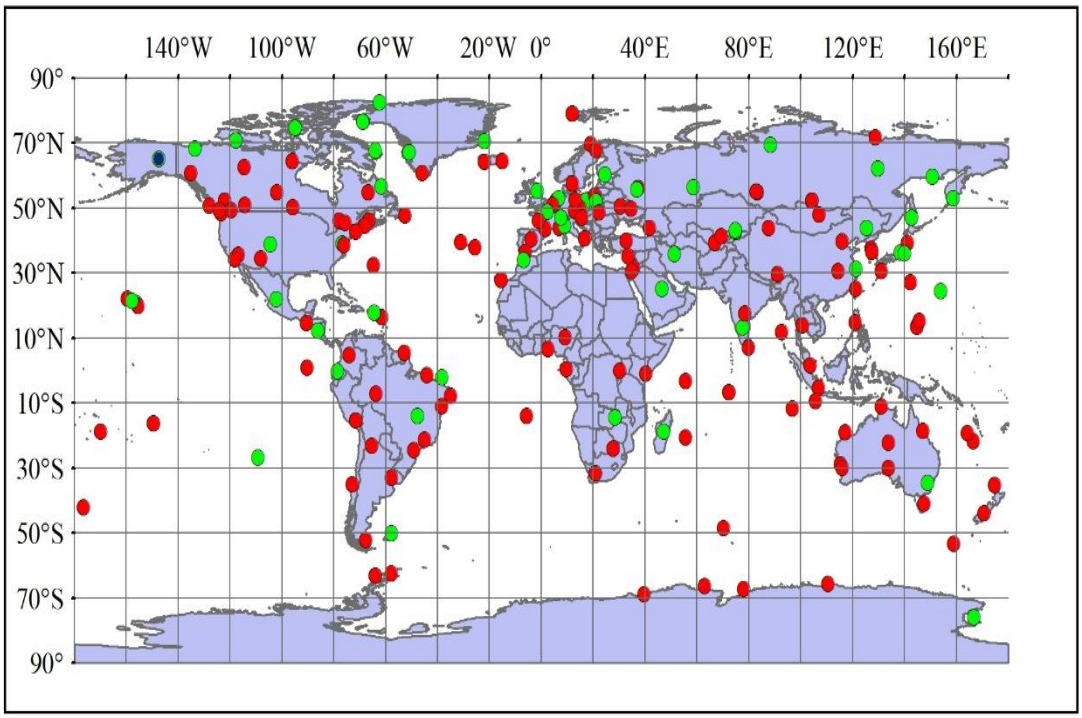


Figure 6-24 GFZ precise products station distribution (GPS only green; GPS+GLO red, unknown: blue) on DOY 12, 2014

3. Epoch-by-Epoch transformation parameters

The precise products are being produced on a daily basis, with the number of stations that are forming the network constant for that day. Therefore, it is interesting to test if the transformation parameters are the same from epoch-to-epoch and this was conducted for DOY 12-18, 2014 for the EMX, ESA and GFZ precise products, with the transformation parameters are summarized in Figure 6-25.

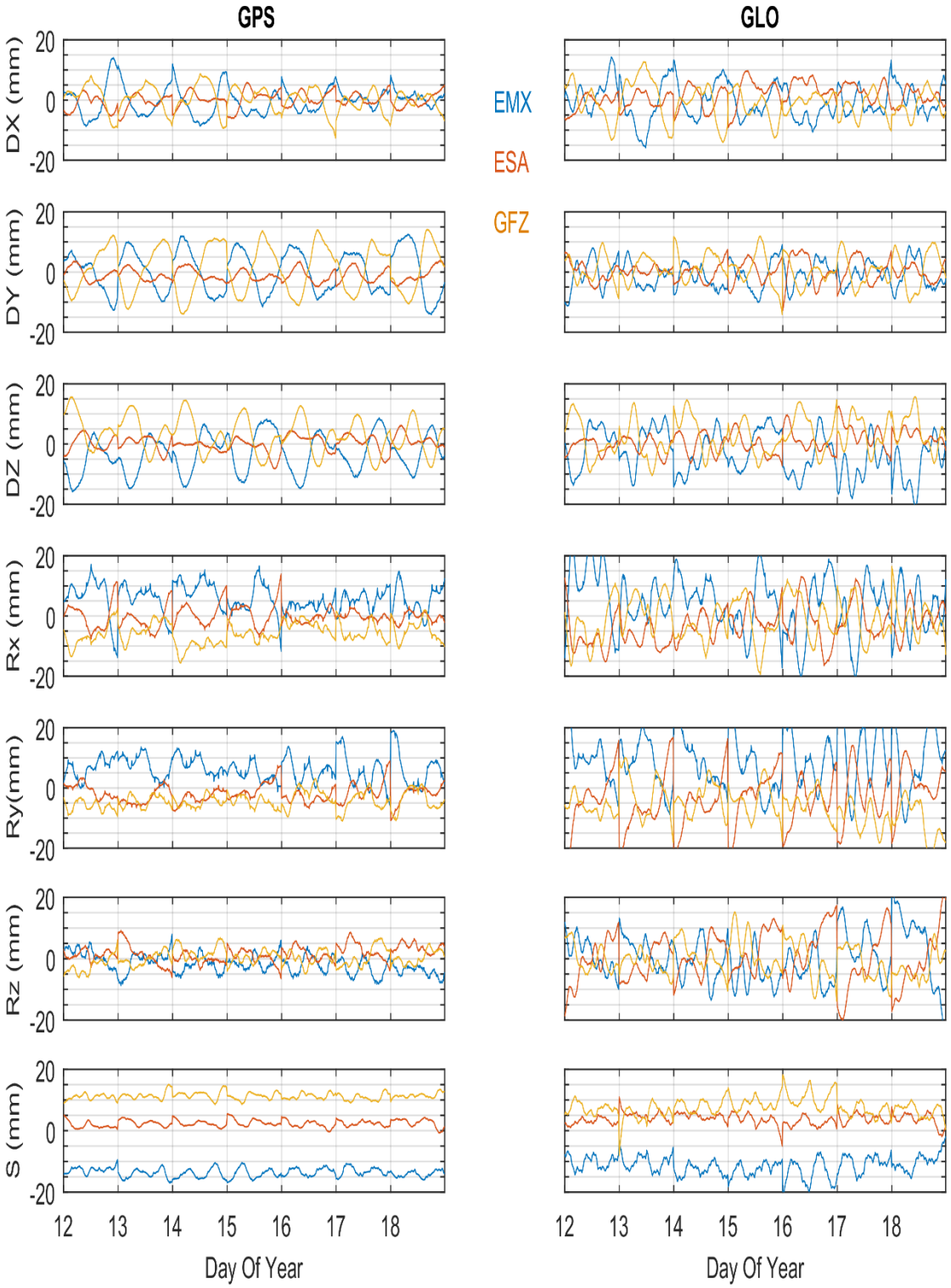


Figure 6-25 Epoch-by-epoch seven parameter Helmert transformation parameters for the EMX, ESA and GFZ precise products on DOY 12-18, 2014

It can be concluded from Figure 6-25 that apart from the scale parameter, the other parameters vary significantly from day to day and within a day. Whereas, the

scale parameter is more stable for the GPS constellation and slightly less stable in the GLO case. This again reflects the network geometry used and the effect of the additional GPS stations that are not available when creating the GLO precise products.

6.7 Chapter Summary

This chapter presents the author's PPP strategy, with details of the modifications that have been done by the author to the POINT software. In terms of PPP accuracy and precision an initial investigation using one-year of data for two stations was presented followed by an extended experiment. It was concluded that PPP can achieve similar accuracy and precision as the GDD in terms of station coordinates. Most interesting was the capability of PPP GLO to produce similar accuracy and precision to both PPP GPS and GDD GPS. This implies that PPP GLO can be used as an independent solution to PPP GPS for station coordinate estimation, rather than being used as increasing observations for the base GPS in PPP GPS+GLO, although PPP GPS+GLO does represent a balance between the PPP GPS and PPP GLO solutions. On closer inspection, it was found that there were noticeable biases between the PPP and the GDD station coordinates station coordinates in the North component. It was also found that these biases are system-dependent, and that the PPP GLO will be affected more than the PPP GPS, while the PPP GPS+GLO will be a balance between both constellations.

The second part of this chapter was an analysis of the precise products from three different analysis centres, as well as their effect on PPP solutions. Firstly, the receiver clock offsets in PPP were shown to be affected by the chosen reference station (time base) which leads to a propagated time offset in all of the estimated satellite clock offsets. However, even though this propagated time offset can reach hundreds of nanoseconds, it can be dealt with if the receiver clock offset is modelled correctly and is allowed to change in order to absorb this effect.

For the station coordinate components, it was found that different precise product satellite coordinate have an effect on the station coordinates at the millimetre level in PPP. It was also found that, it is the number of reference stations and the network geometry used in producing the precise products that affects the satellite

coordinates and leads to slightly more stable GPS orbits than GLO orbits with the reference networks used in 2014.

Chapter 7. Tropospheric Analysis with an alternative strategy for estimating tropospheric Zenith Total Delay from Precise Point Positioning

One of the major sources of error affecting the Precise Point Positioning (PPP) is the tropospheric delay of the GNSS signals. This is the delay of the signals as they propagate between the satellites and the user receiver, which is caused by the increased density of the troposphere. The delay is typically divided into wet and hydrostatic components. The total delay in the vertical direction above the receiver is referred to as the tropospheric zenith total delay (ZTD), which is related to the individual slant delays using an appropriate mapping function. The tropospheric zenith wet delay (ZWD) can then be computed by simple subtraction of the tropospheric zenith hydrostatic delay (ZHD) from the tropospheric ZTD.

This topic has been covered by many researchers using different strategies from the PPP point of view. However, conventional strategies have their limitations. Thus, a new strategy for estimating the tropospheric ZTD is presented in this chapter with its validation.

This chapter summarizes the accuracy of available tropospheric models as well as the conventional strategy. Then, the proposed alternative strategy for tropospheric estimation from PPP is presented, together with its validation over time, different stations, different constellations and various products, when compared to the estimated Global Double-Difference (GDD) tropospheric ZTD. A validation using real-time products is also presented.

It is important to mention that the results in this chapter are presented in a progressive manner, with progressively expanded data sets used in initial tests (~ 85 OSGB stations in the UK over seven weeks for the conventional strategy, 3 OSGB stations over 24 hours for the alternative strategy, 56 OSGB stations in the UK over

seven consecutive days using all PPP scenarios and the alternative strategy), further test (~85 OSGB stations in the UK over seven weeks using all PPP scenarios and the alternative strategy, and 22 OSGB stations in the UK over one year using all PPP scenarios and the alternative strategy), and then for the final test (~76 IGS stations over 12 weeks using PPP GPS and the alternative strategy, with final and real-time precise products).

7.1 Conventional tropospheric strategies used in PPP

For estimating the ZTD from the PPP there are two conventional strategies; using a model for the tropospheric ZTD and using a model for the tropospheric ZHD while estimating the tropospheric ZWD with other unknowns.

7.1.1 Using a model for the tropospheric zenith total delay

To account for the tropospheric ZTD from the PPP, four tropospheric models (Section 3.3.3.1) were tested using the same dataset that had been used for the PPP assessment in Chapter 6. A comparison between the four models for a 24-hour period with a 30-second rate was carried out.

Each of the available tropospheric models calculate a constant value for the day of year (DOY). The four tropospheric models presented in section 3.3.3.1 were tested in order to see their behaviour. The modelled tropospheric ZTD was compared with the estimated tropospheric ZTD from a Global Double Difference (GDD) solution, using a global network of the stations. Figure 7-1 is an example of the comparison of modelled tropospheric ZTD with the estimated tropospheric ZTD_{GDD} for three sample OSGB stations in the UK: DRUM (Drumalbin), FARB (Farnborough), and KEYW (Keyworth) on DOY 12, 2014.

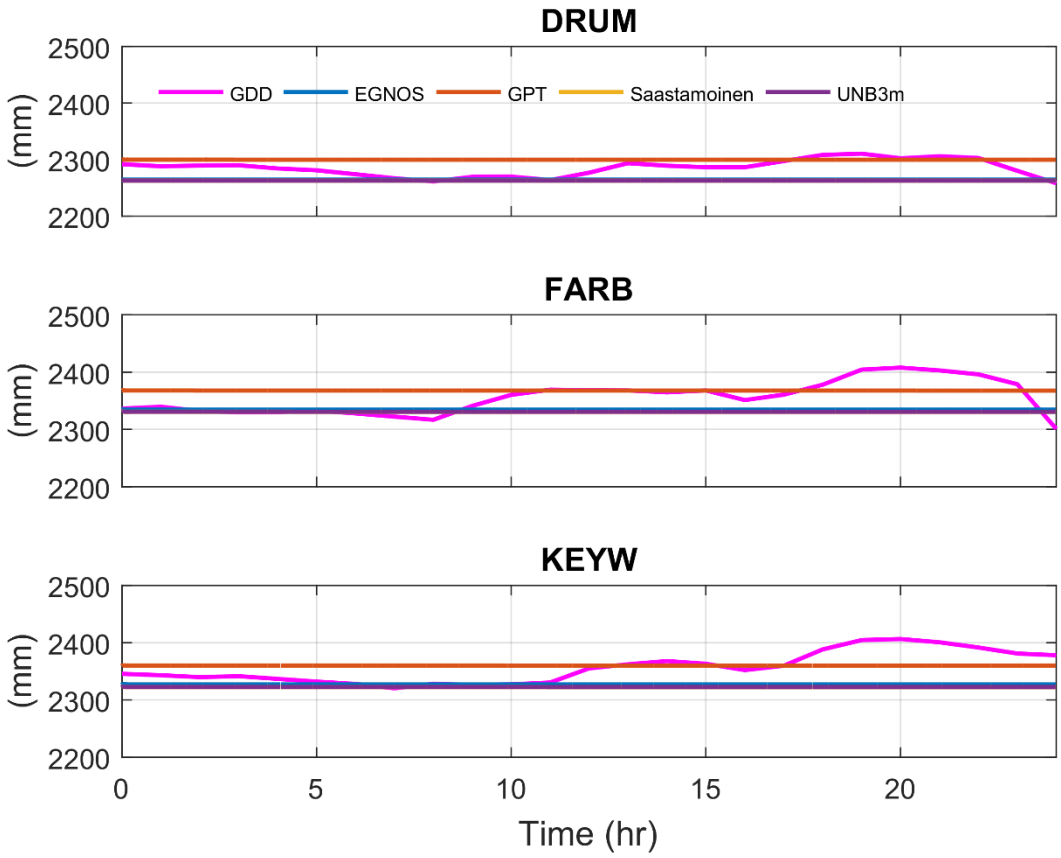


Figure 7-1 Comparison of modelled tropospheric ZTD from four tropospheric models with tropospheric ZTD estimated using GDD

In PPP, any unaccounted tropospheric delay will propagate into the station's coordinates (mainly Up component) and the estimated receiver clock offsets. The differences between the estimated PPP GPS coordinates when using the models and the '*truth*' coordinates from GDD GPS are summarized in Table 7-1.

Table 7-1 Different PPP GPS and solutions for (DRUM, FARB and KEYW) using four models of tropospheric ZTD

Tropospheric Model and Mapping Function	Station	3D (mm)	dE (mm)	dN (mm)	dU (mm)
Saastamoinen with NMF	DRUM	143.1	-4.3	-0.1	143.1
	FARB	159.8	-9.0	4.2	159.5
	KEYW	146.6	-14.9	1.1	145.8
UNB3 with NMF	DRUM	119.6	-1.3	3.7	119.6
	FARB	122.5	-4.4	3.1	122.4
	KEYW	109.5	-4.0	3.9	109.4
GPT with NMF	DRUM	124.7	0.6	2.5	124.6
	FARB	117.3	-5.1	4.0	117.1
	KEYW	110.1	-3.7	3.9	110.0
EGNOS with NMF	DRUM	145.9	-4.7	-0.3	145.8
	FARB	149.1	-8.5	4.3	148.8
	KEYW	141.6	-13.0	1.5	141.0

From Table 7-1, it can be seen that the errors in the station coordinates are mainly in Up component, arising from the unreliable modelling of the ZTD and the un-mitigated tropospheric ZWD propagating into the Up component when using this strategy.

7.1.2 Using a model for the hydrostatic component and estimating the wet component with the other unknowns

To account for the unmitigated ZWD a conventional for PPP is to use a model for the tropospheric ZHD and estimate the tropospheric ZWD along with other unknowns. Many researches have adopted this strategy, which is based on the assumption that the estimated tropospheric ZWD will absorb not only the non-hydrostatic component

(wet delay), but also correct for any errors in the modelled hydrostatic component. Four tropospheric models (Section 3.3.3.1) were used, and to assess their reliability and the obtained tropospheric ZTD accuracy the same dataset (see Section 5.6) was used. The PPP strategy is the same as in Table 6-1 except that the four different tropospheric models were used. To analyse the accuracy of the station coordinates in the PPP solution, the RMS of the daily differences of station coordinates from PPP and GDD GPS for all coordinate components were computed for a 7-week data set and for all scenarios using the PPP GPS, PPP GLO and PPP GPS+GLO. For the assessment of the accuracy of the tropospheric ZTD, the daily differences between the ZTD_{PPP} and the common epochs from the ZTD_{GDD}, which is determined every 1 hour, (ZTD_{PPP}-ZTD_{GDD}), was computed with an overall mean and RMS, as detailed in Table 7-2.

Table 7-2 RMS of the daily differences between PPP GPS, PPP GLO, PPP GPS+GLO and GDD GPS station coordinates and tropospheric ZTD using four models of tropospheric ZHD while solving for the tropospheric ZWD

Tropospheric Model and Mapping Function	Daily station coordinate differences (RMS) (mm)			Tropospheric ZTD differences (mm)		
	E	N	U	Mean	STD	RMS
GPS						
UNB3m with NMF	3.7	3.1	7.5	45.8	9.9	46.8
GPT with NMF	3.7	3.2	7.1	75.7	7.7	76.1
Saastamoinen with NMF	3.6	3.1	7.6	58.3	17.3	60.8
EGNOS with NMF	3.6	3.1	7.5	58.4	16.0	60.6
GLO						
UNB3m with NMF	3.7	4.9	11.5	44.5	11.1	45.9
GPT with NMF	3.7	4.9	12.7	75.0	8.7	75.5
Saastamoinen with NMF	3.7	4.9	10.7	57.0	18.9	60.1
EGNOS with NMF	3.7	4.9	10.8	57.2	17.8	59.8
GPS+GLO						
UNB3m with NMF	3.6	3.9	8.3	44.9	10.5	46.1
GPT with NMF	3.7	3.9	8.6	74.5	8.0	74.9
Saastamoinen with NMF	3.8	4.0	7.8	57.5	17.8	60.1
EGNOS with NMF	3.7	3.9	7.9	57.1	16.2	59.4

It can be seen from Table 7-2 that the estimated station coordinates from all the PPP scenarios are at a very good level of millimetre accuracy. However, the estimated tropospheric ZTD_{PPP} are further from the estimated tropospheric ZTD_{GDD}. These differences in tropospheric ZTD are consistent with the findings of Li et al. (2012) who quoted RMS differences of 5.4, 5 and 4 cm for EGNOS, UNB3m and IGGtrop respectively, and Pace et al. (2010) who quoted residuals in the order of 50-100 mm (as introduced in 2.3).

Even though Zhang and Gao (2001) mentioned that the consistency of the station coordinates could reflect the quality of the troposphere ZTD estimates, the results in Table 7-2 show that this is not entirely true in the PPP scenarios, where large differences in tropospheric ZTD are not always reflected as larger differences in height and vice-versa. Figure 7-2 is an example for the comparison of the PPP GPS estimated tropospheric ZTD using this strategy with the GDD GPS estimated tropospheric ZTD for DRUM, FARB and KEYW, respectively.

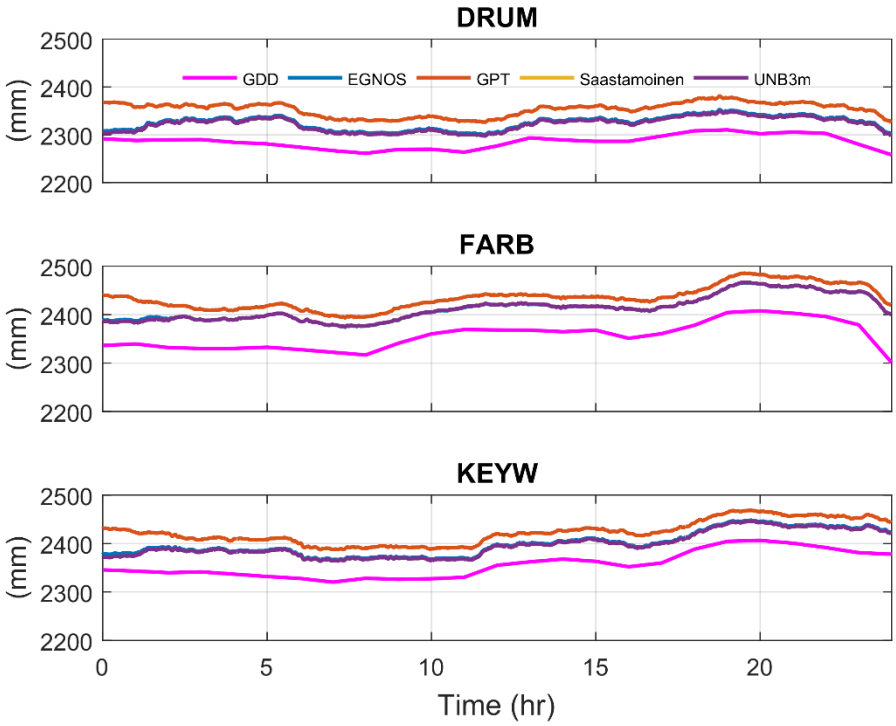


Figure 7-2 Comparison of tropospheric ZTD from GDD GPS and PPP GPS using four tropospheric models of tropospheric ZHD and estimating tropospheric ZWD

Referring back to Figure 7-1, some epochs for the tropospheric ZTD_{GDD} were clearly higher than the value of the tropospheric ZTD_{PPP}. This is clearly not the case in Figure 7-2 where the tropospheric ZTD_{PPP} are always above the tropospheric ZTD_{GDD}.

It can be seen that apart from GPT, the other three have the same performance as each other. Furthermore, the estimated tropospheric ZTD_{PPP} clearly reflects similar temporal variations of the troposphere compared to the estimated tropospheric ZTD_{GDD}. However, the offsets could reflect the uncertainty of the tropospheric ZHD calculated from the tropospheric models and this could affect the long-term repeatability of the estimated station height, as well as affecting the estimated receiver clock offset and ambiguities.

Therefore, there is scope for an alternative strategy for tropospheric estimation in PPP.

7.2 An alternative strategy for estimating tropospheric zenith total delay using PPP

Conventionally in PPP the tropospheric ZTD can be modelled as the hydrostatic part (tropospheric ZHD) and estimated as non-hydrostatic part (tropospheric ZWD). The models that are used rely on meteorological data that should be available in order to form the tropospheric ZHD. These meteorological data should be used from the metrological sensors that are available from the site of observation. However, not all stations are equipped with meteorological sensors, and so rely on meteorological data that are from a meteorological sensor that is nearest to the receiver's station. In this case, the meteorological data will not necessarily reflect the actual weather for that particular site. Therefore, a degradation in the accuracy of the modelled tropospheric ZHD will arise, and this degradation will affect the other part of the troposphere that is the tropospheric ZWD. Hence, it will produce an unreal estimation for the tropospheric ZWD because it will be contaminated with the errors in the tropospheric ZHD.

In other cases the model for computing the tropospheric ZHD will use lookup tables or some assumptions for the meteorological data as standard pressure and temperature (SPT) or global pressure and temperature (GPT). In these cases, the situation will be worse than the previous case as even though these assumptions may be relying on years of meteorological data, they will not accurately reflect the actual elements needed for the tropospheric ZHD.

Estimated station height and tropospheric ZTD values in the GPS analysis will then be corrupted due to not using accurate surface pressure as mentioned by Tregoning and Herring (2006). They also mention that accurate results should come from an accurate tropospheric ZHD. Therefore, to reach a better estimation of the tropospheric ZTD, an alternative strategy is proposed in this research (see Sections 3.3.3.4.1 and 3.3.3.4.2).

A modification was done inside the POINT software to give the ability for changing the tropospheric options. It contains a condition for dealing with different

models of tropospheric ZHD and the potential to include the tropospheric ZWD or not as a part of the estimation process, in addition to a completely new implementation inside the software for the alternative strategy. The alternative strategy adds a further condition for estimating both the tropospheric ZHD and the tropospheric ZWD as unknowns. Thus, implementation of the alternative strategy contains implementing the partial of the tropospheric ZHD in the design matrix for the Extended Kalman Filter (EKF), as well as the observable matrix, with the process noise accounting for the tropospheric ZHD. In addition, the implementation of the observed minus computed was also done with the capability of using the conventional or proposed new. It also contains the standard deviation to be fed inside the covariance matrix, as well as the initial value for both the tropospheric ZHD and the tropospheric ZWD to enable the EKF to start the estimation, in addition to updating the covariance matrix of the EKF over time with a computation for extracting the tropospheric slant total delay to be used for each satellite at each epoch.

Table 7-3 Extended Kalman Filter configurations for the PPP using the alternative tropospheric strategy

State	Initial value	Initial standard deviation	Process noise standard deviation
X	Based on the least squares solution	1,000 m	0.000001 $\frac{m}{\sqrt{s}}$ the X component
Y	Based on the least squares solution	1,000 m	0.000001 $\frac{m}{\sqrt{s}}$ the Y component
Z	Based on the least squares solution	1,000 m	0.000001 $\frac{m}{\sqrt{s}}$ the Z component
Receiver clock error	Based on EKF	1,000 m	100 $\frac{m}{\sqrt{s}}$
Tropospheric Hydrostatic delay	2.2 m	0.1m	10^{-5} $\frac{m}{\sqrt{s}}$
Tropospheric wet delay	0.1 m	0.1m	$3*10^{-5}$ $\frac{m}{\sqrt{s}}$
Troposphere gradient G_N	0	0.001m	$3.1667 * 10^{-6}$ $\frac{m}{\sqrt{s}}$
Troposphere gradient G_E	0	0.001m	$3.1667 * 10^{-6}$ $\frac{m}{\sqrt{s}}$
Carrier phase ambiguities	Based on the estimated range	1,000 cycles	0

7.2.1 Initial Test

For the initial test, the same three OSGB stations (DRUM, FARB and KEYW) that were used in section 7.1.1 were used for testing the alternative tropospheric strategy following the EKF configuration as summarized in Table 7-3. The difference in the station coordinates from the PPP GPS and the GDD GPS are summarized in Table 7-4.

Table 7-4 PPP GPS solution (three stations) using the alternative tropospheric strategy

Tropospheric Model	Station	3D (mm)	dE (mm)	dN (mm)	dU (mm)
The alternative strategy	DRUM	2.5	-0.7	1.8	-1.7
	FARB	13.0	-1.9	0.9	-12.8
	KEYW	5.4	-5.0	-1.0	1.6

A comparison of the tropospheric ZTD between the PPP GPS and the GDD GPS is also shown for the three stations in Figure 7-3.

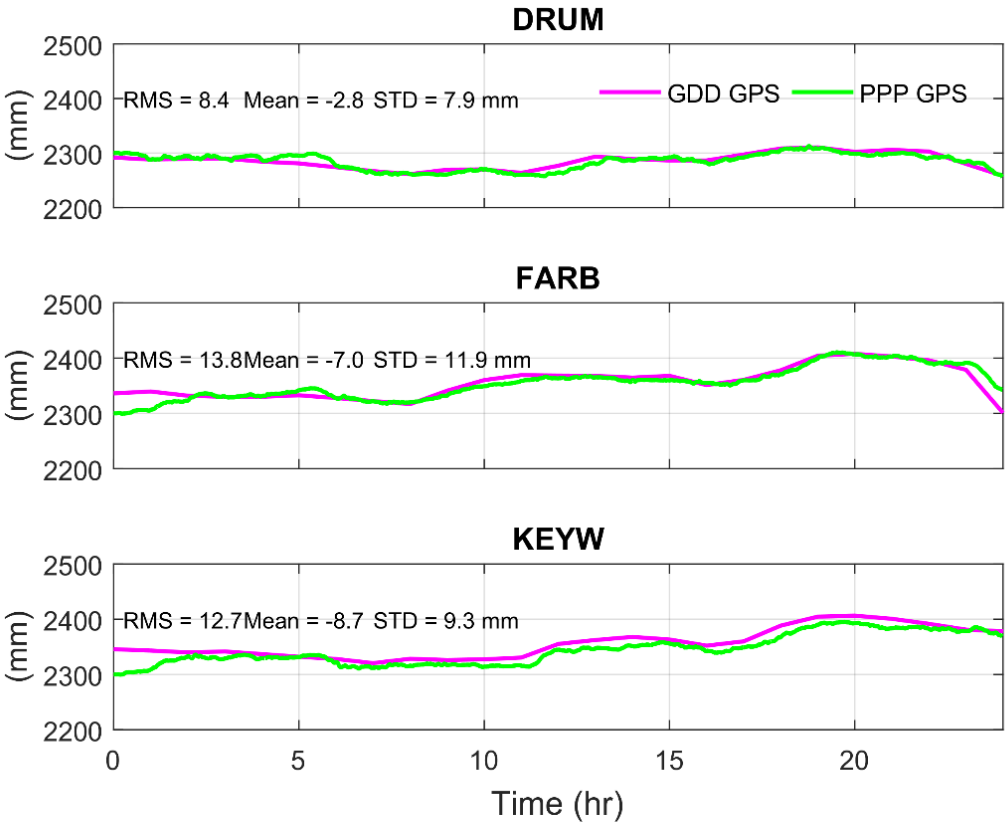


Figure 7-3 Comparison of tropospheric ZTD using PPP GPS with the alternative tropospheric and GDD GPS strategy for three OSGB stations on DOY 12, 2014

It is evident from Figure 7-3 that the tropospheric ZTD from PPP GPS with the alternative tropospheric strategy matches the GDD GPS tropospheric ZTD very closely. This alternative tropospheric strategy gives a tropospheric ZTD without using a model or any real or modelled meteorological data. Moreover, the estimated tropospheric ZTD using the alternative tropospheric strategy depends on the observation rate, which means it can give results at higher rate. In this case, the observation rate was 30 seconds, which means the PPP GPS tropospheric ZTD is available every 30 seconds, as oppose to every hour for GDD GPS.

7.2.2 The correlation between the estimated ZTD and other estimated states

It is important to figure out why the conventional tropospheric strategy in Section 7.1.2 is not sufficient for estimating an accurate tropospheric ZTD from PPP. To investigate that, there is a need to look at the other estimated states from both

scenarios (the conventional and the alternative tropospheric strategies). Figure 7-4, represents the difference between the estimated carrier phase receiver clock offsets when using the conventional and alternative tropospheric strategies.

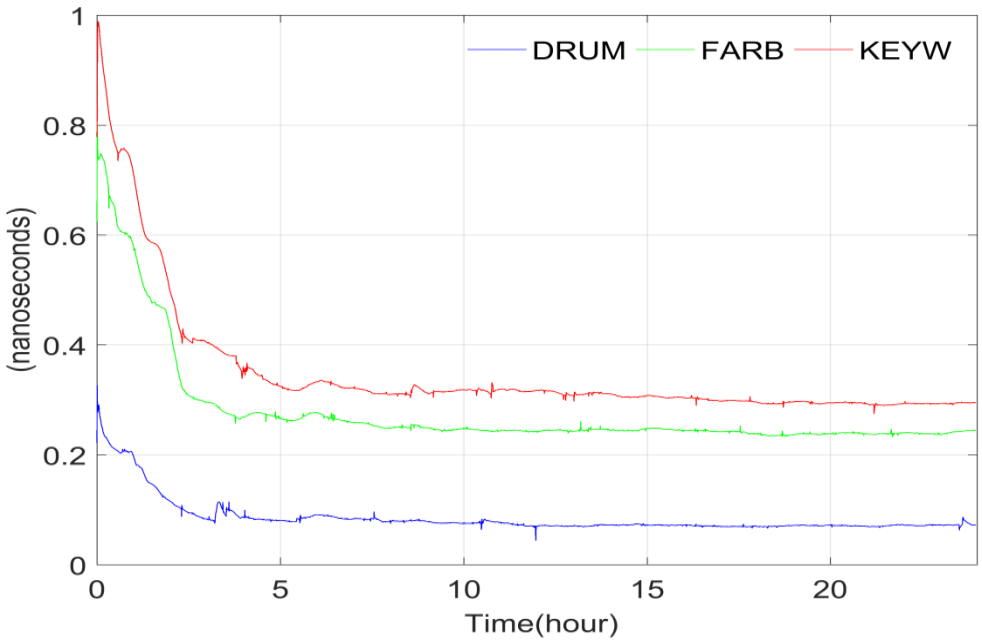


Figure 7-4 The difference between the estimated phase receiver clock offsets for PPP GPS when using the alternative and the conventional tropospheric strategies

From Figure 7-4, it can be concluded that part of the un-mitigated tropospheric ZTD is being absorbed by the receiver clock offsets when using the conventional tropospheric strategy (~0.3 nanosecond equal to ~ 9 cm). This is when the PPP is using the decoupled clock model. It was also found that the affected receiver clock offsets will be the phase receiver clock offsets, with a smaller seen on the code receiver clock offsets (see Figure 7-5).

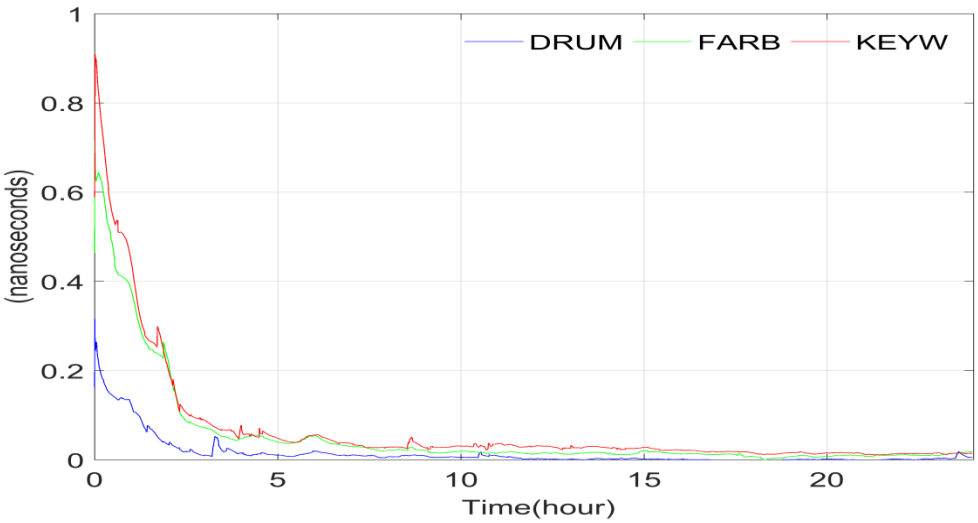


Figure 7-5 The difference between the estimated code receiver clock offsets for PPP GPS when using the alternative and the conventional tropospheric strategies

In contrast, if the PPP is not using the decoupled clock model, it was found that the major effect will be to corrupt the ambiguities, which could because the noise standard deviation that was given to the phase observable is much lower than the noise standard deviation that was given to the code observable.

To see how the ionosphere-free ambiguities are affected by the un-mitigated tropospheric ZHD in the conventional tropospheric strategy, results are shown in Figure 7-6.

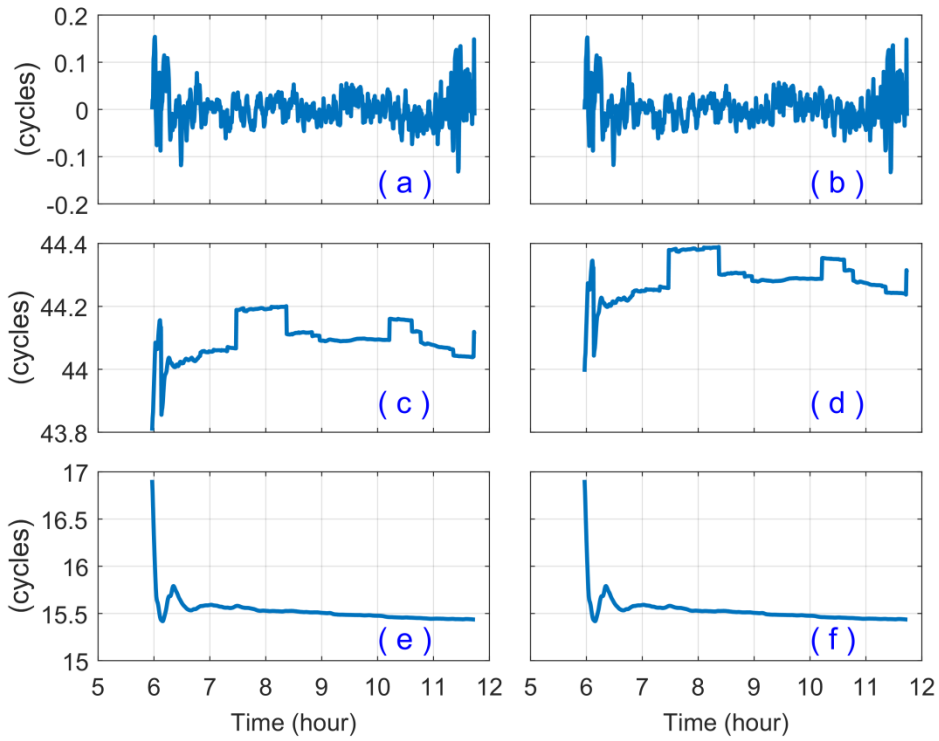


Figure 7-6 Comparison of phase residuals (top), ionosphere-free-ambiguities (middle) and widelane ambiguities (bottom) for PPP GPS when using the conventional tropospheric strategy (left) and the alternative tropospheric strategy (right)

Figure 7-6 shows an example of the phase residuals, the estimated ionosphere-free ambiguity and the widelane ambiguity for satellite PRN 11 at DRUM station when using the conventional and alternative tropospheric strategies in PPP GPS. It can be seen that there is no effect on the phase residuals or the widelane ambiguity. However, it can be seen that in addition to a link between the un-mitigated tropospheric ZTD and the receiver clock offsets, the ionosphere-free ambiguity is also linked. In PPP applications that use ambiguity fixing, an error in the ionosphere-free ambiguity, caused by an un-mitigated tropospheric ZTD could lead to incorrect fixed ambiguities, and hence, incorrect station coordinates in a fixed solution. This is because narrow lane ambiguities are computed from the non-integer ionosphere-free ambiguities and the integer-valued widelane ambiguities. In this research, therefore, in order to better compare the conventional and alternative tropospheric strategies

the ambiguities were not resolved and the solution was float not fixed (Section 3.7). This approach could be taken to agree with the suggestion of Douša (2009) who concluded that the error impact on ZTD depends on the compensation ability of ambiguities and receiver clock offsets in PPP. Furthermore, although Shi and Gao (2012) suggested that the tropospheric ZTD can be improved from 30.1 mm to 17.0 mm by applying ambiguity resolution, Li et al. (2014b) concluded that no significant difference in the tropospheric ZTD between PPP GPS float and fixed solutions remains after a sufficiently long time of convergence, and the effect of fixing the ambiguities will only improve the tropospheric ZTD for the first hour (as introduced in 2.3).

7.3 Validating the alternative tropospheric strategy

To test the reliability of the alternative strategy for tropospheric estimation, there is a need to conduct reasonable validations. All the following validations were conducted using OSGB or IGS stations in the GDD GPS solutions as a reference value for the comparison. In theory, the tropospheric ZTD from the GDD GPS represents a 'truth' value for the tropospheric delay. The reason is that it was computed using a network of stations capable of estimating tropospheric ZHD and ZWD between stations.

The validations were conducted using 7 consecutive days and regional validations at 56 OSGB stations using the PPP GPS, PPP GLO and the PPP GPS+GLO. Further, a long-term validation was also conducted using 22 OSGB stations for one year and using IGS stations.

7.3.1 PPP GPS validation

7.3.1.1 Seven consecutive days validation using PPP GPS

To validate the alternative troposphelric strategy, it is important to test it over consecutive days to evaluate its ability to provide an accurate tropospheric ZTD. It is also interesting to use zero values for initializing the tropospheric ZHD and ZWD in PPP to test if the alternative tropospheric strategy with the used mapping functions is

capable of providing an accurate tropospheric ZTD independent of the initial values. Therefore, this strategy was tested using 56 OSGB stations for seven consecutive days (one continuous solution not 7 x daily solutions) on DOY 12-18, 2014 (GPS week 1775) starting with zero initial values for tropospheric ZHD and ZWD.

The 56 OSGB stations were as shown in Figure 5-2 and were chosen to check the stability of the alternative tropospheric strategy with the variation of the troposphere during the seven days. The data rate was 30 seconds, which means that the tropospheric ZTD can be estimated every 30 seconds from the PPP scenarios.

Figure 7-7 is a sample comparison for station ASAP taken from those 56 OSGB stations (graphs for each station are given in Appendix-D). The degree of consistency between the estimated tropospheric ZTD from PPP GPS using the alternative tropospheric strategy and the tropospheric ZTD derived from the GDD GPS can be clearly seen and the results are summarized in Table 7-5 for the 56 OSGB stations dataset.

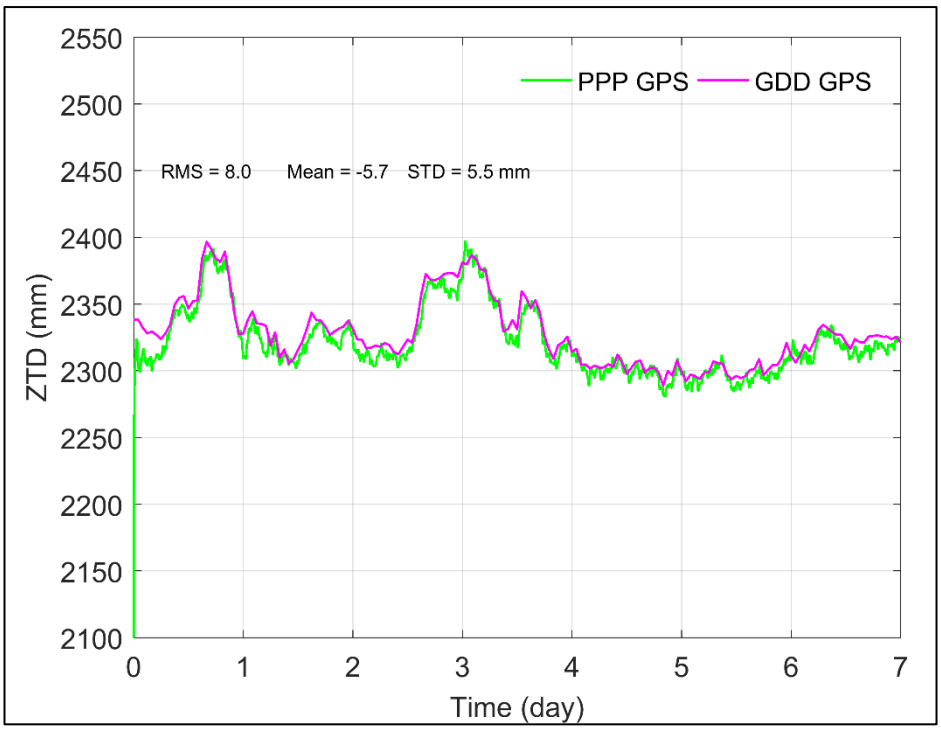


Figure 7-7 Comparison of tropospheric ZTD from GDD GPS and PPP GPS for ASAP station over seven consecutive days

Table 7-5 The difference between the estimated station coordinates and tropospheric ZTD from PPP GPS and GDD GPS for 56 OSGB staptions over seven consecutive days

Daily variation (RMS) (mm)			Tropospheric difference (mm)		
E	**N**	**U**	**Mean**	**STD**	**RMS**
1.9	1.6	14.1	-6.3	5.8	8.5

It is evident from Figure 7-7 that the tropospheric ZTD using PPP GPS, which comes from the estimated tropospheric ZHD and ZWD, agrees strongly with the tropospheric ZTD from the GDD GPS. This alternative tropospheric strategy achieves this without using a model or any assumptions, nor any meteorological data.

The selection of the initial zero values for the tropospheric ZHD and ZWD was performed so as to establish whether the estimated values would converge to the

"*truth*" tropospheric ZTD value, which in this case was taken as the tropospheric ZTD obtained from the GDD GPS. In practice, as this will affect the convergence time, it is possible to choose suitable initial values, and thus for future processing, more realistic initial values will be used. This approach also confirmed the suitability of the selected Niell mapping functions (section 3.3.3.2 Niell (1996)) used throughout this research, as well as the values selected for the process noise in the PPP GPS. Although, it is recognised that the systematic biases and annual errors of NMF could have been reduced with use of the Global Mapping Functions (GMF) as suggested by Boehm et al. (2006a).

7.3.1.2 Regional Validation using PPP GPS

To further evaluate the alternative troposphelric processing strategy, it was important to process the same data set that had previously been processed when assessing the different tropospheric models. They are the same seven weeks as in Table 5-5 that were chosen for producing the tropospheric ZTD from the PPP GPS (see Appendix-B).

To analyse the accuracy of the PPP GPS solution, the RMS values of the daily differences from the GDD GPS solution for all station coordinate components were computed for the 7-week data set. For the assessment of the accuracy of the determination of the tropospheric ZTD, the daily mean of the differences between the GDD ZTD (ZTD_{GDD}), which is estimated every 1 hour, and the common epochs from the PPP ZTD (ZTD_{PPP}) which is estimated every 30 seconds, were computed ($ZTD_{PPP} - ZTD_{GDD}$) with the overall mean and overall RMS, as detailed in Table 7-6 (for each station's coordinate and tropospheric ZTD statistics see Appendix-E)..

To investigate if there is any effect from different precise products on the estimated tropospheric ZTD using the alternative strategy, the analysis of the accuracy of the tropospheric ZTD has been carried out for the EMX, ESA and GFZ precise products for the same datasets.

Table 7-6 The difference between the estimated station coorldinates and tropospheric ZTD from PPP GPS using three precise products (EMX, ESA and GFZ) for 56 OSGB stations and GPS GDD over seven weeks

Products	Station coordinates variation (RMS)(mm)			Tropospheric ZTD (mm)		
	E	N	U	Mean	STD	RMS
EMX	3.6	3.1	8.3	-2.2	6.1	6.5
ESA	3.0	2.0	10.3	-2.6	6.2	6.7
GFZ	3.3	2.0	11.1	-2.7	6.2	6.8

It is evident from Table 7-6 that the tropospheric ZTD derived from PPP GPS compares well with the values obtained from the GDD GPS. In addition, the consistency of the estimated tropospheric ZTD when using different precise products is also clear. These results are better than Li et al. (2015b), who obtained 12.1 mm RMS and -3.1 mm mean of tropospheric ZTD for PPP GPS, and in comparison can be considered to be an improvement in the RMS of tropospheric ZTD of 53.7% 55.4% and 56.2% for EMX, ESA and GFZ respectively. These results are also comparable with Bock et al. (2016) who obtained ±3mm mean with standard deviation ranges from 4 to 8 mm (as introduced in section 2.3). Clearly, if it is the case that the tropospheric parameters may absorb the effect of higher order ionospheric terms such as second-order ionospheric delay if the higher order ionospheric corrections are not applied, as suggested by Fritsche et al. (2005), there is also scope for these results to be further improved by including such higher order ionospheric corrections.

In this case, both PPP GPS and GDD GPS are based on the single constellation (GPS). In this context, it is also interesting to compare the estimated tropospheric ZTD from PPP GLO and GDD GPS.

7.3.2 PPP GLO Validation

7.3.2.1 Seven consecutive days validation using PPP GLO

As mentioned before, the GDD GPS results are based on the GPS observations only for producing the tropospheric ZTD. Therefore, to demonstrate the full potential of the alternative tropospheric strategy and its suitability, it is important to see how it will behave with GLO observations, in which the satellite planes are at a different inclination and represent a completely independent solution. Implementations of the alternative tropospheric strategy were, therefore, conducted for PPP GLO to see its capability for estimating the tropospheric ZTD from the same 56 OSGB stations. In the first instance, the same seven consecutive days for GPS week 1775 for the same datasets were processed to produce the tropospheric ZTD from PPP GLO and compare it with the tropospheric ZTD from GDD GPS, again starting with zero initial values for both tropospheric ZHD and ZWD in PPP GLO. The results for ASAP station as a sample of the tropospheric ZTD from PPP GLO are given in Figure 7-8 (graphs for each station are given in Appendix-D), with the daily variation and ZTD statistics summarized in Table 7-7 for all 56 OSGB stations

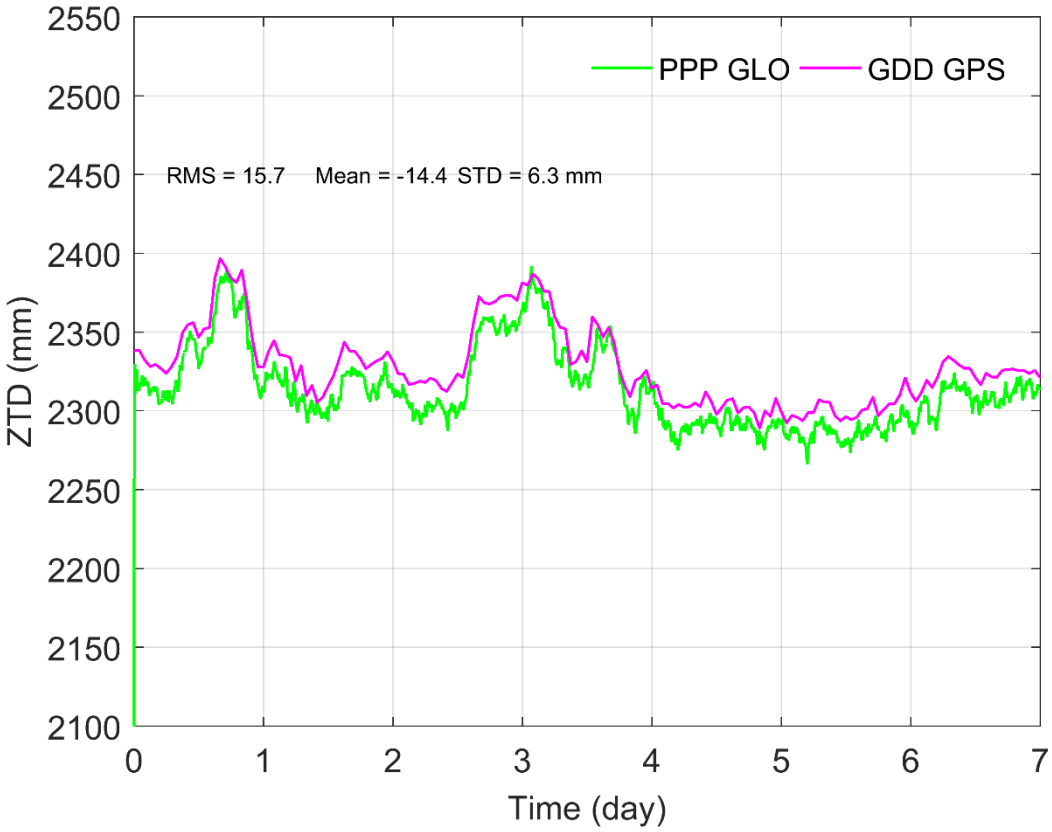


Figure 7-8 Comparison of tropospheric ZTD from GDD GPS and PPP GLO for ASAP station over seven consecutive days

Table 7-7 The difference between the estimated station coordinates and tropospheric ZTD from PPP GLO and GDD GPS for 56 OSGB stations over seven consecutive days

Products	Station coordinates (RMS) (mm)			Tropospheric ZTD (mm)		
	E	N	U	mean	STD	RMS
EMX	3.2	2.2	9.7	-7.7	6.9	10.3

The estimation of the tropospheric ZTD from the PPP GLO alone reflects the suitability of using the alternative tropospheric strategy. This is because the tropospheric ZTD estimation using PPP GLO is completely independent from that using GDD GPS, as the GDD GPS estimation came from the GPS constellation only. It also

comes from a different processing strategy, as well as different frequencies, different precise products and different software.

7.3.2.2 Regional Validation using PPP GLO

To take a step further, the same seven weeks that were processed to produce the tropospheric ZTD from PPP GPS were used here to evaluate the PPP GLO tropospheric ZTD estimation. This was also again done for the three precise products, EMX, ESA and GFZ, as summarized in Table 7-8 (for each station's coordinate and tropospheric ZTD statistics see Appendix-E).

Table 7-8 The difference between the estimated station coordinates and tropospheric ZTD from PPP GLO using three precise products (EMX, ESA and GFZ) and GDD GPS for 56 OSGB stations over seven weeks

Products	Station coordinates (RMS) (mm)			Tropospheric ZTD (mm)		
	E	N	U	mean	STD	RMS
EMX	3.7	4.8	7.3	-3.5	6.4	7.3
ESA	3.3	3.9	11.0	-4.7	7.1	8.5
GFZ	3.2	3.1	6.4	-4.8	6.8	8.1

Table 7-8 gives another indication of the suitability for using the alternative tropospheric strategy. At this level of accuracy for both station coordinate components and tropospheric ZTD, it can be seen that PPP GLO can give an independent check for the alternative strategy. In addition, this gives the potential for PPP users to create two solutions for the same station, instead of one solution of PPP GPS or PPP GPS+GLO.

Although Ding et al. (2017) concluded that PPP GPS is better than PPP GLO for tropospheric ZTD estimation, and Li et al. (2015b) obtained 3.3mm improvement in the RMS of the tropospheric ZTD for PPP GPS over PPP GLO (as introduced in section

2.3), in this research when using the alternative strategy with PPP GLO this leads to RMS values that are similar for PPP GPS and PPP GLO, albeit with PPP GLO being 0.8, 1.8 and 1.3 mm worse than PPP GPS in terms of EMX, ESA and GFZ precise products respectively.

However, it is also interesting to check the combined observations of PPP GPS+GLO using the alternative strategy for estimating the tropospheric ZTD.

7.3.3 PPP GPS+GLO Validation

7.3.3.1 Seven consecutive days validation using PPP GPS+GLO

To evaluate the combination of both constellations, the GPS and GLO, for estimating the tropospheric ZTD, the PPP GPS+GLO was also processed for seven consecutive days with zero initial values for the estimated ZHD and ZWD. Figure 7-9 is an example for ASAP station (graphs for each station are given in Appendix-D), with the daily station coordinate variations and tropospheric ZTD statistics summarized in Table 7-9 for all 56 OSGB stations.

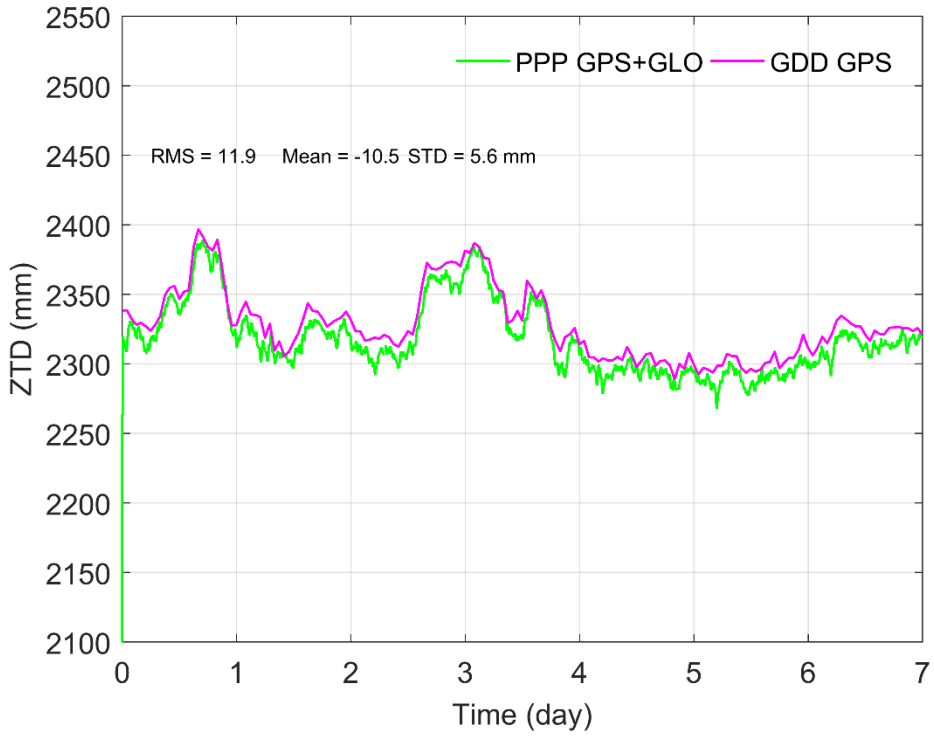


Figure 7-9 Comparison of tropospheric ZTD from GDD GPS and PPP GPS+GLO for ASAP station over seven consecutive days

Table 7-9 The difference between the estimated station coordinates and tropospheric ZTD from PPP GPS+GLO and GDD GPS for 56 OSGB stations over seven consecutive days

Products	Station coordinates (RMS) (mm)			Tropospheric ZTD (mm)		
	E	N	U	mean	STD	RMS
EMX	2.2	1.7	12.8	-6.8	6.0	9.0

7.3.3.2 Regional Validation of the new strategy using PPP GPS+GLO

The same datasets of seven weeks, Table 5-5, that were used for PPP GPS and PPP GLO were also used for producing the tropospheric ZTD from PPP GPS+GLO using three precise products (EMX, ESA and GFZ). Table 7-10 summarizes the daily variations for the station coordinate components and the tropospheric ZTD statistics

for the PPP GPS+GLO scenario (for each station's coordinate and tropospheric ZTD statistics see Appendix-E).

Table 7-10 The difference between the estimated station coordinates and the tropospheric ZTD from PPP GPS+GLO using three precise products (EMX, ESA and GFZ) and GDD GPS for 56 OSGB stations over seven weeks

Products	Station coordinates variation (RMS) (mm)			Tropospheric ZTD (mm)		
	E	N	U	mean	STD	RMS
EMX	3.9	3.9	7.1	-3.9	5.4	6.7
ESA	2.9	3.0	11.0	-5.8	6.5	8.7
GFZ	3.0	2.7	11.7	-6.4	6.5	9.1

Comparing Table 7-10 and Table 7-6, the RMS of the tropospheric ZTD from PPP GPS+GLO are 0.2, 2.0 and 2.3 mm higher than from PPP GPS, when using the precise products of EMX, ESA and GFZ respectively, although there is no significant decrease in the STD when comparing PPP GPS+GLO to PPP GPS. The subtle differences between precise products could be attributed to the different strategies of the ACs (see Appendix-C), where GFZ estimated another parameter for antenna phase centre which will mainly affect the station coordinate Up component and tropospheric ZTD. The results are also similar in their findings to Ding et al. (2017) who concluded that PPP GPS+GLO was not a great improvement over PPP GPS and even made the tropospheric ZTD estimation from some stations worse, and suggested that the reason could be correlated with the different weighting approach that they followed; whereas the weighting approach used for the alternative strategy in this research is the same for both constellations. Nevertheless, when considering their multi-constellation fixed solution, the RMS of the tropospheric ZTD for PPP GPS+GLO found by Ding et al. (2017) was 8mm, which is comparable to that of the PPP GPS+GLO solutions in Table 7-10.

Clearly, with the increasing number of satellites from Galileo (GAL) and BeiDou (BDS) there is potential for further improvement of these results in terms of the mean and RMS of the tropospheric ZTD, as shown by Li et al. (2015b), Lu et al. (2015), Lu et al. (2016) and Lu et al. (2017) (as introduced in 2.3).

7.3.4 Long-term validation

The tropospheric delay varies daily and seasonally. Therefore, it is important to validate the alternative strategy for estimating tropospheric ZTD over a longer term. To achieve this, data from DOY 2 to 365, of 2014, from 22 OSGB stations were used for a complete one-year analysis, of the three PPP scenarios, when using the alternative strategy for tropospheric ZTD estimation. In addition, three precise products (EMX, ESA and GFZ) were also used in this validation.

For each station, the mean and the RMS of the differences between the tropospheric ZTD_{PPP} estimates from the three PPP scenarios (GPS, GLO and GPS+GLO) and tropospheric ZTD_{GDD} from GPS GDD were calculated and are summarised as shown in Figure 7-10 (mean) and Figure 7-11 (RMS), respectively.

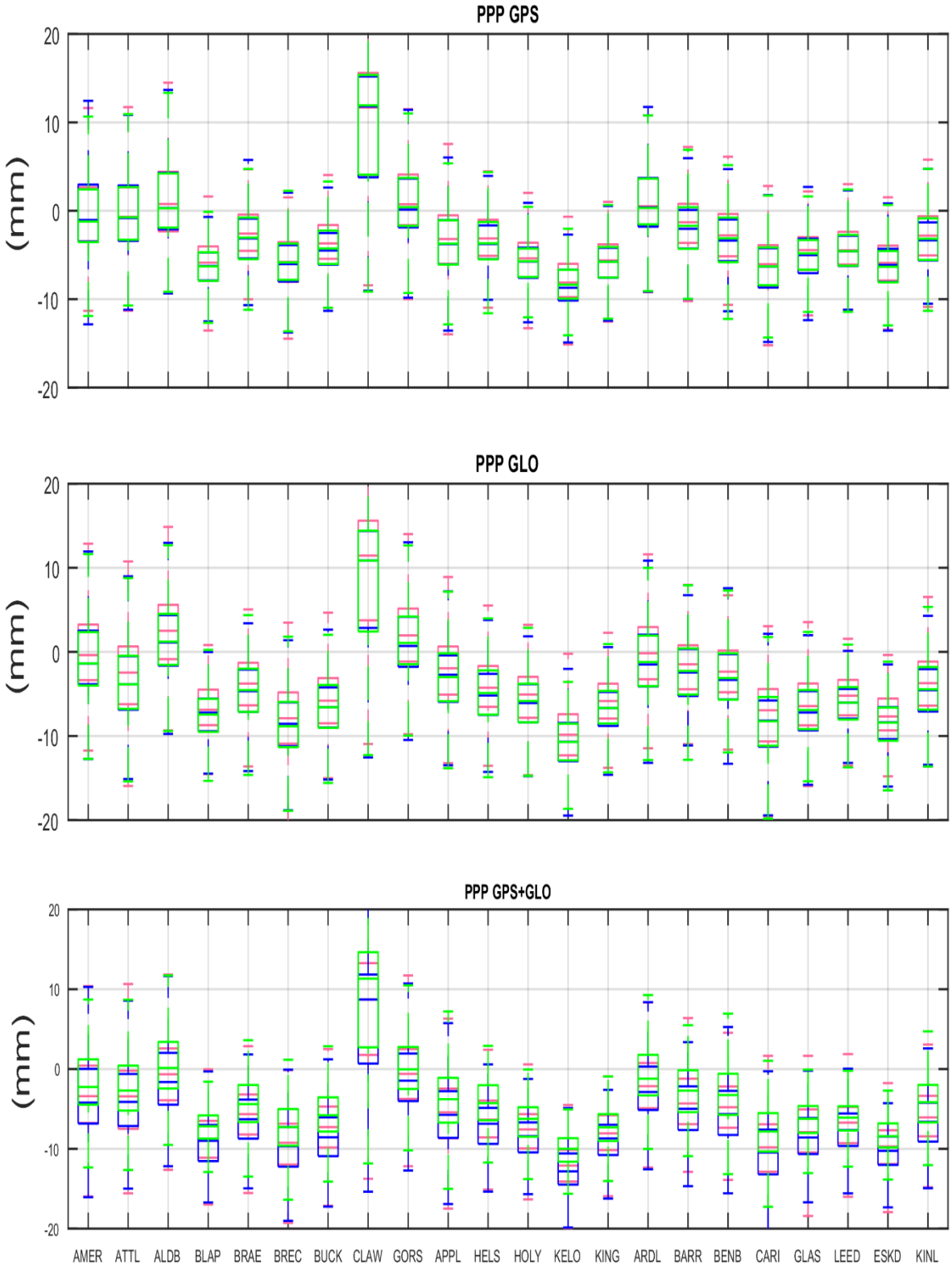


Figure 7-10 The mean statistics between the estimated tropospheric ZTD from PPP GPS PPP GLO and PPP GPS+GLO using three precise products (EMX (pink), ESA (blue) and GFZ (green)) and the estimated tropospheric ZTD from GDD for 22 OSGB stations over one year

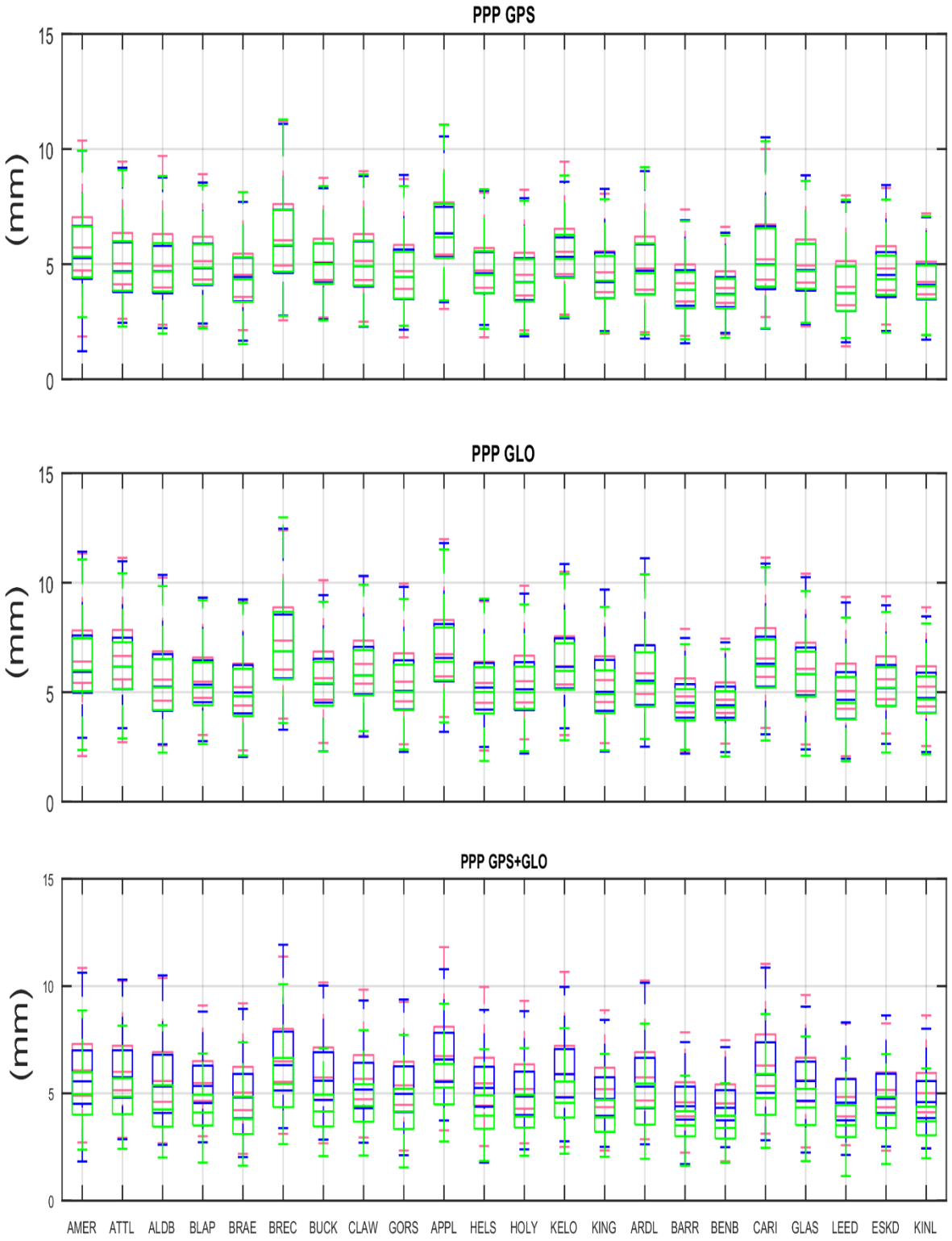


Figure 7-11 The RMS statistics between the estimated tropospheric ZTD from PPP GPS, PPP GLO and PPP GPS+GLO using three precise products(EMX (pink), ESA (blue) and GFZ (green)) and the estimated tropospheric ZTD from GDD GPS for 22 OSGB stations over one year

From Figure 7-10 and 7-11, the achievable accuracy of PPP tropospheric ZTD estimation for these stations can be seen. These illustrate that the alternative strategy may be used at any time of the year, irrespective of the weather conditions, to produce tropospheric ZTD estimates that are consistent with GDD GPS at the 10 to 15mm level. These results are consistent with Rohm et al. (2014), who obtained 15mm when using the Bernese GPS Software (version 5.0) for PPP GPS, and support the findings of Gendt et al. (2004) and Karabatić et al. (2011) who also obtained comparable results between GDD GPS and PPP GPS and suggested that PPP has the potential to become the standard technique for tropospheric ZTD estimation; followed by Dousa et al. (2016) who suggested that PPP gives the potential for advanced GNSS tropospheric products for meteorological applications and emphasized a synergy in GNSS and meteorological data and products.

However, most importantly in terms of these results, the potential of PPP GLO for tropospheric ZTD estimation is clearly highlighted, since the performance of PPP GLO appears to be only slightly worse than PPP GPS, which is the same conclusion as Ding et al. (2017).

7.3.5 Global IGS validation

For a further validation of the alternative tropospheric strategy over different locations, some IGS stations were chosen, as illustrated in Figure 7-12, based on two conditions. Firstly, they had to be available for one continuous week to ensure continuity, and secondly, their solution had to be available from the IGS for the station coordinate estimation and, most importantly, for the final tropospheric solution. The chosen stations ranged between −68.57° and 74.7° latitude, −176.6° and 174.8° longitude, and −27.99 and 2228.3 m height. This degree of variation was selected to provide an indication of the effectiveness of adopting the alternative strategy for the ZTD estimations.

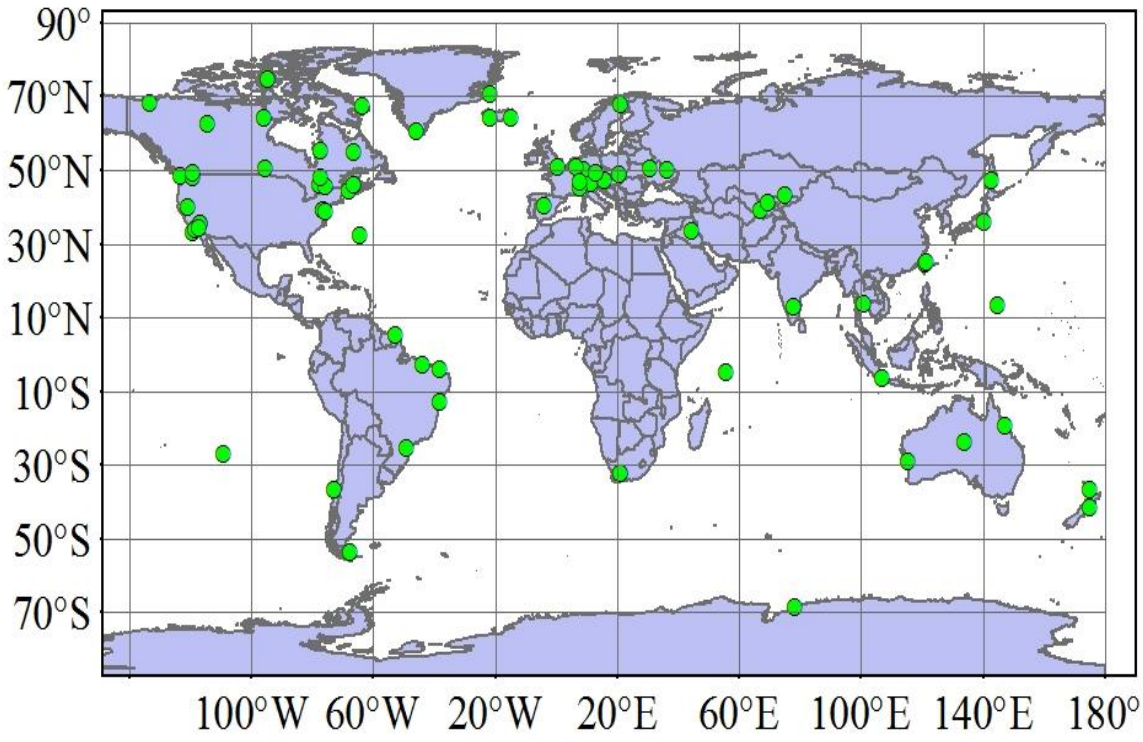


Figure 7-12 IGS stations' used for further validating the alternative tropospheric strategy

To ensure that the method was tested for different weather throughout the year, the first GPS week from each month was chosen as the basis for a dataset. Table 7-11 shows the number of IGS stations available for each of the selected GPS weeks in 2014. Full details of the chosen IGS stations are summarized in Appendix-B.

Table 7-11 GPS week and the number of IGS stations considered in the analysis of each week

GPS week	No. IGS stations
1774	74
1778	76
1782	74
1787	56
1791	64
1795	66
1800	64
1804	71
1809	73
1813	74
1817	68
1822	70

7.3.5.1 Global IGS validation using final precise products

The PPP daily solutions were compared with the IGS weekly solutions. For the PPP daily solution, two precise products were used: the IGS final precise products and the EMX final precise products. For the tropospheric ZTD comparison, two solutions are available from the IGS: one is for near real-time, which has 5-min intervals, and the other is the final produced after four weeks, which is at 2-hour intervals. The estimated tropospheric ZTD values for the common epochs using the alternative strategy were compared with both the IGS near real-time (NS_NRT) and the IGS final (NS_Final) solutions, and the results are summarised in Table 7-12.

Table 7-12 RMS differences between the estimated station coordinates and tropospheric ZTD from the PPP GPS (using two different final precise products) and the IGS near real time and final solutions for IGS stations over 12 weeks

IGS Solution	Station coordinates (RMS) (mm)				Tropospheric ZTD (mm)		
	Precise Products	E	N	U	Mean	STD	RMS
NS_NRT	EMX	4.0	3.8	10.0	1.1	5.8	5.9
NS_Final	EMX				2.0	5.8	6.1
NS_NRT	IGS_final	7.9	4.5	18.7	1.1	5.8	5.7
NS_Final	IGS_final				2.0	5.9	5.5

Table 7-12 summarizes the differences between the PPP GPS estimated tropospheric ZTD compared to the two IGS solutions, as well as by using the two precise products EMX final and IGS final.

In terms of station coordinates, it is found that the EMX final precise products have a better performance than the IGS final precise products. The reason could be that the IGS final precise products are a combination from different Analysis Centres (ACs), which followed different processing strategies. However, the RMS of the differences between the tropospheric ZTD estimated from the alternative strategy and the IGS tropospheric solutions were found to be slightly better when the IGS final precise products were used, in parts of a millimetre.

It is also important to look at the mean values of the tropospheric ZTD differences. Here, it is found that the alternative strategy has a better compatibility with the 5 min IGS tropospheric ZTD rather than the 2-hour, with a similar standard deviation. This can be explained as the estimated tropospheric ZTD from the alternative strategy is available in every epoch, which is a 30-second interval. Therefore, the 5-min IGS tropospheric ZTD product will capture real tropospheric variations better than the 2-hour, the estimated tropospheric ZTD will have better compatibility with the 5-min IGS tropospheric ZTD.

The tropospheric delay is also a challenging issue for the GNSS community in real-time situations. Therefore, it is important to test the alternative tropospheric strategy using real-time precise products.

7.3.5.2 Global Validation using real-time Precise Products

The alternative strategy was evaluated in a pseudo *real-time* situation; the same IGS data sets as considered previously in Table 7-11 were used. The PPP processing strategy was the same as before, except it was performed using IGS real-time precise products (i.e. IGS01, single epoch GPS combination; a single-epoch combination solution produced using software developed by ESA/ESOC). These real-time products

were not available for DOY 10, 11, 128–130, 154–158, 191–193, 279–284, 306–312, and 341–345, and therefore these days were excluded. The estimated tropospheric ZTD from PPP GPS using the alternative strategy was compared with the IGS final and near-real-time tropospheric ZTDs, and the statistics are summarized in Table 7-13 (for each station's coordinate and tropospheric ZTD statistics see Appendix-E).

Table 7-13 RMS differences between the estimated station coordinates and tropospheric ZTD from the PPP GPS (using real-time precise products) and the IGS near real time and final solutions for IGS stations over 12 weeks

IGS Solution	Solution	Station coordinates variation (RMS) (mm)			Tropospheric ZTD (mm)		
		E	N	U	Mean	STD	RMS
NS_NRT	The alternative strategy	20.3	15.7	27.7	1.3	8.0	8.1
NS_Final					2.0	7.8	8.1

Here it is important to highlight that these results compare the IGS final and near real time tropospheric ZTD values to those based on pseudo *real-time* PPP.

These results are significantly better than Ahmed et al. (2014) who obtained a 1 to 3cm bias and 1 to 4 cm standard deviation in tropospheric ZTD, and Yuan et al. (2014) who found that over 90% of their results were within 20 mm RMS for tropospheric ZTD, which could be partly attributed to the software that they used (BNC). In some aspects, these results are consistent with Dousa and Vaclavovic (2014), who obtained 6 to 10mm standard deviation in tropospheric ZTD, but with large biases of up to 20mm, which they suggested were due to missing precise models in their software (as introduced in section 2.3). These results are also slightly better than Li et al. (2015b), who found that the use of PPP GPS gave an RMS of about 10 to 20 mm in tropospheric ZTD, and Lu et al. (2016) who obtained and RMS of 15mm but still with an 11mm mean bias in tropospheric ZTD. Clearly, there is also scope for further improvement of these results by several millimetres, as suggested

by Li et al. (2015b) if multi-GNSS observations are processed simultaneously for enabling outlier elimination in the combined GNSS solution.

This validation clearly shows that the pseudo *real-time* results are almost as good as the post-processed results mentioned in Table 7-12, and therefore that the alternative tropospheric strategy may be used for PPP in real-time when users have access to the real-time products, without the need to implement a tropospheric model or relying on metoerological data.

7.3.5.3 Suitability for different variations

Lastly, it is important to check if PPP with the alternative tropospheric strategy can overcome high different variations in tropospheric ZTD. Therefore, two IGS stations WES2 (Westford, USA) and ALGO (Algonquin Park, Canada) are introduced here as example. Here ALGO has an almost stable tropospheric variation during the day and WES2 has a higher variation during the same day (see Figure 7-13).

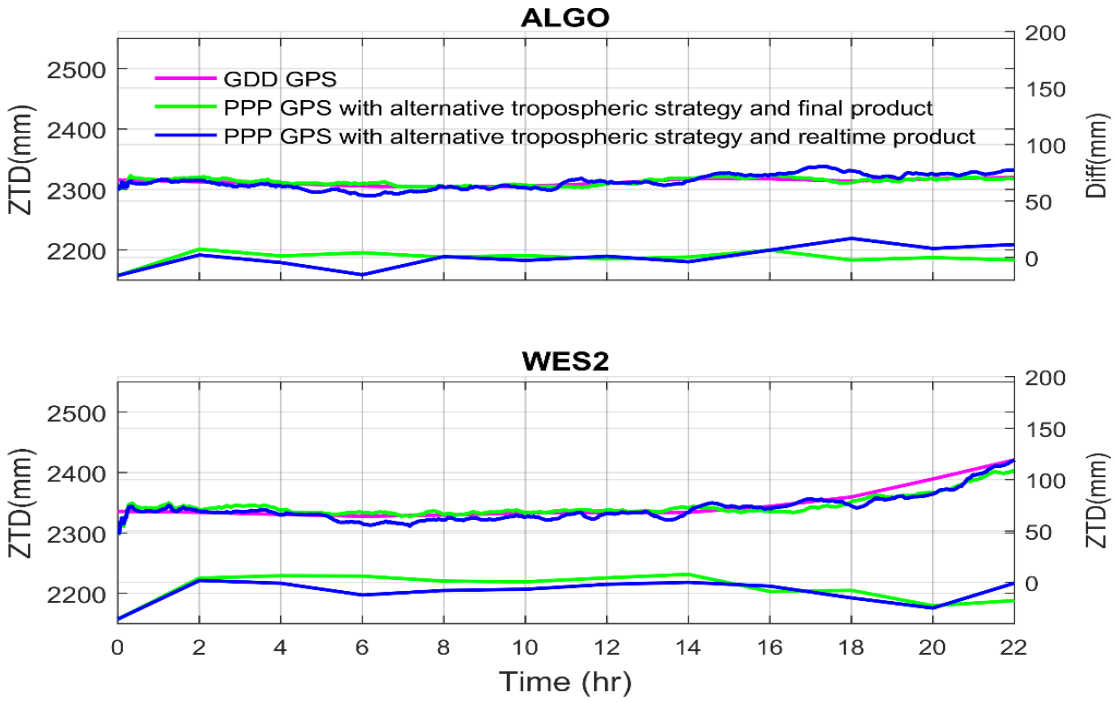


Figure 7-13 Comparison of tropospheric ZTD from GPS GDD and PPP GPS using final and real-time precise products at ALGO and WES2 IGS stations on DOY ,2014

It is apparent from Figure 7-13 that the alternative tropospheric strategy is suitable for different tropospheric variations.

7.4 The effect of the initial values on the estimated tropospheric ZHD and ZWD

All the results produced using PPP with the alternative tropospheric strategy were presented in the previous sections as the tropospheric ZTD. However, using the alternative strategy, actually leads to estimated tropospheric ZHD and ZWD. Therefore, a question may arise as to whether it is possible to go a step further and trust the individual tropospheric ZHD and ZWD estimates separately.

To explain this more, Figure 7-14 represents the estimated tropospheric ZHD and ZWD for ASAP station using the alternative tropospheric strategy over seven days, with the initial values set as zero.

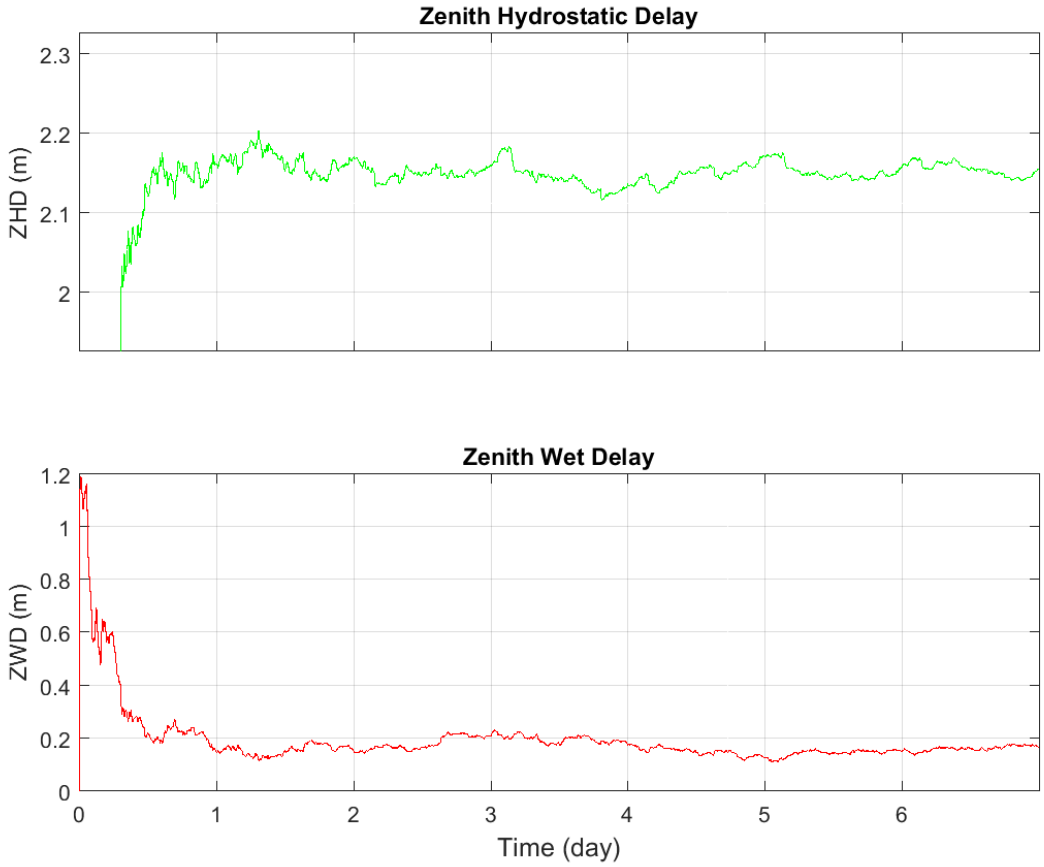


Figure 7-14 Estimated tropospheric ZHD and ZWD starting from zero initial values for ASAP station over seven consecutive days

It can be seen that both tropospheric ZHD and ZWD eventually have converged to these reasonable values (ZHD ~2.15 m and ZWD ~0.2 m), which confirms the suitability of the chosen values for the process noise, and the suitability of using different mapping functions for the two individual components (dry mapping function for the tropospheric ZHD and wet mapping function for the tropospheric ZWD). However, it clearly needs a long time to converge when starting from zero initial values.

To answer the raised question, there is a need to look at Figure 7-15, which represents three OSGB stations that were used previously for evaluating the tropospheric models (DRUM, FARB and KEYW). It shows the estimated ZHD and ZWD for these stations on DOY 12, 2014 for both the PPP GPS and PPP GLO, with 2.2 m and 0.1 m as a-priori values for tropospheric ZHD and ZWD respectively.

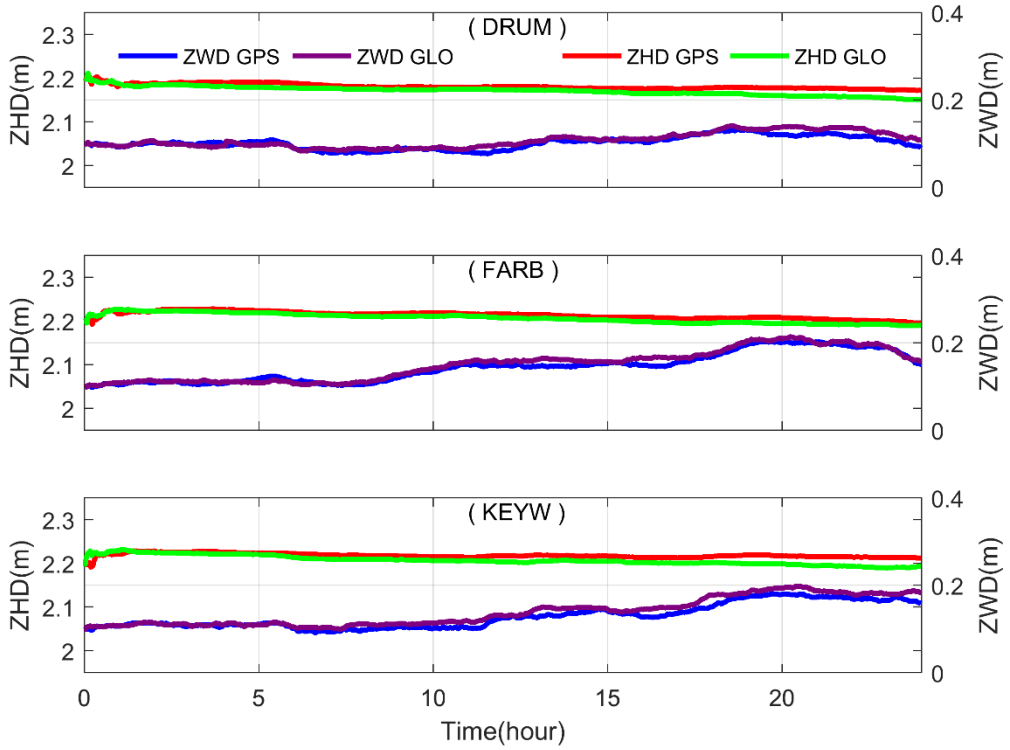


Figure 7-15 Estimated tropospheric ZHD and ZWD for DRUM, FARB, and KEYW stations on DOY 12, 2014, left axis: hydrostatic, right axis: wet

From Figure 7-15, it can be seen that although PPP GLO gives a solution from a different inclination angle, that is independent of the PPP GPS solution, it gives the same tropospheric ZHD and ZWD for all stations.

However, for the individual components, the factor that will affect the accuracy is the initial values as is summarised in Figure 7-16 for DRUM station on DOY 12, 2014, using two different initial values for the tropospheric ZHD and ZWD. Firstly, using 2.2 m for the tropospheric ZHD and 0.1 m for the tropospheric ZWD. Secondly, using a value interpolated by the author from the Vienna mapping function (Boehm et al., 2008).

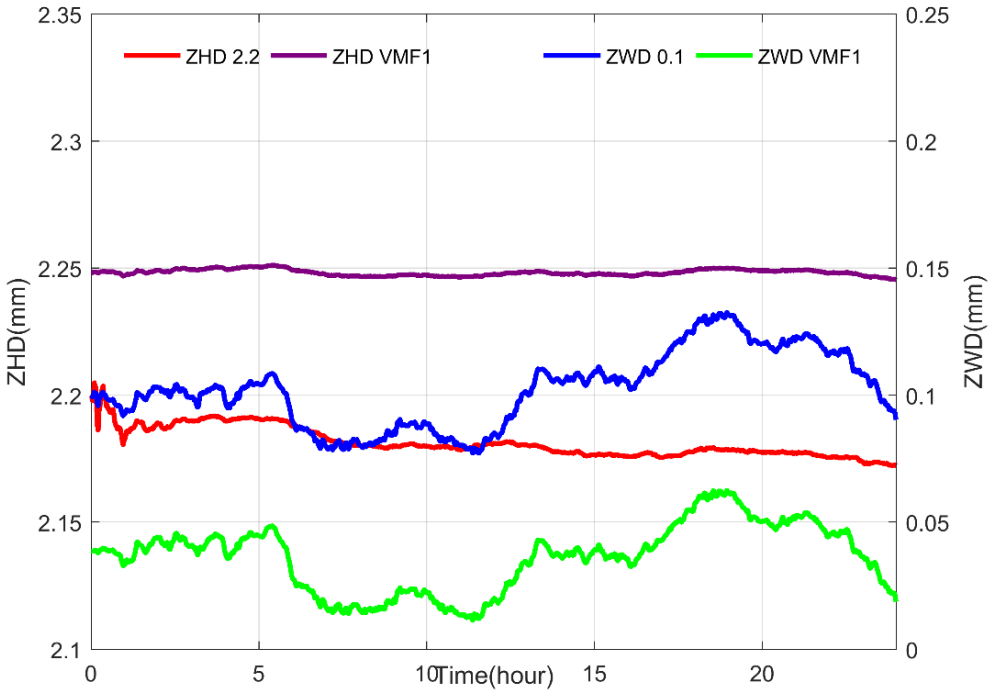


Figure 7-16 The effect of the initial values on the estimated tropospheric ZHD and ZWD for DRUM station on DOY 12, 2014

From Figure 7-16 , it is clear that the initial values have a significant effect on the estimated individual components, as from a visual inspection, the change in the individual component from epoch-to-epoch is the same but the estimates remain offset, depending on the initial values used.

Thus, to use the alternative strategy to estimate tropospheric ZHD and ZWD seperately, it is important to choose a realistic initial values.

However, if the required estimate is simple tropospheric ZTD, then this will be the same no matter what the initial values originally were, as shown in Figure 7-17.

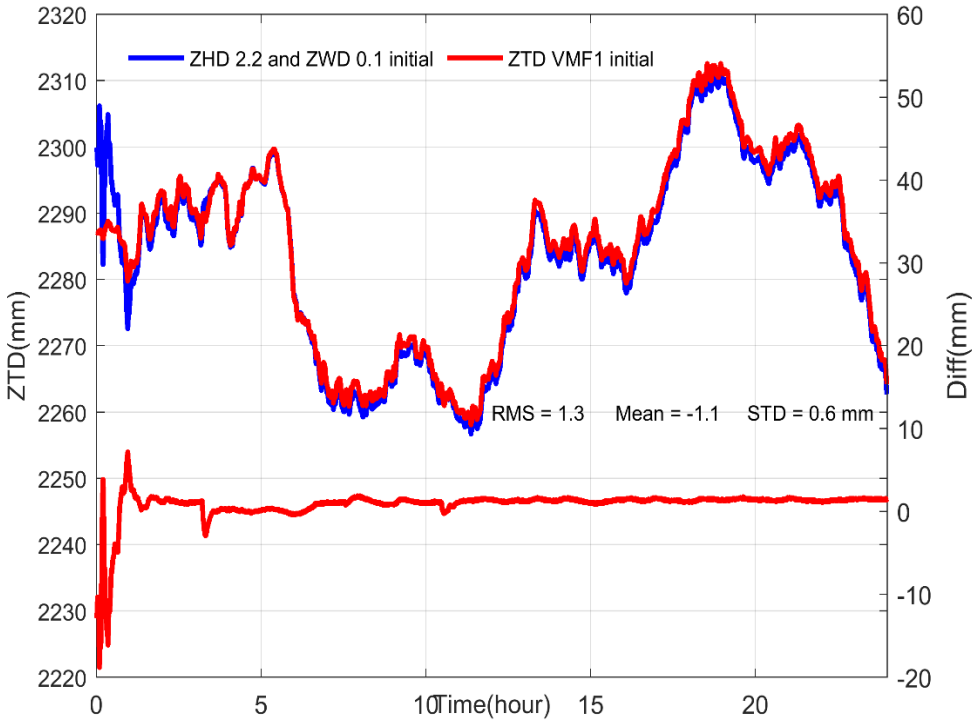


Figure 7-17 The effect of the initial value on the estimated tropospheric ZTD for DRUM station on DOY 12, 2014

Reflecting on Figures 7-16 and 7-17, it is clear from Figure 7-17 that the resultant tropospheric ZTD is the same despite the two different a-priori values, which is acceptable for this research because the interest is in PPP users being able to obtain an accurate tropospheric ZTD without the need for external information or by using any tropospheric models. However, considering Figure 7-16, it could be argued that by starting with VMF1 as an a-priori model of tropospheric ZHD and ZWD, rather than using a simple assumption of 2.2m and 0.1m, means that the resultant separate tropospheric ZHD and ZWD are more physically meaningful in that case (see section 3.3.3.4.1). Such an approach would also be more consistent with Lu et al. (2016) and Bock et al. (2016) who both used VMF1 as an a-priori model of tropospheric ZHD and ZWD (as introduced in section 2.3).

7.5 The correlation between estimated station height and tropospheric ZTD using PPP and Global Double-Difference

To further investigate the differences between the PPP scenarios, the two stations that were used for validating the software and the precise products, as well as the constellation in Section 6.3, were used for all PPP scenarios (PPP GPS, PPP GLO and PPP GPS+GLO). The tropospheric ZTD statistics from one-year of processing for the two stations are summarized in Table 7-14.

Table 7-14 PPP GPS, PPP GLO and PPP GPS +GLO tropospheric ZTD statistics for ALDB and AMER stations over one year

	ALDB			AMER		
	GPS	**GLO**	**GPS+GLO**	**GPS**	**GLO**	**GPS+GLO**
Mean (mm)	1.3	2.4	1.6	-0.5	-0.5	-0.5
STD (mm)	5.3	5.4	5.3	5.3	5.5	5.2
RMS (mm)	5.5	5.8	5.5	5.3	5.5	5.2

It can be seen from Table 7-14 in terms of tropospheric ZTD the alternative strategy is stable for a one-year period according to the results from these two stations.

Concerning any correlation between estimated station heights and tropospheric ZTD from PPP and GDD, Figure 7-18 represents the differences between the estimated tropospheric ZTD from PPP GPS and GDD GPS as well as the difference between the estimated station height.

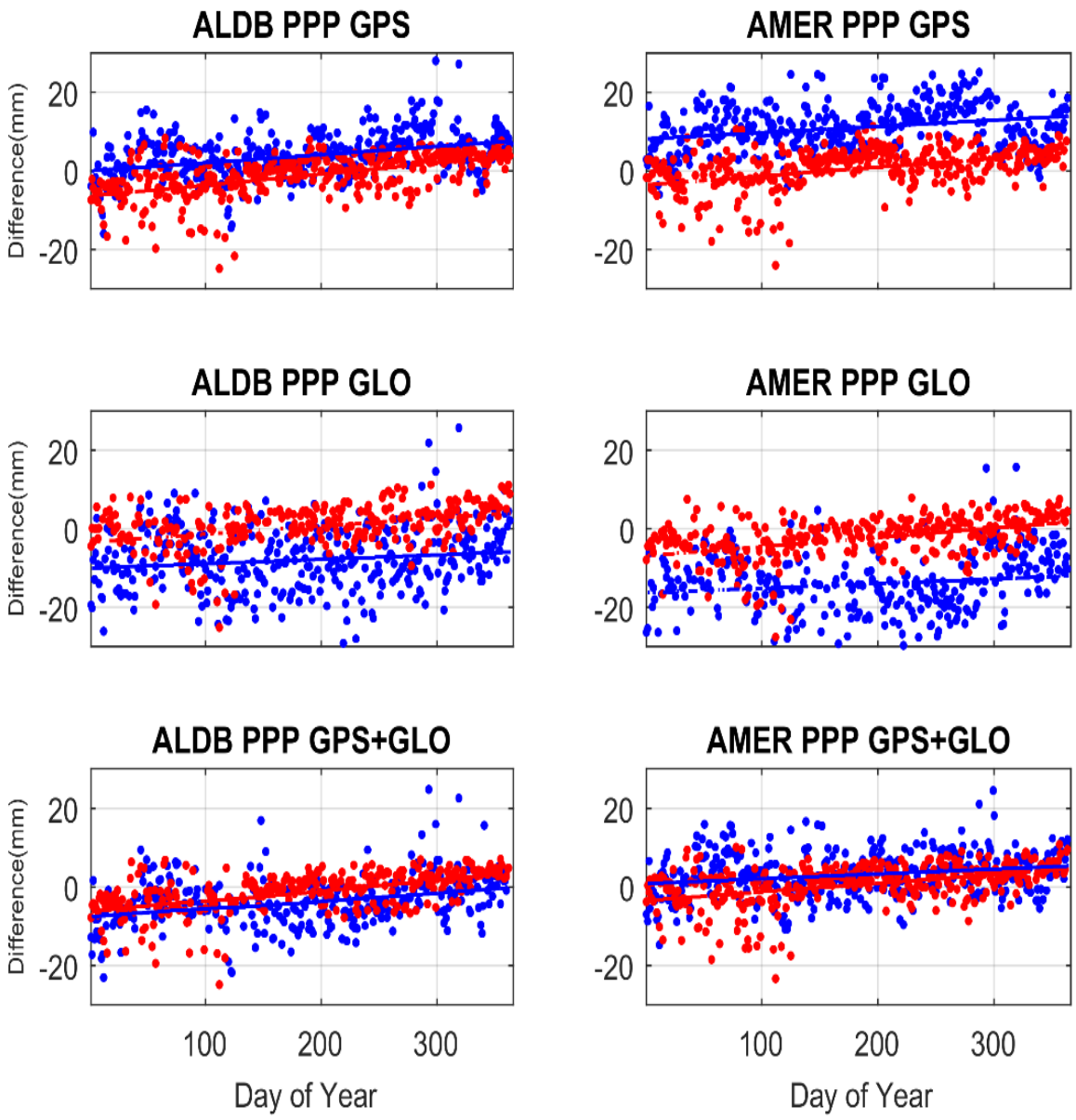


Figure 7-18 The difference between estimated tropospheric ZTD and station heights from PPP GPS, PPP GLO and PPP GPS+GLO, and from GPS GDD for AMER, ALDB stations over one year (dtrop: red, dU: blue)

On first inspection of Figure 7-18 might suggest that there is a correlation between the tropospheric ZTD and station height. However, it can be seen that the estimated station height is high for PPP GPS and low for PPP GLO when compared to GDD GPS for both stations over the year. Clearly this difference in station height is not because of the difference between the tropospheric ZTD because for both PPP GPS

and PPP GLO the effect on tropospheric ZTD is more or less the same. To support this, evidence from the PPP GPS+GLO scenario for both stations indicates that the tropospheric ZTD behaves similar to PPP GPS and PPP GLO while the PPP GPS+GLO balances the error in the PPP GLO station height estimation, which is in the negative direction, with the error that is positive in PPP GPS.

The reason for this could be attributable to imperfections of the models for the antenna phase centres of the receiver antenna with respect to both constellations, which could mask whether the station height from the PPP solutions has reached a significant level. Further, this is true for the two stations as well as the dataset that had been used in Section 5.6, specifically the mean bias for the Up component of the PPP GPS, PPP GLO and PPP GPS+GLO.

It can be concluded, therefore, that the estimated ZTD is consistent in all cases, but that there is further scope for minimizing the station height bias from PPP GPS and PPP GLO.

7.6 Additional PPP improvement when using the alternative tropospheric strategy

The suitability of the alternative strategy for tropospheric ZTD estimation can also be reflected in the PPP performance in terms of the convergence time and repeatability as follows.

7.6.1 Convergence time

It is known that the convergence time for the PPP solution is longer for the station coordinate Up component, and this has a relation with the tropospheric ZTD estimation. Applying the alternative tropospheric strategy not only improves the tropospheric ZTD estimation from the PPP solution, but it also improves the convergence time, as can be seen in Figure 7-19.

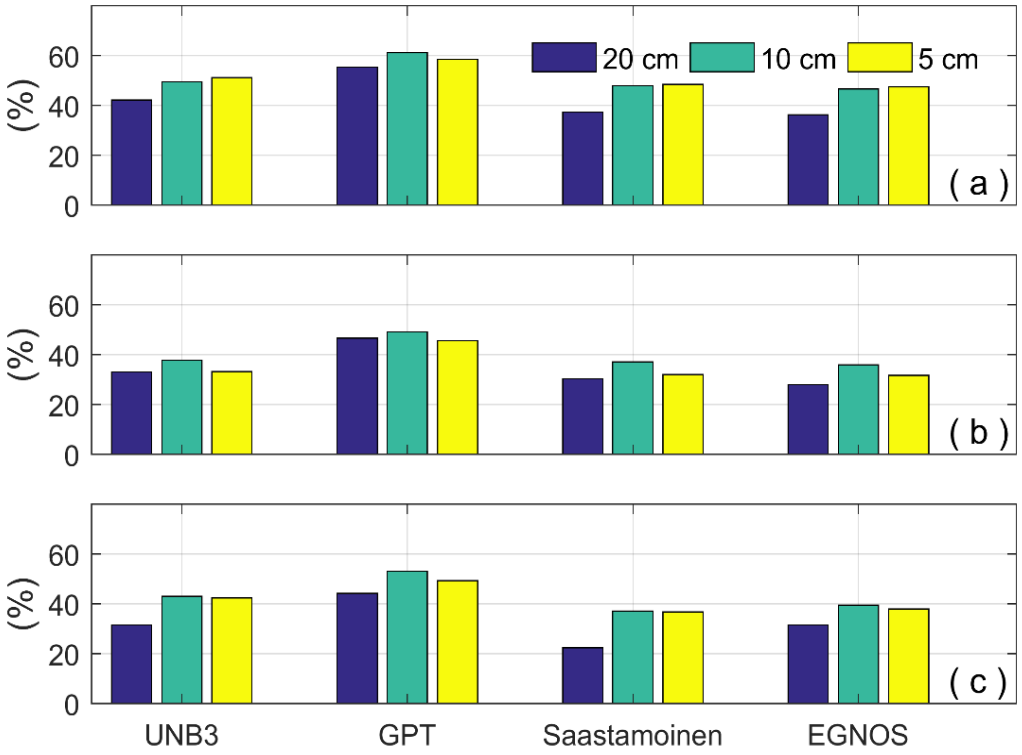


Figure 7-19 Improvements in the convergence time when using the alternative strategy for PPP GPS (top), PPP GLO (middle) and PPP GPS+GLO (bottom)

Figure 7-19 shows a significant improvement in the convergence time for 20, 10, and 5 cm accuracy for the station coordinate Up component for all PPP scenarios and all models used in the case of the conventional strategy. The improvements in the time taken to converge to 5 cm station height accuracy, compared to the conventional strategy using UNB3m, GPT, Saastamoinen SPT and EGNOS models, were 49, 66, 44 and 43 minutes for the PPP GPS (a), 31, 53, 30 and 29 minutes for the PPP GLO (b), and 28, 37, 22 and 23 minutes for the PPP GPS+GLO(c), respectively.

Although the convergence time may not be directly comparable between studies, as its definition can vary, these results are similar to Lu et al. (2017), who showed an improvement in the convergence time of up to 66.7% for the station coordinate Up component when using a NWM-augmented PPP algorithm when compared to a standard PPP solution.

7.6.2 The improvement on one-year repeatability

Another potential improvement is in the repeatability over a long period. This can be seen in Figure 7-20, which represents a comparison of two OSGB stations ALDB and AMER using the conventional and alternative tropospheric strategies.

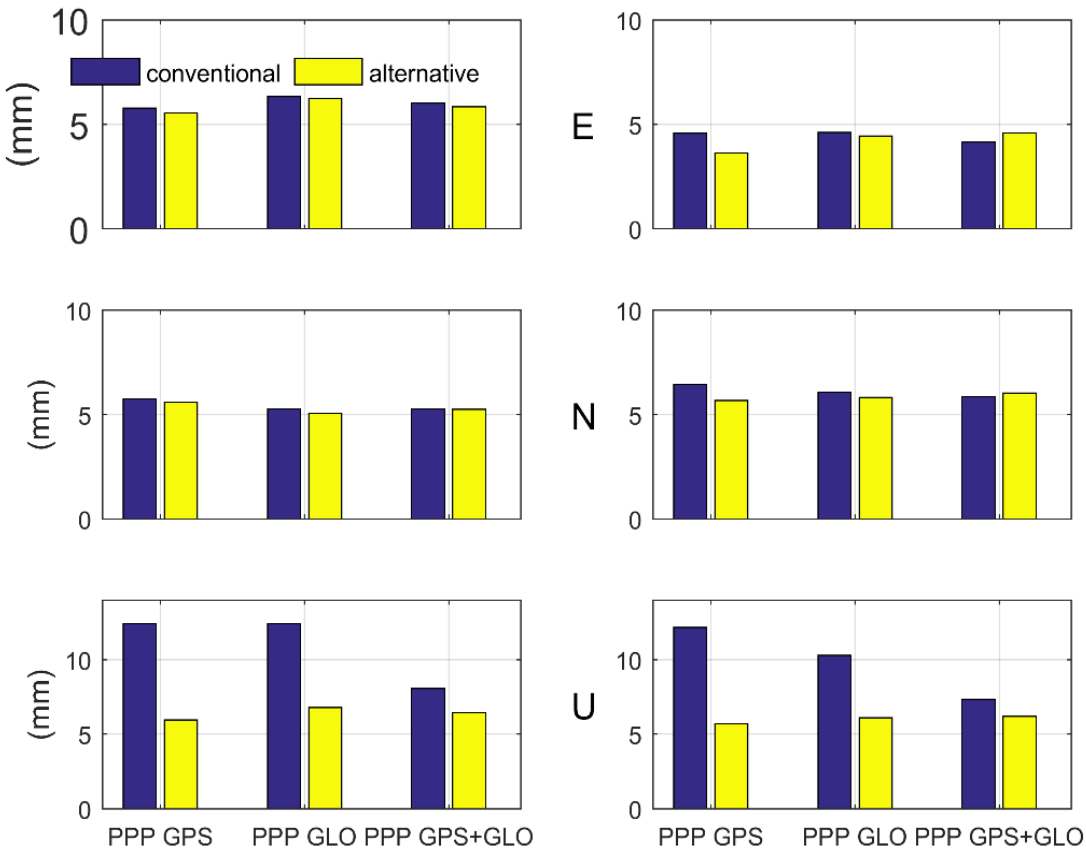


Figure 7-20 Comparison between the repeatability analysis when using a model for troposphere and by using the alternative tropospheric strategy (AMER Left, ALDB Right)

From Figure 7-20, it can be seen that the main improvement obtained is in the repeatability of the station coordinate Up component to be 51.9% (GPS), 45.4% (GLO) and 20.0% (GPS+GLO) for AMER station, 53.2% (GPS), 40.5% (GLO) 15.4% (GPS+GLO) for ALDB station. These results confirm what was said by Liu et al. (2016b) in that degradation in the Up component can be mainly due to the poor

estimation of tropospheric ZTD (as introduced in section 2.3). Furthermore, applying the higher order ionospheric corrections could also further improve the obtained repeatabilities, following Kedar et al. (2003) (Kedar et al., 2003), Steigenberger et al. (2006) and Hernandez-Pajares et al. (2007) (as introduced in section 3.3.2).

In any case, the improvement already obtained from the alternative strategy could give the possibility of enhancing geophysical applications that would benefit from improved velocity estimation based on more precision in the estimated station coordinate Up component over the long-term.

7.7 Chapter summary

In this chapter, tropospheric analysis using PPP has been investigated. The first part of this chapter set out to compare the effect of different tropospheric models for the tropospheric ZTD. It was then concluded that for PPP the conventional tropospheric strategy based on modelling tropospheric ZHD and estimating tropospheric ZWD does not have the ability to produce millimeters accuracy of tropospheric ZTD, even though the station coordinate estimation is accurate, because the receiver clock offsets and the estimated ambiguities absorb any un-mitigated tropospheric ZTD.

The second part of this chapter presented an alternative tropospheric strategy for estimating tropospheric ZTD in PPP, for post-processing and *real-time* estimation, without using any external tropospheric information. It is based on estimating both the tropospheric ZHD and ZWD using different mapping functions and different process noise in the Extended Kalman filter. Following this alternative strategy, the estimated tropospheric ZTD from PPP compares more favorably with that from GDD.

A series of validations were conducted for the alternative tropospheric strategy using PPP GPS, PPP GLO and PPP GPS+GLO. Validation using 7 consecutive days were first performed, followed by an expanded regional validation that was done for a seven week dataset of OSGB stations in the UK, and then a long-term (over one year) validation for 22 OSGB stations. The regional and long-term validations also considered the effect of three different final precise products, namely EMX, ESA and GFZ.

A global validation using ~76 stations IGS stations was then done over a different period, and conducted in three stages, using EMX final, IGS final and IGS real-time precise products. The estimated tropospheric ZTD compared favorably with the IGS final and near real-time solutions. It was also proposed that this approach can

be used in *real-time* as well as in post-processing without a significant difference between the results.

Lastly, it was shown that with the alternative tropospheric strategy, PPP users will not only obtain an accurate tropospheric ZTD, but they will also have an improvement in the convergence time and the repeatability of station height over the long term.

Chapter 8. Estimation of station velocity from PPP GPS, PPP GLO and PPP GPS+GLO

The Global Navigation Satellite System (GNSS) is a valuable tool for monitoring crustal motion, based on its ability to produce daily station coordinates for specific sites. It is also one of the important contributing techniques to the International Terrestrial Reference Frame (ITRF), through the availability of global network of the IGS stations. Some of those IGS stations are GPS only, while others have GLONASS (GLO) in addition to GPS. Many researchers have used PPP GPS or GPS+GLO as a tool for geophysical applications e.g., crustal deformation, but none have investigated PPP GLO alone and whether it is capable of estimating station velocities to a similar level as PPP GPS and PPP GPS+GLO.

Therefore, with the promising results from PPP GLO shown so far in this thesis, it is also reasonable to investigate the possibility of using PPP GLO for crustal motion. This chapter aims to cover a station coordinate repeatability analysis for all PPP scenarios as well as the GDD GPS based on one-year of data for 22 OSGB stations in the UK. In addition, using this one-year of data a comparison of estimated station rates based on PPP GPS, PPP GLO and PPP GPS+GLO will be investigated, to identify any possible long-term biases between the two systems. Further, a comparison between all PPP scenarios (PPP GPS, PPP GLO and PPP GPS+GLO) and GDD GPS will be carried out in term of estimated station rates. While one year is clearly not long enough for the velocity estimation of station, the estimated station rates can provide preliminary results and also allow the consideration of the effect of precise products on long-term processing (station velocity estimation).

8.1 Datasets

The dataset is formed of 22 OSGB stations over one year were used. The stations were chosen based on the maximum record for the stations as well as their availability for 24 hours during a day. Further, the availability of the same stations in

the GDD GPS solution was also considered as a condition for choosing those stations, as well as the distribution of the stations in the UK as a case study (see Figure 8.1).

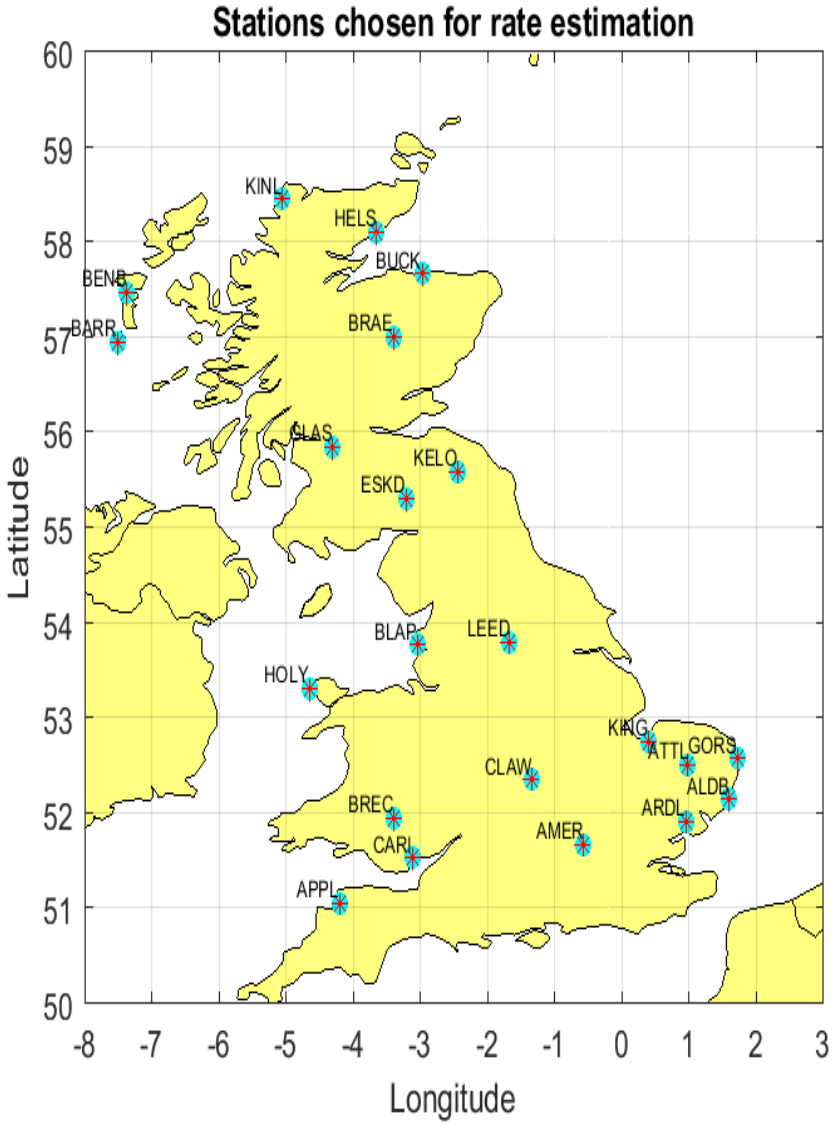


Figure 8-1 22 OSGB stations that were chosen for a one-year assessment of estimated station rates

8.2 Methodology

The aim of the one-year station rate estimation here is to look at the possibilities for station velocity estimation from the PPP scenarios, when compared to GDD. It is also for addressing the potential of estimating station velocity from PPP GLO, which has never been investigated before. Furthermore, the introduction of long-term biases

between the PPP scenarios as well as the effect of different precise products on long-term processing will be considered.

The topic of station velocity estimation is complex and involves time series analysis and consideration of the noise of the station coordinates time series (white, colour, and random walk noise as well as the flicker noise). In this chapter, as there is only one-year time period, no time series analysis is included beyond a least squares implementation using a Matlab script for computing the horizontal station rates for all scenarios (PPP as well as GDD), and only horizontal station rates are considered.

The configuration of the PPP scenarios was carried out using the alternative tropospheric strategy as seen in section 6.3, where three precise products were used (EMX, ESA and GFZ) to assess the quality of these precise products in the long-term as well as the estimated station rates from different constellations.

8.3 One-year Station Coordinates Repeatability Analysis

For assessing the quality of the solutions from different PPP scenarios, it is important to first compare the repeatability of the station coordinates in terms of East and North components for every PPP scenario, with various precise products as well as the GDD solution. The repeatability can represent the stability of a solution for that specific component, enabling constellation as well as precise products assessment. The repeatability analysis was carried out based on the weighted root mean square error (WRMS), as seen in equation (6.1), for all components as follows.

8.3.1 East Coordinate Component Repeatability

Figure 8-2 shows the repeatability of the East coordinate component for all PPP scenarios using EMX, ESA and GFZ precise products and GDD GPS.

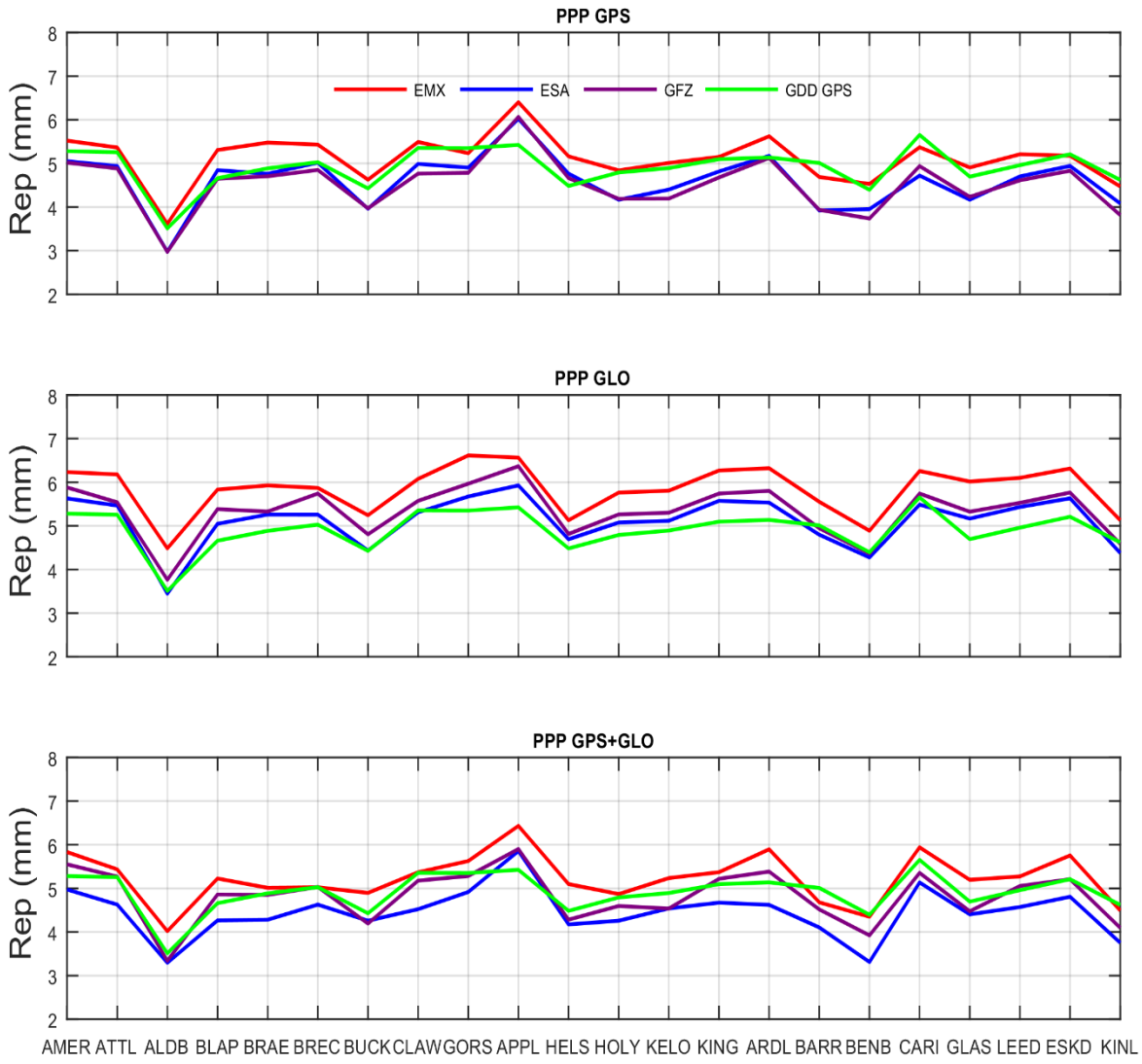


Figure 8-2 Comparison of East coordinate component repeatability for GDD GPS and PPP GPS, PPP GLO and PPP GPS+GLO using EMX, ESA and GFZ precise products

Looking at the precise products' effect on long-term processing, it can be seen that all East coordinate components are made slightly worse when using EMX precise products. Conversely, using ESA and GFZ products has almost the same effect on the PPP GPS with no significant differences, although all the stations in the PPP GLO case have a slightly better performance when using GFZ compared to ESA precise products.

As a constellation performance for the East coordinate component, with the GDD GPS repeatability reflecting a basis for the other solutions, it can be seen that the

repeatability for PPP GPS is almost the same as the GDD GPS. However, this situation is slightly different for PPP GLO because it is coming from a different constellation, with six stations consistent with the repeatability of the GDD GPS when ESA precise products are used, while the GFZ and EMX precise products results are slightly worse than the GDD GPS. This suggests that the stability of the solution will be better when using ESA precise products in the case of the PPP GLO East coordinate component. Lastly, the repeatability from PPP GPS+GLO was generally shifted down, which means a better repeatability and improvement.

These results are comparable to those from Teferle et al. (2007), who obtained 3.0mm repeatability for the East coordinate component using PPP GPS in the Bernese GPS Software (version 5.0). They are also similar to He et al. (2017), who concluded that PPP GPS and GDD GPS can produce very similar results in terms of daily station coordinate repeatability (as introduced in section 2.4). However, there is also scope for improvement in the future, as suggested by Ge et al. (2007) who obtained 27% improvement for the East coordinate component repeatability by ambiguity fixing (as introduced in section 2.5).

8.3.2 North Coordinate Component Repeatability

Figure 8-3 shows the repeatability of the North coordinate component for all PPP scenarios for EMX, ESA and GFZ products as well as the GDD GPS.

Considering a product effects on the North coordinate component, for PPP GPS, it is evident from Figure 8-3 that the GFZ precise products represent the best compared to EMX or ESA. This also applies to the remaining two scenarios of PPP GLO and PPP GPS+GLO, while the other two precise products, ESA and EMX, seem to be more consistent in their repeatability for all PPP scenarios.

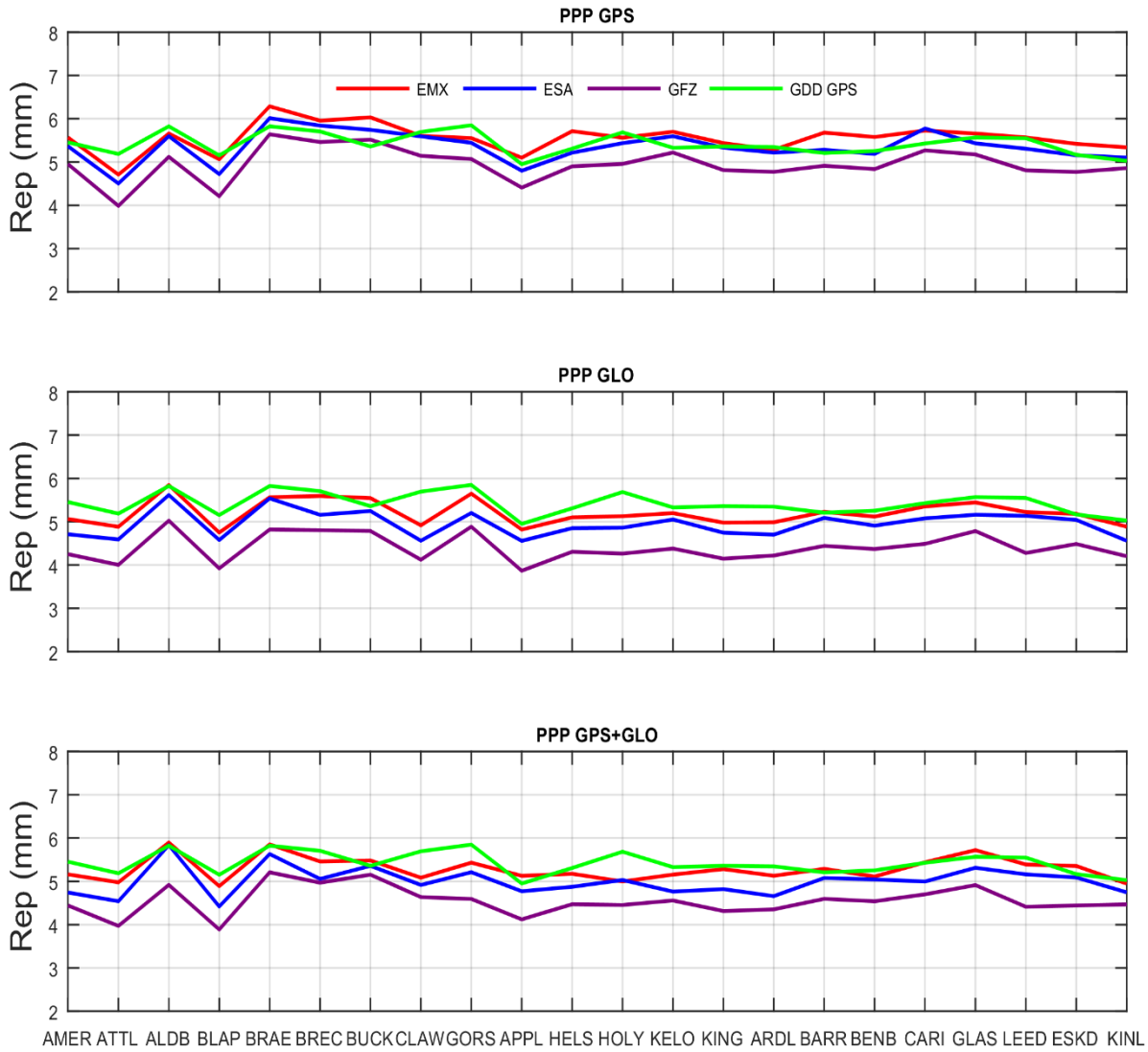


Figure 8-3 Comparison of North coordinate component repeatability for GDD GPS and for PPP GPS, PPP GLO and PPP GPS+GLO using EMX, ESA and GFZ precise products

Looking at the results as constellation differences, it can be seen that PPP GLO has a slightly better repeatability compared to PPP GPS for all stations. This can be attributed to the availability of the GLO satellites to the north as has been discussed in section 6.5. While for the PPP GPS+GLO, it will be as a balance between them. As with the East coordinate component, these results are comparable to those from Teferle et al. (2007), who obtained 3.0mm repeatability for the North coordinate component using PPP GPS in the Bernese GPS Software (version 5.0). They are also consistent with Satirapod et al. (2013) and He et al. (2017) who concluded that PPP GPS can

produce a millimetre-level of station coordinate repeatability (as introduced in section 2.4).

8.4 One-year estimated horizontal station rates

Estimated horizontal station rates were computed for all three PPP scenarios as well as the GDD GPS solutions using a simple least squares rather than a time series analysis, for the reason mentioned before (Section 8.2). This was conducted for the EMX, ESA and GFZ precise products to evaluate the effect of using different precise products and their impact on the estimated station rate. Most importantly, their effect on the PPP GLO was evaluated because no long-term assessment had been done on PPP GLO before.

Here it should be noted that these station rates cannot be used beyond the purpose of the comparison here, and cannot, therefore, be compared to any results from previous research; instead, as was stated at the start of this Chapter, "while one year is clearly not long enough for the velocity estimation of station, the estimated station rates can provide preliminary results and also allow the consideration of the effect of precise products on long-term processing (station velocity estimation)."

Figure 8-4 represents an example of the coordinate time series and station rate estimation for the East component for the ALDB station.

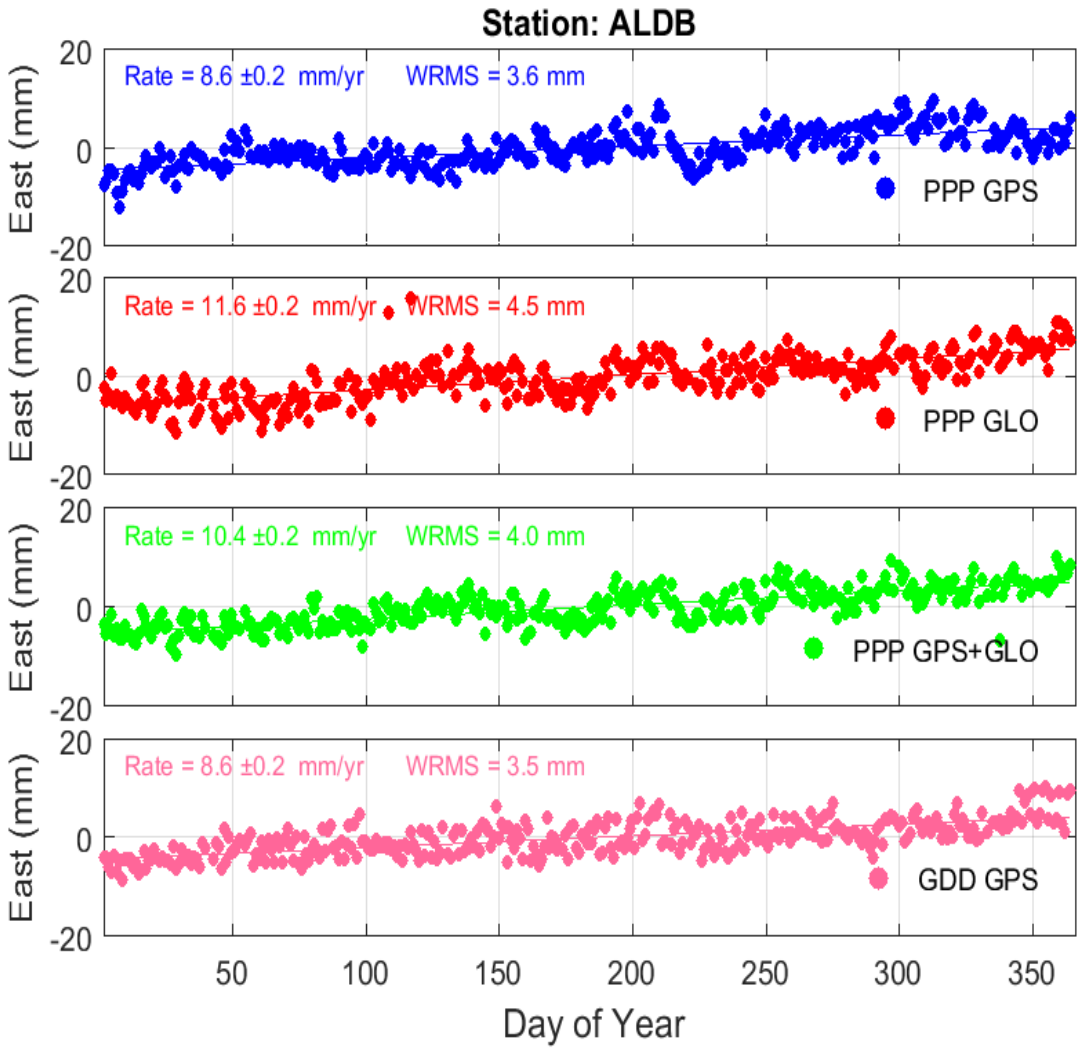


Figure 8-4 Example coordinate time series and station rate estimation for the East component

A summary of all estimated rates for, all scenarios (PPP GPS, PPP GLO, PPP GPS+GLO and GDD) and all products are listed in Appendix-F, noting that only the East and North components are presented for this one-year analysis, and coordinate time series are given in Appendix-G.

8.4.1 Precise Products effect on estimated horizontal station rates

To evaluate the precise products effect on the estimated horizontal station rates, it is important to evaluate each PPP scenario. In order to see their differences from the mean, the estimated rate for each station was computed and the differences from the mean, depending on the precise product type, were then computed.

8.4.1.1 PPP GPS

Starting with PPP GPS, the station rate differences from the mean in the East component were found to be ±1 mm/yr (see Figure 8-5). The differences were found to be biased as precise product type for this component, with the EMX precise product have a positive bias while the other precise products (ESA and GFZ) have a negative bias, and are more consistent with each other.

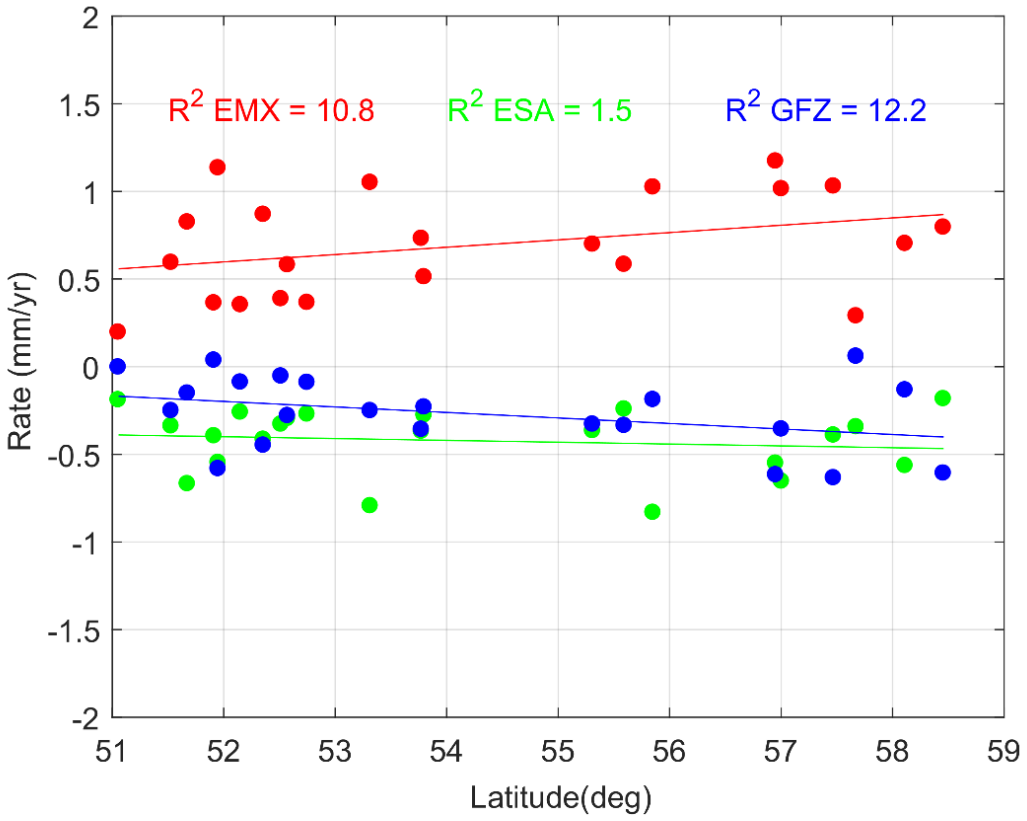


Figure 8-5 The difference between the estimated East station rate and the mean for PPP GPS with EMX, ESA and GFZ precise products

Regarding any effect of the station latitude on the East station rate differences, the correlation (R^2 is a statistical measure of how close the data are to the fitted regression line) is weak for all the precise products; however, the correlation is ten times higher for the EMX.

Similarly, for the North component, it is found that EMX precise products still have a positive direction in order to be higher than the other precise products for all stations. However, when using ESA precise products the results vary and the GFZ has the lowest North station rate for all the stations (see Figure 8-6).

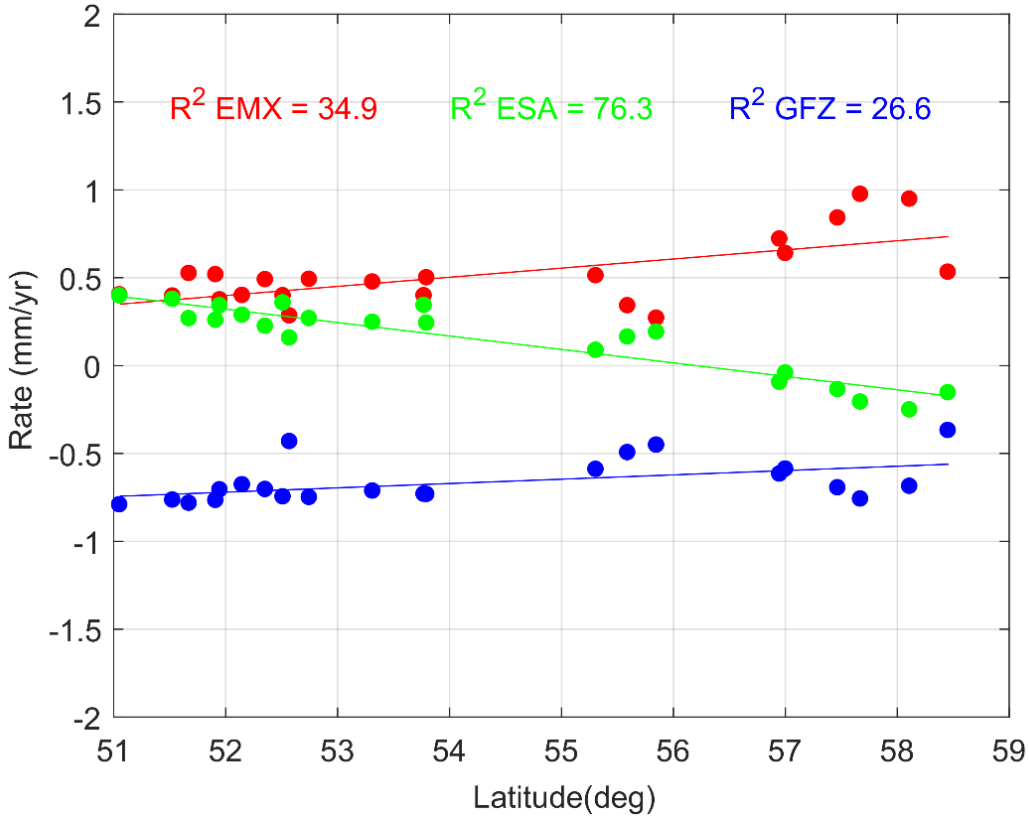


Figure 8-6 The difference between the estimated North station rate and the mean for PPP GPS with EMX, ESA and GFZ precise products

From the trend analysis, it was found that the ESA has 76.3% correlation dependence with the station latitude, while the second highest correlation is found when using the EMX precise products, as 34.8% correlation while the GFZ precise products is 26.5%.

All PPP configurations were the same except for the product types, which means that the differences are coming from the precise products. Therefore, It can be concluded that the precise products have the effect of ±1mm on the stations rate estimates.

8.4.1.2 PPP GLO

For the East component, the station rate differences from the mean were also found to be within 1 mm/yr. The ESA precise products were found to be negative from the mean except for two stations, KELO and GLAS, which were found to be the most consistent stations for this component. The highest difference from the mean was found in the EMX precise products (see Figure 8-7).

To evaluate the effect of the station latitude dependence on these differences, the correlation (R^2) was also computed. It was found that the East component using EMX precise products had the smallest correlation with the PPP GLO station rate differences. The correlation using the other two precise products was found to be 3-4 times higher. However, the visual difference between the two precise products (EMX and GFZ) is changing in different directions, with an increase for the EMX and a decrease for the GFZ.

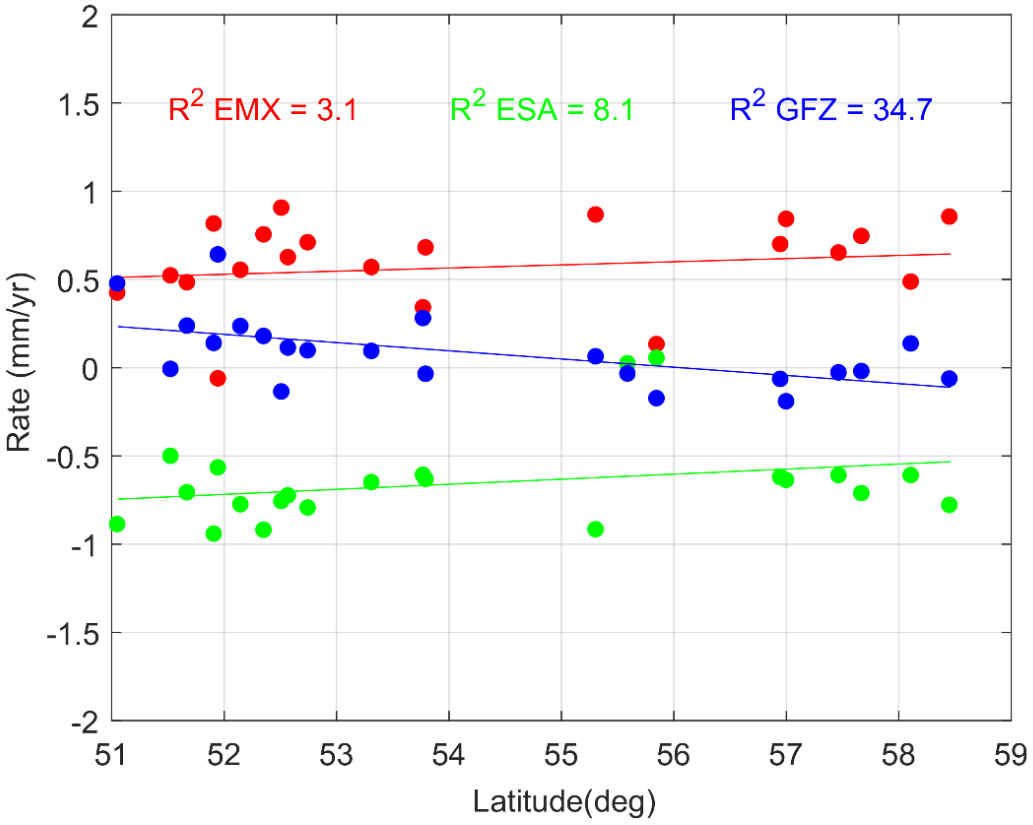


Figure 8-7 The difference between the estimated East station rate and the mean for PPP GLO with EMX, ESA and GFZ precise products

For the North component, this different behaviour compared to the East component. No correlation with the latitude was found for the ESA precise products which is the nearest to the mean (zero value). The EMX differences are higher compared to the other precise products, and the North rate differences are more than 1 mm/yr (see Figure 8-8).

The correlation for the trend lines was found to be 50.4% for the EMX precise products and 36.1% for the GFZ precise products relating to the station latitude. Although these differences are small, a correlation still exists.

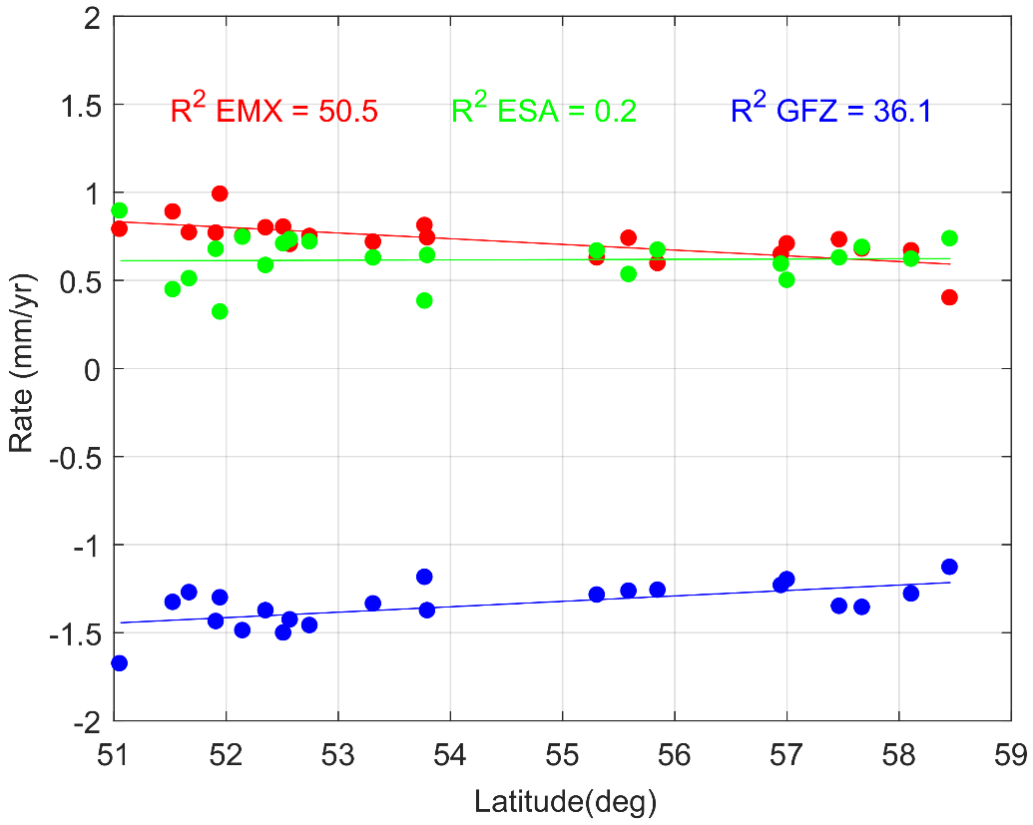


Figure 8-8 The difference between the estimated North station rate and the mean for PPP GLO with EMX, ESA and GFZ precise products

8.4.1.3 PPP GPS+GLO

From the PPP GPS+GLO scenario, the East component is still within a 1 mm/yr difference between the three precise products. These differences increase with an increase of the latitude, 20.5% correlation with the latitude for the EMX precise products, 11.5% correlation for the GFZ precise products and no significant correlation for the ESA precise products (see Figure 8-9).

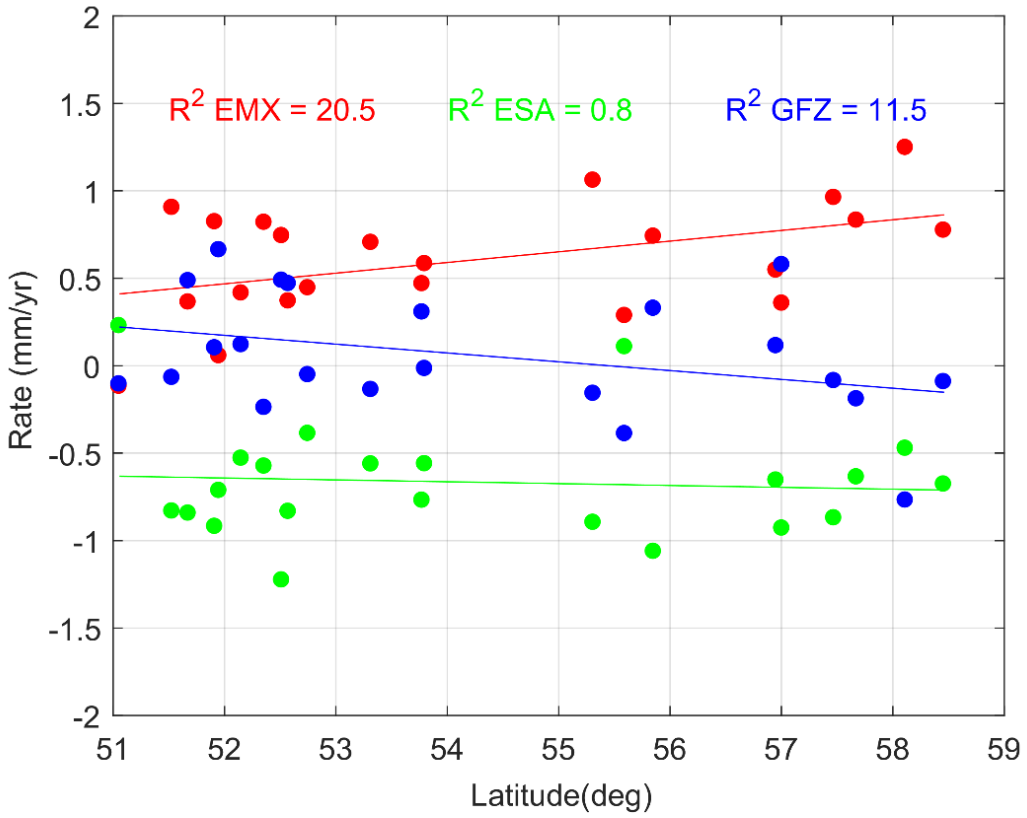


Figure 8-9 The difference between the estimated East station rate and the mean for PPP GPS+GLO with EMX, ESA and GFZ precise products

Similarly, EMX precise products still have a similar correlation at 22.69% for the North component as well as the GFZ precise products which was found to be 11.9% correlation, but this time as a mirror with almost no change in the correlation for the ESA precise products, which is negligible for both components (Figure 8-10).

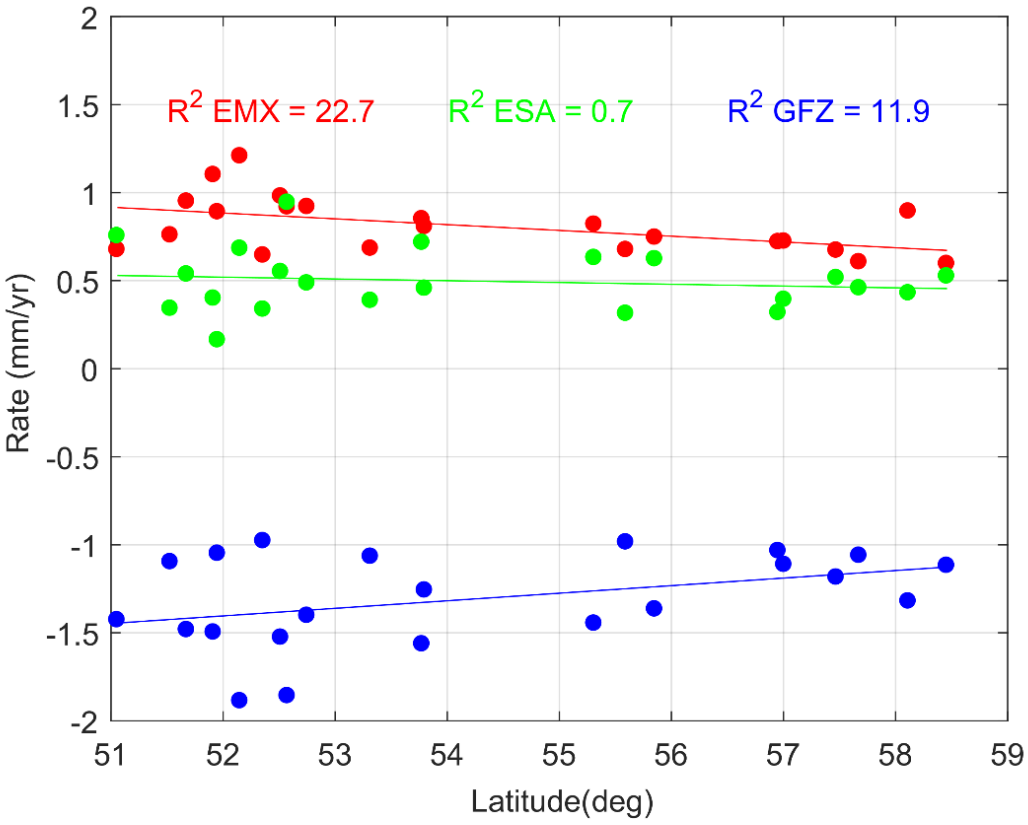


Figure 8-10 The difference between the estimated North station rate and the mean for PPP GPS+GLO with EMX, ESA and GFZ precise products

As a conclusion for the precise products effects, the ESA precise products represented the middle for all of the three precise products.

8.4.2 System effects on estimated horizontal station rates

To see if the horizontal station rate differences are a system bias or a precise products bias, it is important to analyse the difference between the PPP scenarios using the same precise products for the common components. If the differences between these scenarios is found to be the same for different precise products, then these biases are likely to be a system-dependent bias rather than a product-dependent bias. To achieve that, the mean of each daily solution was computed for different PPP scenarios, and the difference from the mean for each PPP solution was computed. To remove the observation noise, a moving average was computed with a time window of 10 days.

It was found that the East component behaves differently with time. Sometimes the PPP GLO was higher and sometimes lower than the PPP GPS, except for the APPL (Figure 8-11) and BLAP (Figure 8-12) stations in which the PPP GLO is higher than the PPP GPS for all three precise products. Both of them are coastal stations (being on the edge of the UK).

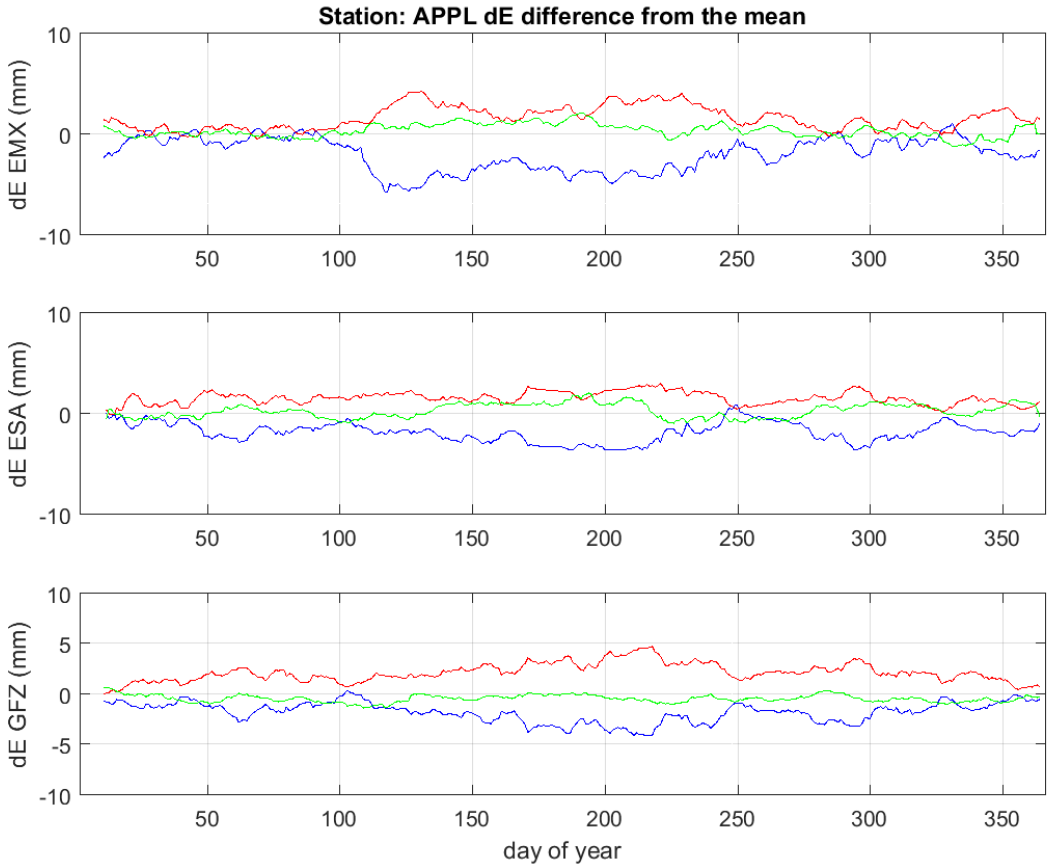


Figure 8-11 Comparison of Moving average East station coordinates for the PPP scenarios using the EMX, ESA and GFZ precise products for the APPL station. (Blue: PPP GPS, Red: PPP GLO, Green: PPP GPS+GLO)

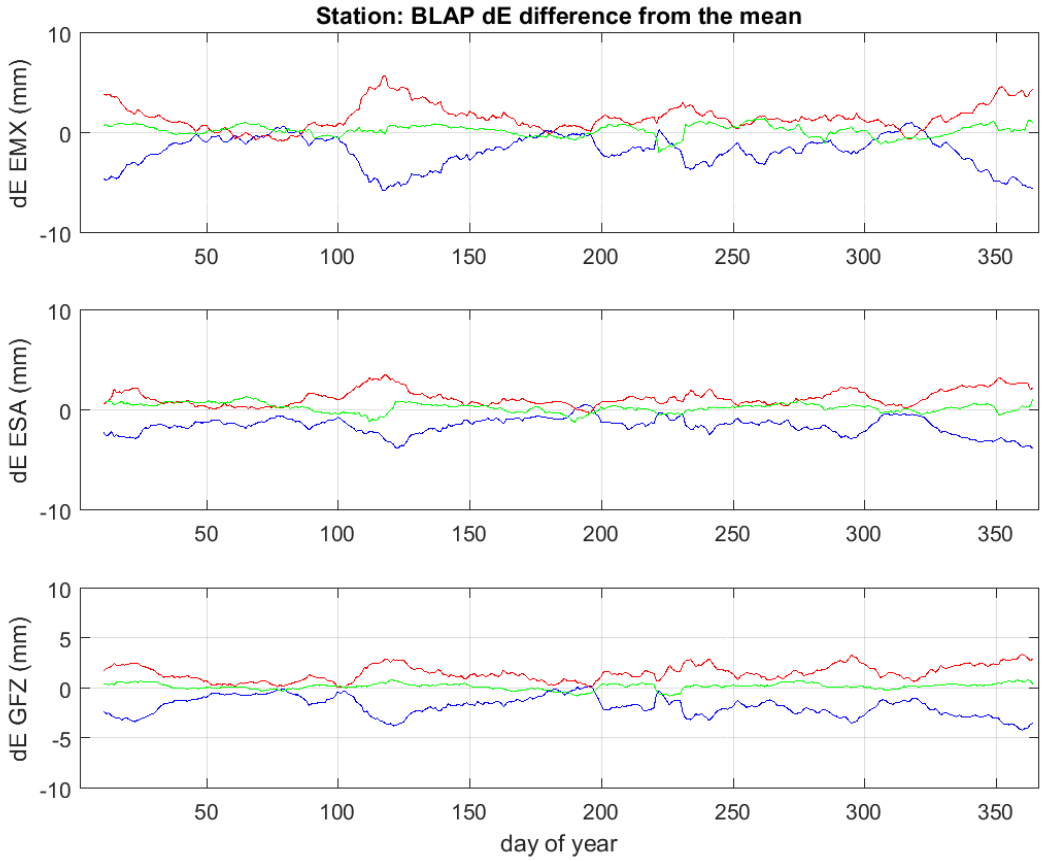


Figure 8-12 Comparison of Moving average East coordinate components for the PPP scenarios using the EMX, ESA and GFZ precise products for the BLAP station. (Blue: PPP GPS, Red: PPP GLO, Green: PPP GPS+GLO)

For the North component, it is found that for all stations that had been used, the PPP GLO station coordinates are higher than for PPP GPS for all precise products (except for: (ARDL, BUCK, CLAW, ESKD, HELS, HOLY, and LEED from >DOY 290), (ATTL BREC KELO KING (sometimes higher, sometimes lower)). This supports the idea that was mentioned before about the PPP GLO station coordinates being more northerly than the PPP GPS because of the GLONASS.

8.5 Differences in estimated horizontal station rates

Considering all three precise products it was found that the estimated horizontal station rates from PPP GPS were the most consistent with the estimated horizontal rates from GDD GPS. Whereas, the PPP GLO gave different estimated horizontal station rates from the GDD GPS, as well as from the PPP GPS, while the PPP GPS+GLO

estimated horizontal station rates were a balance between the PPP GPS and PPP GLO. The differences in estimated horizontal station rates are summarized in Figure 8-13, Figure 8-14 and Figure 8-15 for GDD GPS and PPP GPS , PPP GLO and PP GPS+GLO using EMX, ESA and GFZ precise products respectively.

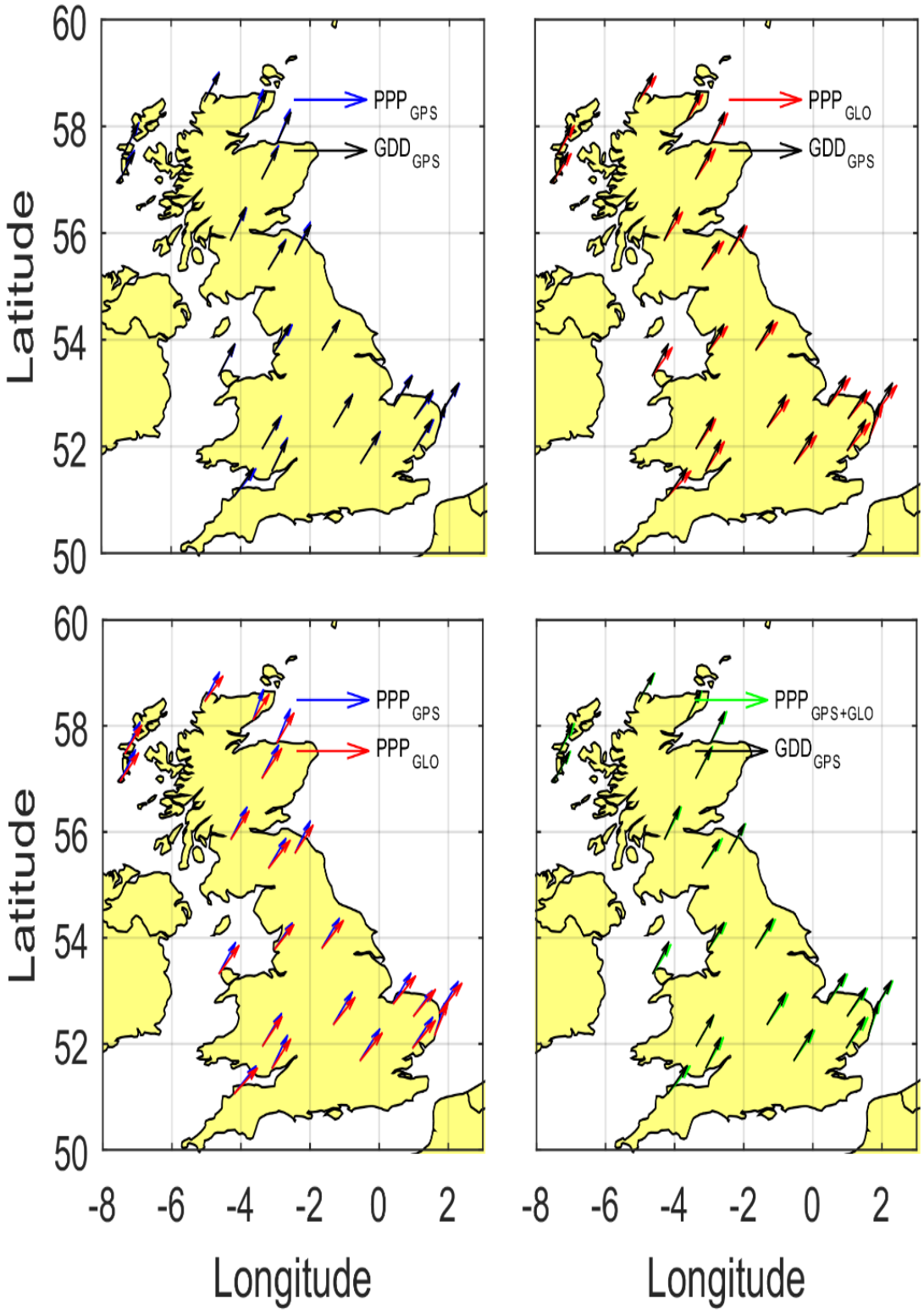


Figure 8-13 Horizontal station Rate comparisons using EMX precise products

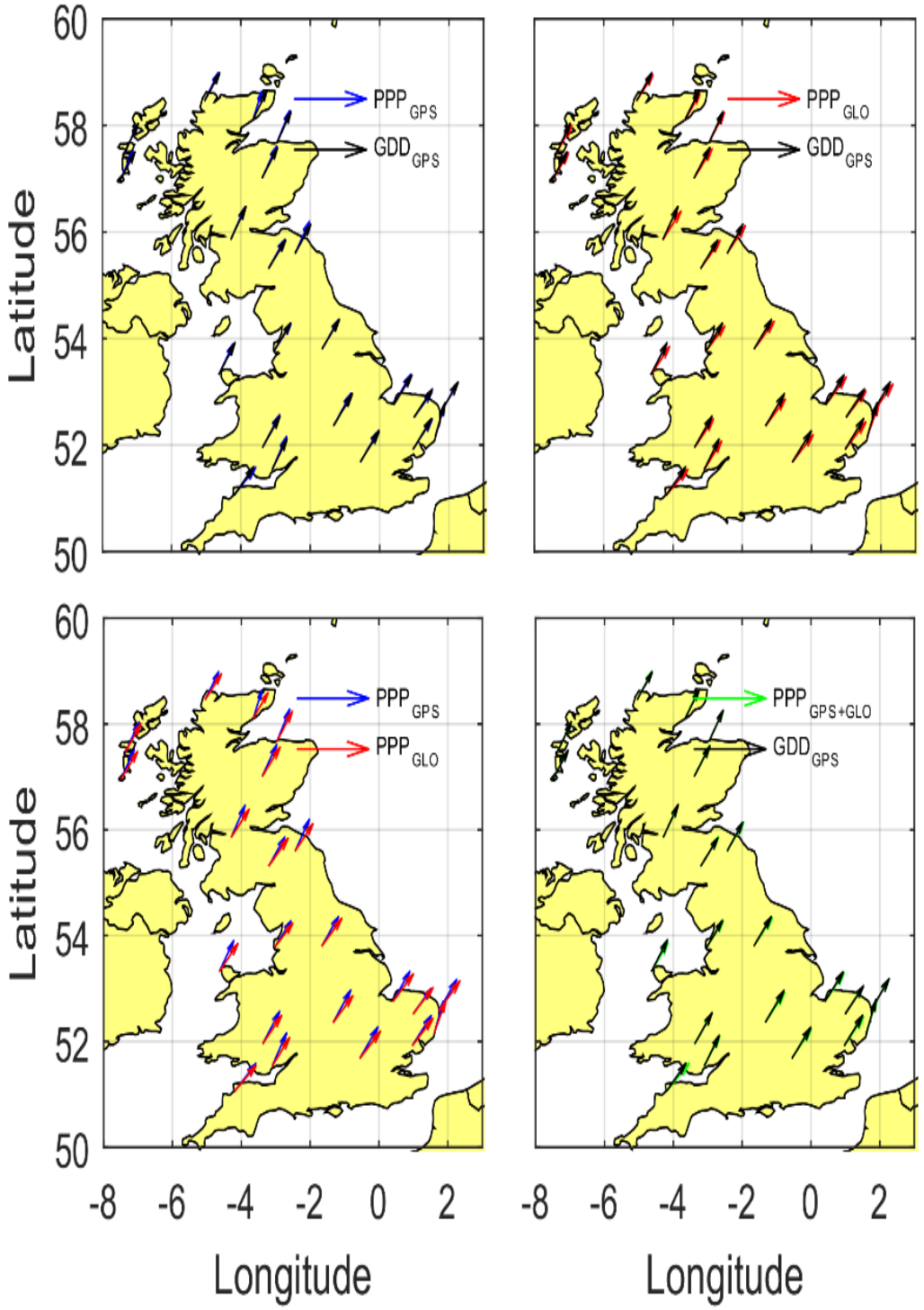


Figure 8-14 Horizontal station rate comparisons using ESA precise products

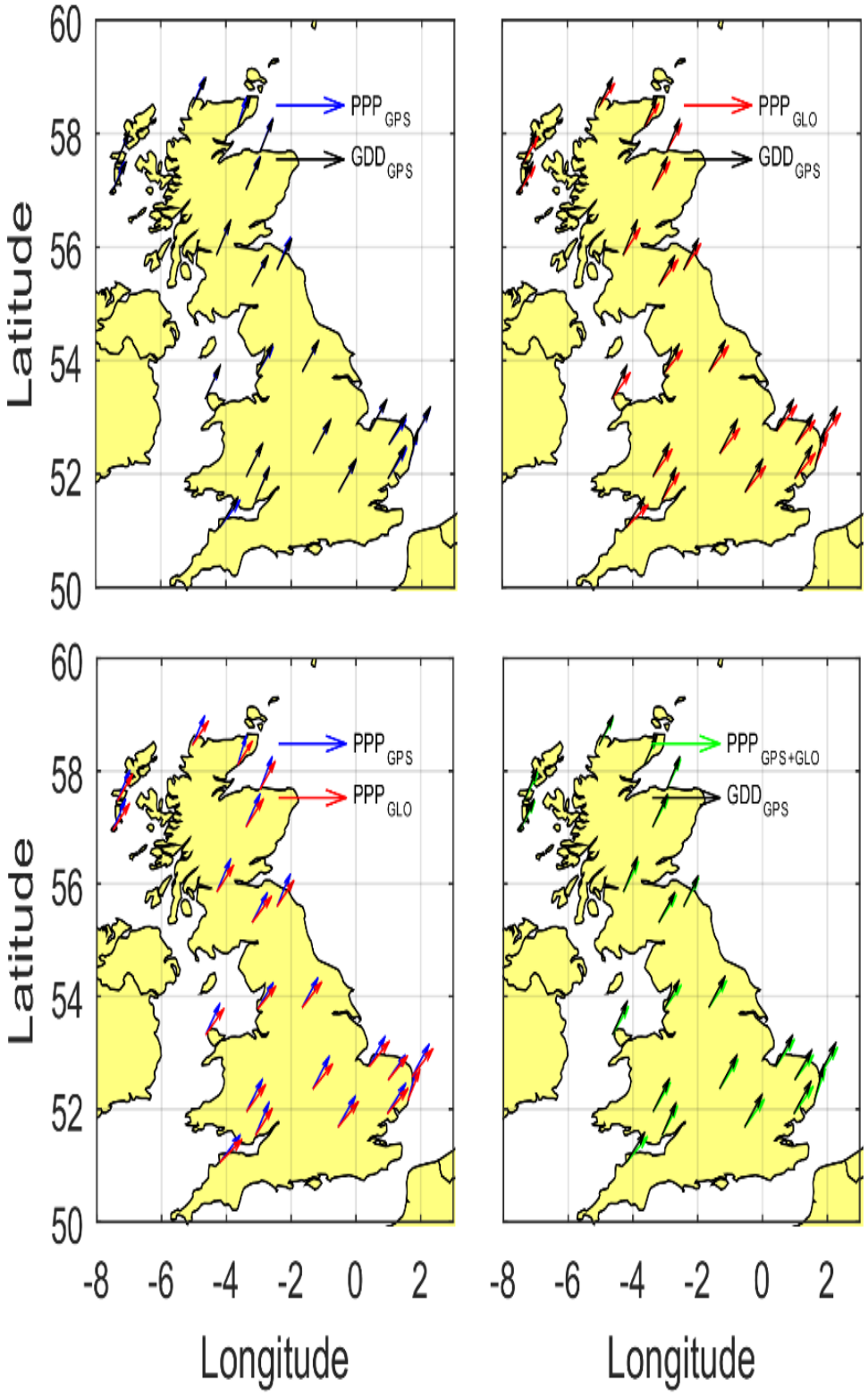


Figure 8-15 Horizontal station Rate comparisons using GFZ precise products

This indicates that the difference between the estimated horizontal station rates is a system-dependence rather than being a product-dependence. Thus, there is a need to investigate the two components of the rate, the magnitude, and the orientation to see if any significant differences are present.

As summarized in Figure 8-16 and 8-17 for both constellations and all precise products, it is found that the major difference originates in the orientation (bearing computed from the north), for PPP GPS this ranges from ~ 25° to 50° whereas for PPP GLO this ranges from ~38° to 55°. Whereas, for magnitude this is more consistent, in the range of 17 to 25 mm/yr for both PPP GPS and PPP GLO.

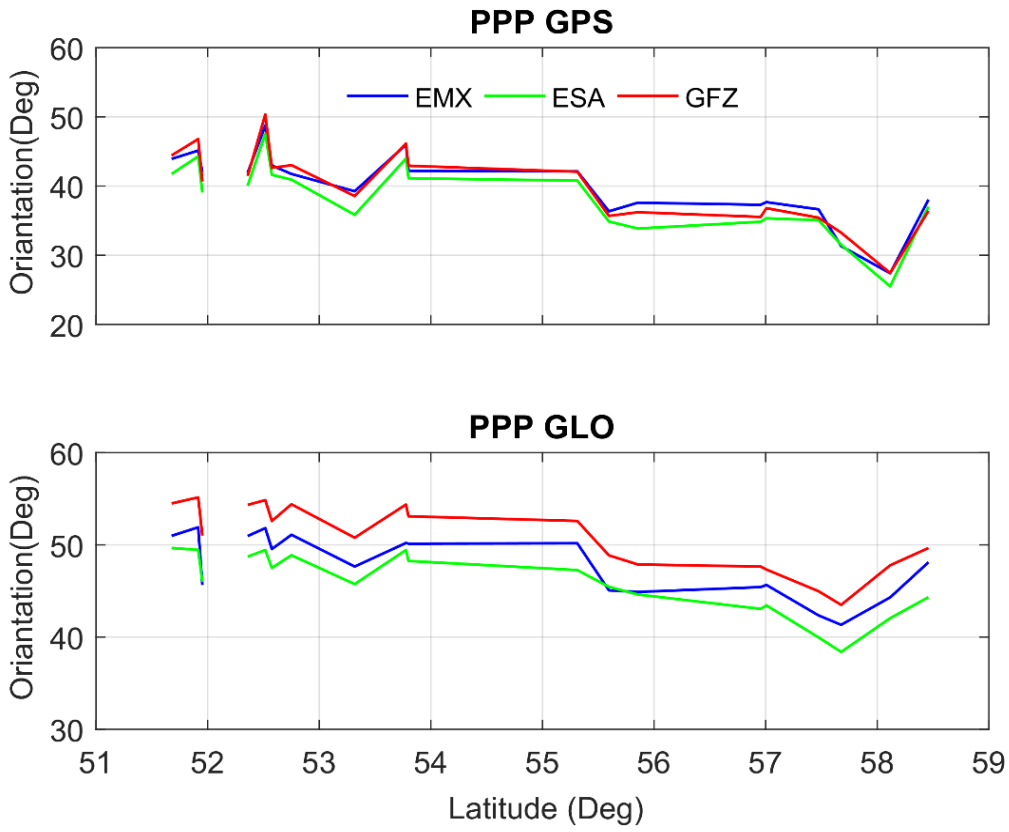


Figure 8-16 Comparison of the horizontal station rate orientations from PPP GPS and PPP GLO using the EMX, ESA and GFZ precise products

The precise products have a smaller effect on the orientation and magnitude.

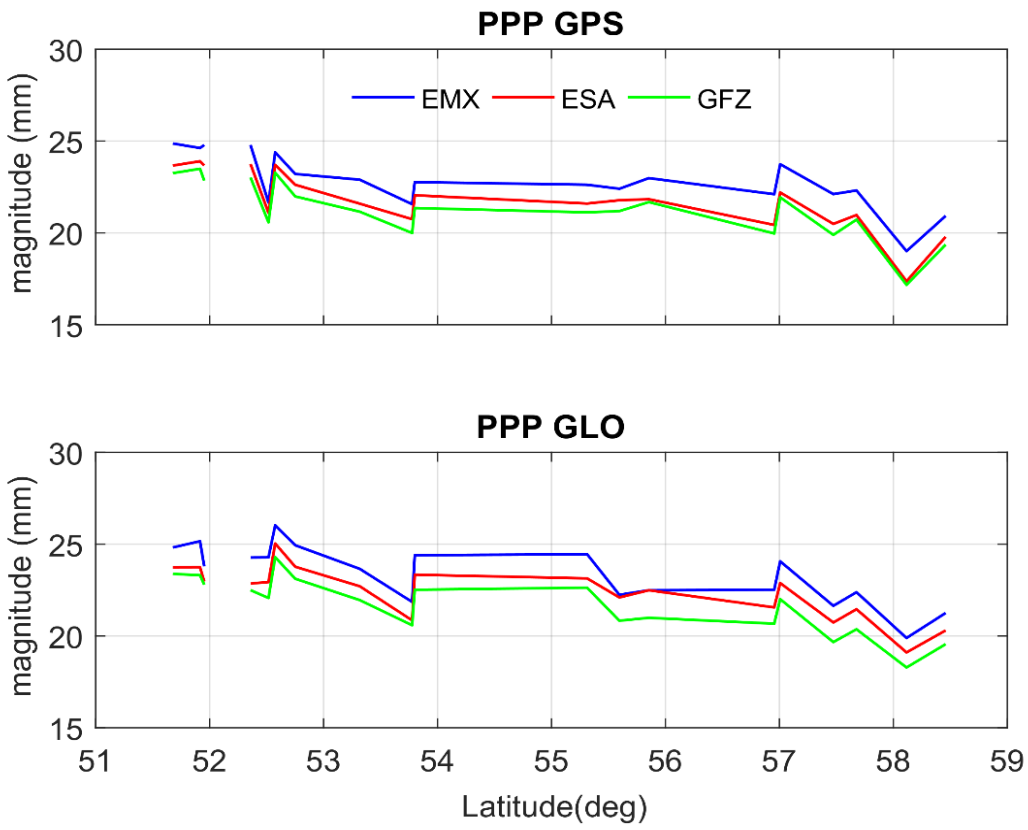


Figure 8-17 Comparison of horizontal station rate magnitudes from PPP GPS and PPP GLO using the EMX, ESA and GFZ precise products

A potential reason for these differences is the reference frame; as ITRF2008 only contains a limited number of GPS+GLO stations, which will affect the ITRF to be more consistent with GPS rather than with GLO. For that reason, PPP GPS could be more consistent than PPP GLO in terms of estimating horizontal station rates because all GPS precise products are more closely aligned to the reference frame than GLO precise products, at this moment in time.

8.6 Chapter Summary

This chapter set out to analyse the potential of using PPP GLO for station velocity estimation, though comparison of horizontal station rates with PPP GPS as well as GDD GPS, for a one-year dataset. In addition, the effect of different precise products on the station coordinates repeatability and the horizontal rate estimation were considered. This was done using 22 OSGB stations in the UK.

It was found that the East coordinate repeatability is almost the same for PPP GPS compared to GDD GPS while it is worse for PPP GLO. However, this was within the range of less than 1 mm. The PPP GPS+GLO repeatability was found to be a balance between the PPP GPS and PPP GLO. By looking to the PPP GLO, it can be seen that in terms of the North coordinate repeatability it is performing better than the GDD GPS for all the stations, which reflects the availability of the satellites to the north for the GLONASS. The GPS+GLO scenario improves the coordinate repeatability for the majority of stations with respect to PPP GPS, however, some stations still have better coordinate repeatability in PPP GLO.

It was also found that the estimated horizontal station rates from PPP GPS are consistent with GDD GPS, even when they are coming from a different strategy, which suggests the stability of the PPP GPS solution over the long-term. However, a noticeable bias between the estimated horizontal station rates from PPP GLO and the others (PPP GPS and GDD GPS) was found and considered to be a system difference effect with the significant effect being on orientation rather than magnitude, suggesting that GPS precise products are more closely aligned to the reference frame than GLO precise products at this moment of time.

Chapter 9. Conclusions and recommendations

The PPP multi-constellation GNSS is a growing tool for research. GPS and GLONASS are of particular interest to this study, because they are fully operational and present the possibility of using PPP GPS or PPP GPS+GLONASS, but also to consider PPP GLO as an independent solution for which there is little-published research to date.

These conclusions and recommendations are presented in six parts and follow the thread of the thesis in providing a comprehensive review of the main research and developments that have focused on the improvement of PPP over the last few decades, and then presenting the contributions that have been made by the author through three assessments.

9.1 PPP background and initial analyses

The first part of the thesis was a theoretical part, in which PPP was reviewed and background on all of the errors, biases and models involved in PPP were introduced. Considering these, a problem statement and research aims were introduced, with attention drawn to the fact that PPP GLO has not been closely studied, even for station coordinate estimation or station velocities. Furthermore, a potential for improving PPP tropospheric zenith total delay (ZTD) estimation, beyond the current use of models for tropospheric ZHD combined with an estimation of tropospheric ZWD, was also identified.

Thus, a need to cover these gaps in knowledge was considered, in terms of investigating the achievable accuracy from PPP GPS, PPP GLO and PPP GPS+GLO for station coordinates, tropospheric ZTD, and station velocities, through carrying out further developments to the POINT software made available to the author and using a variety of test datasets.

To support the main research aims, some initial analysis was carried out, This included: the development of an alternative approach for evaluating the constellation

geometry based on cumulative Dilation of Precision (DOP); studies on the effect of weighting functions on PPP convergence time and station coordinate accuracy, which found that without using weighting functions gave the best performance and also presented a better approach for evaluating the observables as well as the constellations; studies of the mp1 and mp2 values at 85 OSGB stations, which found that a few stations exhibited abnormal behaviour and were potential high multipath sites; studies on convergence time, which found this to be slightly better for PPP GPS than PPP GLO, but that PPP GPS+GLO was the best overall.

9.2 PPP station coordinate assessment

The first part of the assessment considered the use of PPP GPS, PPP GLO and PPP GPS+GLO in terms of station coordinate accuracy and precision when using precise products from EMX, ESA and GFZ, with a suggested strategy to be followed for achieving high accuracy PPP results from all PPP scenarios.

In terms of station coordinate accuracy and precision, an initial investigation using one-year of data for two OSGB stations was presented followed by an extended experiment, and it was concluded that PPP can achieve similar accuracy and precision as GDD in term of station coordinates. Most interesting was the capability of PPP GLO to produce similar accuracy and precision to both PPP GPS and GDD GPS, which implies that PPP GLO can be used as an independent solution to PPP GPS for station coordinate estimation, rather than being used as simply increasing the number of observations for the base GPS in PPP GPS+GLO. On closer inspection, it was found that there were noticeable biases between the PPP and the GDD station coordinates in the North component. It was also found that these biases are system-dependent, and that the PPP GLO will be affected more than the PPP GPS, while the PPP GPS+GLO will be a balance between both constellations.

Moving to the analysis of the precise products from three different analysis centres, as well as their effect on PPP solutions, it was found that the receiver clock

offsets in PPP were shown to be affected by the chosen reference station (time base) which leads to a propagated time offset in all of the estimated satellite clock offsets However, even though this propagated time offset can reach hundreds of nanoseconds, it can be dealt with if the receiver clock offset is modelled correctly and is allowed to change in order to absorb this effect. While for the precise products effect on the station coordinates, it was found that the satellite coordinates from different precise products have an effect on the station coordinates at the millimetre level in PPP, and that it is the number of reference stations and the network geometry used in producing the precise products that affects the satellite coordinates, which led to slightly more stable GPS orbits than GLO orbits with the reference networks used 2014.

9.3 PPP tropospheric ZTD assessment, including an alternative tropospheric strategy

The second part of the assessment was to investigate the troposphere in PPP, to compare the effect of different tropospheric models for tropospheric ZTD, the effect of using the conventional tropospheric strategy for estimating tropospheric ZTD, and to present an alternative tropospheric strategy for estimating tropospheric ZTD. It was concluded that for PPP, the conventional tropospheric strategy based on modelling tropospheric ZHD and estimating tropospheric ZWD does not have the ability to produce millimetre accuracy for tropospheric ZTD, even though the estimated station coordinates are accurate, because the estimated receiver clock offsets and ambiguities absorb any un-mitigated tropospheric ZTD. While for the alternative tropospheric strategy, which is based on estimating both the tropospheric ZHD and ZWD using different mapping functions and different process noise in the Extended Kalman filter, it was found that this results in tropospheric ZTD which compares more favourably with that from GDD. These conclusions were based on validations that were conducted for the alternative tropospheric strategy using PPP GPS, PPP GLO and PPP GPS+GLO, on OSGB stations in the UK, using 7 consecutive days first, followed by an expanded regional validation for a seven week dataset of up to 85 OSGB stations, then a long-

term (over one year) validation for 22 OSGB stations. This research also considered the effect of three different final precise products, namely EMX, ESA and GFZ. Furthermore, a global validation using ~76 IGS stations was also done over a different period and conducted in three stages, using EMX final, IGS final and IGS real-time precise products, and showed that the estimated tropospheric ZTD compared favourably with the IGS final and near real-time solutions, suggesting that this approach can be used in real-time as well as post processing without significant differences between the results.

9.4 PPP station rate/velocity assessment

The third part of the assessment was conducted to analyse the potential of using PPP GLO for station rate/velocity estimation, though a comparison of horizontal station rates with PPP GPS as well as GDD GPS, for a one-year dataset for 22 OSGB stations in the UK. In addition, the effect of different precise products on station coordinate repeatability and horizontal station rate estimation were considered.

It was found that the East coordinate repeatability is almost the same for PPP GPS as it is for GDD GPS, while it is slightly worse for PPP GLO (within the range of less than 1 mm), and the PPP GPS+GLO repeatability was found to be a balance between the PPP GPS and PPP GLO. For PPP GLO, however, it was found that in terms of the North coordinate repeatability, it is actually performing better than GDD GPS for all stations, which reflects the availability of satellites to the north from the GLONASS. Furthermore, it was found that the estimated horizontal station rates from PPP GPS are consistent with GDD GPS, even when they are coming from a different strategy, which suggests the stability of the PPP GPS solution over the long-term. However, a noticeable bias between the estimated horizontal station rates from PPP GLO and the others (PPP GPS and GDD GPS) was found and considered to be a system difference, with the significant effect being on orientation rather than magnitude, suggesting that GPS precise products were more closely aligned to the reference frame than GLO precise products at that moment of time in 2014.

9.5 Conclusion summary

Returning to the aims that were set in the beginning of this study, it is now possible to state that:

- The PPP is an efficient tool that is capable of producing the same station coordinate precision as the Global Double-Difference (GDD).
- PPP GLO has the same station coordinate precision and almost the same station coordinate accuracy as PPP GPS, as well as GDD GPS, and so can provide an accurate and independent solution.
- The precise products lead to almost the same precision but slightly different accuracy of station coordinates, especially in the Up component, because of the different strategy and the different number of stations that formulated the network.
- The conventional tropospheric strategy used in PPP is not capable of producing accurate tropospheric ZTD; whereas, the alternative tropospheric strategy proposed by the author is, and presents the possibility to turn the PPP into an accurate and precise tool not just for station coordinates but for tropospheric ZTD as well.
- In terms of station rates/velocities, the PPP GLO is a promising technique which has the potential to be used as an independent tool for crustal motion studies, provided the observed bias between the PPP GPS and the PPP GLO station rates/velocities can be addressed.

It is noteworthy to mention that the objectives of this study have also been achieved, although there are clear opportunities for further development and studies, as discussed in the following section.

9.6 Recommendations for Future Work

As with any research, this research has been conducted with certain restrictions, some of which could be addressed in the future.

Ambiguity resolution for the PPP was kept as a float solution because there is a need for the fractional cycle biases to be defined from other sources and because the models in the POINT software are not identical to those used in the production of the precise products. Despite this, obtained accuracy and precision in this research does reflect the actual capability of PPP for 24 hours observation in static mode. However, ambiguity resolution in the POINT software could be studied for improving other issues, e.g. convergence time.

Concerning the alternative tropospheric strategy, it is important for further research to test this over a longer time period, and with different initial values, so that a further validation of the two separated components (the estimated tropospheric ZHD and ZWD) can be carried out against a trusted source that can provide a high temporal resolution as well as high spatial resolution. It would also be interesting to test the alternative tropospheric strategy using a fixed solution, and with consideration of higher order ionosphere. In addition, a test of the alternative tropospheric strategy in kinematic mode would be interesting, as this could make an improvement to the estimated components, and could be done with a static receiver processed as kinematic or from a moving receiver.

In addition to further testing of PPP GLO over the longer term, with improved reference frames and precise products, the inclusion of Beidou, and Galileo could also be evaluated in terms of station coordinate accuracy and precision, as well as the alternative tropospheric strategy, and it would be interesting to test and validate them using real data rather than simulated data.

References

ABDEL-SALAM, M. A. T. 2005. *Precise Point Positioning Using Un-Differenced Code and Carrier Phase Observations.* PhD, University of Calgary.

ABDI, N., ARDALAN, A. A., KARIMI, R. & REZVANI, M. H. 2017. Performance assessment of multi-GNSS real-time PPP over Iran. *Advances in Space Research,* 59**,** 2870-2879.

ABRAHA, K. E., TEFERLE, F. N., HUNEGNAW, A. & DACH, R. 2017. GNSS related periodic signals in coordinate time-series from Precise Point Positioning. *Geophysical Journal International,* 208**,** 1449-1464.

AFIFI, A. & EL-RABBANY, A. 2016. Precise Point Positioning Using Triple GNSS Constellations in Various Modes. *Sensors (Basel),* 16.

AGRELL, E., ERIKSSON, T., VARDY, A. & ZEGER, K. 2002. Closest point search in lattices. *Ieee Transactions on Information Theory,* 48**,** 2201-2214.

AHMED, F., VÁCLAVOVIC, P., TEFERLE, F. N., DOUŠA, J., BINGLEY, R. & LAURICHESSE, D. 2014. Comparative analysis of real-time precise point positioning zenith total delay estimates. *GPS Solutions,* 20**,** 187-199.

ALINIA, H. S., TIAMPO, K. F. & JAMES, T. S. 2017. GPS coordinate time series measurements in Ontario and Quebec, Canada. *Journal of Geodesy,* 91**,** 653-683.

ALTAMIMI, Z., COLLILIEUX, X., LEGRAND, J., GARAYT, B. & BOUCHER, C. 2007. ITRF2005: A new release of the International Terrestrial Reference Frame based on time series of station positions and earth orientation parameters. *Journal of Geophysical Research-Solid Earth,* 112.

ALTAMIMI, Z., COLLILIEUX, X. & METIVIER, L. 2011. ITRF2008: an improved solution of the international terrestrial reference frame. *Journal of Geodesy,* 85**,** 457-473.

ALTAMIMI, Z., SILLARD, P. & BOUCHER, C. 2002. ITRF2000: A new release of the International Terrestrial Reference frame for earth science applications. *Journal of Geophysical Research-Solid Earth,* 107.

AMIRI-SIMKOOEI, A. R., MOHAMMADLOO, T. H. & ARGUS, D. F. 2017. Multivariate analysis of GPS position time series of JPL second reprocessing campaign. *Journal of Geodesy,* 91**,** 685-704.

ANQUELA, A. B., MARTIN, A., BERNE, J. L. & PADIN, J. 2013. GPS and GLONASS Static and Kinematic PPP Results. *Journal of Surveying Engineering-Asce,* 139**,** 47-58.

ARGUS, D. F. & HEFLIN, M. B. 1995. Plate Motion and Crustal Deformation Estimated with Geodetic Data from the Global Positioning System. *Geophysical Research Letters,* 22**,** 1973-1976.

ARGUS, D. F., PELTIER, W. R. & WATKINS, M. M. 1999. Glacial isostatic adjustment observed using very long baseline interferometry and satellite laser ranging geodesy. *Journal of Geophysical Research-Solid Earth,* 104**,** 29077-29093.

ASHBY, N. 2003. Relativity in the Global Positioning System. *Living Rev Relativ,* 6**,** 1.

BAKER, H. C., DODSON, A. H., PENNA, N. T., HIGGINS, M. & OFFILER, D. 2001. Ground-based GPS water vapour estimation: potential for meteorological forecasting. *Journal of Atmospheric and Solar-Terrestrial Physics,* 63**,** 1305-1314.

BALAEI, A., WU, J. & DEMPSTER, A. G. 2007. Comparison between GPS and Galileo satellite availability in the presence of CW interference. *International Global Navigation Satellite Systems Society IGNSS Symposium 2007.* Sydney, Australia.

BANVILLE, S. 2016. GLONASS ionosphere-free ambiguity resolution for precise point positioning. *Journal of Geodesy,* 90**,** 487-496.

BANVILLE, S. & LANGLEY, R. B. 2009. Improving Real-Time Kinematic PPP with Instantaneous Cycle-Slip Correction. *Journal of The Institute of Navigation,* 57**,** 325-334.

BAR-SEVER, Y. E., KROGER, P. M. & BORJESSON, J. A. 1998. Estimating horizontal gradients of tropospheric path delay with a single GPS receiver. *Journal of Geophysical Research-Solid Earth,* 103**,** 5019-5035.

BASSIRI, S. & HAJJ, G. A. 1993. Higher-order ionospheric effects on the global positioning system observables and means of modeling them. *Manuscripta geodaetica,* 18**,** 280-280.

BDS-OS-PS-2.0 2013. BeiDou Navigation Satellite SystemSignal In Space Interface Control Document v 2.0.

BEVIS, M., BUSINGER, S., HERRING, T. A., ROCKEN, C., ANTHES, R. A. & WARE, R. H. 1992. Gps Meteorology - Remote-Sensing of Atmospheric Water-Vapor Using the Global Positioning System. *Journal of Geophysical Research-Atmospheres,* 97**,** 15787-15801.

BHATTA, B. 2011. *Global Navigation Satellite Systems: Insights Into GPS, GLONASS, Galileo, Compass, and Others*, BS Publications.

BIGF 2014. The services of the Natural Environment Research Council (NERC) British Isles continuous GNSS Facility (BIGF).

BISNATH, S. B., MENDES, V. B. & LANGLEY, R. B. 1997. Effects of tropospheric mapping functions on space geodetic data. *1997 IGS Analysis Center Workshop.* Pasadena, Canada.

BLACK, H. D. & EISNER, A. 1984. Correcting Satellite Doppler Data for Tropospheric Effects. *Journal of Geophysical Research-Atmospheres,* 89**,** 2616-2626.

BLEWITT, G. 1989. Carrier Phase Ambiguity Resolution for the Global Positioning System Applied to Geodetic Baselines up to 2000 Km. *Journal of Geophysical Research-Solid Earth and Planets,* 94**,** 10187-10203.

BLEWITT, G. 2014. *Nevada Geodetic Laboratory (NGL), Position time*

series.NevadaGeodetic Laboratory, Reno,NV. http://geodesy.unr.

edu/index.php. [Online]. [Accessed].

BLEWITT, G. & LAVALLEE, D. 2002. Effect of annual signals on geodetic velocity. *Journal of Geophysical Research-Solid Earth,* 107**,** ETG 9-1-ETG 9-11.

BOCK, O., BOSSER, P., BOURCY, T., DAVID, L., GOUTAIL, F., HOAREAU, C., KECKHUT, P., LEGAIN, D., PAZMINO, A., PELON, J., PIPIS, K., POUJOL, G., SARKISSIAN, A., THOM, C., TOURNOIS, G. & TZANOS, D. 2013. Accuracy assessment of water vapour measurements from in situ and remote sensing techniques during the DEMEVAP 2011 campaign at OHP. *Atmospheric Measurement Techniques,* 6**,** 2777-2802.

BOCK, O., BOSSER, P., PACIONE, R., NURET, M., FOURRIE, N. & PARRACHO, A. 2016. A high-quality reprocessed ground-based GPS dataset for atmospheric process studies, radiosonde and model evaluation, and reanalysis of HyMeX Special Observing Period. *Quarterly Journal of the Royal Meteorological Society,* 142**,** 56-71.

BOCK, Y., ABBOT, R. I., COUNSELMAN, C. C. & KING, R. W. 1986. A demonstration of 1–2 parts in 107 accuracy using GPS. *Bulletin Géodésique,* 60**,** 241-254.

BOEHM, J., HEINKELMANN, R. & SCHUH, H. 2007. Short Note: A global model of pressure and temperature for geodetic applications. *Journal of Geodesy,* 81**,** 679-683.

BOEHM, J., KOUBA, J. & SCHUH, H. 2008. Forecast Vienna Mapping Functions 1 for real-time analysis of space geodetic observations. *Journal of Geodesy,* 83**,** 397-401.

BOEHM, J., NIELL, A., TREGONING, P. & SCHUH, H. 2006a. Global Mapping Function (GMF): A new empirical mapping function based on numerical weather model data. *Geophysical Research Letters,* 33.

BOEHM, J. & SCHUH, H. 2004. Vienna mapping functions in VLBI analyses. *Geophysical Research Letters,* 31.

BOEHM, J., WERL, B. & SCHUH, H. 2006b. Troposphere mapping functions for GPS and very long baseline interferometry from European Centre for Medium-Range Weather Forecasts operational analysis data. *Journal of Geophysical Research-Solid Earth,* 111.

BOGUSZ, J. & KLOS, A. 2015. On the significance of periodic signals in noise analysis of GPS station coordinates time series. *GPS Solutions,* 20**,** 655-664.

BÖHM, J., MÖLLER, G., SCHINDELEGGER, M., PAIN, G. & WEBER, R. 2014. Development of an improved empirical model for slant delays in the troposphere (GPT2w). *GPS Solutions,* 19**,** 433-441.

BOS, M. S., FERNANDES, R. M. S., WILLIAMS, S. D. P. & BASTOS, L. 2012. Fast error analysis of continuous GNSS observations with missing data. *Journal of Geodesy,* 87**,** 351-360.

BOSSER, P., BOCK, O., THOM, C., PELON, J. & WILLIS, P. 2009. A case study of using Raman lidar measurements in high-accuracy GPS applications. *Journal of Geodesy,* 84**,** 251-265.

BRACK, A. 2014. On reliable data-driven partial GNSS ambiguity resolution. *GPS Solutions,* 19**,** 411-422.

BRACK, A. & GUNTHER, C. 2014. Generalized integer aperture estimation for partial GNSS ambiguity fixing. *Journal of Geodesy,* 88**,** 479-490.

BYUN, S. H. & BAR-SEVER, Y. E. 2009. A new type of troposphere zenith path delay product of the international GNSS service. *Journal of Geodesy,* 83**,** 367-373.

CAI, C. 2009. *Precise point positioning using dual-frequency GPS and GLONASS measurements.* Msc.

CAI, C. & GAO, Y. 2007. Precise Point Positioning Using Combined GPS and GLONASS Observations. *Journal of Global Positioning Systems,* 6**,** 13-22.

CAI, C. & GAO, Y. 2008. Estimation of GPS-GLONASS System Time Difference with Application to PPP. *Proceedings of the 21st International Technical Meeting of the Satellite Division of The Institute of Navigation (ION GNSS 2008).* Savannah, GA.

CAI, C., LIU, Z. & LUO, X. 2013. Single-frequency Ionosphere-free Precise Point Positioning Using Combined GPS and GLONASS Observations. *Journal of Navigation,* 66**,** 417-434.

CAI, C. S. & GAO, Y. 2009. A Combined GPS/GLONASS Navigation Algorithm for use with Limited Satellite Visibility. *Journal of Navigation,* 62**,** 671-685.

CAI, C. S. & GAO, Y. 2013a. GLONASS-based precise point positioning and performance analysis. *Advances in Space Research,* 51**,** 514-524.

CAI, C. S. & GAO, Y. 2013b. Modeling and assessment of combined GPS/GLONASS precise point positioning. *Gps Solutions,* 17**,** 223-236.

CAI, C. S., GAO, Y., PAN, L. & ZHU, J. J. 2015. Precise point positioning with quad-constellations: GPS, BeiDou, GLONASS and Galileo. *Advances in Space Research,* 56**,** 133-143.

CALAIS, E., HAN, J. Y., DEMETS, C. & NOCQUET, J. M. 2006. Deformation of the North American plate interior from a decade of continuous GPS measurements. *Journal of Geophysical Research-Solid Earth,* 111.

CAPILLA, R. M., BERNE, J. L., MARTIN, A. & RODRIGO, R. 2016. Simulation case study of deformations and landslides using real-time GNSS precise point positioning technique. *Geomatics Natural Hazards & Risk,* 7**,** 1856-1873.

CARDELLACH, E., ELOSEGUI, P. & DAVIS, J. L. 2007. Global distortion of GPS networks associated with satellite antenna model errors. *Journal of Geophysical Research-Solid Earth,* 112.

CHEN, G. & HERRING, T. A. 1997. Effects of atmospheric azimuthal asymmetry on the analysis of space geodetic data. *Journal of Geophysical Research-Solid Earth,* 102**,** 20489-20502.

CHEN, J. P., ZHANG, Y. Z., WANG, J. G., YANG, S. N., DONG, D. A., WANG, J. X., QU, W. J. & WU, B. 2015. A simplified and unified model of multi-GNSS precise point positioning. *Advances in Space Research,* 55**,** 125-134.

CHEN, W. R., GAO, C. F. & PAN, S. G. 2014. Assessment of GPT2 Empirical Troposphere Model and Application Analysis in Precise Point Positioning. *China Satellite Navigation Conference (CSNC) 2014 Proceedings: Volume II.*

COLLINS, P., BISNATH, S., LAHAYE, F. & HÉROUX, P. 2010. Undifferenced GPS Ambiguity Resolution Using the Decoupled Clock Model and Ambiguity Datum Fixing. *Navigation,* 57**,** 123-135.

DACH, R. & DIETRICH, R. 2000. Influence of the ocean loading effect on GPS derived precipitable water vapor. *Geophysical Research Letters,* 27**,** 2953-2956.

DACH, R., HUGENTOBLER, U., FRIDEZ, P. & MEINDL, M. 2007. Bernese GPS software version 5.0 (user manual of the Bernese GPS software version 5.0). *AIUB—Astronomical Institute, University of Bern, Switzerland.*

DACH, R., LUTZ, S., WALSER, P. & FRIDEZ, P. 2015. Bernese GNSS Software Version 5.2. Astronomical Institute, University of Bern.

DAI, L., ESLINGER, D. & SHARPE, T. Innovative algorithms to improve long range RTK reliability and availability. Proceedings of the 2007 National Technical Meeting of the Institute of Navigation, 2007. 860-872.

DESAI, S., BERTIGER, W., HAINES, B., HARVEY, N., MILLER, M., SELLE, C., SIBTHORPE, A. & WEISS, J. Long-Term Evaluation of Precise Point Positioing wimth Single Receiver Phase Ambiguity Resolution using JPL' GPS Products. EGU General Assembly, 2011 Vienna, Austria.

DING, W. W., TEFERLE, F. N., KAZMIERSKI, K., LAURICHESSE, D. & YUAN, Y. B. 2017. An evaluation of real-time troposphere estimation based on GNSS Precise Point Positioning. *Journal of Geophysical Research-Atmospheres,* 122**,** 2779-2790.

DIXON, T., FARINA, F., DEMETS, C., SUAREZ-VIDAL, F., FLETCHER, J., MARQUEZ-AZUA, B., MILLER, M., SANCHEZ, O. & UMHOEFER, P. 2000. New kinematic models for Pacific-North America motion from 3 ma to present, II: Evidence for a "Baja California shear zone". *Geophysical Research Letters,* 27**,** 3961-3964.

DODSON, A. H., BINGLEY, R. M., PENNA, N. T. & AQUINO, M. H. O. 2000. A national network of continuously operating GPS receivers for the UK. *Geodesy Beyond 2000.*

DODSON, A. H., SHARDLOW, P. J., HUBBARD, L. C. M., ELGERED, G. & JARLEMARK, P. O. J. 1996. Wet tropospheric effects on precise relative GPS height determination. *Journal of Geodesy,* 70**,** 188-202.

DONG, D., FANG, P., BOCK, Y., WEBB, F., PRAWIRODIRDJO, L., KEDAR, S. & JAMASON, P. 2006. Spatiotemporal filtering using principal component analysis and Karhunen-Loeve expansion approaches for regional GPS network analysis. *Journal of Geophysical Research-Solid Earth,* 111**,** n/a-n/a.

DONG, D., HERRING, T. A. & KING, R. W. 1998. Estimating regional deformation from a combination of space and terrestrial geodetic data. *Journal of Geodesy,* 72**,** 200-214.

DOUŠA, J. 2009. The impact of errors in predicted GPS orbits on zenith troposphere delay estimation. *GPS Solutions,* 14**,** 229-239.

DOUSA, J., DICK, G., KACMARIK, M., BROZKOVA, R., ZUS, F., BRENOT, H., STOYCHEVA, A., MOLLER, G. & KAPLON, J. 2016. Benchmark campaign and case study episode in central Europe for development and assessment of advanced GNSS tropospheric models and products. *Atmospheric Measurement Techniques,* 9**,** 2989-3008.

DOUSA, J. & VACLAVOVIC, P. 2014. Real-time zenith tropospheric delays in support of numerical weather prediction applications. *Advances in Space Research,* 53**,** 1347-1358.

DUAN, J. P., BEVIS, M., FANG, P., BOCK, Y., CHISWELL, S., BUSINGER, S., ROCKEN, C., SOLHEIM, F., VANHOVE, T., WARE, R., MCCLUSKY, S., HERRING, T. A. & KING, R. W. 1996. GPS meteorology: Direct estimation of the absolute value of precipitable water. *Journal of Applied Meteorology,* 35**,** 830-838.

ELSOBEIEY, M. 2014. Precise Point Positioning using Triple-Frequency GPS Measurements. *Journal of Navigation,* 68**,** 480-492.

ELSOBEIEY, M. & EL-RABBANY, A. 2010. On stochastic modeling of the modernized global positioning system (GPS) L2C signal. *Measurement Science and Technology,* 21**,** 055105.

ESTEY, L. & WIER, S. 2014. Teqc Tutorial: Basics of Teqc Use and Teqc Products.

ESTEY, L. H. & MEERTENS, C. M. 1999. TEQC: The Multi-Purpose Toolkit for GPS/GLONASS Data. *GPS Solutions,* 3**,** 42-49.

FENG, S., OCHIENG, W., MOORE, T., HILL, C. & HIDE, C. 2008. Carrier phase-based integrity monitoring for high-accuracy positioning. *GPS Solutions,* 13**,** 13-22.

FRITSCHE, M., DIETRICH, R., KNOFEL, C., RULKE, A., VEY, S., ROTHACHER, M. & STEIGENBERGER, P. 2005. Impact of higher-order ionospheric terms on GPS estimates. *Geophysical Research Letters,* 32.

GABOR, M. & NEREM, R. 2000. Characteristics of Satellite-Satellite Single Difference Widelane Fractional Carrier Phase Biases. *ION GPS 2000.* Salt Lake City, UT.

GABOR, M. J. & NEREM, R. S. 1999. GPS Carrier phase Ambiguity Resolution Using Satellite-Satellite Single Differences. *ION GPS 1999.* Nashville, TN.

GAO, Z., ZHANG, H., GE, M., NIU, X., SHEN, W., WICKERT, J. & SCHUH, H. 2016. Tightly coupled integration of multi-GNSS PPP and MEMS inertial measurement unit data. *GPS Solutions,* 21**,** 377-391.

GE, M., GENDT, G., ROTHACHER, M., SHI, C. & LIU, J. 2007. Resolution of GPS carrier-phase ambiguities in Precise Point Positioning (PPP) with daily observations. *Journal of Geodesy,* 82**,** 389-399.

GE, M. R., CALAIS, E. & HAASE, J. 2002. Sensitivity of zenith total delay accuracy to GPS orbit errors and implications for near-real-time GPS meteorology. *Journal of Geophysical Research-Atmospheres,* 107.

GENDT, G., DICK, G., REIGBER, C., TOMASSINI, M., LIU, Y. & RAMATSCHI, M. 2004. Near Real Time GPS Water Vapor Monitoring for Numerical Weather Prediction in Germany. *Journal of the Meteorological Society of Japan. Ser. II,* 82**,** 361-370.

GENDT, G., REIGBER, C. & DICK, G. 2001. Near real-time water vapor estimation in a German GPS network-first results from the ground program of the HGF GASP project. *Physics and Chemistry of the Earth, Part A: Solid Earth and Geodesy,* 26**,** 413-416.

GENG, J., SHI, C., GE, M., DODSON, A. H., LOU, Y., ZHAO, Q. & LIU, J. 2011a. Improving the estimation of fractional-cycle biases for ambiguity resolution in precise point positioning. *Journal of Geodesy,* 86**,** 579-589.

GENG, J., TEFERLE, F. N., MENG, X. & DODSON, A. H. 2011b. Towards PPP-RTK: Ambiguity resolution in real-time precise point positioning. *Advances in Space Research,* 47**,** 1664-1673.

GENG, J., ZHAO, Q., SHI, C. & LIU, J. 2016. A review on the inter-frequency biases of GLONASS carrier-phase data. *Journal of Geodesy,* 91**,** 329-340.

GENG, J. H., MENG, X. L., DODSON, A. H., GE, M. R. & TEFERLE, F. N. 2010a. Rapid re-convergences to ambiguity-fixed solutions in precise point positioning. *Journal of Geodesy,* 84**,** 705-714.

GENG, J. H., MENG, X. L., DODSON, A. H. & TEFERLE, F. N. 2010b. Integer ambiguity resolution in precise point positioning: method comparison. *Journal of Geodesy,* 84**,** 569-581.

GRIFFITHS, J. & RAY, J. R. 2009. On the precision and accuracy of IGS orbits. *Journal of Geodesy,* 83**,** 277-287.

GROUP, R. O. O. B. G. R. 2012. *Tropospheric Delay and GNSS Signals: Tutorial* [Online]. Available: http://gnss.be/troposphere_tutorial.php [Accessed 2015].

GU, S. F., LOU, Y. D., SHI, C. & LIU, J. N. 2015. BeiDou phase bias estimation and its application in precise point positioning with triple-frequency observable. *Journal of Geodesy,* 89**,** 979-992.

GUEROVA, G., JONES, J., DOUSA, J., DICK, G., DE HAAN, S., POTTIAUX, E., BOCK, O., PACIONE, R., ELGERED, G., VEDEL, H. & BENDER, M. 2016. Review of the state of the art and future prospects of the ground-based GNSS meteorology in Europe. *Atmospheric Measurement Techniques,* 9**,** 5385-5406.

GUO, Q. 2014. Precision comparison and analysis of four online free PPP services in static positioning and tropospheric delay estimation. *GPS Solutions,* 19**,** 537-544.

GUTMAN, S. I. & BENJAMIN, S. G. 2001. The Role of Ground-Based GPS Meteorological Observations in Numerical Weather Prediction. *GPS Solutions,* 4**,** 16-24.

HAASE, J., CALAIS, E., TALAYA, J., RIUS, A., VESPE, F., SANTANGELO, R., HUANG, X. Y., DAVILA, J. M., GE, M., CUCURULL, L., FLORES, A., SCIARRETTA, C., PACIONE, R., BOCCOLARI, M., PUGNAGHI, S., VEDEL, H., MOGENSEN, K., YANG, X. & GARATE, J. 2001. The contributions of the MAGIC project to the COST 716 objectives of assessing the operational potential of ground-based GPS meteorology on an international scale. *Physics and Chemistry of the Earth Part a-Solid Earth and Geodesy,* 26**,** 433-437.

HAASE, J., GE, M. R., VEDEL, H. & CALAIS, E. 2003. Accuracy and variability of GPS tropospheric delay measurements of water vapor in the western Mediterranean. *Journal of Applied Meteorology,* 42**,** 1547-1568.

HÅKANSSON, M., JENSEN, A. B. O., HOREMUZ, M. & HEDLING, G. 2016. Review of code and phase biases in multi-GNSS positioning. *GPS Solutions*.

HE, X. X., MONTILLET, J. P., FERNANDES, R., BOS, M., YU, K., HUA, X. H. & JIANG, W. P. 2017. Review of current GPS methodologies for producing accurate time series and their error sources. *Journal of Geodynamics,* 106**,** 12-29.

HERNANDEZ-PAJARES, M., ARAGON-ANGEL, A., DEFRAIGNE, P., BERGEOT, N., PRIETO-CERDEIRA, R. & GARCIA-RIGO, A. 2014. Distribution and mitigation of higher-order ionospheric effects on precise GNSS processing. *Journal of Geophysical Research-Solid Earth,* 119**,** 3823-3837.

HERNANDEZ-PAJARES, M., JUAN, J. M., SANZ, J. & ORUS, R. 2007. Second-order ionospheric term in GPS: Implementation and impact on geodetic estimates. *Journal of Geophysical Research-Solid Earth,* 112.

HEROUX, P. & KOUBA, J. 2001. GPS precise point positioning using IGS orbit products. *Physics and Chemistry of the Earth Part a-Solid Earth and Geodesy,* 26**,** 573-578.

HOFMANN-WELLENHOF, B., LICHTENEGGER, H. & WASLE, E. 2007. *GNSS–global navigation satellite systems: GPS, GLONASS, Galileo, and more*, Springer Science & Business Media.

HOLDEN, L., SILCOCK, D., CHOY, S., CAS, R., AILLERES, L. & FOURNIER, N. 2017. Evaluating a campaign GNSS velocity field derived from an online precise point positioning service. *Geophysical Journal International,* 208**,** 246-256.

HOQUE, M. M. & JAKOWSKI, N. 2008. Mitigation of higher order ionospheric effects on GNSS users in Europe. *GPS Solutions,* 12**,** 87-97.

HUANG, J. 2007. *A high-integrity carrier phase batch processor for differential satellite positioning*, ProQuest.

JI, S. Y., CHEN, W., DING, X. L., CHEN, Y. Q., ZHAO, C. M. & HU, C. W. 2010. Potential Benefits of GPS/GLONASS/GALILEO Integration in an Urban Canyon - Hong Kong. *Journal of Navigation,* 63**,** 681-693.

JOKINEN, A., FENG, S., OCHIENG, W., HIDE, C., MOORE, T. & HILL, C. 2012a. Fixed ambiguity Precise Point Positioning (PPP) using tropospheric corrections based on Numeric Weather Modeling (NWM). *Proceedings of the ION 2013 Pacific PNT Meeting.* Honolulu, Hawaii.

JOKINEN, A., FENG, S., OCHIENG, W., HIDE, C., MOORE, T. & HILL, C. 2012b. Fixed ambiguity Precise Point Positioning (PPP) with FDE RAIM. *Proceedings of IEEE/ION PLANS 2012.* Myrtle Beach, South Carolina

JOKINEN, A., FENG, S., SCHUSTER, W., OCHIENG, W., HIDE, C., MOORE, T. & HILL, C. 2013a. Integrity monitoring of fixed ambiguity Precise Point Positioning (PPP) solutions. *Geo-spatial Information Science,* 16**,** 141-148.

JOKINEN, A., FENG, S. J., SCHUSTER, W., OCHIENG, W., HIDE, C., MOORE, T. & HILL, C. 2013b. GLONASS Aided GPS Ambiguity Fixed Precise Point Positioning. *Journal of Navigation,* 66**,** 399-416.

JOKINEN, A., FENG, S. J., SCHUSTER, W., OCHIENG, W. Y., HIDE, C. D., MOORE, T. & HILL, C. J. 2012c. Precise Point Positioning and Integrity Monitoring with GPS and GLONASS. *European Navigation Conference.*

JOKINEN, A., FENG, S. J., SCHUSTER, W., OCHIENG, W. Y., HIDE, C. D., MOORE, T. & HILL, C. J. 2013c. GLONASS Aided GPS Ambiguity Fixed Precise Point Positioning. *Journal of Navigation,* 66**,** 399-416.

JOKINEN, A., FENG, S. J., SCHUSTER, W., OCHIENG, W. Y., YANG, L., MOORE, T. & HILL, C. J. 2013d. Improving ambiguity validation and integrity monitoring of Precise Point Positioning (PPP). *Proceedings of the 26th International Technical Meeting of The Satellite Division of the Institute of Navigation (ION GNSS+ 2013).* Nashville, TN.

KANAMITSU, M., EBISUZAKI, W., WOOLLEN, J., YANG, S. K., HNILO, J. J., FIORINO, M. & POTTER, G. L. 2002. NCEP-DOE AMIP-II reanalysis (R-2). *Bulletin of the American Meteorological Society,* 83**,** 1631-1643.

KAPLAN, E. D. & HEGARTY, C. J. 2005. *Understanding GPS: principles and applications*, Artech House.

KARABATIĆ, A., WEBER, R. & HAIDEN, T. 2011. Near real-time estimation of tropospheric water vapour content from ground based GNSS data and its potential contribution to weather now-casting in Austria. *Advances in Space Research,* 47**,** 1691-1703.

KEDAR, S., HAJJ, G. A., WILSON, B. D. & HEFLIN, M. B. 2003. The effect of the second order GPS ionospheric correction on receiver positions. *Geophysical Research Letters,* 30.

KHAN & KNUDSEN, P. 2012. comparison between GIPSY OASIS 6.0 and BERNESE 5.0 time series for long term GPS stations in Denmark. *EUREF Symposium 2011.*

KHAN, S. A. 2005. *Surface deformations analyzed using GPS time series.* PhD, Danish National Space Center.

KHANAFSEH, S. & PERVAN, B. 2010. New Approach for Calculating Position Domain Integrity Risk for Cycle Resolution in Carrier Phase Navigation Systems. *Ieee Transactions on Aerospace and Electronic Systems,* 46**,** 296-307.

KING, M. A. & WATSON, C. S. 2010. Long GPS coordinate time series: Multipath and geometry effects. *Journal of Geophysical Research-Solid Earth,* 115.

KING, M. A., WATSON, C. S., PENNA, N. T. & CLARKE, P. J. 2008. Subdaily signals in GPS observations and their effect at semiannual and annual periods. *Geophysical Research Letters,* 35.

KING, M. A., WHITEHOUSE, P. L. & VAN DER WAL, W. 2015. Incomplete separability of Antarctic plate rotation from glacial isostatic adjustment deformation within geodetic observations. *Geophysical Journal International,* 204**,** 324-330.

KING, M. A. & WILLIAMS, S. D. P. 2009. Apparent stability of GPS monumentation from short-baseline time series. *Journal of Geophysical Research-Solid Earth,* 114.

KLEIJER, F. 2004. *Troposphere modeling and filtering for precise GPS leveling*, TU Delft, Delft University of Technology.

KOGAN, M. G. & STEBLOV, G. M. 2008. Current global plate kinematics from GPS (1995-2007) with the plate-consistent reference frame. *Journal of Geophysical Research-Solid Earth,* 113.

KOUBA, J. 2009. *A guide to using International GNSS Service (IGS) products* [Online]. ftp://ftp.igs.org/pub/resource/pubs/UsingIGSProductsVer21.pdf. Available: ftp://ftp.igs.org/pub/resource/pubs/UsingIGSProductsVer21.pdf [Accessed].

KRUEGER, E., SCHUELER, T. & ARBESSER-RASTBURG, B. 2005. The standard tropospheric correction model for the European satellite navigation system Galileo. *XXVIIIth General Assembly of the International Union of Radio Science (URSI).* New Delhi, India.

KUO, Y. H., ZOU, X. & GUO, Y. R. 1996. Variational Assimilation of Precipitable Water Using a Nonhydrostatic Mesoscale Adjoint Model. Part I: Moisture Retrieval and Sensitivity Experiments. *Monthly Weather Review,* 124**,** 122-147.

LAGLER, K., SCHINDELEGGER, M., BOHM, J., KRASNA, H. & NILSSON, T. 2013. GPT2: Empirical slant delay model for radio space geodetic techniques. *Geophysical Research Letters*

40**,** 1069-1073.

LANGLEY, R. B. 1997. GPS receiver system noise. *GPS World,* 8**,** 40-45.

LARSON, K. M., FREYMUELLER, J. T. & PHILIPSEN, S. 1997. Global plate velocities from the Global Positioning System. *Journal of Geophysical Research-Solid Earth,* 102**,** 9961-9981.

LARSON, K. M., LOWRY, A. R., KOSTOGLODOV, V., HUTTON, W., SANCHEZ, O., HUDNUT, K. & SUAREZ, G. 2004. Crustal deformation measurements in Guerrero, Mexico. *Journal of Geophysical Research-Solid Earth,* 109.

LAURICHESSE, D. 2011. The CNES Real-time PPP with undifferenced integer ambiguity resolution demonstrator. *Proceedings of the 24th International Technical Meeting of the Satellite Division of the Institute of Navigation (Ion Gnss 2011)***,** 654-662.

LAURICHESSE, D., MERCIER, F., BERTHIAS, J.-P., BROCA, P. & CERRI, L. 2009. Integer Ambiguity Resolution on Undifferenced GPS Phase Measurements and Its Application to PPP and Satellite Precise Orbit Determination. *Navigation,* 56**,** 135-149.

LAURICHESSE, D., MERCIER, F., BERTHIAS, J. & BIJAC, J. 2008. Real time zero-difference ambiguities fixing and absolute RTK. *Proceedings of the 2008 National Technical Meeting of The Institute of Navigation.*

LAURICHESSE, D. & PRIVAT, A. An open-source PPP client implementation for the CNES PPP-WIZARD demonstrator. ION GNSS, 2015.

LEANDRO, R., SANTOS, M. & LANGLEY, R. UNB Neutral Atmosphere Models: Development and Performance. Proceedings of the 2006 National Technical Meeting of The Institute of Navigation, 18-20 January 2006 Monterey, CA. 564-73.

LI, D., SHI, C., GONG, J., ZHAO, Q., GENG, J., WU, H., LOU, Y., GE, M. & LIU, J. 2008. Recent development of PANDA software in GNSS data processing. 7285**,** 72851S.

LI, M., QU, L., ZHAO, Q., GUO, J., SU, X. & LI, X. 2014a. Precise point positioning with the BeiDou navigation satellite system. *Sensors (Basel),* 14**,** 927-43.

LI, W., TEUNISSEN, P., ZHANG, B. & VERHAGEN, S. Precise Point Positioning Using GPS and Compass Observations. China Satellite Navigation Conference (CSNC) 2013 Proceedings, 2013a. 367-378.

LI, W., YUAN, Y. B., OU, J. K., LI, H. & LI, Z. S. 2012. A new global zenith tropospheric delay model IGGtrop for GNSS applications. *Chinese Science Bulletin,* 57**,** 2132-2139.

LI, X., ZHANG, X. & GUO, F. 2009. Study on Precise Point Positioning Based on Combined GPS and GLONASS. *Proceedings of the 22nd International Technical Meeting of The Satellite Division of the Institute of Navigation (ION GNSS 2009).* Savannah, GA.

LI, X., ZHANG, X., REN, X., FRITSCHE, M., WICKERT, J. & SCHUH, H. 2015a. Precise positioning with current multi-constellation Global Navigation Satellite Systems: GPS, GLONASS, Galileo and BeiDou. *Sci Rep,* 5**,** 8328.

LI, X. X., DICK, G., GE, M. R., HEISE, S., WICKERT, J. & BENDER, M. 2014b. Real-time GPS sensing of atmospheric water vapor: Precise point positioning with orbit, clock, and phase delay corrections. *Geophysical Research Letters,* 41**,** 3615-3621.

LI, X. X., DICK, G., LU, C. X., GE, M. R., NILSSON, T., NING, T., WICKERT, J. & SCHUH, H. 2015b. Multi-GNSS Meteorology: Real-Time Retrieving of Atmospheric Water Vapor From BeiDou, Galileo, GLONASS, and GPS Observations. *Ieee Transactions on Geoscience and Remote Sensing,* 53**,** 6385-6393.

LI, X. X., GE, M. R., DAI, X. L., REN, X. D., FRITSCHE, M., WICKERT, J. & SCHUH, H. 2015c. Accuracy and reliability of multi-GNSS real-time precise positioning: GPS, GLONASS, BeiDou, and Galileo. *Journal of Geodesy,* 89**,** 607-635.

LI, X. X., GE, M. R., ZHANG, H. P., NISCHAN, T. & WICKERT, J. 2013b. The GFZ real-time GNSS precise positioning service system and its adaption for COMPASS. *Advances in Space Research,* 51**,** 1008-1018.

LI, X. X., GE, M. R., ZHANG, H. P. & WICKERT, J. 2013c. A method for improving uncalibrated phase delay estimation and ambiguity-fixing in real-time precise point positioning. *Journal of Geodesy,* 87**,** 405-416.

LI, X. X., GE, M. R., ZHANG, X. H., ZHANG, Y., GUO, B. F., WANG, R. J., KLOTZ, J. & WICKERT, J. 2013d. Real-time high-rate co-seismic displacement from ambiguity-fixed precise point positioning: Application to earthquake early warning. *Geophysical Research Letters,* 40**,** 295-300.

LI, X. X. & ZHANG, X. H. 2012. Improving the Estimation of Uncalibrated Fractional Phase Offsets for PPP Ambiguity Resolution. *Journal of Navigation,* 65**,** 513-529.

LIANG, S. M., GAN, W. J., SHEN, C. Z., XIAO, G. R., LIU, J., CHEN, W. T., DING, X. G. & ZHOU, D. M. 2013. Three-dimensional velocity field of present-day crustal motion of the Tibetan Plateau derived from GPS measurements. *Journal of Geophysical Research-Solid Earth,* 118**,** 5722-5732.

LIU, T., YUAN, Y., ZHANG, B., WANG, N., TAN, B. & CHEN, Y. 2016a. Multi-GNSS precise point positioning (MGPPP) using raw observations. *Journal of Geodesy,* 91**,** 253-268.

LIU, Y., SONG, W., LOU, Y., YE, S. & ZHANG, R. 2016b. GLONASS phase bias estimation and its PPP ambiguity resolution using homogeneous receivers. *GPS Solutions,* 21**,** 427-437.

LIU, Y., YE, S., SONG, W., LOU, Y. & CHEN, D. 2016c. Integrating GPS and BDS to shorten the initialization time for ambiguity-fixed PPP. *GPS Solutions,* 21**,** 333-343.

LIU, Z. Z. 2011. A new automated cycle slip detection and repair method for a single dual-frequency GPS receiver. *Journal of Geodesy,* 85**,** 171-183.

LU, C., LI, X., ZUS, F., HEINKELMANN, R., DICK, G., GE, M., WICKERT, J. & SCHUH, H. 2017. Improving BeiDou real-time precise point positioning with numerical weather models. *Journal of Geodesy*.

LU, C. X., LI, X. X., NILSSON, T., NING, T., HEINKELMANN, R., GE, M. R., GLASER, S. & SCHUH, H. 2015. Real-time retrieval of precipitable water vapor from GPS and BeiDou observations. *Journal of Geodesy,* 89**,** 843-856.

LU, C. X., ZUS, F., GE, M. R., HEINKELMANN, R., DICK, G., WICKERT, J. & SCHUH, H. 2016. Tropospheric delay parameters from numerical weather models for multi-GNSS precise positioning. *Atmospheric Measurement Techniques,* 9**,** 5965-5973.

MACMILLAN, D. S. 1995. Atmospheric gradients from very long baseline interferometry observations. *Geophysical Research Letters,* 22**,** 1041-1044.

MARQUEZ-AZUA, B. & DEMETS, C. 2009. Deformation of Mexico from continuous GPS from 1993 to 2008. *Geochemistry Geophysics Geosystems,* 10**,** n/a-n/a.

MARTIN, A., ANQUELA, A. B., CAPILLA, R. & BERNE, J. L. 2011. PPP Technique Analysis Based on Time Convergence, Repeatability, IGS Products, Different

Software Processing, and GPS plus GLONASS Constellation. *Journal of Surveying Engineering-Asce,* 137**,** 99-108.

MCCARTHY, D. D. & PETIT, G. 2004. IERS conventions (2003). Germany: DTIC Document.

MCCLUSKY, S., BALASSANIAN, S., BARKA, A., DEMIR, C., ERGINTAV, S., GEORGIEV, I., GURKAN, O., HAMBURGER, M., HURST, K., KAHLE, H., KASTENS, K., KEKELIDZE, G., KING, R., KOTZEV, V., LENK, O., MAHMOUD, S., MISHIN, A., NADARIYA, M., OUZOUNIS, A., PARADISSIS, D., PETER, Y., PRILEPIN, M., REILINGER, R., SANLI, I., SEEGER, H., TEALEB, A., TOKSOZ, M. N. & VEIS, G. 2000. Global Positioning System constraints on plate kinematics and dynamics in the eastern Mediterranean and Caucasus. *Journal of Geophysical Research-Solid Earth,* 105**,** 5695-5719.

MEINDL, M., SCHAER, S., HUGENTOBLER, U. & BEUTLER, G. 2004. Tropospheric gradient estimation at CODE: Results from global solutions. *Journal of the Meteorological Society of Japan,* 82**,** 331-338.

MELGARD, T., VIGEN, E., DE JONG, K., LAPUCHA, D., VISSER, H. & OERPEN, O. G2-the first real-time GPS and GLONASS precise orbit and clock service. Proceedings of the 22nd International Technical Meeting of The Satellite Division of the Institute of Navigation (ION GNSS 2009), 2009. 1885-1891.

MENDES, V. B. 1998. *Modeling the Neutral Atmosphere Propagation Delay in Radiometric Space Techniques.* PhD, The University of New Brunswick.

MERVART, L., LUKES, Z., ROCKEN, C. & IWABUCHI, T. Precise Point Positioning With Ambiguity Resolution In Real-Time. Proceedings of ION GNSS, 2008. 397-405.

MONTENBRUCK, O. 2003. Kinematic GPS positioning of LEO satellites using ionosphere-free single frequency measurements. *Aerospace Science and Technology,* 7**,** 396-405.

MUSTAFAR, M. A., SIMONS, W. J. F., TONGKUL, F., SATIRAPOD, C., OMAR, K. M. & VISSER, P. N. A. M. 2017. Quantifying deformation in North Borneo with GPS. *Journal of Geodesy*.

NADARAJAH, N. & TEUNISSEN, P. J. G. 2013. Instantaneous GPS/BeiDou/Galileo attitude determination: A single-frequency robustness analysis under

constrained environments. *Proceedings of the ION 2013 Pacific PNT Meeting.* Honolulu, Hawaii.

NAIF. 2014. *The Navigation and Ancillary Information Facility* [Online]. Available: http://naif.jpl.nasa.gov/naif/ [Accessed 1/4/2014 2014].

NIELL, A. E. 1996. Global mapping functions for the atmosphere delay at radio wavelengths. *Journal of Geophysical Research-Solid Earth,* 101**,** 3227-3246.

NIK, S. A. & PETOVELLO, M. G. 2010. Implementation of a Dual-Frequency GLONASS and GPS L1 C/A Software Receiver. *Journal of Navigation,* 63**,** 269-287.

NOCQUET, J. M. & CALAIS, E. 2003. Crustal velocity field of western Europe from permanent GPS array solutions, 1996-2001. *Geophysical Journal International,* 154**,** 72-88.

OCALAN, T., ERDOGAN, B., TUNALIOGLU, N. & DURDAG, U. M. 2016. Accuracy Investigation of PPP Method Versus Relative Positioning Using Different Satellite Ephemerides Products Near/Under Forest Environment. *Earth Sciences Research Journal,* 20**,** 1.

OCHIENG, W. Y., FENG, S., MOORE, T., HILL, C. & HIDE, C. 2008. User Level Integrity Monitoring and Quality Control for High Accuracy Positioning using GPS/INS Measurements. *Journal of Global Positioning Systems,* 7**,** 104-114.

OCHSENBEIN, J. 2 February 2015. *RE: Personal Correspondence jessica.ochsenbein@aiub.unibe.ch.*

ODIJK, D., ARORA, B. S. & TEUNISSEN, P. J. G. 2014. Predicting the Success Rate of Long-baseline GPS+Galileo (Partial) Ambiguity Resolution. *Journal of Navigation,* 67**,** 385-401.

ODIJK, D., ZHANG, B., KHODABANDEH, A., ODOLINSKI, R. & TEUNISSEN, P. J. G. 2015. On the estimability of parameters in undifferenced, uncombined GNSS network and PPP-RTK user models by means of S-system theory. *Journal of Geodesy,* 90**,** 15-44.

ODOLINSKI, R., TEUNISSEN, P. J. G. & ODIJK, D. 2013. An analysis of combined COMPASS/BeiDou-2 and GPS single- and multiple-frequency RTK positioning. *Proceedings of the ION 2013 Pacific PNT Meeting.* Honolulu, Hawaii.

PACE, B., PACIONE, R., SCIARRETTA, C. & VESPE, F. 2010. Estimating Zenith Total Delay Residual Fields by using Ground-Based GPS network. *Proceedings of XX EUREF Symposium.* Gävle, Sweden.

PAN, L., XIAOHONG, Z. & FEI, G. 2016. Ambiguity resolved precise point positioning with GPS and BeiDou. *Journal of Geodesy,* 91**,** 25-40.

PAN, L., ZHANG, X. H., LIU, J. N., LI, X. X. & LI, X. 2017a. Performance Evaluation of Single-frequency Precise Point Positioning with GPS, GLONASS, BeiDou and Galileo. *Journal of Navigation,* 70**,** 465-482.

PAN, Z., CHAI, H. & KONG, Y. 2017b. Integrating multi-GNSS to improve the performance of precise point positioning. *Advances in Space Research*.

PANY, A., WRESNIK, J., BÖHM, J. & SCHUH, H. 2007. Optimum modeling of troposphere and clock parameters in VLBI. *Proceedings of the 18th European VLBI for Geodesy and Astrometry Working Meeting.* Vienna.

PARK, J. K., KIM, M. G. & LEE, J. S. 2013a. Analysis of Crustal Movement About Antarctica Using Distributed GPS Network. *Proceedings, The 5th International Conference on Advanced Science and Technology.*

PARK, J. K., KIM, M. G. & LEE, J. S. 2013b. Tectonic Motion Monitoring of Antarctica Using GPS Measurements. *International Journal of Control and Automation,* 6**,** 215-224.

PARKINS, A. 2011. Increasing GNSS RTK availability with a new single-epoch batch partial ambiguity resolution algorithm. *Gps Solutions,* 15**,** 391-402.

PENNA, N., BOS, M., BAKER, T. & SCHERNECK, H. G. 2008. Assessing the accuracy of predicted ocean tide loading displacement values. *Journal of Geodesy,* 82**,** 893-907.

PENNA, N., DODSON, A. & CHEN, W. 2001. Assessment of EGNOS tropospheric correction model. *Journal of Navigation,* 54**,** 37-55.

PENNA, N. T., KING, M. A. & STEWART, M. P. 2007. GPS height time series: Short-period origins of spurious long-period signals. *Journal of Geophysical Research-Solid Earth,* 112.

PEREZ, J., MONICO, J. & CHAVES, J. 2003. Velocity field estimation using GPS precise point positioning: The South American Plate Case. *Journal of Global Positioning Systems,* 2**,** 90-99.

REILINGER, R. E., MCCLUSKY, S. C., SOUTER, B. J., HAMBURGER, M. W., PRILEPIN, M. T., MISHIN, A., GUSEVA, T. & BALASSANIAN, S. 1997. Preliminary estimates of plate convergence in the Caucasus collision zone from global positioning system measurements. *Geophysical Research Letters,* 24**,** 1815-1818.

REUSSNER, N. & WANNINGER, L. 2011. GLONASS Inter-frequency Biases and Their Effects on RTK and PPP Carrier-phase Ambiguity Resolution. *Proceedings of the 24th International Technical Meeting of The Satellite Division of the Institute of Navigation (ION GNSS 2011).* Portland, Oregon.

RIZOS, C., MONTENBRUCK, O., WEBER, R., WEBER, G., NEILAN, R. & HUGENTOBLER, U. 2013. The IGS MGEX experiment as a milestone for a comprehensive Multi-GNSS service. *Proceedings of the ION 2013 Pacific PNT Meeting.* Honolulu, Hawaii.

ROCKEN, C., VAN HOVE, T. & WARE, R. 1997. Near real-time GPS sensing of atmospheric water vapor. *Geophysical Research Letters,* 24**,** 3221-3224.

ROCKEN, C., VANHOVE, T., JOHNSON, J., SOLHEIM, F., WARE, R., BEVIS, M., CHISWELL, S. & BUSINGER, S. 1995. Gps/Storm - Gps Sensing of Atmospheric Water-Vapor for Meteorology. *Journal of Atmospheric and Oceanic Technology,* 12**,** 468-478.

ROCKEN, C., WARE, R., VANHOVE, T., SOLHEIM, F., ALBER, C. & JOHNSON, J. 1993. Sensing Atmospheric Water-Vapor with the Global Positioning System. *Geophysical Research Letters,* 20**,** 2631-2634.

ROHM, W., YUAN, Y. B., BIADEGLGNE, B., ZHANG, K. F. & LE MARSHALL, J. 2014. Ground-based GNSS ZTD/IWV estimation system for numerical weather prediction in challenging weather conditions. *Atmospheric Research,* 138**,** 414-426.

RTCA 1996. *Minimum Operational Performance Standards for Global Positioning System/Wide Area Augmentation System Airborne Equipment: Hauptbd*, RTCA.

RTCA 1999. Minimum Operational Performance Standards for Global Positioning System/Wide Area Augmentation System Airborne Equipment. *RTCA Documentation Number DO-229B***,** 255.

SAASTAMOINEN, J. 1972. Atmospheric correction for the troposphere and stratosphere in radio ranging satellites. *The Use of Artificial Satellites for Geodesy.* Washington, D. C: American Geophysical Union.

SAASTAMOINEN, J. 1973. Contributions to the theory of atmospheric refraction. *Bulletin Géodésique,* 107**,** 13-34.

SAKIDIN, H., ABU BAKAR, M. R., SHARIFF, M., RASHID, A., NOORANI, M., SALMI, M., MATORI, A. & MOHAMED, A. 2009. Effect of GPS Tropospheric Delay Neill Mapping Function Simplification. *Malaysian Journal of Mathematical Sciences,* 3**,** 95-107.

SATIRAPOD, C., SIMONS, W. J. F., PANUMASTRAKUL, E. & TRISIRISATAYAWONG, I. 2013. Updating Thai Reference Frame to ITRF2005 Using GPS: Diversion Between ITRF2000 and 2005 in Southeast Asia. *Survey Review,* 43**,** 45-53.

SCHMID, R., STEIGENBERGER, P., GENDT, G., GE, M. & ROTHACHER, M. 2007. Generation of a consistent absolute phase-center correction model for GPS receiver and satellite antennas. *Journal of Geodesy,* 81**,** 781-798.

SCHUELER, T., HEIN, G. W. & EISSFELLER, B. 2000a. Improved Tropospheric Delay Modeling Using an Integrated Approach of Numerical Weather Models and GPS. *Proceedings of the 13th International Technical Meeting of the Satellite Division of The Institute of Navigation (ION GPS 2000).* Salt Lake City, UT.

SCHUELER, T., HEIN, G. W. & EISSFELLER, B. 2000b. Towards an optimal strategy for GPS wet delay Kalman filtering. *Proceedings of the IAIN World Congress and the 56th Annual Meeting of The Institute of Navigation (2000).* San Diego, CA.

SEGALL, P. & DAVIS, J. L. 1997. GPS applications for geodynamics and earthquake studies. *Annual Review of Earth and Planetary Sciences,* 25**,** 301-336.

SELLA, G. F., STEIN, S., DIXON, T. H., CRAYMER, M., JAMES, T. S., MAZZOTTI, S. & DOKKA, R. K. 2007. Observation of glacial isostatic adjustment in "stable" North America with GPS. *Geophysical Research Letters,* 34.

SHI, J. & GAO, Y. 2012. Improvement of PPP-inferred tropospheric estimates by integer ambiguity resolution. *Advances in Space Research,* 50**,** 1374-1382.

SHIMADA, S. & BOCK, Y. 1992. Crustal Deformation Measurements in Central Japan Determined by a Global Positioning System Fixed-Point Network. *Journal of Geophysical Research-Solid Earth,* 97**,** 12437-12455.

SIDOROV, D. & TEFERLE, F. N. 2015. Impact of Antenna Phase Centre Calibrations on Position Time Series: Preliminary Results. 143**,** 117-123.

SIMONS, W. J. F., SOCQUET, A., VIGNY, C., AMBROSIUS, B. A. C., ABU, S. H., PROMTHONG, C., SUBARYA, C., SARSITO, D. A., MATHEUSSEN, S., MORGAN, P. & SPAKMAN, W. 2007. A decade of GPS in Southeast Asia: Resolving Sundaland motion and boundaries. *Journal of Geophysical Research-Solid Earth,* 112.

SONG, W., ZHANG, R., YAO, Y., LIU, Y. & HU, Y. 2016. PPP Sliding Window Algorithm and Its Application in Deformation Monitoring. *Sci Rep,* 6**,** 26497.

STEIGENBERGER, P., ROTHACHER, M., DIETRICH, R., FRITSCHE, M., RULKE, A. & VEY, S. 2006. Reprocessing of a global GPS network. *Journal of Geophysical Research-Solid Earth,* 111**,** n/a-n/a.

STEIGENBERGER, P., ROTHACHER, M., FRITSCHE, M., RUELKE, A. & DIETRICH, R. 2009. Quality of reprocessed GPS satellite orbits. *Journal of Geodesy,* 83**,** 241-248.

STERLE, O., STOPAR, B. & PRESEREN, P. P. 2015. Single-frequency precise point positioning: an analytical approach. *Journal of Geodesy,* 89**,** 793-810.

STEWART, M. P., PENNA, N. T. & LICHTI, D. D. 2005. Investigating the propagation mechanism of unmodelled systematic errors on coordinate time series estimated using least squares. *Journal of Geodesy,* 79**,** 479-489.

STOSIUS, R., BEYERLE, G., HOECHNER, A., WICKERT, J. & LAUTERJUNG, J. 2011. The impact on tsunami detection from space using GNSS-reflectometry when combining GPS with GLONASS and Galileo. *Advances in Space Research,* 47**,** 843-853.

TAKASU, T. 2014. RTKLIB: An Open Source Program Package for GNSS Positioning.

TEFERLE, F. N., BINGLEY, R. M., ORLIAC, E. J., WILLIAMS, S. D. P., WOODWORTH, P. L., MCLAUGHLIN, D., BAKER, T. F., SHENNAN, I., MILNE, G. A., BRADLEY, S. L. & HANSEN, D. N. 2009. Crustal motions in Great Britain: evidence from

continuous GPS, absolute gravity and Holocene sea level data. *Geophysical Journal International,* 178**,** 23-46.

TEFERLE, F. N., ORLIAC, E. J. & BINGLEY, R. M. 2007. An assessment of Bernese GPS software precise point positioning using IGS final products for global site velocities. *GPS Solutions,* 11**,** 205-213.

TEGEDOR, J., ØVSTEDAL, O. & VIGEN, E. 2014. Precise orbit determination and point positioning using GPS, Glonass, Galileo and BeiDou. *Journal of Geodetic Science,* 4.

TEUNISSEN, P. J. GNSS ambiguity bootstrapping: theory and application. Proceedings of international symposium on kinematic systems in geodesy, geomatics and navigation, 2001. 246-254.

TEUNISSEN, P. J. G. 1995. The Invertible Gps Ambiguity Transformations. *Manuscripta Geodaetica,* 20**,** 489-497.

TEUNISSEN, P. J. G. 1999. An optimality property of the integer least-squares estimator. *Journal of Geodesy,* 73**,** 587-593.

TEUNISSEN, P. J. G. 2003. Integer Aperture GNSS Ambiguity Resolution. *Artificial Satellites,* 38**,** 79-88.

TEUNISSEN, P. J. G., JONGE, P. J. D. & TIBERIUS, C. C. J. M. 1995. The LAMBDA method for fast GPS surveying. *International Symposium "GPS Technology Applications".* Bucharest, Romania.

TEUNISSEN, P. J. G. & KHODABANDEH, A. 2014. Review and principles of PPP-RTK methods. *Journal of Geodesy,* 89**,** 217-240.

TEUNISSEN, P. J. G., ODIJK, D. & ZHANG, B. 2010. PPP-RTK: Results of CORS network-based PPP with integer ambiguity resolution. *Journal of Aeronautics,* 42**,** 223-230.

TOLMAN, B. W., KERKHOFF, A., RAINWATER, D., MUNTON, D. & BANKS, J. 2010. Absolute Precise Kinematic Positioning With GPS and GLONASS. *Proceedings of the 23rd International Technical Meeting of The Satellite Division of the Institute of Navigation (ION GNSS 2010).* Portland, OR.

TREGONING, P., BOERS, R., O'BRIEN, D. & HENDY, M. 1998. Accuracy of absolute precipitable water vapor estimates from GPS observations. *Journal of Geophysical Research-Atmospheres,* 103**,** 28701-28710.

TREGONING, P. & HERRING, T. A. 2006. Impact of a priori zenith hydrostatic delay errors on GPS estimates of station heights and zenith total delays. *Geophysical Research Letters,* 33.

TREGONING, P. & WATSON, C. 2009. Atmospheric effects and spurious signals in GPS analyses. *Journal of Geophysical Research-Solid Earth,* 114.

VERHAGEN, S., TEUNISSEN, P. J., VAN DER MAREL, H. & LI, B. GNSS ambiguity resolution: which subset to fix. Proceedings of IGNSS Symposium, Sydney, Australia, 2011.

VINCENTY, T. 2013. Direct and Inverse Solutions of Geodesics on the Ellipsoid with Application of Nested Equations. *Survey Review,* 23**,** 88-93.

WANG, F., CHEN, X. & GUO, F. 2015a. GPS/GLONASS Combined Precise Point Positioning with Receiver Clock Modeling. *Sensors (Basel),* 15**,** 15478-93.

WANG, G. Q. 2013. Millimeter-accuracy GPS landslide monitoring using Precise Point Positioning with Single Receiver Phase Ambiguity (PPP-SRPA) resolution: a case study in Puerto Rico. *Journal of Geodetic Science,* 3.

WANG, G. Q., BAO, Y., CUDDUS, Y., JIA, X. Y., SERNA, J. & JING, Q. 2015b. A methodology to derive precise landslide displacement time series from continuous GPS observations in tectonically active and cold regions: a case study in Alaska. *Natural Hazards,* 77**,** 1939-1961.

WARREN, D. L. M. & RAQUET, J. F. 2003. Broadcast vs. precise GPS ephemerides: a historical perspective. *GPS Solutions,* 7**,** 151-156.

WDOWINSKI, S., SUDMAN, Y. & BOCK, Y. 2001. Geodetic detection of active faults in S. California. *Geophysical Research Letters,* 28**,** 2321-2324.

WIESER, A. & BRUNNER, F. K. 2014. An extended weight model for GPS phase observations. *Earth, Planets and Space,* 52**,** 777-782.

WILLIAMS, S. D. P. 2003a. The effect of coloured noise on the uncertainties of rates estimated from geodetic time series. *Journal of Geodesy,* 76**,** 483-494.

WILLIAMS, S. D. P. 2003b. Offsets in Global Positioning System time series. *Journal of Geophysical Research-Solid Earth,* 108.

WING, S., JOHNSON, J. R., JEN, J., MENG, C. I., SIBECK, D. G., BECHTOLD, K., FREEMAN, J., COSTELLO, K., BALIKHIN, M. & TAKAHASHI, K. 2005. Kp forecast models. *Journal of Geophysical Research-Space Physics,* 110.

WU, J., WU, S., HAJJ, G., BERTIGER, W. & LICHTEN, S. 1993. Effects of antenna orientation on GPS carrier phase. *Manuscripta Geodaetica,* 18**,** 91-98.

XIANG JIN, X. & DE JONG, C. D. 2009. Relationship Between Satellite Elevation and Precision of GPS Code Observations. *Journal of Navigation,* 49**,** 253-265.

YANG, L., ELMAS, Z., HILL, C., AQUINO, M. & MOORE, T. 2011a. An Innovative Approach for Atmospheric Error Mitigation Using New GNSS Signals. *Journal of Navigation,* 64**,** S211-S232.

YANG, L., HILL, C. & MOORE, T. 2013. Numerical weather modeling-based slant tropospheric delay estimation and its enhancement by GNSS data. *Geo-spatial Information Science,* 16**,** 186-200.

YANG, X. H., SASS, B. H., ELGERED, G., JOHANSSON, J. M. & EMARDSON, T. R. 1999. A comparison of precipitable water vapor estimates by an NWP simulation and GPS observations. *Journal of Applied Meteorology,* 38**,** 941-956.

YANG, Y. X., LI, J. L., XU, J. Y., TANG, J., GUO, H. R. & HE, H. B. 2011b. Contribution of the Compass satellite navigation system to global PNT users. *Chinese Science Bulletin,* 56**,** 2813-2819.

YAO, Y., CHANG-YONG, H., BAO, Z. & CHAO-QIAN, X. 2013. A new global zenith tropospheric delay model GZTD. *Chinese Journal Geophysics,* 56**,** 2218-2227.

YAO, Y. B., HU, Y. F., YU, C., ZHANG, B. & GUO, J. J. 2016. An improved global zenith tropospheric delay model GZTD2 considering diurnal variations. *Nonlinear Processes in Geophysics,* 23**,** 127-136.

YI, W., SONG, W., LOU, Y., SHI, C., YAO, Y., GUO, H., CHEN, M. & WU, J. 2017. Improved method to estimate undifferenced satellite fractional cycle biases using network observations to support PPP ambiguity resolution. *GPS Solutions*.

YIBIN, Y. 2006. Earth rotation parameter estimation by GPS observations. *Geo-spatial Information Science,* 9**,** 260-264.

YIGIT, C. O., GIKAS, V., ALCAY, S. & CEYLAN, A. 2013. Performance evaluation of short to long term GPS, GLONASS and GPS/GLONASS post-processed PPP. *Survey Review,* 46**,** 155-166.

YU, J. & WANG, G. 2016. Introduction to the GNSS geodetic infrastructure in the Gulf of Mexico Region. *Survey Review,* 49**,** 51-65.

YUAN, Y. B., ZHANG, K. F., ROHM, W., CHOY, S., NORMAN, R. & WANG, C. S. 2014. Real-time retrieval of precipitable water vapor from GPS precise point positioning. *Journal of Geophysical Research-Atmospheres,* 119**,** 10044-10057.

ZHANG, B. C., OU, J. K., LI, Z. S. & YUAN, Y. B. 2011. Determination of ionospheric observables with precise point positioning. *Chinese Journal of Geophysics-Chinese Edition,* 54**,** 950-957.

ZHANG, M. Y., ZHANG, J. & QIN, Y. 2008. Satellite Selection for Multi-Constellation. *2008 IEEE/ION Position, Location and Navigation Symposium.* Monterey, CA.

ZHANG, Y. & GAO, Y. 2001. Influence Analysis of Tropospheric Model and Mapping Function on Precise Tropospheric Delay Estimation Using PPP. *Proceedings of the 19th International Technical Meeting of the Satellite Division of The Institute of Navigation (ION GNSS 2006).* Fort Worth, TX.

ZHAO, Q. L., GUO, J., LI, M., QU, L. Z., HU, Z. G., SHI, C. & LIU, J. N. 2013. Initial results of precise orbit and clock determination for COMPASS navigation satellite system. *Journal of Geodesy,* 87**,** 475-486.

ZUMBERGE, J. F., HEFLIN, M. B., JEFFERSON, D. C., WATKINS, M. M. & WEBB, F. H. 1997. Precise point positioning for the efficient and robust analysis of GPS data from large networks. *Journal of Geophysical Research-Solid Earth,* 102**,** 5005-5017.

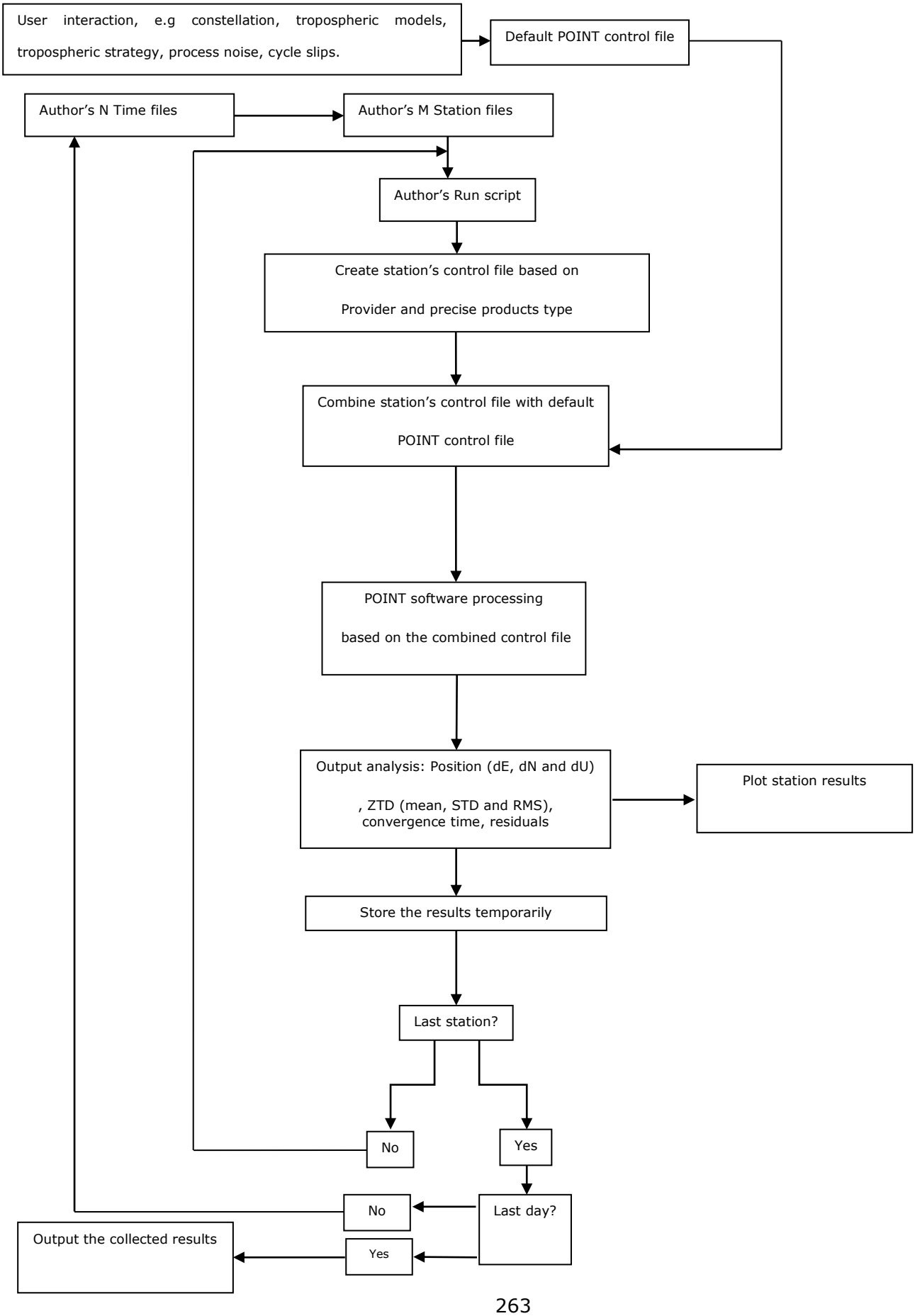
ZUS, F., DICK, G., DOUŠA, J., HEISE, S. & WICKERT, J. 2014a. The rapid and precise computation of GPS slant total delays and mapping factors utilizing a numerical weather model. *Radio Science,* 49**,** 207-216.

ZUS, F., DICK, G., DOUSA, J. & WICKERT, J. 2014b. Systematic errors of mapping functions which are based on the VMF1 concept. *GPS Solutions,* 19**,** 277-286.

Appendices

Appendix-A- Flow chart for automation of the POINT software via Matlab

Figure A- 1 Flow char for automated the POINT software in MATLAB



Appendix-B- Station coordinates for 85 OSGB stations in the UK and 76 IGS stations

Code	Station name	Longitude	Latitude	Height	Receiver type	Antenna type
ABEP	Aberporth	355° 25 43.3"	52° 8 21.9"	188.5	LEICA GRX1200+GNSS	LEIAR25 LEIT
ALDB	Aldeburgh	1° 36 10.2"	52° 9 11.4"	57	LEICA GRX1200+GNSS	LEIAR25 NONE
AMER	Amersham	359° 26 26.3"	51° 40 37.9"	134.2	LEICA GRX1200+GNSS	LEIAR25 LEIT
ANLX	Angle	354° 55 15"	51° 41 21.5"	74.2	LEICA GRX1200+GNSS	LEIAR25 LEIT
APPL	Appledore	355° 48 1.3"	51° 3 24.9"	68.7	LEICA GRX1200+GNSS	LEIAR25 LEIT
ARDL	Ardleigh	0° 57 42.8"	51° 54 56.8"	91.5	LEICA GRX1200+GNSS	LEIAR25 LEIT
ASAP	St Asaph	356° 31 11.6"	53° 15 4.9"	103.4	LEICA GRX1200+GNSS	LEIAR25 LEIT
ATTL	Attleborough	0° 59 17.3"	52° 31 0.6"	81.5	LEICA GRX1200+GNSS	LEIAR25 LEIT
BARR	Barra	352° 29 58.1"	56° 57 15.8"	70.4	LEICA GRX1200+GNSS	LEIAR25 NONE
BEES	St Bees	356° 23 36.4"	54° 29 27.4"	66.2	LEICA GRX1200+GNSS	LEIAR25 LEIT
BENB	Benbecula	352° 38 9.1"	57° 28 23.1"	67.2	LEICA GRX1200+GNSS	LEIAR25 LEIT
BLAP	Blackpool	356° 57 54.1"	53° 46 36.9"	66	LEICA GRX1200+GNSS	LEIAR25 LEIT
BRAE	Braemar	356° 36 15.8"	57° 0 24.3"	400.9	LEICA GRX1200+GNSS	LEIAR25 LEIT
BREC	Brecon	356° 37 5.8"	51° 57 10.4"	242.3	LEICA GRX1200+GNSS	LEIAR25 LEIT
BUCK	Buckie	357° 2 18.6"	57° 40 34.1"	81.8	LEICA GRX1200+GNSS	LEIAR25 LEIT
CAML	Campbeltown	354° 23 53.1"	55° 25 30.7"	66.8	LEICA GRX1200+GNSS	LEIAR25 LEIT
CARI	Cardiff	356° 53 35.5"	51° 31 51.8"	93.1	LEICA GRX1200+GNSS	LEIAR25 LEIT
CARL	Carlisle	357° 3 42.2"	54° 53 43.5"	93.6	LEICA GRX1200+GNSS	LEIAR25 LEIT
CLAW	Church Lawford	358° 40 6.6"	52° 21 31.6"	159.1	LEICA GRX1200+GNSS	LEIAR25 LEIT
DARE	DARESBURY	357° 21 34.2"	53° 20 41.3"	88.4	LEICA GRX1200+GNSS	LEIAR25 LEIT
DRUM	Drumalbin	356° 15 50.2"	55° 37 37.8"	302.6	LEICA GRX1200+GNSS	LEIAR25 LEIT
DUDE	Dundee	357° 7 21.7"	56° 27 50.1"	57.5	LEICA GRX1200+GNSS	LEIAR25 LEIT
DUNG	Dungeness	0° 58 35.3"	50° 55 35.6"	56	LEICA GRX1200+GNSS	LEIAR25 LEIT
EASN	Easington	0° 6 59.2"	53° 38 56.4"	52.1	LEICA GRX1200+GNSS	LEIAR25 LEIT

Table B- 1 Station coordinates for 85 stations in the UK

Code	Station name	Longitude	Latitude	Height	Receiver type	Antenna type
ESKD	Eskdalemuir	356° 47 35"	55° 18 44.6"	297.5	LEICA GRX1200+GNSS	LEIAR25 LEIT
EXMO	Exmouth	356° 35 23.8"	50° 36 48.4"	65.7	LEICA GRX1200+GNSS	LEIAR25 LEIT
FARB	Farnborough	359° 13 38.3"	51° 16 47.8"	112.7	LEICA GRX1200+GNSS	LEIAR25 LEIT
FAUG	Fort Augustus	355° 18 41.5"	57° 8 8.5"	99.3	LEICA GRX1200+GNSS	LEIAR25 LEIT
GIGG	Giggleswick	357° 41 28.2"	54° 4 33.2"	284.2	LEICA GRX1200+GNSS	LEIAR25 LEIT
GIRA	Girvan	355° 8 32.7"	55° 14 36.4"	65.3	LEICA GRX1200+GNSS	LEIAR25 LEIT
GLAS	Glasgow	355° 42 12.7"	55° 51 14.4"	71.7	LEICA GRX1200+GNSS	LEIAR25 LEIT
GORS	Gorleston	1° 43 55"	52° 34 32"	51.9	LEICA GRX1200+GNSS	LEIAR25 LEIT
HARD	Hardham	359° 28 16.8"	50° 56 58.9"	65.9	LEICA GRX1200+GNSS	LEIAR25 LEIT
HELS	Helmsdale	356° 21 2.3"	58° 6 55.1"	66.8	LEICA GRX1200+GNSS	LEIAR25 LEIT
HOLY	Holyhead	355° 21 28.6"	53° 19 3.8"	67.9	LEICA GRX1200+GNSS	LEIAR25 LEIT
HOOB	Hoober	358° 37 13.2"	53° 28 58.3"	186.1	LEICA GRX1200+GNSS	LEIAR25 LEIT
HUNG	Hungerford	358° 29 9.8"	51° 24 15.5"	183.2	LEICA GRX1200+GNSS	LEIAR25 LEIT
INVR	Inverness	355° 46 50.7"	57° 29 10.5"	66.2	LEICA GRX1200+GNSS	LEIAR25 LEIT
KELO	Kelso	357° 33 35.8"	55° 35 44.3"	93	LEICA GRX1200+GNSS	LEIAR25 LEIT
KEYW	Keyworth	358° 55 18.8"	52° 52 44.2"	122.9	LEICA GRX1200+GNSS	LEIAR25 LEIT
KILN	Killin	355° 40 45.4"	56° 27 17.8"	232.2	LEICA GRX1200+GNSS	LEIAR25 LEIT
KING	Kings Lynn	0° 24 5.5"	52° 45 4.9"	66.4	LEICA GRX1200+GNSS	LEIAR25 LEIT
KINL	Kinlochbervie	354° 56 51.6"	58° 27 31.6"	65	LEICA GRX1200+GNSS	LEIAR25 LEIT
KIRK	Kirkcudbright	355° 57 9.5"	54° 50 22.4"	67.1	LEICA GRX1200+GNSS	LEIAR25 LEIT
LCAR	Lochcarron	354° 32 9.2"	57° 25 13.1"	71.9	LEICA GRX1200+GNSS	LEIAR25 LEIT
LEED	Leeds	358° 20 10.4"	53° 48 0.8"	215.6	LEICA GRX1200+GNSS	LEIAR25 LEIT
LEEK	Leek	358° 1 7.3"	53° 7 40.1"	352.8	LEICA GRX1200+GNSS	LEIAR25 LEIT
LICF	Lichfield	358° 11 10.6"	52° 42 35.9"	129.4	LEICA GRX1200+GNSS	LEIAR25 LEIT

Table B- 2 Station coordinates for 85 stations in the UK

Code	Station name	Longitude	Latitude	Height	Receiver type	Antenna type
LINO	Lincoln	359° 28 47.7"	53° 15 0.9"	103.5	LEICA GRX1200+GNSS	LEIAR25 LEIT
LOFT	Loftus	359° 8 11.7"	54° 33 46.6"	209.4	LEICA GRX1200+GNSS	LEIAR25 LEIT
MACY	Machynlleth	356° 8 53.6"	52° 35 20.1"	76.7	LEICA GRX1200+GNSS	LEIAR25 LEIT
MART	Margate	1° 22 58.4"	51° 23 30.1"	58.3	LEICA GRX1200+GNSS	LEIAR25 LEIT
NCAS	Newcastle	358° 23 0.3"	54° 58 44.9"	125.9	LEICA GRX1200+GNSS	LEIAR25 LEIT
NEWR	Newmarket2	0° 24 55"	52° 16 0.5"	75.8	LEICA GRX1200+GNSS	LEIAR25 LEIT
OBAN	Oban	354° 33 33.1"	56° 27 4.8"	74.5	LEICA GRX1200+GNSS	LEIAR25 LEIT
OXFR	Oxford	358° 42 41.3"	51° 49 26.3"	119.8	LEICA GRX1200+GNSS	LEIAR25 LEIT
PADT	Padstow	355° 3 47.6"	50° 32 28"	65.5	LEICA GRX1200+GNSS	LEIAR25 LEIT
PETE	Peterborough	359° 44 12.6"	52° 35 1.5"	72.9	LEICA GRX1200+GNSS	LEIAR25 LEIT
PMTH	Plymouth	355° 52 25.8"	50° 24 59.3"	175.6	LEICA GRX1200+GNSS	LEIAR25 LEIT
POOL	Poole	358° 5 22"	50° 46 33.1"	68.7	LEICA GRX1200+GNSS	LEIAR25 LEIT
PRAE	Prawle Point	356° 16 47.1"	50° 12 10.4"	112.5	LEICA GRX1200+GNSS	LEIAR25 LEIT
RICM	Richmond	358° 15 48.9"	54° 24 46.5"	271.1	LEICA GRX1200+GNSS	LEIAR25 LEIT
SABB	St Abbs	357° 52 17.1"	55° 53 55.9"	61.8	LEICA GRX1200+GNSS	LEIAR25 LEIT
SANO	Sandown	358° 47 13.3"	50° 39 1.2"	91.1	LEICA GRX1200+GNSS	LEIAR25 LEIT
SCAO	Scarborough	359° 37 12"	54° 15 9.1"	150.2	LEICA GRX1200+GNSS	LEIAR25 LEIT
SCIL	Scilly Isles	353° 42 15.1"	49° 54 52.4"	85.4	LEICA GRX1200+GNSS	LEIAR25 LEIT
SHOB	Shobdon	357° 6 51.1"	52° 14 34.3"	153.4	LEICA GRX1200+GNSS	LEIAR25 LEIT
SHOE	Shoeburyness	0° 49 37.3"	51° 33 17.2"	49	TRIMBLE NETR5	TRM55971.00 NONE
SHRE	Shrewsbury	357° 17 0.8"	52° 43 4.6"	110.6	LEICA GRX1200+GNSS	LEIAR25 LEIT
SKEE	Skegness	0° 20 48.4"	53° 8 30.8"	58.7	LEICA GRX1200+GNSS	LEIAR25 LEIT
SOTN	Southampton	358° 31 46.5"	50° 56 15.8"	73.7	LEICA GRX1200+GNSS	LEIAR25 LEIT
STEE	Stevenage	359° 49 17.4"	51° 54 5.4"	158.7	LEICA GRX1200+GNSS	LEIAR25 LEIT

Table B- 3 Station coordinates for 85 stations in the UK

Code	Station name	Longitude	Latitude	Height	Receiver type	Antenna type
STOR	Stornoway	353° 37 28.6"	58° 12 11.2"	63.9	LEICA GRX1200+GNSS	LEIAR25 LEIT
STRA	Stratford	0° 0 34.3"	51° 32 40.6"	80.5	TRIMBLE NETR9	TRM55971.00 NONE
SWAN	Swanland	359° 29 41.9"	53° 44 11.3"	149	LEICA GRX1200+GNSS	LEIAR25 LEIT
TAUT	Taunton	356° 55 16.6"	51° 1 24.2"	80.5	LEICA GRX1200+GNSS	LEIAR25 LEIT
TEDD	Teddington	359° 39 23.3"	51° 25 31"	70.1	LEICA GRX1200+GNSS	LEIAT504GG NONE
THUS	Thurso2	356° 16 29.9"	58° 34 53.7"	94.3	LEICA GRX1200+GNSS	LEIAR25 LEIT
TIRE	Tiree	353° 7 9.7"	56° 30 0"	70.8	LEICA GRX1200+GNSS	LEIAR25 LEIT
WARS	Warminster	357° 49 5.9"	51° 12 17.4"	177.6	LEICA GRX1200+GNSS	LEIAR25 LEIT
WEAR	Wear Head	357° 46 10.7"	54° 44 56.8"	408.4	LEICA GRX1200+GNSS	LEIAR25 LEIT
WEIW	Weir Wood	0° 0 27.5"	51° 6 3.7"	115.9	LEICA GRX1200+GNSS	LEIAR25 LEIT
WELL	Wellingborough	359° 22 31.3"	52° 18 27"	97.5	LEICA GRX1200+GNSS	LEIAR25 LEIT
WEYB	Weybourne	1° 7 49.2"	52° 56 41.5"	74.2	LEICA GRX1200+GNSS	LEIAR25 LEIT
YEAS	Yearsley	358° 53 59.7"	54° 9 44.4"	225.4	LEICA GRX1200+GNSS	LEIAR25 LEIT

Table B- 4 Station coordinates for 85 stations in the UK

Code	Station name	Longitude	Latitude	Height	Receiver type	Antenna type
ALBH	Victoria, CA	236° 30 45.1"	48° 23 23.2"	31.7	AOA BENCHMARK	AOAD/M_T SCIS
ALGO	Algonquin Park, CA	281° 55 43.1"	45° 57 20.9"	200.9	TPS NET-G3A	AOAD/M_T NONE
ALIC	Alice Springs, AU	133° 53 7.9"	-23° 40 12.4"	603.2	LEICA GRX1200GGPRO	LEIAR25.R3 NONE
AUCK	Whangaparaoa, NZ	174° 50 3.8"	-36° 36 10.2"	132.7	TRIMBLE NETR9	TRM55971.00 NONE
BAKE	Baker Lake, CA	263° 59 51.5"	64° 19 4.2"	4.5	TPS NET-G3A	TPSCR.G3 NONE
BAKO	Cibinong, ID	106° 50 56.1"	-6° 29 27.8"	158.1	LEICA GRX1200GGPRO	LEIAT504GG LEIS
BARH	Bar Harbor, US	291° 46 41.9"	44° 23 42.2"	6.8	LEICA GRX1200GGPRO	LEIAX1202GG NONE
BREW	Brewster, United State	240° 19 2.5"	48° 7 53.5"	238.6	ASHTECH UZ-12	ASH701945C_M SCIT
BRFT	Eusebio, BR	321° 34 28.1"	-3° 52 38.8"	21.7	LEICA GRX1200PRO	LEIAT504 NONE
BRMU	Bermuda, GB	295° 18 13.4"	32° 22 13.4"	-11.6	LEICA GRX1200GGPRO	JAVRINGANT_DM NONE
BZRG	Bolzano - Bozen, Italy	11° 20 12.5"	46° 29 56.4"	328.8	LEICA GRX1200+GNSS	LEIAR25.R4 LEIT
CAGS	Gatineau, CA	284° 11 33.6"	45° 35 6.1"	235	TRIMBLE NETR8	TRM59800.00 NONE
CHUM	Chumysh, Kazakhstan	74° 45 4"	42° 59 54.6"	714.4	TRIMBLE NETRS	AOAD/M_T NONE
CIT1	Pasadena, United State	241° 52 21.8"	34° 8 12.2"	215.3	TRIMBLE NETR9	TRM57971.00 NONE
CONZ	Concepcion, CL	286° 58 28.1"	-36° 50 37.6"	180.6	LEICA GRX1200+GNSS	LEIAR25.R3 LEIT
CUSV	BANGKOK, THAILAND	100° 32 2.1"	13° 44 9.3"	74.7	TRIMBLE NETRS	TRM41249.00 NONE
DAV1	Davis, AQ	77° 58 21.4"	-68° 34 38.4"	44.4	LEICA GRX1200GGPRO	LEIAR25.R3 LEIT
DRAO	Penticton, CA	240° 22 30.1"	49° 19 21.4"	541.9	TRIMBLE NETR8	TRM59800.00 SCIS
DUBO	Lac Du Bonnet, CA	264° 8 1.7"	50° 15 31.7"	245.3	TPS NETG3	AOAD/M_T NONE
FFMJ	Frankfurt / Main, Germ	8° 39 53.9"	50° 5 26.1"	178.2	JPS LEGACY	LEIAR25.R4 LEIT
GANP	Ganovce, SK	20° 19 22.6"	49° 2 5"	746	TRIMBLE NETR9	TRM55971.00 NONE
GLSV	Kiev, UA	30° 29 48.2"	50° 21 51.1"	226.3	NOV OEMV3	NOV702GG NONE
GODE	Greenbelt, US	283° 10 23.4"	39° 1 18.2"	14.5	ASHTECH UZ-12	AOAD/M_T JPLA
GODZ	Greenbelt, US	283° 10 23.4"	39° 1 18.2"	14.5	JPS EGGDT	AOAD/M_T JPLA
GOL2	Goldstone_2SCIGN	243° 6 38.7"	35° 25 30.6"	986.6	ASHTECH UZ-12	AOAD/M_T NONE
GOLD	Goldstone, US	243° 6 38.7"	35° 25 30.6"	986.7	JPS EGGDT	AOAD/M_T NONE

Table B- 5 Station coordinates for 76 IGS stations

Code	Station name	Longitude	Latitude	Height	Receiver type	Antenna type
GRAZ	Graz, AT	15° 29 36.5"	47° 4 1.7"	538.3	LEICA GRX1200+GNSS	LEIAR25.R3 LEIT
GUUG	Mangilao, USA	144° 48 9.8"	13° 25 59.5"	134.7	TRIMBLE NETR5	TRM55971.00 NONE
HERS	Hailsham, GB	0° 20 10.6"	50° 52 2.3"	76.5	SEPT POLARX3ETR	LEIAR25.R3 NONE
HNPT	Cambridge, US	283° 52 10.6"	38° 35 19.7"	-28	LEICA GRX1200GGPRO	LEIAX1202GG NONE
HOFN	Hoefn, IS	344° 48 7.5"	64° 16 2.3"	82.8	LEICA GR25	LEIAR25.R4 LEIT
IENG	Torino_Italy	7° 38 21.9"	45° 0 54.5"	316.6	ASHTECH Z-XII3T	ASH701945C_M NONE
IISC	Bangalore, IN	77° 34 13.4"	13° 1 16.2"	843.7	ASHTECH UZ-12	ASH701945E_M NONE
INVK	Inuvik, CA	226° 28 22.9"	68° 18 22.3"	46.4	ASHTECH UZ-12	ASH701945C_M SCIS
ISBA	Baghdad, IQ	44° 26 18.3"	33° 20 29.1"	72.4	TRIMBLE NETR5	TRM57971.00 NONE
ISPA	Easter Island, CL	250° 39 20.1"	-27° 7 29.9"	112.5	ASHTECH UZ-12	ASH701945E_M SCIT
KHAR	Kharkiv, UA	36° 14 20.4"	50° 0 18.4"	201	NOV OEMV3	NOV702GG NONE
KIRU	KIRUNA, SWEDEN	20° 58 6.4"	67° 51 26.5"	391.6	SEPT POLARX4	SEPCHOKE_MC SPKE
KIT3	Kitab, UZ	66° 53 7.6"	39° 8 5.2"	622.5	JAVAD TRE_G3TH	JAV_RINGANT_G3T NONE
KOUR	Kourou, GF	307° 11 38.5"	5° 15 7.9"	-25.8	SEPT POLARX4	SEPCHOKE_MC NONE
KUUJ	KUUJJUARAPIK, CANADA	282° 15 16.4"	55° 16 42.1"	0.2	TPS NET-G3A	TPSCR.G3 NONE
QAQ1	Qaqortoq, GL	313° 57 8"	60° 42 55"	110.5	ASHTECH UZ-12	ASH701945E_M SCIS
QIKI	QIKIQTARJUAQ (BAFFIN I	295° 57 58.8"	67° 33 33.6"	13.3	ASHTECH UZ-12	ASH701945E_M NONE
QUIN	Quincy, US	239° 3 20.1"	39° 58 28.4"	1105.8	ASHTECH UZ-12	ASH701945E_M SNOW
RESO	Resolute, CA	265° 6 22.7"	74° 41 27"	20	ASHTECH UZ-12	ASH700936A_M NONE
REYK	Reykjavik, IS	338° 2 40.2"	64° 8 19.6"	93	LEICA GR25	LEIAR25.R4 LEIT
RIO2	Rio Grande, AR	292° 14 56"	-53° 47 7.7"	32	JAVAD TRE_G3TH	JAV_RINGANT_G3T NONE
SALU	Sao Luis, BR	315° 47 15.1"	-2° 35 36.4"	19	TRIMBLE NETR8	TRM59800.00 NONE
SAVO	Salvador, BR	321° 34 3.9"	-12° 56 21.3"	76.3	TRIMBLE NETR5	TRM55971.00 NONE
SCH2	Schefferville, CA	293° 10 2.6"	54° 49 55.5"	498.3	TPS NET-G3A	ASH701945E_M NONE
SCOR	Scoresbysund, GL	338° 2 58.8"	70° 29 7.2"	128.5	ASHTECH UZ-12	ASH701941.B SCIS
SEY1	Seychelles	55° 28 45.9"	-4° 40 25.4"	537.2	JAVAD TRE_G3TH	ASH701945E_M NONE

Table B- 6 Station coordinates for 76 IGS stations

Code	Station name	Longitude	Latitude	Height	Receiver type	Antenna type
SNI1	SNI1_SCGN_CS1995	240° 28 32.3"	33° 14 52.4"	239.6	TPS NET-G3A	ASH701945B_M SCIS
SPK1	Saddle Peak, CA	241° 21 13.8"	34° 3 33.6"	440.1	TPS NET-G3A	TPSCR.G3 NONE
SUTH	Sutherland, ZA	20° 48 37.7"	-32° 22 48.8"	1799.8	ASHTECH UZ-12	ASH701945G_M NONE
SUTM	Sutherland, ZA	20° 48 39.3"	-32° 22 53.2"	1797.6	JAVAD TRE_G3TH	JAV_RINGANT_G3T NONE
TABL	Wrightwood, US	242° 19 18.2"	34° 22 54.7"	2228	TRIMBLE NETR9	TRM57971.00 NONE
TASH	Tashkent, UZ	69° 17 44"	41° 19 41"	439.7	JAVAD TRE_G3TH	JAV_RINGANT_G3T NONE
TITZ	Titz, Germany	6° 25 53.9"	51° 2 7.1"	155.6	JPS LEGACY	LEIAR25.R4 LEIT
TNML	HSINCHU, REPUBLIC OF C	120° 59 14.4"	24° 47 52.6"	75.9	AOA BENCHMARK	AOAD/M_T NONE
TOW2	Cape Ferguson, AU	147° 3 20.5"	-19° 16 9.4"	88.1	LEICA GRX1200GGPRO	LEIAR25.R3 NONE
TSKB	Tsukuba, JP	140° 5 15"	36° 6 20.4"	67.2	TRIMBLE NETR9	AOAD/M_T DOME
TWTF	Taoyuan, TW	121° 9 52.2"	24° 57 12.8"	201.5	ASHTECH Z-XII3T	ASH701945C_M SCIS
UFPR	Curitiba, BR	310° 46 8.6"	-25° 26 54.1"	925.8	TRIMBLE NETR5	TRM55971.00 NONE
UNBJ	Fredericton, CA	293° 21 29.9"	45° 57 0.8"	22.8	TPS LEGACY	TRM57971.00 NONE
VALD	Val d'Or, CA	282° 26 9"	48° 5 49.4"	312.8	TPS NET-G3A	TPSCR.G3 NONE
VILL	Villafranca, ES	356° 2 52.9"	40° 26 36.9"	647.3	SEPT POLARX4	SEPCHOKE_MC NONE
WAB2	Wabern, Switzerland	7° 27 51.3"	46° 55 25.5"	609.3	ASHTECH Z-XII3T	ASH700936F_C SNOW
WGTN	Wellington, NZ	174° 48 21.2"	-41° 19 24.4"	26	TRIMBLE NETR9	TRM55971.00 NONE
WTZA	Wettzell_/_Germa	12° 52 44.1"	49° 8 39.2"	665.9	ASHTECH Z-XII3T	ASH700936C_M SNOW
WTZR	Koetzting, DE	12° 52 44.1"	49° 8 39.1"	666	LEICA GRX1200+GNSS	LEIAR25.R3 LEIT
WTZZ	Koetzting, DE	12° 52 44.1"	49° 8 39.2"	665.9	JAVAD TRE_G3TH	LEIAR25.R3 LEIT
YAR3	Dongara, AU	115° 20 49.8"	-29° 2 47.4"	242.4	LEICA GRX1200GGPRO	LEIAR25 NONE
YELL	Yellowknife, CA	245° 31 9.5"	62° 28 51.2"	181	JAVAD TRE_G3T	AOAD/M_T NONE
YSSK	Yuzhno-Sakhalinsk, RU	142° 43 0.2"	47° 1 47"	91.3	ASHTECH Z-XII3	ASH701933B_M DOME

Table B- 7 Station coordinates for 76 IGS stations

Appendix-C- Summary of the differences between EMX, ESA and GFZ analysis centre strategies

	EMX	ESA	GFZ
software	GIPSY/OASISII v6.3 , developed by JPL	NAPEOS v3.6	EPOS.P8 developed at GFZ
GNSS system (s)	GPS, GLO.	GPS,GLO,(Galileo)	GPS, GLO
Pre-processing	Pre-screened using PPP matrics to reject small /incomplete files (<50%), slips (>500), phase residual (> 1cm), code residual (> 1m). Outliers, slips, 1 ms jump fixed. Code bias using CODE	Pre-screened on small /incomplete files. Rejected receivers if little data, many outliers, many cycle slip. Start with 300 stations. (ESA station with the IGS reference frame sites). CODE bias using cc2noncc.	PPP cleaning of phase data using rapid products.
Basic observables	Undifferenced carrier phases & smoothed pseudoranges	Undifferenced carrier phases and pseudoranges	Carrier phase and pseudoranges
Elevation angle	10	10	7
Sampling rate	5 min	5 min	5 min
Weighting	Elevation angle Another down weighting: station specific based on PPP results.	1/sin(e)	Elevation dependent angle with unit weight until 30 deg, then 1/2sin(e)
GPS attitude model	GPS satellites yaw applied	Yaw rates applied for GLONASS GPS not implemented yet	Applied for both GPS and GLONASS

Table C- 1 Summary of the differences between EMX, ESA and GFZ analysis centre strategies

	EMX	ESA	GFZ
Troposphere a priori model	VMF1 Gradient: none	Saastamoinen(T and P from GPT model) Gradient: none	empirical model Global Pressure and Temperature (GPT) according to Boehm et al. 2007; Relative humidity set to 60 % for all sites. Gradient: None
Mapping Function	GMF for Dry. GMF for Wet.	Using Dry GMF	GMF
Ionosphere	1st applied , 2nd applied	1st applied, 2nd not applied	1st applied, 2nd not applied
Tidal displacement	IERS 2010	IERS 2003	Mixed 2010 & 2003
Earth orientation variation	IERS 2010	IERS 2003	IERS 2003
Tracking Network	80 daily stations dynamically selected based on geometry with priority on IGS08 core stations. Stations are processed in one global network.	Maximum number of stations used 150 from ~ 300 stations.	Use all available reference frame stations plus others based mostly on geometry and location on earth
Inter connection	IAU 2006 precession Theory	IAU 2000A Precession-Nutation Theory	IAU 2000A Precession-Nutation Theory
Orbit Models			
Geopotential	EGM2008 to degree & order 12. C20 … IERS 2010	EIGEN-GLO5C to degree order 12. C20 .. IERS 2003	EGM2008 to degree & order 12. C20 … temporal variation

Table C- 2 Summary of the differences between EMX, ESA and GFZ analysis centre strategies

	EMX	ESA	GFZ
Equatorial radius of Earth	AE = 6378136 , 6378136.46 for gravity field expansion.	6378136.55	6378137
Tidal variation	IERS 2010	IERS 2003	IERS 2010
Third body	Applied , GM_sun = 132712440017.9870	Applied , GM_sun not mentioned	Applied GM_sun = 132712442076.0
Solar radiation	JPL empirical SRP model GSPM_2013	None	None
Relativistic effects	Dynamical correction not applied.	Dynamical correction applied.	Dynamical correction applied.
Adjustment Method			
	Square root information filter SRIF.	Bayesian weight least squares	Least square adjustments according to Ge et al.(2006)
Data span	24 hr	24 hr	Not mentioned
Station coordinates	All stations coordinates are adjusted, relative to the a priori values from IGb08.snx. The IGb08 velocities are used for daily coordinates updates.	All stations coordinates are adjusted, relative to the a priori values from selected IGS reference frame.	Stations coordinates constrained to IGb08.snx
Troposphere			
Zenith delay	Estimated for each observation epoch as a random walk.	Estimated as linear parameters every one hour.	Zenith delay parameters for each station with 1 hour intervals.
Mapping function	GMF.	GMF wet.	GMF wet.

Table C- 3 Summary of the differences between EMX, ESA and GFZ analysis centre strategies

	EMX	ESA	GFZ
Zenith delay epoch	Each epoch.	Value for middle of 1 hour interval.	Each integer hour.
gradients	Estimated for each epoch.	Linear per day.	For each station in daily intervals.
Ambiguity	Real except when DD ambiguities can be resolved (about 65% of global ambiguities resolved).	Real except when DD ambiguities can be resolved. Integer ambiguities resolution scheme from GFZ (G2 2005).	Fixed according to Ge et al. (2005).
Other parameters			
	None	1 bias for GLONASS per observation period for each receiver. These values are taken as reference by setting them to zero, all others are estimated. This bias is estimated as a clock bias between the GPS part and the GLONASS part of the receiver. Satellites antenna offsets are set-up so that they are included in our SINEX submissions.	GPS satellite phase centre offsets estimated daily.

Table C- 4 Summary of the differences between EMX, ESA and GFZ analysis centre strategies

Appendix-D- Comparison of tropospheric ZTD from GDD GPS and PPP GPS, PPP GLO and PPP GPS+GLO for 56 OSGB stations over seven consecutive days (figure summary)

Figure D-1 Comparison of tropospheric ZTD from GDD GPS and PPP GPS, PPP GLO and PPP GPS+GLO for 56 OSGB stations over seven consecutive days

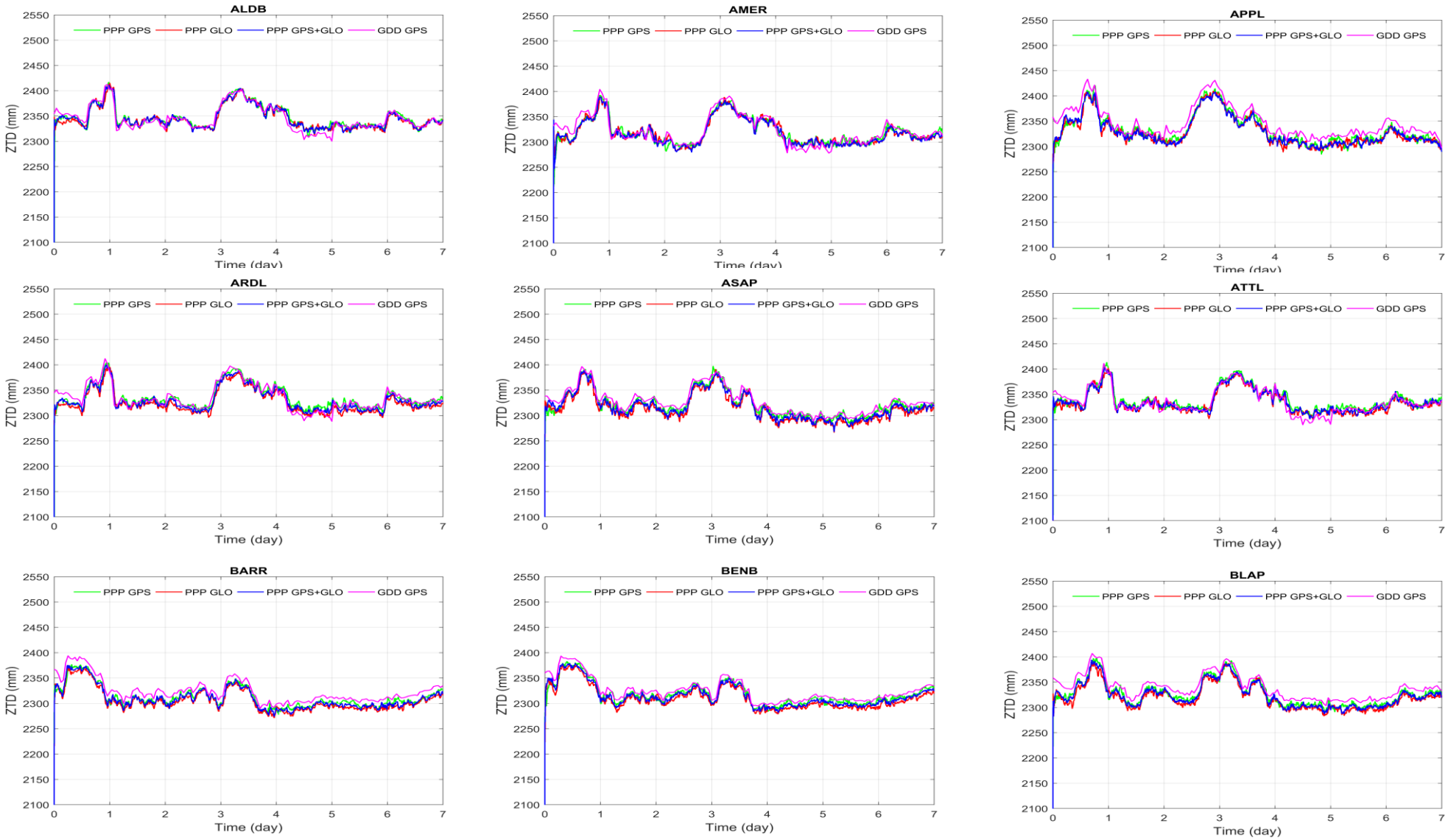


Figure D- 2 Comparison of tropospheric ZTD from GDD GPS and PPP GPS, PPP GLO and PPP GPS+GLO for 56 OSGB stations over seven consecutive days

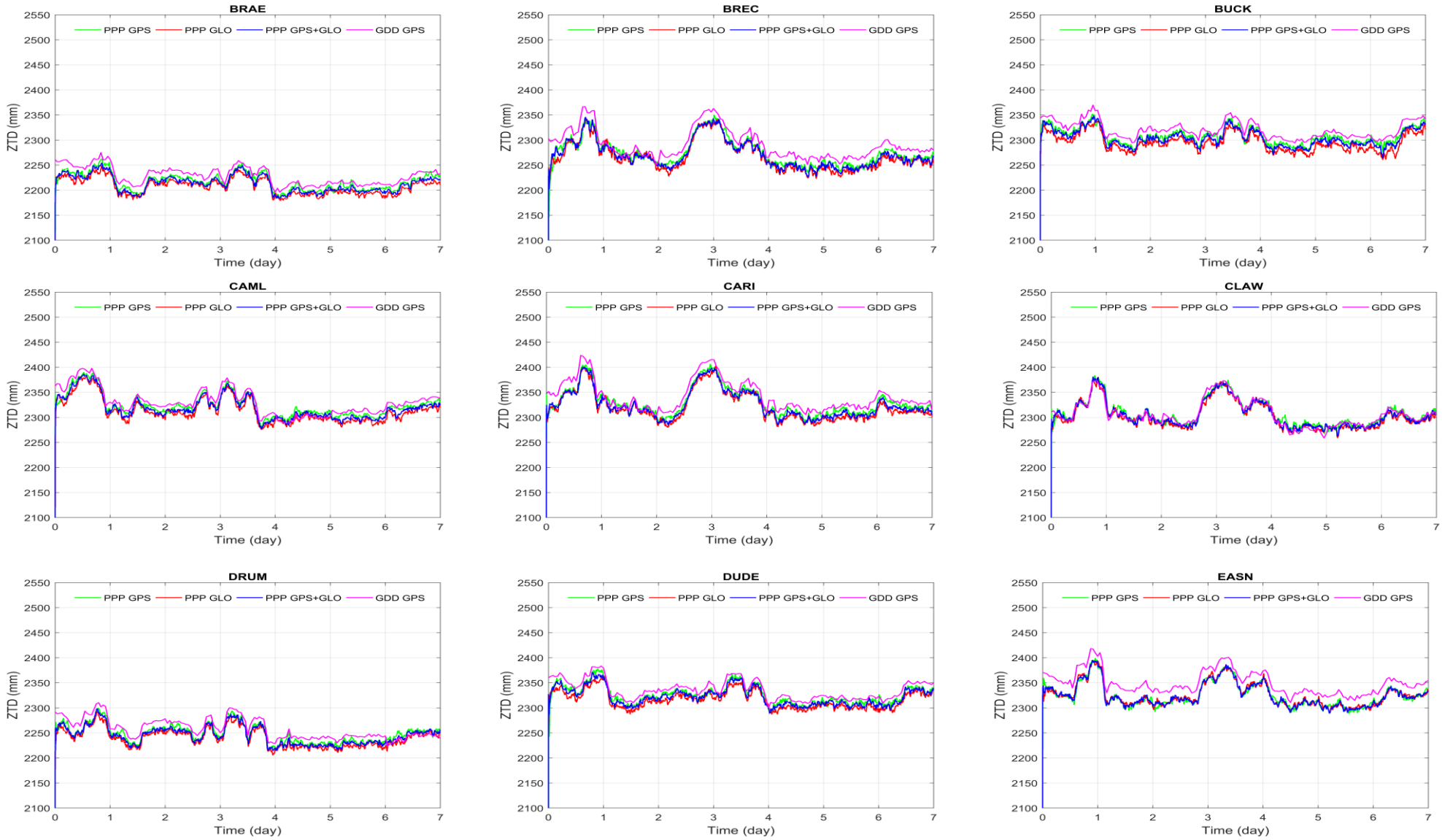


Figure D- 3 Comparison of tropospheric ZTD from GDD GPS and PPP GPS, PPP GLO and PPP GPS+GLO for 56 OSGB stations over seven consecutive days

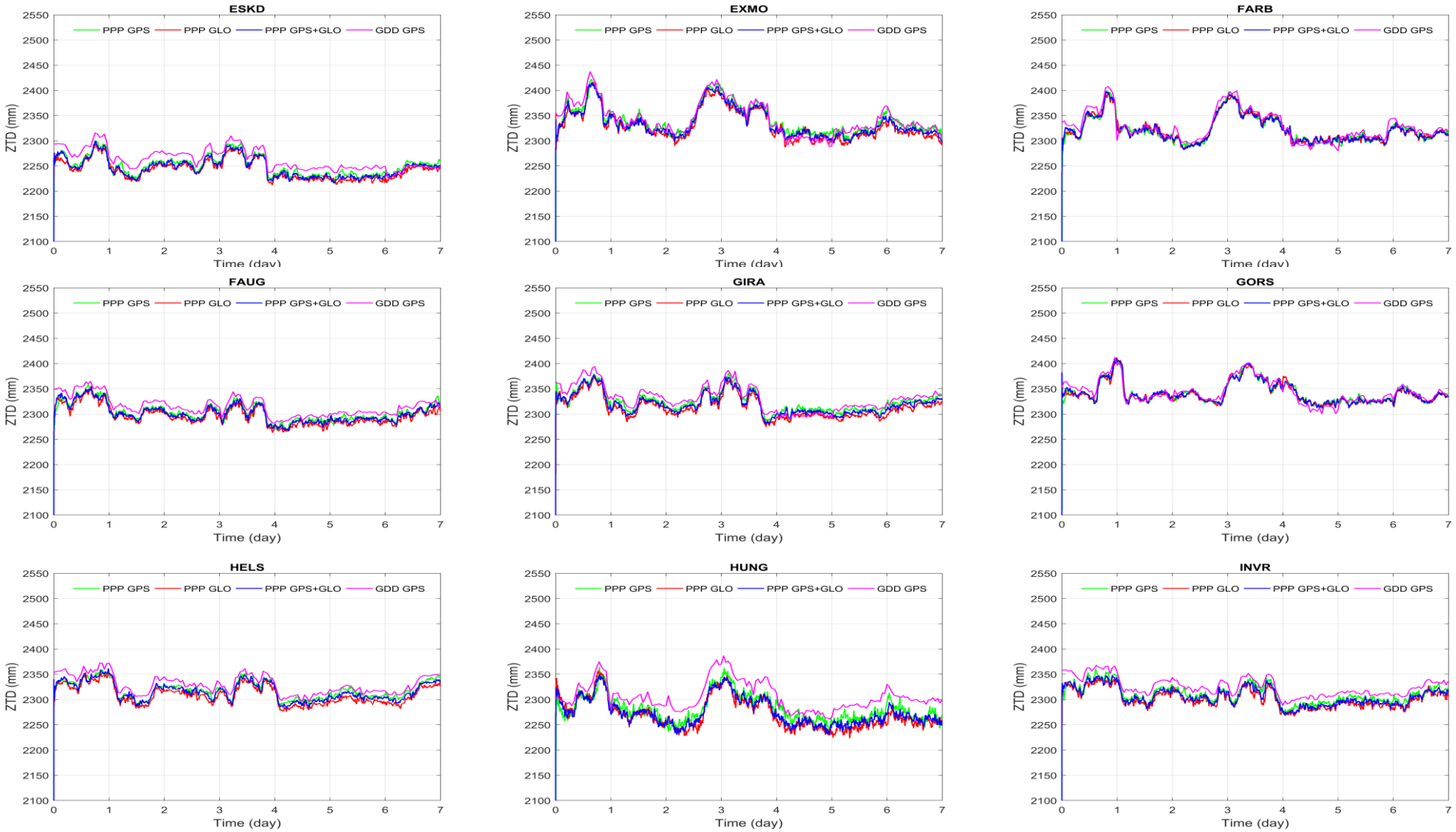


Figure D- 4 Comparison of tropospheric ZTD from GDD GPS and PPP GPS, PPP GLO and PPP GPS+GLO for 56 OSGB stations over seven consecutive days

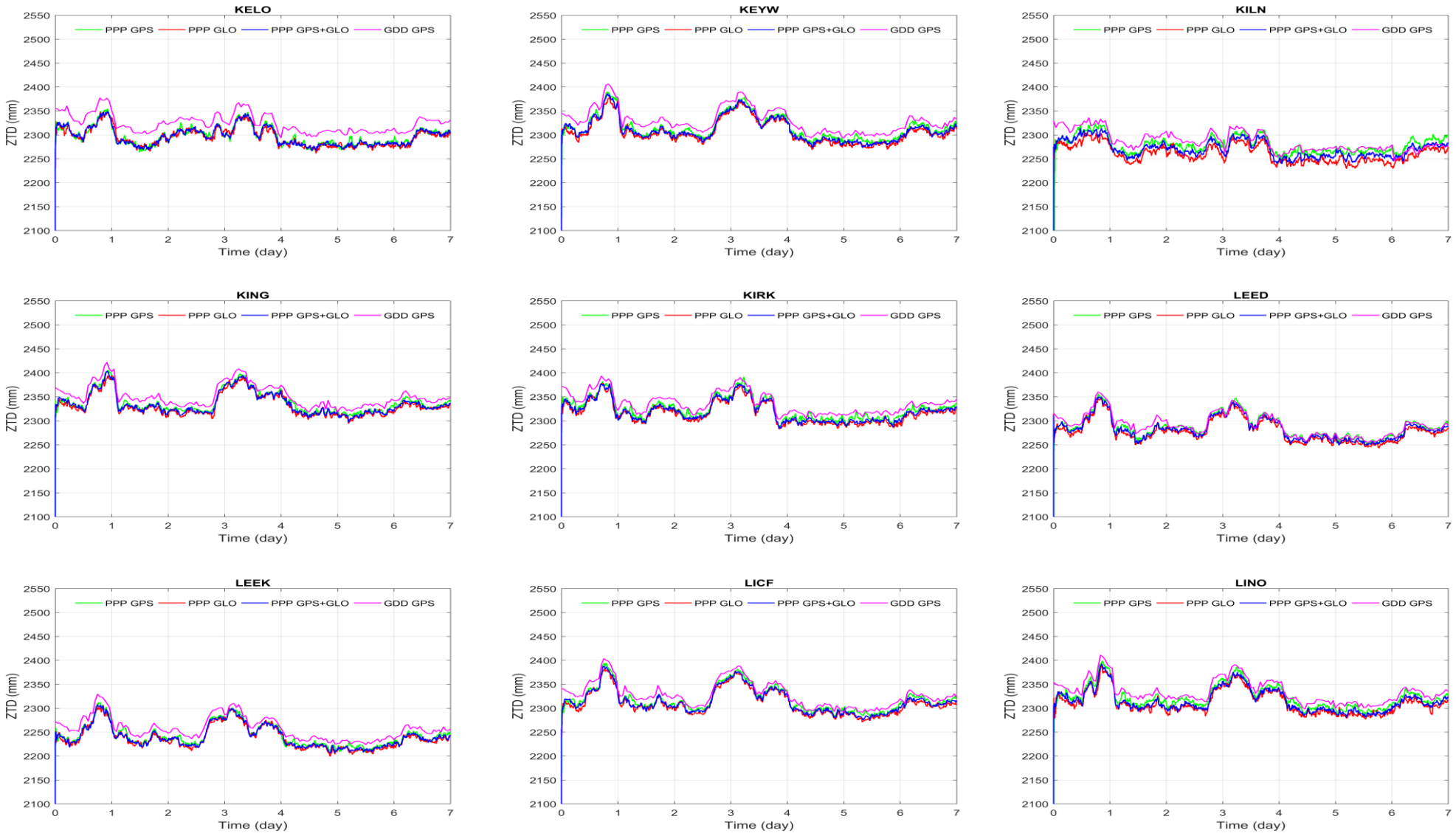


Figure D- 5 Comparison of tropospheric ZTD from GDD GPS and PPP GPS, PPP GLO and PPP GPS+GLO for 56 OSGB stations over seven consecutive days

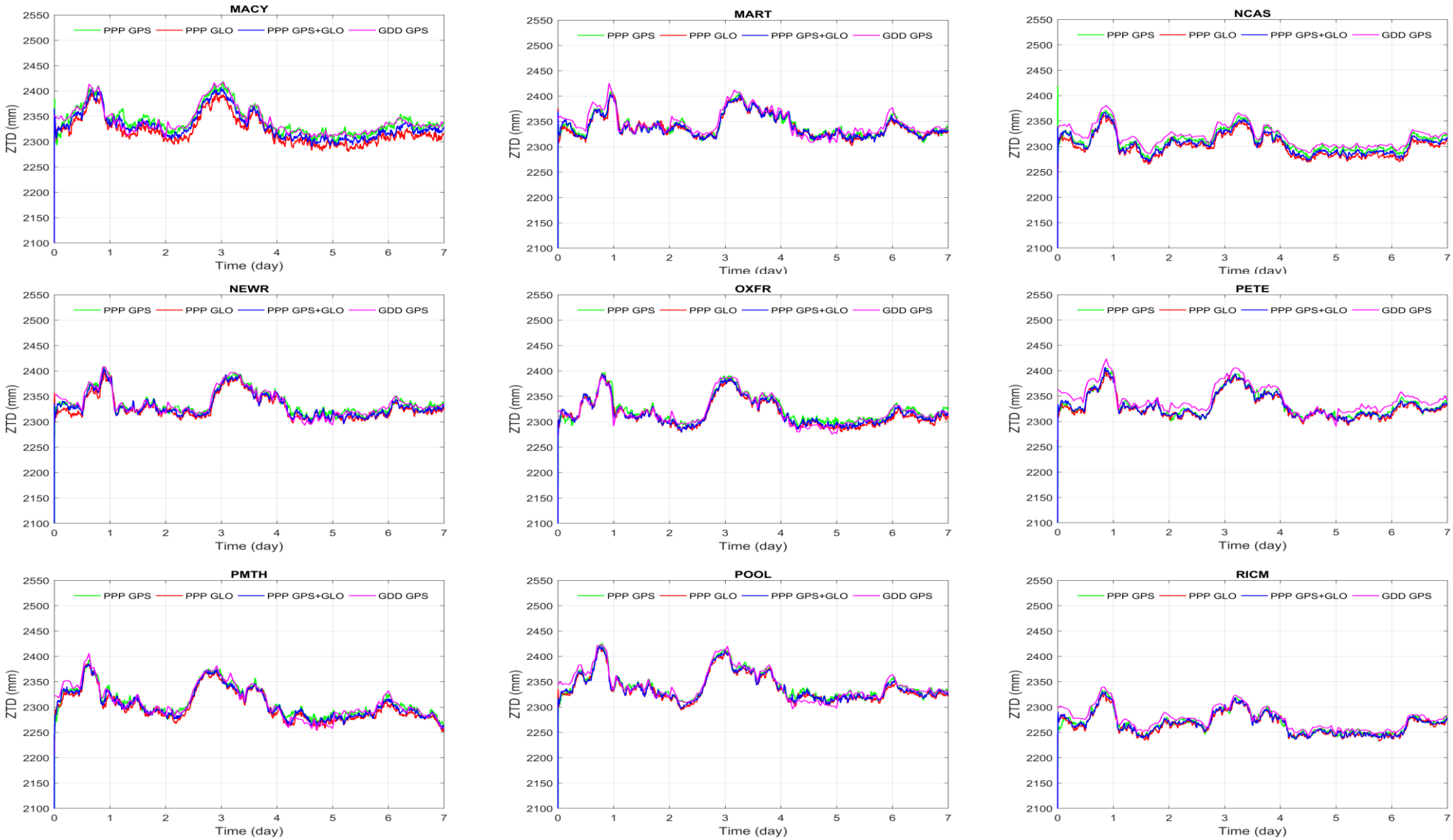


Figure D- 6 Comparison of tropospheric ZTD from GDD GPS and PPP GPS, PPP GLO and PPP GPS+GLO for 56 OSGB stations over seven consecutive days

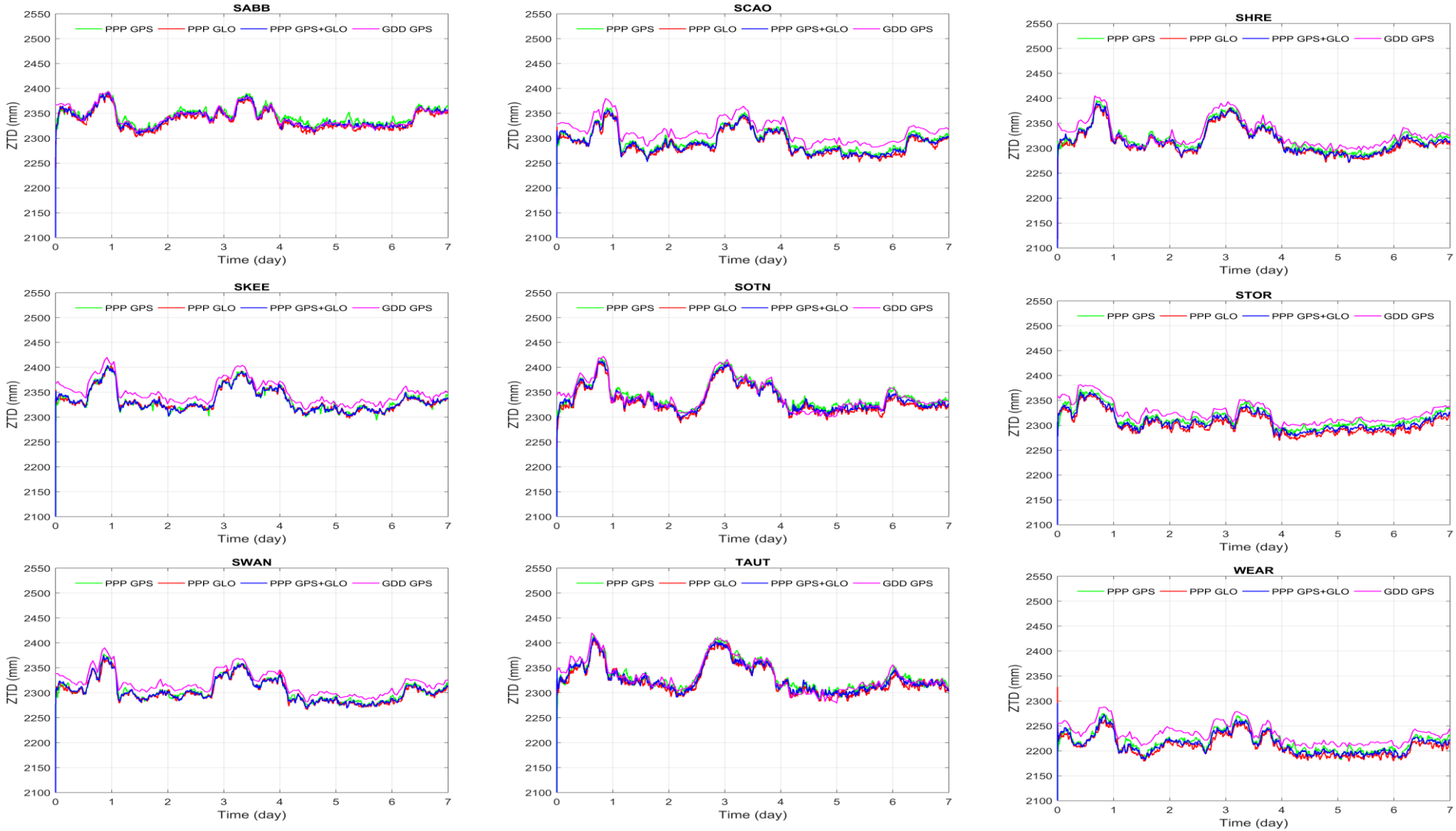
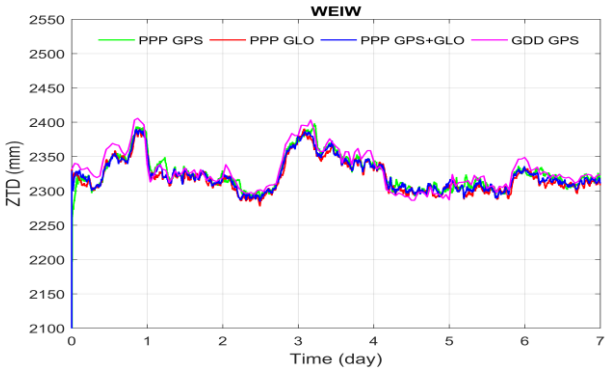
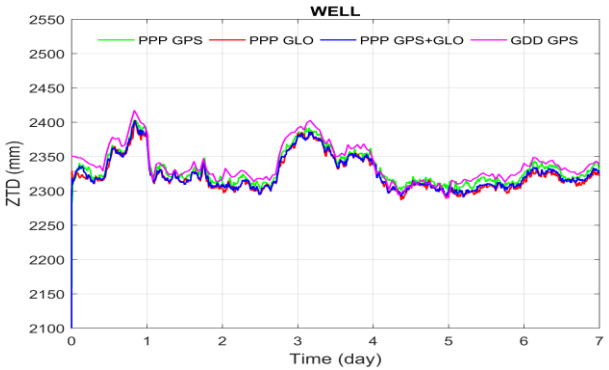


Figure D- 7 Comparison of tropospheric ZTD from GDD GPS and PPP GPS, PPP GLO and PPP GPS+GLO for 56 OSGB stations over seven consecutive days





Appendix-E- Station coordinates and tropospheric ZTD differences between all PPP scenarios using EMX, ESA and GFZ precise products and GDD GPS for 85 OSGB stations in the UK over seven weeks and between PPP GPS (using real-time precise products) and the IGS near real time solutions for 76 IGS stations over 12 weeks

Station	Station coordinates variation (RMS) (mm)			Tropospheric ZTD (mm)		
	E	N	U	Mean	STD	RMS
ABEP	3.1	3.2	7.7	-3.2	4.3	5.4
ALDB	3.0	3.4	6.7	-3.5	6.4	7.3
AMER	4.6	3.5	11.9	5.0	5.7	7.6
ANLX	3.9	3.3	6.5	2.1	5.8	6.1
APPL	3.9	2.6	10.4	-2.2	6.3	6.7
ARDL	3.1	3.0	8.5	-4.7	4.8	6.8
ASAP	4.4	2.7	8.8	3.9	5.6	6.8
ATTL	3.0	2.6	10.7	-4.4	1.9	4.8
BARR	3.8	2.8	4.6	4.0	5.6	6.9
BEES	3.9	2.4	11.1	-2.5	2.2	3.3
BENB	3.4	3.1	6.1	-4.3	3.8	5.8
BLAP	3.6	2.8	7.9	-5.2	1.8	5.4
BRAE	4.8	2.6	6.8	-4.9	2.1	5.3
BREC	3.5	3.0	9.2	-5.0	2.3	5.5
BUCK	3.3	5.2	8.3	-4.4	5.1	6.7
CAML	3.3	2.9	8.3	-5.5	2.2	5.9
CARI	3.3	2.5	9.4	-0.6	8.2	8.2
CARL	3.1	3.3	8.1	-5.8	4.8	7.5
CLAW	3.8	2.9	10.8	-3.5	5.4	6.4
DARE	3.7	2.8	7.6	7.1	7.2	10.1
DRUM	3.4	3.4	7.6	-1.9	6.1	6.4
DUDE	3.0	2.7	8.7	-1.2	7.6	7.7
DUNG	4.2	5.2	7.8	-5.0	1.6	5.2
EASN	3.2	2.5	8.0	0.5	7.0	7.1
ESKD	3.2	3.2	6.9	-6.3	2.7	6.8
EXMO	5.7	3.0	5.3	-1.5	7.0	7.2
FARB	3.2	3.5	4.5	-1.4	6.0	6.1
FAUG	5.3	3.6	7.0	6.6	5.7	8.7
GIGG	3.4	3.0	9.5	-3.7	5.4	6.5
GIRA	4.3	2.6	6.4	-0.2	4.7	4.7
GLAS	4.8	3.5	7.9	-0.1	7.9	7.9
GORS	3.0	3.2	7.8	-0.2	8.5	8.5
HARD	2.4	3.0	9.4	2.6	5.4	6.0
HELS	3.7	3.2	7.3	4.1	5.7	7.0
HOLY	2.9	3.2	6.6	-5.2	1.6	5.4
HOOB	3.4	2.9	7.4	-5.1	1.9	5.4
HUNG	3.6	3.1	8.2	-3.7	5.1	6.3
INVR	4.2	2.9	10.1	8.0	8.0	11.3
KELO	4.6	2.3	12.5	-4.3	2.3	4.9

Table E-1 The differences between the estimated station coordinates and tropospheric ZTD from GPS GDD and PPP GPS using EMX precise products for 85 OSGB stations over seven weeks

Station	Station coordinates variation (RMS) (mm)			Tropospheric ZTD (mm)		
	E	N	U	Mean	STD	RMS
KEYW	3.0	2.4	7.7	-7.5	3.3	8.2
KILN	3.5	3.1	8.3	-2.3	6.1	6.5
KING	3.0	2.8	6.3	-6.6	2.5	7.0
KINL	3.8	2.9	7.6	-5.6	2.4	6.1
KIRK	5.1	2.6	7.9	-5.1	1.9	5.4
LCAR	4.1	3.3	7.2	-4.3	4.2	6.0
LEED	3.1	2.8	5.7	-4.7	2.1	5.2
LEEK	4.0	2.6	5.5	-2.7	4.4	5.2
LICF	3.0	2.9	8.6	-3.9	4.2	5.7
LINO	4.2	4.1	7.0	-6.4	2.3	6.8
LOFT	3.6	3.7	7.4	-4.7	2.7	5.4
MACY	3.6	3.0	8.3	-2.3	6.2	6.7
MART	3.1	3.3	8.7	-4.3	1.9	4.7
NCAS	3.2	3.2	7.1	4.3	5.8	7.2
NEWR	3.3	3.0	13.5	-4.6	2.2	5.0
OBAN	5.5	4.2	7.2	1.2	5.4	5.5
OXFR	3.1	2.4	12.7	-4.3	4.5	6.2
PADT	3.5	3.1	8.3	-2.2	6.3	6.5
PETE	3.2	2.7	6.6	4.3	6.5	7.8
PMTH	3.0	3.6	7.9	-4.9	5.2	7.2
POOL	3.6	3.1	7.0	-1.5	6.3	6.4
PRAE	3.3	3.1	8.0	2.3	7.1	7.4
RICM	3.6	3.1	8.2	-2.2	6.2	6.5
SABB	4.1	3.7	12.2	-1.7	6.2	6.4
SANO	3.7	3.4	9.0	-5.2	3.5	6.3
SCAO	3.2	3.2	6.6	1.8	6.6	6.8
SCIL	3.2	3.3	7.6	-3.3	2.9	4.4
SHOB	3.0	2.8	7.0	-3.4	5.1	6.2
SHOE	3.6	3.1	8.4	-2.1	6.2	6.5
SHRE	3.0	2.4	7.3	-4.7	4.5	6.5
SKEE	3.3	3.3	8.0	-4.5	5.9	7.4
SOTN	3.0	2.9	9.6	-6.6	2.5	7.1
STEE	3.4	3.4	8.0	1.6	5.8	6.0
STOR	3.0	2.9	5.2	3.5	5.0	6.0
STRA	3.6	3.1	8.2	-2.4	6.2	6.6
SWAN	3.2	2.8	7.1	-3.1	4.3	5.3
TAUT	3.2	3.2	8.9	-6.5	2.3	6.9
TEDD	3.7	3.1	8.3	-2.3	6.1	6.6
THUS	3.1	3.0	5.1	-5.1	4.9	7.1

Table E-2 The differences between the estimated station coordinates and tropospheric ZTD from GPS GDD and PPP GPS using EMX precise products for 85 OSGB stations over seven weeks

Station	Station coordinates variation (RMS) (mm)			Tropospheric ZTD (mm)		
	E	N	U	Mean	STD	RMS
TIRE	3.6	3.1	8.4	-2.3	6.0	6.6
WARS	3.7	3.1	8.3	-2.3	6.2	6.6
WEAR	4.5	2.5	11.0	-2.8	4.1	5.0
WEIW	3.4	3.7	10.5	-6.3	3.9	7.5
WELL	3.4	3.1	7.4	2.5	5.7	6.2
WEYB	3.9	3.0	7.4	-5.2	4.6	6.9
YEAS	3.9	2.4	8.4	-0.6	7.3	7.3

Table E-3 The differences between the estimated station coordinates and tropospheric ZTD from GPS GDD and PPP GPS using EMX precise products for 85 OSGB stations over seven weeks

Station	Station coordinates variation (RMS) (mm)			Tropospheric ZTD (mm)		
	E	N	U	Mean	STD	RMS
ABEP	2.7	2.0	10.2	-3.8	4.4	5.8
ALDB	3.3	2.1	8.4	-4.1	6.3	7.5
AMER	3.2	2.3	13.8	4.6	5.7	7.3
ANLX	2.8	1.8	7.8	2.1	5.8	6.2
APPL	2.9	2.2	11.8	-2.2	6.7	7.1
ARDL	3.2	2.0	10.6	-5.0	4.5	6.8
ASAP	3.4	1.8	10.8	3.6	5.8	6.8
ATTL	2.6	1.9	13.2	-4.7	2.0	5.1
BARR	3.2	1.4	5.2	3.8	5.8	6.9
BEES	3.0	2.1	14.7	-3.1	2.3	3.9
BENB	2.5	1.8	8.0	-5.3	3.8	6.5
BLAP	4.0	1.8	10.2	-5.7	1.8	6.0
BRAE	4.0	1.9	8.5	-5.5	2.2	5.9
BREC	3.1	1.7	11.4	-5.5	2.2	5.9
BUCK	2.7	3.8	9.8	-4.8	5.3	7.2
CAML	3.1	1.7	11.0	-5.8	1.9	6.1
CARI	2.6	1.8	11.8	-1.2	8.2	8.3
CARL	3.2	2.0	8.6	-5.9	4.9	7.7
CLAW	3.9	2.0	14.1	-3.9	5.6	6.8
DARE	3.1	1.9	10.3	6.4	7.0	9.5
DRUM	2.2	2.0	8.7	-2.0	6.3	6.6
DUDE	2.6	1.3	10.7	-1.6	7.7	7.9
DUNG	2.4	2.9	11.8	-5.1	1.5	5.3
EASN	2.1	2.0	9.8	0.5	7.4	7.4
ESKD	2.4	1.7	8.0	-6.8	2.4	7.2
EXMO	6.5	1.6	7.8	-2.1	7.2	7.5
FARB	1.7	1.7	5.0	-1.1	6.4	6.5
FAUG	4.4	1.8	8.4	6.2	5.9	8.6
GIGG	2.9	1.8	11.3	-4.4	5.4	7.0
GIRA	4.3	1.4	8.6	-0.9	4.5	4.6
GLAS	3.7	1.9	9.4	-0.7	7.8	7.9
GORS	2.7	2.0	9.2	-0.7	8.7	8.8
HARD	4.0	1.8	10.7	2.5	5.5	6.0
HELS	3.8	2.0	9.3	3.8	5.8	6.9
HOLY	2.4	2.0	8.3	-5.5	1.6	5.8
HOOB	2.4	1.7	8.3	-5.6	1.9	6.0
HUNG	3.0	2.0	10.3	-4.0	5.0	6.4
INVR	3.3	2.0	11.9	5.7	8.2	10.0
KELO	2.8	2.8	14.1	-4.8	2.3	5.3

Table E-4 The differences between the estimated station coordinates and tropospheric ZTD from GPS GDD and PPP GPS using ESA precise products for 85 OSGB stations over seven weeks

Station	Station coordinates variation (RMS) (mm)			Tropospheric ZTD (mm)		
	E	N	U	Mean	STD	RMS
KEYW	2.4	1.8	9.9	-7.7	3.1	8.3
KILN	3.0	2.0	10.4	-2.7	6.1	6.8
KING	2.8	1.8	8.3	-6.7	2.4	7.2
KINL	2.9	1.8	10.3	-6.0	2.5	6.5
KIRK	3.4	1.7	9.4	-5.7	2.0	6.0
LCAR	3.9	2.0	8.2	-4.9	4.0	6.3
LEED	2.3	1.6	7.0	-5.2	2.0	5.6
LEEK	4.4	2.0	8.3	-2.9	4.5	5.3
LICF	2.4	1.8	10.9	-4.4	4.2	6.1
LINO	2.7	2.5	8.5	-6.8	2.2	7.1
LOFT	2.8	2.0	8.8	-5.1	2.6	5.8
MACY	3.0	2.0	10.3	-2.5	6.1	6.8
MART	2.8	2.1	10.5	-4.7	2.0	5.1
NCAS	3.0	1.8	8.7	3.8	5.9	7.0
NEWR	2.2	1.9	15.9	-4.9	2.0	5.3
OBAN	4.3	2.3	8.8	1.3	5.3	5.5
OXFR	2.2	1.9	15.2	-4.8	5.9	7.6
PADT	3.0	2.0	10.3	-2.5	6.3	6.8
PETE	2.8	1.9	7.9	4.5	6.5	7.9
PMTH	2.3	2.3	9.8	-5.2	5.3	7.5
POOL	2.3	1.9	8.7	-1.7	6.4	6.7
PRAE	3.8	2.1	9.8	2.0	7.0	7.3
RICM	3.0	2.0	10.5	-2.5	6.3	6.8
SABB	3.7	2.4	14.5	-2.1	6.4	6.7
SANO	2.5	2.3	10.9	-5.3	3.3	6.2
SCAO	2.5	1.9	8.1	1.6	6.4	6.6
SCIL	2.9	1.9	9.3	-3.8	2.6	4.6
SHOB	2.8	1.8	8.7	-3.8	5.2	6.4
SHOE	3.1	2.0	10.4	-2.7	6.1	6.8
SHRE	2.9	1.6	9.8	-5.1	4.6	6.8
SKEE	2.0	1.9	10.2	-4.9	5.8	7.7
SOTN	3.1	1.9	11.7	-7.1	2.5	7.5
STEE	4.3	2.2	10.2	1.3	5.9	6.0
STOR	2.5	1.7	7.0	3.2	4.9	5.8
STRA	2.9	2.0	10.3	-2.5	6.1	6.7
SWAN	2.6	1.9	9.6	-3.9	4.5	6.0
TAUT	2.7	2.4	11.5	-7.0	2.2	7.3
TEDD	3.1	2.0	10.2	-2.6	6.2	6.7
THUS	2.8	1.6	5.8	-5.4	4.4	7.0

Table E-5 The differences between the estimated station coordinates and tropospheric ZTD from GPS GDD and PPP GPS using ESA precise products for 85 OSGB stations over seven weeks

Station	Station coordinates variation (RMS) (mm)			Tropospheric ZTD (mm)		
	E	N	U	Mean	STD	RMS
TIRE	3.0	1.9	10.4	-2.6	6.1	6.7
WARS	3.0	1.9	10.3	-2.7	6.2	6.8
WEAR	3.3	1.8	13.5	-3.2	4.4	5.5
WEIW	2.7	2.3	13.0	-6.5	4.0	7.7
WELL	1.9	2.0	9.5	2.5	5.8	6.3
WEYB	2.5	1.8	9.0	-5.8	4.7	7.5
YEAS	3.2	1.5	11.9	-1.2	7.2	7.3

Table E-6 The differences between the estimated station coordinates and tropospheric ZTD from GPS GDD and PPP GPS using ESA precise products for 85 OSGB stations over seven weeks

Station	Station coordinates variation (RMS) (mm)			Tropospheric ZTD (mm)		
	E	N	U	Mean	STD	RMS
ABEP	3.2	2.0	11.1	-3.9	4.4	5.9
ALDB	3.7	1.9	9.0	-4.2	6.4	7.6
AMER	2.5	2.0	14.7	4.6	5.8	7.4
ANLX	2.6	1.8	8.2	2.1	5.7	6.1
APPL	3.6	2.4	13.2	-2.5	6.6	7.0
ARDL	3.8	1.9	11.6	-5.1	4.5	6.8
ASAP	3.2	1.8	11.3	3.6	5.7	6.8
ATTL	3.2	2.1	13.9	-4.8	2.1	5.2
BARR	3.6	1.7	6.0	3.8	5.8	6.9
BEES	3.7	2.7	15.1	-3.1	2.3	3.9
BENB	2.5	1.8	8.9	-5.2	3.8	6.5
BLAP	4.4	1.9	11.1	-5.9	1.6	6.1
BRAE	4.4	2.2	9.4	-5.5	2.1	5.9
BREC	3.3	1.8	12.3	-5.7	2.0	6.1
BUCK	3.3	3.5	9.9	-4.7	5.1	6.9
CAML	2.9	1.8	11.1	-5.8	1.9	6.1
CARI	2.9	2.2	12.8	-1.2	8.2	8.3
CARL	3.4	1.9	9.2	-5.9	5.1	7.8
CLAW	4.5	2.0	14.4	-4.0	5.7	7.0
DARE	2.9	2.0	10.7	6.4	7.0	9.5
DRUM	2.4	2.1	10.6	-2.0	6.3	6.6
DUDE	3.0	1.7	11.4	-1.8	7.6	7.9
DUNG	2.3	2.6	12.7	-5.3	1.6	5.6
EASN	2.5	2.5	11.4	0.3	7.4	7.4
ESKD	2.8	2.0	9.4	-6.8	2.5	7.3
EXMO	6.5	1.9	9.1	-2.3	7.2	7.5
FARB	1.9	1.6	6.4	-1.8	5.9	6.2
FAUG	3.9	1.9	9.1	5.9	5.8	8.3
GIGG	3.4	2.0	11.8	-4.5	5.5	7.1
GIRA	4.8	1.5	9.3	-0.9	4.5	4.6
GLAS	2.9	2.0	10.0	-0.7	7.8	7.8
GORS	3.3	2.0	10.1	-0.8	8.6	8.7
HARD	4.1	1.7	11.4	2.4	5.4	5.9
HELS	4.2	1.9	10.0	3.7	5.7	6.8
HOLY	3.1	1.8	9.0	-5.6	1.5	5.8
HOOB	2.8	1.9	9.1	-5.7	1.9	6.0
HUNG	3.2	2.0	11.1	-4.2	5.0	6.6
INVR	3.3	2.1	12.8	6.9	8.6	11.1
KELO	2.6	3.5	15.8	-4.8	2.3	5.3

Table E-7 The differences between the estimated station coordinates and tropospheric ZTD from GPS GDD and PPP GPS using GFZ precise products for 85 OSGB stations over seven weeks

Station	Station coordinates variation (RMS) (mm)			Tropospheric ZTD (mm)		
	E	N	U	Mean	STD	RMS
KEYW	2.7	2.1	10.7	-7.8	3.1	8.4
KILN	3.3	2.0	11.0	-2.7	6.0	6.9
KING	3.3	1.9	9.2	-6.8	2.3	7.2
KINL	2.7	2.1	10.7	-6.1	2.5	6.6
KIRK	3.0	1.7	10.6	-5.6	1.9	5.9
LCAR	3.6	2.1	9.2	-4.9	4.1	6.4
LEED	2.6	1.7	8.1	-5.4	2.0	5.7
LEEK	4.9	2.1	9.0	-3.1	4.3	5.3
LICF	2.6	1.9	11.8	-4.5	4.3	6.2
LINO	2.2	2.0	9.1	-6.9	2.2	7.2
LOFT	3.1	1.9	9.5	-5.1	2.6	5.7
MACY	3.3	2.0	11.2	-2.8	6.3	6.8
MART	2.8	1.9	11.4	-4.7	1.8	5.1
NCAS	3.7	1.7	9.8	3.7	5.8	6.8
NEWR	2.2	1.8	17.0	-5.0	2.1	5.4
OBAN	4.7	2.1	8.2	1.3	5.4	5.5
OXFR	2.3	2.3	16.0	-4.4	5.9	7.4
PADT	3.3	2.0	11.1	-2.7	6.2	6.9
PETE	3.2	2.1	8.8	4.4	6.4	7.8
PMTH	2.6	2.0	10.5	-5.3	5.3	7.5
POOL	2.2	1.7	9.8	-2.1	6.3	6.7
PRAE	4.3	2.1	10.6	2.0	7.0	7.2
RICM	3.2	2.0	11.1	-2.6	6.4	6.8
SABB	3.4	2.0	14.2	-2.1	6.3	6.6
SANO	2.6	2.1	11.8	-5.2	3.4	6.2
SCAO	2.9	1.8	9.0	1.5	6.3	6.5
SCIL	3.3	1.8	10.1	-3.9	2.5	4.7
SHOB	3.5	2.0	9.7	-3.9	5.2	6.5
SHOE	3.3	2.0	11.0	-2.8	6.2	6.8
SHRE	3.1	1.9	10.8	-5.3	4.6	7.0
SKEE	2.5	1.9	11.2	-4.9	5.8	7.6
SOTN	3.6	1.8	12.5	-7.2	2.4	7.6
STEE	5.0	2.1	11.0	1.3	5.7	5.9
STOR	2.8	1.8	7.9	3.3	5.0	6.0
STRA	3.3	2.0	11.0	-2.5	6.2	6.8
SWAN	2.9	2.0	10.4	-4.1	4.3	5.9
TAUT	3.2	1.9	12.8	-7.0	2.2	7.3
TEDD	3.3	2.0	11.2	-2.8	6.3	6.8
THUS	3.3	1.8	6.2	-5.8	4.3	7.2

Table E-8 The differences between the estimated station coordinates and tropospheric ZTD from GPS GDD and PPP GPS using GFZ precise products for 85 OSGB stations over seven weeks

Station	Station coordinates variation (RMS) (mm)			Tropospheric ZTD (mm)		
	E	N	U	Mean	STD	RMS
TIRE	3.3	2.0	11.0	-2.9	6.1	6.7
WARS	3.3	2.1	11.0	-2.8	6.2	6.8
WEAR	3.0	2.3	14.7	-3.5	3.8	5.2
WEIW	3.1	2.1	14.1	-6.9	4.0	8.0
WELL	2.0	1.8	10.3	2.1	5.7	6.1
WEYB	2.9	1.9	9.9	-5.8	4.7	7.4
YEAS	3.3	1.8	12.3	-1.4	7.0	7.2

Table E-9 The differences between the estimated station coordinates and tropospheric ZTD from GPS GDD and PPP GPS using GFZ precise products for 85 OSGB stations over seven weeks

Station	Station coordinates variation (RMS) (mm)			Tropospheric ZTD (mm)		
	E	N	U	Mean	STD	RMS
ABEP	3.7	3.3	6.9	-2.8	5.4	6.1
ALDB	3.9	4.2	11.2	-4.4	6.6	7.9
AMER	3.5	6.1	8.5	5.0	5.7	7.6
ANLX	3.7	2.5	9.3	1.7	5.7	6.0
APPL	4.0	4.6	9.0	-2.3	6.7	7.1
ARDL	3.7	3.9	5.7	-4.0	5.3	6.6
ASAP	4.3	3.9	5.2	2.1	5.6	6.0
ATTL	3.7	2.6	9.8	-6.2	3.1	6.9
BARR	3.0	6.0	11.8	0.3	5.5	5.5
BEES	3.8	3.6	6.0	-3.8	2.8	4.7
BENB	3.3	5.7	10.1	-5.3	4.7	7.1
BLAP	3.6	4.5	5.3	-5.5	1.9	5.8
BRAE	3.5	5.3	4.9	-6.6	2.6	7.1
BREC	3.4	3.2	7.2	-7.0	2.4	7.4
BUCK	3.9	6.5	5.2	-7.4	5.0	8.9
CAML	3.6	5.3	6.9	-8.7	2.5	9.0
CARI	3.9	4.3	6.5	-1.6	8.3	8.4
CARL	3.3	4.9	5.4	-7.0	5.2	8.8
CLAW	2.9	5.1	5.9	-5.4	5.6	7.8
DARE	3.3	4.2	5.4	6.3	9.6	11.5
DRUM	3.2	5.9	5.6	-5.4	5.7	7.8
DUDE	3.6	4.7	5.0	-4.5	7.3	8.6
DUNG	3.9	6.6	7.5	-6.9	1.7	7.1
EASN	3.1	4.4	10.0	0.1	7.7	7.7
ESKD	3.2	4.1	5.8	-6.2	2.6	6.7
EXMO	3.2	5.3	8.7	-4.5	7.1	8.4
FARB	3.4	5.6	14.8	-4.9	5.9	7.6
FAUG	3.5	6.7	7.2	4.1	6.1	7.3
GIGG	3.6	5.8	5.6	-4.9	5.6	7.4
GIRA	3.9	4.7	5.2	-1.7	5.0	5.3
GLAS	4.3	7.3	6.4	-0.8	8.0	8.0
GORS	3.8	4.8	10.6	-2.3	8.5	8.8
HARD	3.6	3.5	7.2	2.8	5.8	6.5
HELS	3.4	4.5	5.7	4.4	5.7	7.2
HOLY	3.6	4.1	9.6	-6.9	2.2	7.2
HOOB	3.2	4.5	5.9	-5.0	2.8	5.8
HUNG	3.7	4.8	7.3	-5.1	4.3	6.7
INVR	4.5	4.8	5.5	6.2	8.1	10.2
KELO	4.6	2.7	9.2	-7.2	2.3	7.6

Table E-10 The differences between the estimated station coordinates and tropospheric ZTD from GPS GDD and PPP GLO using EMX precise products for 85 OSGB stations over seven weeks

Station	Station coordinates variation (RMS) (mm)			Tropospheric ZTD (mm)		
	E	N	U	Mean	STD	RMS
KEYW	3.4	4.0	5.2	-8.5	3.9	9.3
KILN	3.7	4.8	7.2	-3.4	6.6	7.2
KING	3.7	2.7	6.8	-7.7	2.6	8.1
KINL	3.9	5.8	5.1	-5.9	2.7	6.5
KIRK	4.2	8.2	4.9	-6.4	3.5	7.3
LCAR	3.5	5.6	5.7	-4.9	4.6	6.7
LEED	3.3	4.2	4.9	-7.1	2.4	7.5
LEEK	3.7	3.1	5.0	-4.3	3.2	5.3
LICF	3.7	4.0	5.0	-6.1	4.2	7.4
LINO	3.8	5.8	8.8	-8.4	2.8	8.9
LOFT	3.4	6.7	6.1	-5.7	2.7	6.3
MACY	3.7	4.8	7.3	-3.4	6.5	7.2
MART	3.3	2.8	8.8	-6.2	2.2	6.6
NCAS	3.4	4.9	4.2	3.0	6.4	7.0
NEWR	3.5	5.2	6.8	-6.3	2.1	6.6
OBAN	5.0	5.9	8.9	1.2	5.4	5.5
OXFR	3.4	4.0	5.5	-5.2	4.4	6.8
PADT	3.7	4.8	7.4	-3.4	6.4	7.5
PETE	3.3	4.4	8.4	6.0	7.8	9.8
PMTH	3.7	3.8	5.4	-5.4	4.7	7.2
POOL	3.7	4.9	6.5	-3.8	5.8	6.9
PRAE	3.6	4.2	5.0	1.3	6.4	6.6
RICM	3.7	4.8	7.3	-3.5	6.4	7.3
SABB	3.9	5.2	5.3	-2.8	5.7	6.4
SANO	3.8	5.0	9.2	-6.3	4.3	7.6
SCAO	3.5	4.3	8.9	1.3	6.8	7.0
SCIL	3.8	5.5	8.0	-4.7	2.5	5.3
SHOB	3.7	4.2	5.2	-4.0	5.5	6.7
SHOE	3.7	4.8	7.4	-3.5	6.6	7.5
SHRE	3.3	3.9	4.8	-6.8	4.7	8.3
SKEE	3.4	5.2	6.1	-6.0	5.6	8.2
SOTN	4.1	4.6	5.5	-7.3	2.7	7.8
STEE	5.7	3.1	8.4	0.6	6.5	6.5
STOR	3.4	5.3	5.2	0.3	4.7	4.8
STRA	3.7	4.8	7.2	-3.5	6.4	7.2
SWAN	3.3	4.1	5.0	-4.9	4.5	6.7
TAUT	4.4	3.6	7.8	-7.8	2.4	8.2
TEDD	3.6	4.7	7.2	-3.5	6.6	7.3
THUS	3.0	4.9	5.4	-4.3	4.7	6.4

Table E-11 The differences between the estimated station coordinates and tropospheric ZTD from GPS GDD and PPP GLO using EMX precise products for 85 OSGB stations over seven weeks

Station	Station coordinates variation (RMS) (mm)			Tropospheric ZTD (mm)		
	E	N	U	Mean	STD	RMS
TIRE	3.7	4.8	7.4	-3.5	6.4	7.3
WARS	3.7	4.8	7.4	-3.4	6.5	7.3
WEAR	3.7	4.2	12.4	-4.8	4.4	6.5
WEIW	4.4	4.4	6.0	-8.9	5.0	10.2
WELL	3.6	4.2	8.8	2.4	5.8	6.3
WEYB	4.5	5.2	8.9	-4.6	4.2	6.2
YEAS	3.2	5.0	7.2	-0.9	7.4	7.4

Table E-12 The differences between the estimated station coordinates and tropospheric ZTD from GPS GDD and PPP GLO using EMX precise products for 85 OSGB stations over seven weeks

Station	Station coordinates variation (RMS) (mm)			Tropospheric ZTD (mm)		
	E	N	U	Mean	STD	RMS
ABEP	3.0	2.6	4.7	-4.3	5.7	7.1
ALDB	3.3	3.4	8.8	-5.8	6.9	9.0
AMER	2.4	5.5	7.6	3.6	6.1	7.1
ANLX	2.6	2.0	7.8	0.9	5.9	6.0
APPL	3.7	3.7	7.9	-3.4	7.0	7.8
ARDL	3.4	3.2	6.6	-4.7	5.3	7.1
ASAP	4.1	3.1	5.9	1.1	5.8	5.9
ATTL	3.8	2.1	11.6	-7.6	3.7	8.5
BARR	2.8	5.1	9.9	-0.9	6.2	6.3
BEES	2.9	2.9	4.8	-4.9	2.6	5.5
BENB	3.1	4.7	8.6	-6.5	4.6	8.0
BLAP	3.1	3.7	6.0	-6.6	2.2	6.9
BRAE	3.3	4.7	5.1	-7.5	2.9	8.0
BREC	2.9	2.8	8.7	-8.0	2.5	8.4
BUCK	3.8	5.9	5.7	-7.1	15.9	17.4
CAML	3.5	4.2	6.5	-10.0	2.8	10.4
CARI	3.4	3.7	7.9	-2.6	8.1	8.5
CARL	3.1	3.7	5.6	-9.1	5.8	10.8
CLAW	2.2	4.5	7.3	-7.0	5.7	9.0
DARE	2.9	3.1	6.6	5.3	9.4	10.8
DRUM	3.0	4.4	5.6	-6.4	5.9	8.7
DUDE	4.1	3.4	5.9	-5.0	7.4	8.9
DUNG	4.5	5.4	5.9	-8.5	2.6	8.9
EASN	2.1	3.2	8.9	-0.9	8.0	8.0
ESKD	3.2	2.8	5.5	-8.6	8.9	12.4
EXMO	3.2	4.6	7.5	-5.7	7.1	9.1
FARB	2.6	4.5	12.3	-5.6	5.8	8.1
FAUG	3.1	5.3	6.3	3.0	5.9	6.6
GIGG	2.8	4.6	5.6	-6.4	5.8	8.6
GIRA	3.9	3.4	5.4	-2.7	5.1	5.8
GLAS	4.1	6.1	5.6	-1.7	7.7	7.9
GORS	3.0	3.8	7.7	-3.4	8.7	9.3
HARD	3.0	2.8	6.3	1.8	5.7	6.0
HELS	2.8	3.7	5.7	2.9	6.0	6.7
HOLY	3.0	3.0	8.1	-7.9	2.1	8.2
HOOB	2.4	3.4	5.3	-6.2	2.3	6.6
HUNG	3.3	3.9	7.1	-6.0	4.4	7.4
INVR	4.5	3.6	7.0	4.0	8.3	9.2
KELO	3.9	2.4	10.4	-8.5	3.0	9.0

Table E-13 The differences between the estimated station coordinates and tropospheric ZTD from GPS GDD and PPP GLO using ESA precise products for 85 OSGB stations over seven weeks

Station	Station coordinates variation (RMS) (mm)			Tropospheric ZTD (mm)		
	E	N	U	Mean	STD	RMS
KEYW	2.6	3.2	5.3	-10.1	3.7	10.7
KILN	3.2	3.9	7.1	-4.7	7.1	8.6
KING	3.3	1.9	5.6	-8.6	2.6	9.0
KINL	4.6	4.3	7.3	-7.2	2.7	7.7
KIRK	3.6	7.0	4.9	-8.3	7.6	11.3
LCAR	3.5	4.5	6.8	-5.7	4.4	7.2
LEED	2.6	3.2	4.6	-8.5	2.8	8.9
LEEK	2.7	2.3	4.4	-5.6	3.1	6.4
LICF	2.5	3.1	6.1	-7.3	4.4	8.5
LINO	3.3	5.0	7.2	-9.5	3.1	10.0
LOFT	3.0	6.0	5.2	-6.6	2.9	7.3
MACY	3.3	3.9	6.8	-4.3	7.1	8.2
MART	3.1	2.2	8.5	-7.3	2.2	7.6
NCAS	2.9	4.1	4.6	1.6	6.6	6.8
NEWR	2.5	4.5	7.4	-7.1	2.3	7.5
OBAN	5.2	4.2	9.6	0.4	5.6	5.6
OXFR	2.8	3.3	6.9	-7.9	9.0	12.0
PADT	3.3	4.0	7.0	-4.8	7.2	8.7
PETE	2.1	3.7	7.2	4.5	8.3	9.4
PMTH	3.1	3.0	5.5	-7.1	5.6	9.1
POOL	2.6	4.3	5.6	-5.3	6.3	8.2
PRAE	2.9	3.3	5.7	0.3	6.5	6.5
RICM	3.3	3.9	6.9	-4.8	7.1	8.6
SABB	3.6	4.2	6.2	-3.9	5.8	7.0
SANO	3.3	4.1	7.5	-7.3	3.9	8.3
SCAO	3.1	3.7	7.7	0.5	6.9	6.9
SCIL	2.9	4.7	7.0	-5.8	2.5	6.3
SHOB	2.8	3.2	6.1	-5.0	5.2	7.3
SHOE	3.3	3.9	6.9	-4.8	7.1	8.5
SHRE	2.4	3.3	5.3	-7.8	4.9	9.2
SKEE	2.7	4.3	4.7	-7.4	6.3	9.7
SOTN	3.9	3.8	6.0	-8.4	3.0	8.9
STEE	5.1	2.1	9.5	-0.6	6.8	6.8
STOR	3.5	4.7	5.8	-0.3	5.4	5.4
STRA	3.2	4.0	7.0	-4.4	7.2	8.4
SWAN	2.6	3.4	4.4	-6.0	4.3	7.4
TAUT	3.9	3.0	7.2	-9.0	2.5	9.3
TEDD	3.3	3.9	7.1	-4.6	7.1	8.5
THUS	2.6	4.1	5.0	-5.8	9.7	11.3

Table E-14 The differences between the estimated station coordinates and tropospheric ZTD from GPS GDD and PPP GLO using ESA precise products for 85 OSGB stations over seven weeks

Station	Station coordinates variation (RMS) (mm)			Tropospheric ZTD (mm)		
	E	N	U	Mean	STD	RMS
TIRE	3.3	4.0	7.0	-4.6	7.1	8.4
WARS	3.3	3.9	7.0	-4.8	7.2	8.6
WEAR	3.5	3.1	13.4	-5.2	6.3	8.1
WEIW	4.4	3.8	6.4	-10.9	5.3	12.1
WELL	3.1	3.5	7.4	1.5	5.9	6.1
WEYB	4.5	3.8	7.4	-6.8	5.2	8.6
YEAS	2.3	4.1	5.4	-2.3	7.4	7.7

Table E-15 The differences between the estimated station coordinates and tropospheric ZTD from GPS GDD and PPP GLO using ESA precise products for 85 OSGB stations over seven weeks

Station	Station coordinates variation (RMS) (mm)			Tropospheric ZTD (mm)		
	E	N	U	Mean	STD	RMS
ABEP	3.4	1.9	4.0	-4.1	5.3	6.7
ALDB	3.9	2.8	7.8	-5.6	6.4	8.6
AMER	2.5	4.6	6.7	3.7	5.9	7.0
ANLX	2.9	1.9	6.1	0.5	5.7	5.7
APPL	2.9	3.1	6.7	-3.4	6.7	7.6
ARDL	4.0	2.6	7.0	-5.1	5.2	7.2
ASAP	4.2	2.4	4.5	0.9	5.7	5.8
ATTL	4.0	2.3	12.0	-7.9	3.2	8.6
BARR	2.4	3.9	9.0	-0.8	5.8	5.9
BEES	3.1	2.1	4.6	-4.8	2.6	5.5
BENB	3.0	3.6	7.6	-6.6	4.6	8.1
BLAP	2.7	2.7	5.3	-6.5	1.8	6.7
BRAE	3.1	3.5	5.1	-7.8	2.6	8.2
BREC	3.1	2.2	9.4	-8.1	2.2	8.4
BUCK	3.2	4.8	5.9	-9.0	5.1	10.3
CAML	3.6	3.4	5.6	-10.0	2.6	10.3
CARI	3.5	2.8	8.4	-2.6	8.0	8.4
CARL	3.1	2.5	5.4	-9.3	5.5	10.8
CLAW	2.4	3.8	7.3	-6.5	5.5	8.6
DARE	2.7	2.7	6.5	5.3	9.5	10.9
DRUM	2.8	3.5	4.3	-6.4	6.0	8.8
DUDE	3.5	2.6	5.4	-5.7	6.9	9.0
DUNG	4.1	4.9	4.2	-8.5	2.3	8.8
EASN	2.4	2.7	6.4	-1.0	7.9	7.9
ESKD	3.0	2.3	4.5	-7.5	2.7	8.0
EXMO	2.3	3.5	6.1	-5.9	7.0	9.2
FARB	2.8	3.5	10.2	-6.0	6.0	8.5
FAUG	2.4	4.5	5.0	2.8	5.9	6.5
GIGG	3.0	3.9	4.3	-6.2	5.6	8.4
GIRA	3.7	2.7	4.6	-2.8	5.0	5.7
GLAS	3.4	5.1	5.1	-2.0	7.9	8.1
GORS	3.3	3.3	7.6	-3.4	8.5	9.1
HARD	2.2	2.0	4.2	2.1	5.7	6.1
HELS	2.6	2.8	5.3	3.0	6.0	6.7
HOLY	3.0	2.4	6.5	-7.9	2.0	8.2
HOOB	2.4	2.6	3.6	-6.1	2.2	6.5
HUNG	3.2	3.1	6.5	-6.4	4.2	7.7
INVR	4.2	2.7	6.3	3.9	8.3	9.2
KELO	3.2	3.1	11.1	-8.3	2.7	8.8

Table E-16 The differences between the estimated station coordinates and tropospheric ZTD from GPS GDD and PPP GLO using GFZ precise products for 85 OSGB stations over seven weeks

Station	Station coordinates variation (RMS) (mm)			Tropospheric ZTD (mm)		
	E	N	U	Mean	STD	RMS
KEYW	2.6	2.6	5.5	-10.2	3.5	10.8
KILN	3.3	3.2	6.5	-4.7	6.6	8.2
KING	3.7	1.5	4.3	-9.0	2.4	9.3
KINL	3.5	3.4	4.6	-7.3	2.6	7.8
KIRK	4.3	6.2	4.1	-7.3	3.5	8.1
LCAR	3.4	3.5	6.6	-6.1	4.5	7.6
LEED	2.7	2.4	3.5	-8.6	2.7	9.0
LEEK	2.7	1.9	4.0	-5.7	3.4	6.6
LICF	2.2	2.3	5.6	-7.4	4.2	8.5
LINO	3.4	4.1	5.8	-9.6	2.7	10.0
LOFT	2.9	4.9	3.7	-7.1	2.7	7.6
MACY	3.2	3.2	6.5	-4.7	6.6	8.2
MART	2.7	2.1	6.0	-7.4	2.1	7.7
NCAS	2.9	3.1	4.2	1.5	6.6	6.8
NEWR	2.6	3.7	7.8	-7.4	2.0	7.7
OBAN	4.1	3.5	7.8	0.0	5.5	5.5
OXFR	2.7	2.4	7.6	-7.0	6.2	9.4
PADT	3.2	3.1	6.3	-4.8	6.5	8.0
PETE	2.6	3.0	5.3	4.2	8.2	9.3
PMTH	3.3	2.4	5.7	-7.2	5.5	9.1
POOL	2.4	3.3	4.3	-5.1	5.9	7.8
PRAE	3.4	2.6	4.6	0.2	6.4	6.4
RICM	3.3	3.2	6.5	-4.7	6.4	8.0
SABB	3.4	3.1	5.1	-4.1	5.8	7.1
SANO	3.7	3.5	5.8	-7.4	3.8	8.3
SCAO	3.2	2.8	5.7	0.2	6.7	6.7
SCIL	3.0	3.8	5.6	-6.0	2.4	6.5
SHOB	3.4	2.4	6.1	-5.0	5.3	7.3
SHOE	3.3	3.1	6.4	-4.8	6.5	8.1
SHRE	2.2	2.2	4.1	-7.7	4.6	8.9
SKEE	2.8	3.7	4.2	-7.2	5.7	9.2
SOTN	4.4	3.2	6.5	-8.0	2.5	8.4
STEE	6.2	2.2	10.5	-0.7	6.8	6.8
STOR	3.2	3.1	3.9	-1.2	5.4	5.5
STRA	3.3	3.1	6.5	-4.8	6.5	8.1
SWAN	2.6	2.6	4.0	-6.2	4.3	7.6
TAUT	3.3	2.4	7.8	-8.8	2.1	9.1
TEDD	3.2	3.1	6.4	-4.8	6.4	8.1
THUS	2.8	2.9	3.4	-5.1	4.7	6.9

Table E-17 The differences between the estimated station coordinates and tropospheric ZTD from GPS GDD and PPP GLO using GFZ precise products for 85 OSGB stations over seven weeks

Station	Station coordinates variation (RMS) (mm)			Tropospheric ZTD (mm)		
	E	N	U	Mean	STD	RMS
TIRE	3.3	3.2	6.5	-4.8	6.5	8.2
WARS	3.2	3.1	6.5	-4.7	6.5	8.0
WEAR	3.3	2.4	14.8	-5.8	4.4	7.3
WEIW	4.8	3.1	5.8	-11.4	5.3	12.6
WELL	3.5	2.6	5.7	1.5	5.8	6.0
WEYB	4.6	3.3	5.0	-7.1	5.1	8.8
YEAS	2.5	3.4	5.3	-1.9	7.1	7.4

Table E-18 The differences between the estimated station coordinates and tropospheric ZTD from GPS GDD and PPP GLO using GFZ precise products for 85 OSGB stations over seven weeks

Station	Station coordinates variation (RMS) (mm)			Tropospheric ZTD (mm)		
	E	N	U	Mean	STD	RMS
ABEP	3.3	3.0	4.0	-3.4	4.7	5.8
ALDB	3.4	3.7	6.2	-5.1	5.1	7.2
AMER	3.3	4.7	8.5	3.4	4.7	5.8
ANLX	3.4	3.0	5.8	0.4	4.9	4.9
APPL	3.7	3.2	6.0	-4.2	5.5	6.9
ARDL	5.1	3.9	9.8	-5.9	3.3	6.8
ASAP	3.7	3.4	6.4	1.2	4.7	4.9
ATTL	2.8	2.7	11.8	-5.9	2.2	6.3
BARR	3.2	4.6	8.1	1.6	5.5	5.7
BEES	4.0	2.9	7.9	-3.7	2.1	4.3
BENB	2.8	4.5	5.5	-5.1	4.0	6.5
BLAP	3.2	4.0	5.6	-5.4	1.6	5.6
BRAE	4.6	3.8	5.0	-6.2	1.7	6.5
BREC	3.0	2.8	8.5	-6.4	1.9	6.7
BUCK	3.1	5.5	5.8	-6.4	3.2	7.2
CAML	4.8	3.8	7.9	-7.4	1.8	7.6
CARI	3.9	3.2	8.5	-2.6	7.8	8.3
CARL	3.1	3.8	7.2	-7.5	4.4	8.7
CLAW	7.9	5.1	8.5	-4.8	6.2	7.9
DARE	3.3	3.4	7.2	3.5	7.2	8.0
DRUM	2.7	4.5	4.8	-4.0	6.0	7.2
DUDE	2.7	3.3	6.0	-4.0	6.5	7.6
DUNG	8.7	6.5	6.1	-6.5	2.1	6.8
EASN	2.8	3.3	4.5	-0.9	6.8	6.9
ESKD	2.9	3.1	5.7	-7.1	2.0	7.4
EXMO	3.9	4.0	4.5	-3.2	7.3	8.0
FARB	3.8	5.4	7.5	-4.6	4.9	6.7
FAUG	3.5	5.1	5.5	3.1	4.4	5.4
GIGG	3.4	4.5	7.1	-5.0	4.9	7.0
GIRA	4.4	3.9	5.4	-2.1	3.6	4.1
GLAS	3.6	4.5	5.7	-2.5	5.6	6.2
GORS	4.2	4.0	7.2	-3.8	6.3	7.4
HARD	6.3	3.2	8.9	1.9	5.4	5.8
HELS	2.9	3.5	5.8	2.1	4.8	5.2
HOLY	4.0	3.3	4.4	-5.9	1.7	6.2
HOOB	2.9	3.5	5.4	-5.6	1.9	6.0
HUNG	3.9	3.8	10.5	-5.9	3.5	6.9
INVR	3.9	3.9	7.1	5.5	4.8	7.3
KELO	4.6	2.7	11.9	-6.1	1.7	6.4

Table E-19 The differences between the estimated station coordinates and tropospheric ZTD from GPS GDD and PPP GPS+GLO using EMX precise products for 85 OSGB stations over seven weeks

Station	Station coordinates variation (RMS) (mm)			Tropospheric ZTD (mm)		
	E	N	U	Mean	STD	RMS
KEYW	2.9	3.0	7.0	-8.8	3.3	9.4
KILN	3.8	3.9	7.0	-4.2	5.4	6.6
KING	3.3	2.7	6.4	-8.1	2.0	8.3
KINL	4.2	3.6	6.7	-6.9	2.3	7.3
KIRK	3.9	6.3	6.1	-6.3	1.9	6.6
LCAR	3.2	4.1	6.0	-5.5	4.2	6.9
LEED	3.9	3.5	5.6	-6.6	1.9	6.9
LEEK	5.0	3.0	5.4	-3.9	3.6	5.3
LICF	3.2	3.3	7.9	-6.3	2.3	6.7
LINO	2.9	4.6	5.4	-8.0	2.1	8.3
LOFT	3.1	5.3	5.6	-6.3	2.0	6.6
MACY	4.0	3.9	7.0	-4.0	5.4	6.6
MART	4.0	2.6	7.5	-5.9	1.5	6.1
NCAS	3.1	3.7	5.0	2.1	4.9	5.3
NEWR	3.1	4.1	10.8	-6.0	1.3	6.2
OBAN	4.3	4.9	6.1	1.2	4.5	4.6
OXFR	3.8	3.3	9.9	-5.4	4.6	7.1
PADT	3.9	4.0	7.1	-3.9	5.5	6.8
PETE	7.2	4.5	6.6	4.1	6.2	7.4
PMTH	5.0	3.7	8.2	-5.5	4.4	7.0
POOL	3.1	4.0	5.7	-3.6	5.3	6.4
PRAE	2.8	3.3	5.6	0.1	6.1	6.1
RICM	3.9	4.0	7.0	-3.7	5.5	6.6
SABB	4.0	4.4	7.2	-3.6	5.0	6.2
SANO	3.8	5.6	7.4	-5.4	3.9	6.7
SCAO	2.9	3.7	5.2	-0.1	5.5	5.5
SCIL	7.2	6.4	5.6	-5.0	1.9	5.3
SHOB	3.2	3.4	7.5	-4.4	4.9	6.6
SHOE	3.9	3.9	7.1	-3.9	5.3	6.8
SHRE	3.1	3.0	4.9	-7.0	2.4	7.4
SKEE	4.0	3.5	6.6	-6.4	4.3	7.7
SOTN	4.3	3.7	7.9	-8.0	2.2	8.2
STEE	4.5	2.8	8.6	-0.3	5.8	5.8
STOR	2.7	3.7	4.0	1.2	4.7	4.8
STRA	3.8	3.9	7.1	-3.8	5.4	6.6
SWAN	3.1	3.1	5.6	-4.5	4.3	6.3
TAUT	3.6	3.1	7.2	-7.8	2.1	8.1
TEDD	4.0	3.9	7.2	-3.8	5.4	6.6
THUS	4.9	4.4	6.9	-5.1	4.6	6.9

Table E-20 The differences between the estimated station coordinates and tropospheric ZTD from GPS GDD and PPP GPS+GLO using EMX precise products for 85 OSGB stations over seven weeks

Station	Station coordinates variation (RMS) (mm)			Tropospheric ZTD (mm)		
	E	N	U	Mean	STD	RMS
TIRE	4.0	4.0	6.9	-3.9	5.3	6.6
WARS	3.9	4.0	7.0	-3.8	5.5	6.7
WEAR	3.7	2.7	11.1	-4.2	3.6	5.6
WEIW	4.8	4.4	8.7	-8.3	4.2	9.3
WELL	3.1	3.9	6.1	1.8	3.8	4.2
WEYB	3.3	4.1	4.5	-6.1	3.5	7.0
YEAS	2.8	3.6	6.1	-1.5	6.0	6.2

Table E-21 The differences between the estimated station coordinates and tropospheric ZTD from GPS GDD and PPP GPS+GLO using EMX precise products for 85 OSGB stations over seven weeks

Station	Station coordinates variation (RMS) (mm)			Tropospheric ZTD (mm)		
	E	N	U	Mean	STD	RMS
ABEP	2.9	2.1	8.8	-5.7	5.1	7.7
ALDB	3.4	2.5	6.6	-7.8	6.9	10.4
AMER	2.7	4.0	12.5	2.1	5.6	6.0
ANLX	2.5	2.1	8.0	-1.2	6.1	6.3
APPL	3.0	3.1	10.3	-5.2	5.9	7.9
ARDL	3.1	2.6	12.5	-6.8	5.2	8.6
ASAP	3.0	2.2	8.7	0.7	5.2	5.3
ATTL	4.2	3.4	15.2	-8.6	2.7	9.1
BARR	2.4	3.3	4.7	0.8	6.1	6.2
BEES	3.2	2.1	10.2	-6.8	2.8	7.3
BENB	2.4	3.4	5.3	-7.7	4.1	8.7
BLAP	2.8	2.9	9.7	-8.6	2.2	8.9
BRAE	3.4	3.1	11.2	-7.9	3.4	8.6
BREC	2.7	2.3	13.6	-9.0	2.5	9.4
BUCK	2.8	5.0	11.6	-8.8	5.4	10.3
CAML	2.8	2.8	9.4	-11.3	2.2	11.5
CARI	2.8	2.6	13.4	-3.9	7.9	8.8
CARL	3.2	2.5	10.6	-9.8	5.6	11.3
CLAW	2.5	3.3	14.3	-6.6	7.1	9.7
DARE	2.5	2.7	11.8	4.1	6.8	8.0
DRUM	2.5	2.9	8.7	-6.1	6.5	8.9
DUDE	3.1	1.4	9.0	-5.1	7.7	9.2
DUNG	2.6	3.8	13.2	-8.8	2.5	9.2
EASN	1.9	2.2	6.2	-3.2	7.1	7.8
ESKD	2.6	1.8	10.5	-8.4	2.2	8.7
EXMO	3.8	3.2	8.5	-6.7	7.4	9.9
FARB	1.9	2.9	5.5	-5.8	6.5	8.7
FAUG	2.6	3.5	8.7	2.4	6.2	6.6
GIGG	2.8	3.3	10.6	-8.4	5.1	9.8
GIRA	3.3	2.7	8.4	-3.2	5.1	6.0
GLAS	3.4	3.2	10.5	-3.1	7.9	8.5
GORS	2.8	2.9	6.6	-4.4	8.4	9.5
HARD	3.6	2.7	11.7	1.1	5.0	5.1
HELS	2.5	2.9	10.8	1.7	6.1	6.3
HOLY	2.6	2.3	5.5	-9.0	2.5	9.3
HOOB	2.2	2.3	10.0	-8.3	2.4	8.6
HUNG	4.6	4.8	20.0	-7.6	5.1	9.1
INVR	3.6	2.8	12.5	0.2	6.3	6.3
KELO	3.4	2.4	18.9	-10.2	2.8	10.5

Table E-22 The differences between the estimated station coordinates and tropospheric ZTD from GPS GDD and PPP GPS+GLO using ESA precise products for 85 OSGB stations over seven weeks

Station	Station coordinates variation (RMS) (mm)			Tropospheric ZTD (mm)		
	E	N	U	Mean	STD	RMS
KEYW	2.4	2.4	11.2	-11.2	3.4	11.7
KILN	2.8	3.0	11.0	-5.8	6.6	8.7
KING	3.1	1.9	8.3	-9.8	2.5	10.1
KINL	2.7	2.8	11.5	-8.4	2.5	8.8
KIRK	2.7	4.6	9.9	-9.1	2.1	9.3
LCAR	3.0	3.3	13.1	-7.2	4.7	8.6
LEED	3.3	2.5	12.2	-9.3	3.4	9.9
LEEK	2.8	1.9	10.0	-5.7	5.7	8.1
LICF	2.2	2.5	11.7	-7.4	6.1	9.6
LINO	2.4	3.7	9.0	-8.5	5.3	10.0
LOFT	2.5	4.3	8.4	-8.8	3.6	9.5
MACY	2.9	2.9	11.2	-5.6	6.5	8.6
MART	2.4	2.0	11.0	-8.4	2.2	8.6
NCAS	2.5	3.1	9.7	-0.1	6.1	6.1
NEWR	2.3	3.2	14.0	-8.2	2.1	8.5
OBAN	3.4	3.6	10.6	-0.6	5.1	5.2
OXFR	4.0	4.4	13.6	-7.7	4.4	8.8
PADT	2.9	2.9	10.9	-5.8	6.5	8.5
PETE	2.1	2.8	7.9	4.3	6.6	7.9
PMTH	2.9	2.7	10.7	-8.1	5.6	9.8
POOL	2.2	3.0	9.8	-5.3	6.6	8.5
PRAE	3.3	3.7	13.4	-0.2	7.4	7.4
RICM	3.0	3.0	11.1	-5.7	6.5	8.9
SABB	2.4	2.6	7.0	-3.6	6.8	7.7
SANO	5.0	3.3	9.4	-7.0	4.5	8.3
SCAO	2.3	2.5	7.8	0.0	6.6	6.6
SCIL	2.6	3.3	8.1	-7.3	3.2	7.9
SHOB	2.3	2.2	11.6	-6.7	5.2	8.5
SHOE	2.9	3.0	11.2	-5.7	6.5	8.8
SHRE	2.3	2.1	9.4	-8.7	4.8	10.0
SKEE	2.3	2.4	10.9	-7.9	6.0	9.9
SOTN	3.8	3.2	12.0	-8.9	4.9	10.2
STEE	4.8	2.1	14.5	-1.2	6.3	6.4
STOR	2.3	2.9	8.4	-0.7	5.3	5.3
STRA	2.9	3.0	10.9	-5.8	6.5	8.8
SWAN	2.8	2.9	10.8	-7.4	4.3	8.5
TAUT	2.9	2.3	12.0	-10.7	2.5	11.0
TEDD	2.9	2.9	11.0	-5.7	6.7	8.7
THUS	2.4	2.8	8.0	-7.4	4.7	8.8

Table E-23 The differences between the estimated station coordinates and tropospheric ZTD from GPS GDD and PPP GPS+GLO using ESA precise products for 85 OSGB stations over seven weeks

Station	Station coordinates variation (RMS) (mm)			Tropospheric ZTD (mm)		
	E	N	U	Mean	STD	RMS
TIRE	2.9	3.0	11.0	-5.8	6.6	8.6
WARS	2.9	3.0	11.2	-5.7	6.4	8.8
WEAR	3.3	2.5	22.2	-6.9	4.6	8.3
WEIW	3.5	2.8	13.6	-12.5	6.0	13.9
WELL	2.5	2.5	7.7	-1.1	5.8	5.9
WEYB	2.7	3.0	6.5	-8.0	5.1	9.5
YEAS	2.5	2.9	9.2	-3.7	7.5	8.3

Table E-24 The differences between the estimated station coordinates and tropospheric ZTD from GPS GDD and PPP GPS+GLO using ESA precise products for 85 OSGB stations over seven weeks

Station	Station coordinates variation (RMS) (mm)			Tropospheric ZTD (mm)		
	E	N	U	Mean	STD	RMS
ABEP	3.3	1.8	9.6	-6.0	5.0	7.8
ALDB	4.1	2.3	7.0	-8.2	6.5	10.5
AMER	2.4	3.8	12.9	1.7	6.0	6.2
ANLX	2.6	2.0	8.0	-1.9	5.5	5.8
APPL	2.6	2.7	11.1	-5.5	6.9	8.8
ARDL	4.1	3.5	14.6	-7.9	5.0	9.3
ASAP	3.5	2.1	9.1	-0.3	5.8	5.8
ATTL	3.0	2.2	15.5	-8.8	2.4	9.1
BARR	2.4	3.0	4.7	-0.5	5.7	5.7
BEES	2.7	1.9	10.8	-7.1	2.9	7.6
BENB	2.6	3.0	5.5	-8.3	4.0	9.2
BLAP	2.9	2.4	10.4	-8.8	2.1	9.1
BRAE	3.5	2.9	12.5	-9.1	2.5	9.4
BREC	3.1	2.0	15.2	-9.5	2.3	9.8
BUCK	2.7	4.6	12.2	-9.4	5.4	10.9
CAML	3.0	2.3	9.7	-11.4	2.2	11.6
CARI	3.2	2.6	15.0	-4.3	8.1	9.2
CARL	3.1	2.1	11.7	-10.7	5.2	11.9
CLAW	3.0	3.0	14.7	-7.7	5.4	9.4
DARE	2.5	2.4	12.4	3.2	7.9	8.5
DRUM	3.4	3.1	9.3	-6.7	6.8	9.6
DUDE	3.3	1.7	10.6	-5.4	8.2	9.8
DUNG	2.8	4.0	10.6	-9.2	2.5	9.5
EASN	2.1	2.3	6.9	-3.2	7.2	7.8
ESKD	2.9	2.0	11.9	-9.0	2.1	9.3
EXMO	3.2	3.0	10.0	-7.3	7.2	10.3
FARB	2.2	2.9	7.8	-7.0	6.6	9.7
FAUG	2.7	3.6	9.8	1.8	6.2	6.4
GIGG	2.8	3.2	10.9	-8.7	5.1	10.1
GIRA	3.4	2.4	9.3	-4.1	4.8	6.3
GLAS	3.1	3.1	11.1	-3.6	8.0	8.8
GORS	3.4	2.7	6.9	-4.8	8.4	9.7
HARD	2.2	2.0	9.8	0.1	5.4	5.4
HELS	2.4	2.6	11.8	1.3	5.8	5.9
HOLY	2.7	2.1	6.2	-9.6	2.3	9.9
HOOB	2.3	2.2	10.7	-9.0	2.4	9.3
HUNG	3.5	3.7	18.9	-8.0	5.0	9.4
INVR	3.6	2.4	13.1	1.3	7.3	7.4
KELO	3.2	2.9	20.8	-10.3	2.3	10.6

Table E-25 The differences between the estimated station coordinates and tropospheric ZTD from GPS GDD and PPP GPS+GLO using GFZ precise products for 85 OSGB stations over seven weeks

Station	Station coordinates variation (RMS) (mm)			Tropospheric ZTD (mm)		
	E	N	U	Mean	STD	RMS
KEYW	2.6	2.2	12.5	-12.1	3.3	12.5
KILN	3.0	2.7	11.8	-6.3	6.5	9.2
KING	3.6	1.8	9.1	-10.5	2.4	10.7
KINL	2.4	2.7	12.4	-8.9	2.4	9.2
KIRK	2.9	4.4	11.1	-9.6	2.1	9.8
LCAR	2.8	2.7	14.0	-7.6	4.7	8.9
LEED	2.7	1.9	9.4	-9.7	3.1	10.2
LEEK	3.3	1.8	10.6	-6.3	4.5	7.7
LICF	2.1	2.0	12.6	-8.6	4.1	9.5
LINO	2.7	3.4	9.5	-9.9	3.2	10.4
LOFT	2.6	4.0	9.2	-10.0	2.6	10.4
MACY	3.0	2.7	11.8	-6.1	6.5	9.0
MART	2.8	1.9	11.5	-8.7	2.4	9.0
NCAS	2.9	2.8	11.1	-0.9	6.4	6.4
NEWR	2.5	2.9	15.6	-8.6	2.2	8.9
OBAN	3.2	3.5	11.1	-1.6	5.2	5.5
OXFR	2.3	2.2	13.8	-8.6	6.3	10.7
PADT	2.9	2.7	11.7	-6.4	6.4	9.1
PETE	2.5	2.4	8.4	3.2	7.3	7.9
PMTH	3.1	2.2	12.2	-8.7	5.3	10.2
POOL	2.1	2.9	9.9	-5.9	6.3	8.6
PRAE	3.2	2.2	10.2	-1.4	6.7	6.9
RICM	3.0	2.7	11.7	-6.4	6.4	9.1
SABB	2.4	2.3	6.8	-4.9	6.1	7.8
SANO	3.2	2.9	7.5	-7.9	3.8	8.8
SCAO	2.8	2.3	8.5	-1.1	6.2	6.3
SCIL	2.9	3.0	8.1	-8.1	2.4	8.5
SHOB	3.3	2.0	12.3	-7.0	5.1	8.7
SHOE	3.0	2.7	11.6	-6.5	6.5	9.1
SHRE	2.2	1.9	11.0	-9.1	4.8	10.3
SKEE	2.6	2.3	12.0	-8.6	6.0	10.4
SOTN	4.5	3.0	12.6	-10.5	2.8	10.9
STEE	5.7	2.1	15.9	-1.6	6.3	6.5
STOR	2.9	2.4	9.5	-1.3	5.3	5.4
STRA	3.0	2.7	11.7	-6.5	6.5	9.2
SWAN	2.6	2.6	11.4	-7.8	4.2	8.9
TAUT	2.9	2.0	13.1	-10.8	2.3	11.1
TEDD	3.0	2.7	11.7	-6.3	6.5	9.3
THUS	2.7	2.4	8.2	-7.9	4.6	9.2

Table E-26 The differences between the estimated station coordinates and tropospheric ZTD from GPS GDD and PPP GPS+GLO using GFZ precise products for 85 OSGB stations over seven weeks

Station	Station coordinates variation (RMS) (mm)			Tropospheric ZTD (mm)		
	E	N	U	Mean	STD	RMS
TIRE	3.0	2.6	11.8	-6.4	6.5	9.2
WARS	3.0	2.7	11.7	-6.4	6.5	9.1
WEAR	3.0	2.3	24.2	-7.2	4.4	8.5
WEIW	4.0	2.6	14.3	-14.0	5.4	15.1
WELL	3.3	2.4	8.2	-1.2	5.7	5.9
WEYB	3.6	3.0	7.2	-8.9	5.1	10.3
YEAS	2.5	2.7	9.5	-3.8	7.4	8.3

Table E-27 The differences between the estimated station coordinates and tropospheric ZTD from GPS GDD and PPP GPS+GLO using GFZ precise products for 85 OSGB stations over seven weeks

The differences between the estimated station coordinates and tropospheric ZTD from GPS GDD and PPP GPS+GLO using EMX precise products for 85 OSGB stations over seven weeks

Station	Station coordinates variation (RMS) (mm)			Tropospheric ZTD (mm)		
	E	N	U	Mean	STD	RMS
ALBH	19.9	17.1	27.0	0.6	3.7	3.8
ALGO	14.5	13.2	20.4	1.1	5.8	5.9
ALIC	15.2	6.2	16.5	11.5	6.4	13.1
AUCK	15.0	7.8	19.4	2.0	3.9	4.4
BAKE	10.2	14.8	29.9	-2.4	7.1	7.4
BAKO	25.8	7.4	31.2	-3.9	5.1	6.5
BARH	18.7	12.9	13.2	1.2	8.1	8.2
BREW	28.3	16.3	23.0	-3.9	9.6	10.4
BRFT	26.1	19.7	22.2	1.6	4.8	5.1
BRMU	20.9	13.9	28.9	-0.7	4.4	4.5
BZRG	9.8	8.0	28.7	2.5	4.6	5.2
CAGS	18.2	13.3	29.4	1.7	5.7	5.9
CHUM	31.9	15.1	48.9	-3.2	10.1	10.6
CIT1	13.8	8.6	18.0	-4.8	6.8	8.3
CONZ	21.0	8.9	21.8	-6.3	12.5	14.0
CUSV	33.6	15.0	26.7	-6.4	3.9	7.5
DAV1	12.2	19.6	25.5	7.3	6.2	9.6
DRAO	11.6	9.7	31.1	-0.6	5.1	5.2
DUBO	16.5	12.3	22.4	-5.3	4.4	6.9
FFMJ	14.1	9.6	28.5	3.9	6.4	7.5
GANP	11.4	9.7	36.1	2.4	4.3	4.9
GLSV	16.3	11.4	30.2	2.5	6.0	6.5
GODE	30.1	27.7	33.9	2.2	5.7	6.1
GODZ	20.2	12.2	23.3	11.8	5.5	13.0
GOL2	21.9	12.7	30.4	8.8	7.3	11.5
GOLD	13.0	8.1	30.5	-3.4	7.0	7.8
GRAZ	25.5	19.2	33.3	-5.4	8.9	10.5
GUUG	20.2	10.5	24.5	-4.7	3.4	5.8
HERS	21.7	19.1	24.8	-4.2	4.9	6.4
HNPT	16.2	13.1	12.1	-5.7	4.0	6.9
HOFN	18.4	16.6	17.4	1.2	5.8	6.0
IENG	25.9	18.2	40.8	6.8	6.9	9.7
IISC	23.1	10.6	33.1	-0.4	5.1	5.1
INVK	15.8	18.7	22.7	4.8	8.1	9.5
ISBA	21.4	7.9	24.0	-4.9	8.6	10.0
ISPA	30.6	17.2	30.1	4.2	4.8	6.4
KHAR	15.7	27.1	28.8	-1.3	5.3	5.5
KIRU	9.4	14.2	26.1	5.8	9.8	11.4
KIT3	12.8	5.3	31.9	-4.5	7.8	9.0

Table E-28 The differences between the estimated station coordinates and tropospheric ZTD from IGS and PPP GPS (using real-time precise products) for 76 IGS stations over 12 weeks

Station	Station coordinates variation (RMS) (mm)			Tropospheric ZTD (mm)		
	E	N	U	Mean	STD	RMS
KOUR	28.2	11.5	28.9	2.0	3.9	4.4
KUUJ	16.2	13.5	31.0	2.5	7.5	7.9
QAQ1	17.8	10.4	30.5	1.9	6.4	6.6
QIKI	18.9	14.4	17.6	9.1	4.7	10.3
QUIN	32.1	13.3	27.0	0.6	3.0	3.0
RESO	18.9	12.8	21.4	-5.1	4.1	6.5
REYK	21.0	35.5	17.5	4.1	4.3	5.9
RIO2	16.0	11.5	24.8	-2.4	9.1	9.4
SALU	27.3	13.6	23.2	-5.4	8.3	9.9
SAVO	21.4	21.3	21.7	2.9	4.5	5.4
SCH2	26.0	14.5	31.5	3.3	4.2	5.4
SCOR	23.7	17.6	43.4	-3.4	16.0	16.4
SEY1	27.3	10.6	35.9	7.4	5.5	9.2
SNI1	13.3	9.0	23.9	8.9	6.0	10.7
SPK1	13.3	8.5	32.4	16.0	9.1	18.4
SUTH	31.4	17.6	26.0	13.4	5.1	14.3
SUTM	16.6	16.8	15.2	10.2	10.6	14.7
TABL	14.6	10.0	24.5	0.0	4.7	4.7
TASH	13.1	6.3	17.3	-4.6	9.3	10.4
TITZ	20.3	26.2	29.4	-2.7	7.1	7.6
TNML	33.4	21.2	34.7	-2.6	3.4	4.3
TOW2	15.0	37.3	23.9	1.3	5.3	5.4
TSKB	17.4	8.0	23.5	-1.0	7.3	7.4
TWTF	35.6	25.0	26.1	-0.5	6.8	6.8
UFPR	23.6	7.5	19.8	-2.1	4.7	5.2
UNBJ	18.4	11.1	19.8	-2.4	7.0	7.4
VALD	16.3	13.7	31.2	2.9	5.3	6.0
VILL	20.0	13.0	43.9	2.3	3.4	4.1
WAB2	20.0	12.8	42.8	3.5	4.8	5.9
WGTN	14.0	12.0	21.8	-2.5	6.8	7.2
WTZA	18.1	26.0	47.2	-0.5	4.6	4.7
WTZR	17.9	22.5	24.6	0.3	7.7	7.7
WTZZ	12.4	12.7	26.9	-0.4	4.3	4.3
YAR3	16.6	7.3	13.6	3.1	4.4	5.3
YELL	15.3	12.7	29.1	-2.1	7.7	7.9
YSSK	25.5	16.3	26.3	4.1	5.3	6.8

Table E-29 The differences between the estimated station coordinates and tropospheric ZTD from IGS and PPP GPS (using real-time precise products) for 76 IGS stations over 12 weeks

Appendix-F- Horizontal Station rate estimates (mm/yr) for 22 OSGB stations in the UK (table summary)

Name	E PPP GPS	N PPP GPS	E PPP GLO	N PPP GLO	E PPP GPS+GLO	N PPP GPS +GLO	E GDD GPS	N GDD GPS
AMER	17.3	17.9	19.3	15.6	18.3	17.2	16.5	17.5
ATTL	16.3	14.3	19.1	15.0	17.8	15.7	16.1	15.9
ALDB	8.6	18.2	11.6	18.5	10.4	19.7	8.6	19.1
BLAP	15.5	15.0	16.8	14.0	15.9	15.0	13.8	15.2
BRAE	14.5	18.8	17.2	16.8	14.8	18.0	13.7	17.2
BREC	16.6	18.4	17.0	16.6	15.5	17.5	15.2	17.5
BUCK	11.6	19.1	14.8	16.8	14.0	17.6	12.2	17.3
CLAW	16.6	18.4	18.9	15.3	18.4	17.1	16.4	18.0
GORS	16.6	17.8	19.8	16.9	17.4	18.2	16.1	18.2
APPL	19.1	15.6	20.2	14.4	19.3	15.6	16.9	15.8
HELS	8.7	16.9	13.9	14.2	12.9	16.0	12.0	15.9
HOLY	14.5	17.7	17.5	15.9	15.9	16.6	14.1	18.0
KELO	13.3	18.0	15.7	15.7	14.7	16.6	13.7	16.3
KING	15.5	17.3	19.4	15.7	17.8	16.7	16.0	16.9
ARDL	17.4	17.4	19.8	15.5	18.9	17.2	16.1	17.4
BARR	13.4	17.6	16.0	15.8	14.5	16.8	13.4	16.4
BENB	13.2	17.7	14.6	16.0	13.8	16.9	12.0	16.9
CARI	13.6	18.7	16.3	16.6	15.5	17.5	13.1	17.4
GLAS	14.0	18.2	15.9	15.9	14.6	18.2	13.2	18.7
LEED	15.3	16.9	18.7	15.6	17.3	16.3	15.2	16.6
ESKD	15.2	16.8	18.8	15.7	17.6	16.7	15.0	16.0
KINL	12.9	16.5	15.8	14.2	14.2	16.0	13.2	15.7

Table F-1 Horizontal station rate estimates (mm/yr) for 22 OSGB stations in the UK using PPP with EMX precise products

Name	E PPP GPS	N PPP GPS	E PPP GLO	N PPP GLO	E PPP GPS+GLO	N PPP GPS +GLO	E GDD GPS	N GDD GPS
AMER	15.8	17.7	18.1	15.4	17.1	16.8	16.5	17.5
ATTL	15.6	14.2	17.4	14.9	15.8	15.3	16.1	15.9
ALDB	8.0	18.1	10.2	18.5	9.5	19.2	8.6	19.1
BLAP	14.4	14.9	15.8	13.6	14.6	14.8	13.8	15.2
BRAE	12.8	18.1	15.7	16.6	13.5	17.6	13.7	17.2
BREC	14.9	18.4	16.5	16.0	14.7	16.7	15.2	17.5
BUCK	11.0	17.9	13.3	16.8	12.6	17.5	12.2	17.3
CLAW	15.3	18.2	17.2	15.1	17.0	16.8	16.4	18.0
GORS	15.7	17.7	18.5	16.9	16.2	18.2	16.1	18.2
APPL	18.7	15.6	18.8	14.5	19.7	15.7	16.9	15.8
HELS	7.5	15.7	12.8	14.2	11.2	15.5	12.0	15.9
HOLY	12.6	17.5	16.3	15.8	14.7	16.3	14.1	18.0
KELO	12.5	17.9	15.7	15.5	14.6	16.3	13.7	16.3
KING	14.8	17.1	17.9	15.6	17.0	16.3	16.0	16.9
ARDL	16.7	17.1	18.0	15.4	17.1	16.5	16.1	17.4
BARR	11.7	16.8	14.7	15.7	13.3	16.4	13.4	16.4
BENB	11.8	16.8	13.3	15.9	12.0	16.8	12.0	16.9
CARI	12.6	18.7	15.3	16.1	13.7	17.1	13.1	17.4
GLAS	12.2	18.1	15.8	16.0	12.8	18.1	13.2	18.7
LEED	14.5	16.6	17.4	15.5	16.1	16.0	15.2	16.6
ESKD	14.1	16.4	17.0	15.7	15.6	16.5	15.0	16.0
KINL	11.9	15.8	14.2	14.5	12.7	15.9	13.2	15.7

Table F-2 Horizontal station rate estimates (mm/yr) for 22 OSGB stations in the UK using PPP with ESA precise products

Name	E PPP GPS	N PPP GPS	E PPP GLO	N PPP GLO	E PPP GPS+GLO	N PPP GPS +GLO	E GDD GPS	N GDD GPS
AMER	16.3	16.6	19.0	13.6	18.4	14.8	16.5	17.5
ATTL	15.8	13.1	18.0	12.7	17.6	13.2	16.1	15.9
ALDB	8.2	17.1	11.2	16.3	10.1	16.6	8.6	19.1
BLAP	14.4	13.9	16.7	12.0	15.7	12.6	13.8	15.2
BRAE	13.1	17.6	16.2	14.9	15.0	16.1	13.7	17.2
BREC	14.9	17.3	17.7	14.3	16.1	15.5	15.2	17.5
BUCK	11.4	17.3	14.0	14.8	13.0	16.0	12.2	17.3
CLAW	15.2	17.3	18.3	13.1	17.3	15.5	16.4	18.0
GORS	15.8	17.1	19.3	14.8	17.5	15.4	16.1	18.2
APPL	18.9	14.4	20.2	11.9	19.3	13.5	16.9	15.8
HELS	7.9	15.2	13.5	12.3	10.9	13.8	12.0	15.9
HOLY	13.2	16.5	17.0	13.9	15.1	14.8	14.1	18.0
KELO	12.4	17.2	15.7	13.7	14.1	15.0	13.7	16.3
KING	15.0	16.1	18.8	13.5	17.3	14.4	16.0	16.9
ARDL	17.1	16.1	19.1	13.3	18.1	14.6	16.1	17.4
BARR	11.6	16.2	15.3	13.9	14.1	15.1	13.4	16.4
BENB	11.5	16.2	13.9	13.9	12.8	15.1	12.0	16.9
CARI	12.7	17.6	15.8	14.3	14.5	15.7	13.1	17.4
GLAS	12.8	17.5	15.6	14.1	14.2	16.1	13.2	18.7
LEED	14.5	15.6	18.0	13.5	16.7	14.3	15.2	16.6
ESKD	14.1	15.7	18.0	13.7	16.3	14.4	15.0	16.0
KINL	11.5	15.6	14.9	12.7	13.3	14.3	13.2	15.7

Table F-3 Horizontal station rate estimates (mm/yr) for 22 OSGB stations in the UK using PPP with GFZ precise products

Appendix-G- Horizontal station rate estimates (mm/yr) for 22 OSGB stations in the UK (figures summary)

Figure G- 1 Coordinate time series and station rate estimation for the East component using EMX (left), ESA (middle) and GFZ (right) precise products for all PPP scenarios as well as GDD GPS

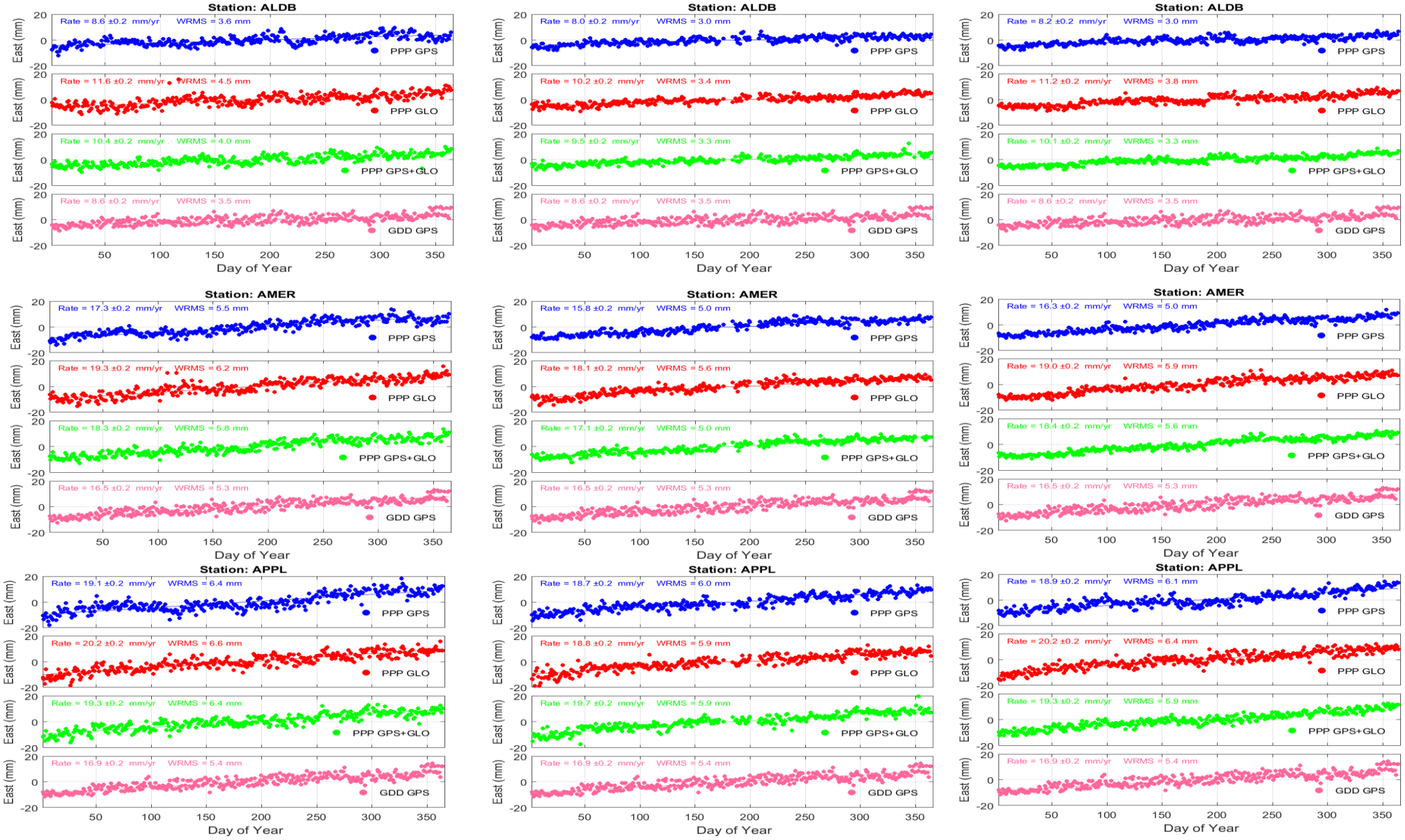


Figure G- 2 Coordinate time series and station rate estimation for the East component using EMX (left), ESA (middle) and GFZ (right) precise products for all PPP scenarios as well as GDD GPS

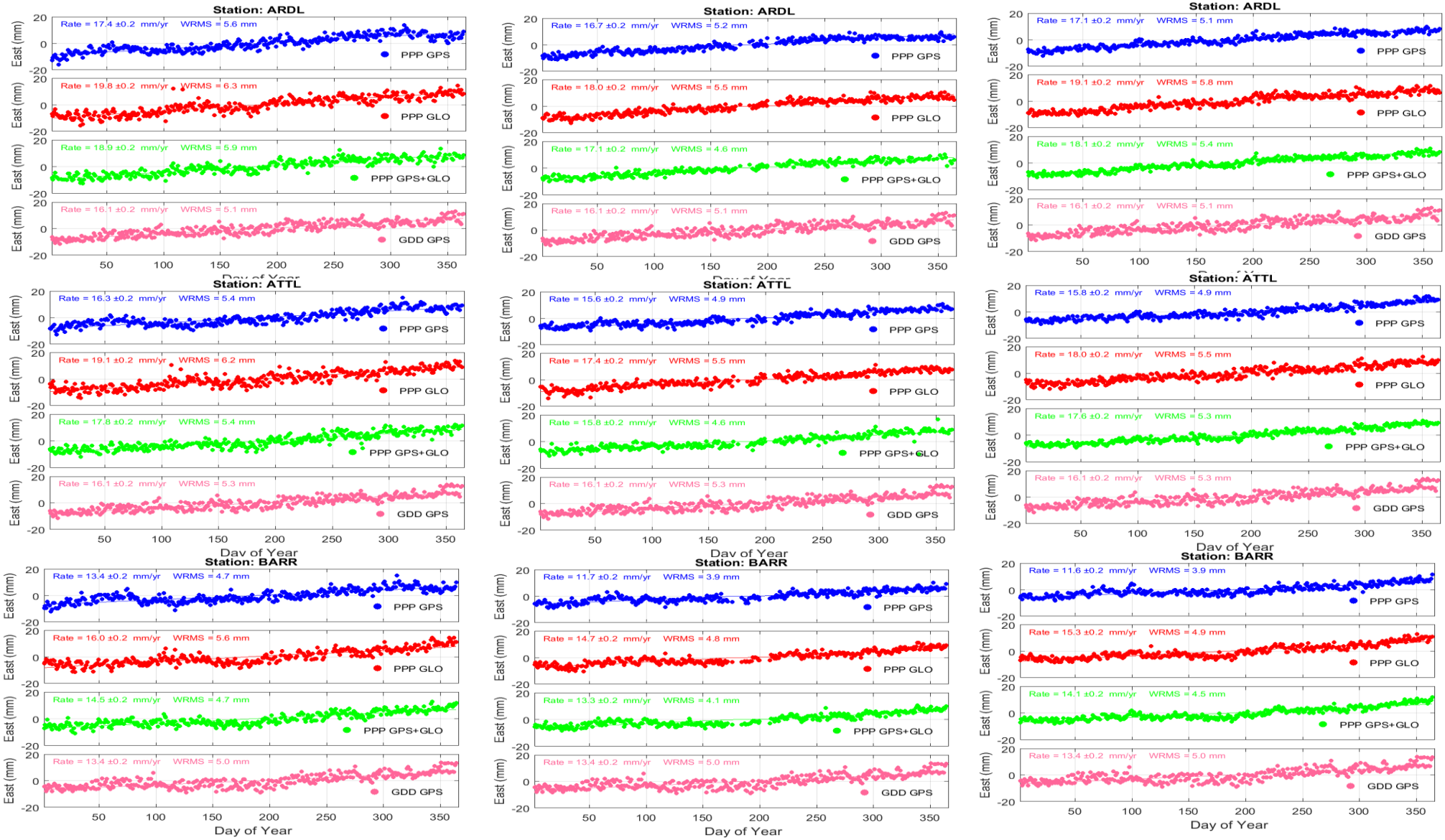


Figure G- 3 Coordinate time series and station rate estimation for the East component using EMX (left), ESA (middle) and GFZ (right) precise products for all PPP scenarios as well as GDD GPS

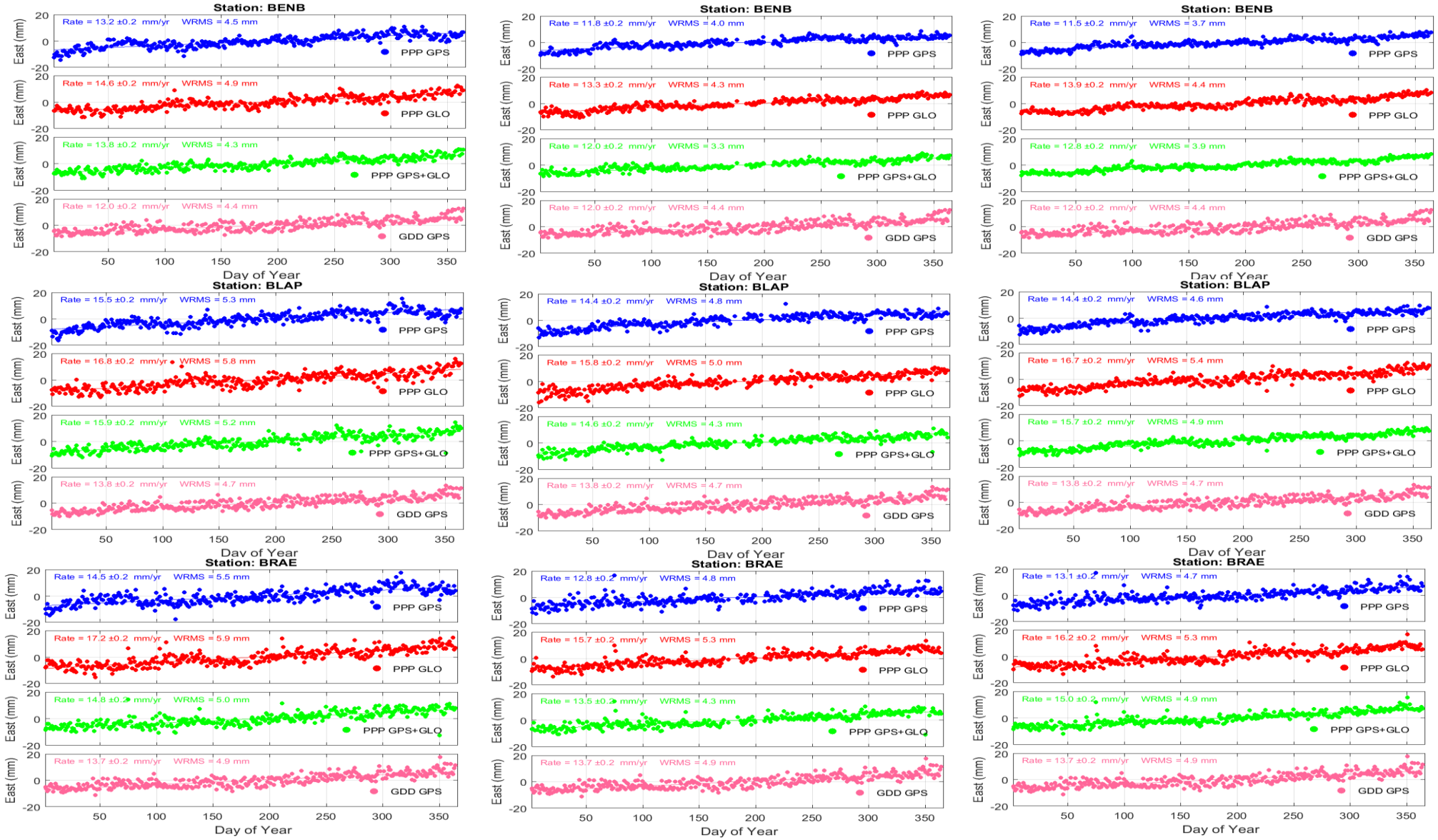


Figure G- 4 Coordinate time series and station rate estimation for the East component using EMX (left), ESA (middle) and GFZ (right) precise products for all PPP scenarios as well as GDD GPS

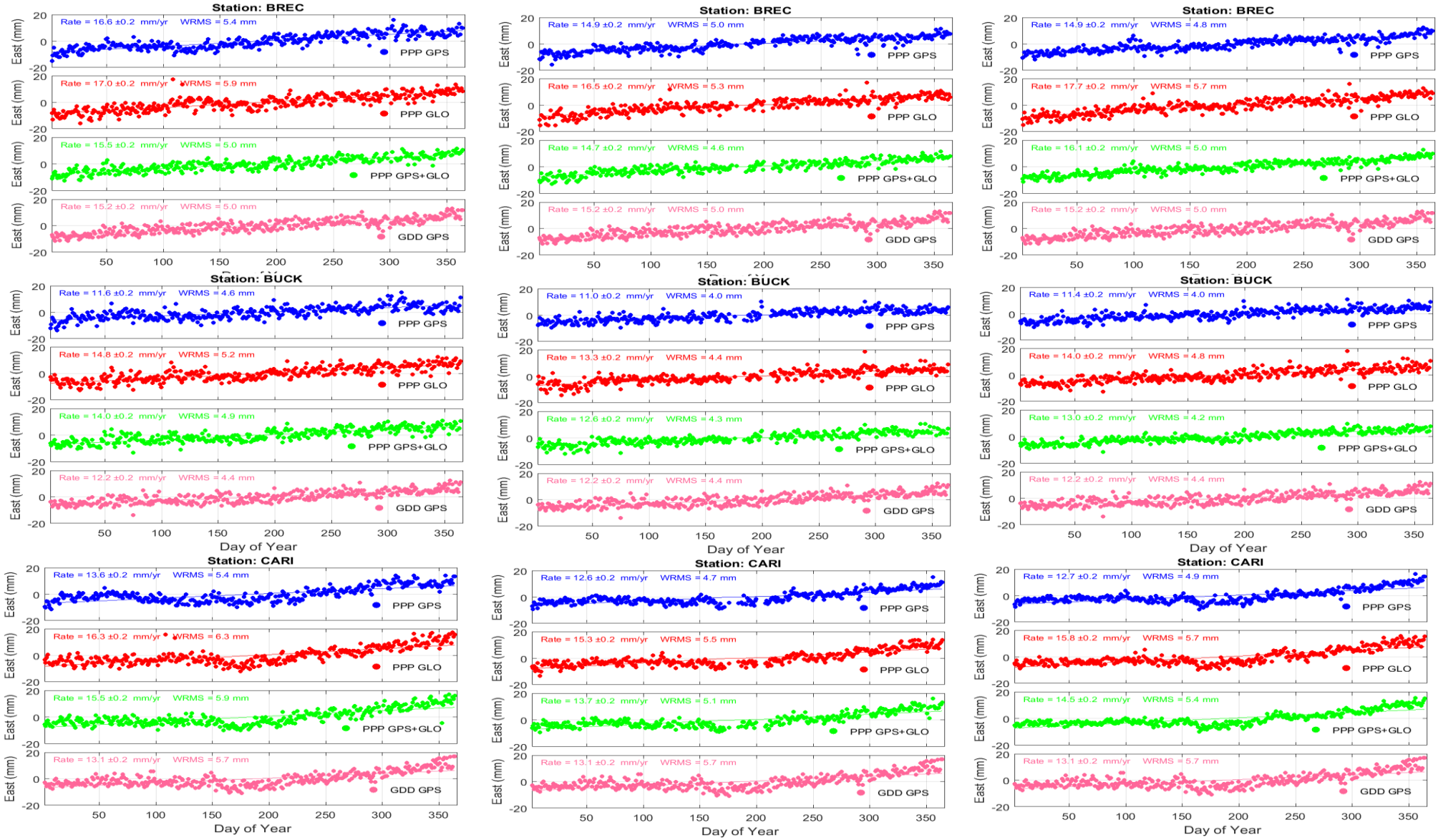


Figure G- 5 Coordinate time series and station rate estimation for the East component using EMX (left), ESA (middle) and GFZ (right) precise products for all PPP scenarios as well as GDD GPS

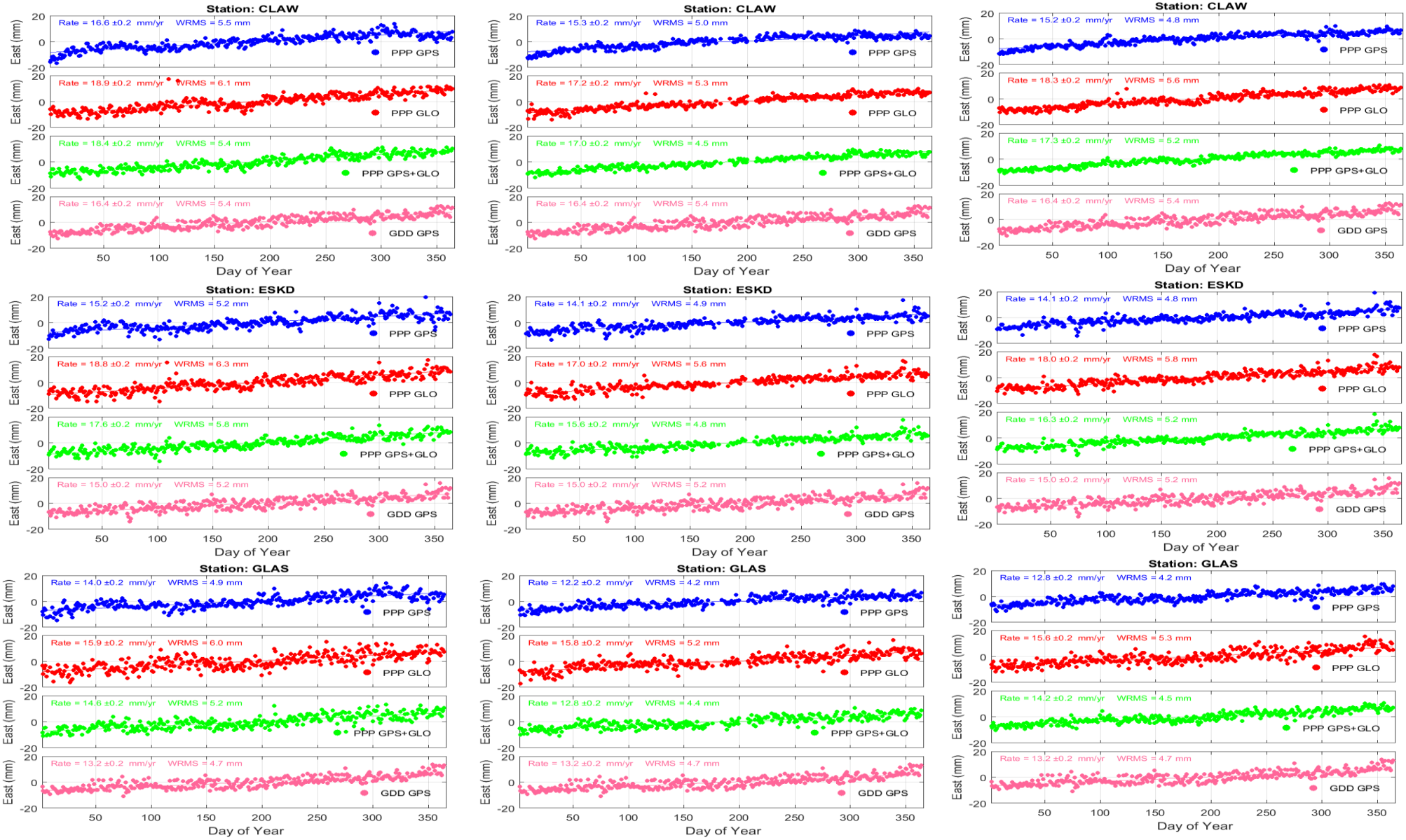


Figure G- 6 Coordinate time series and station rate estimation for the East component using EMX (left), ESA (middle) and GFZ (right) precise products for all PPP scenarios as well as GDD GPS

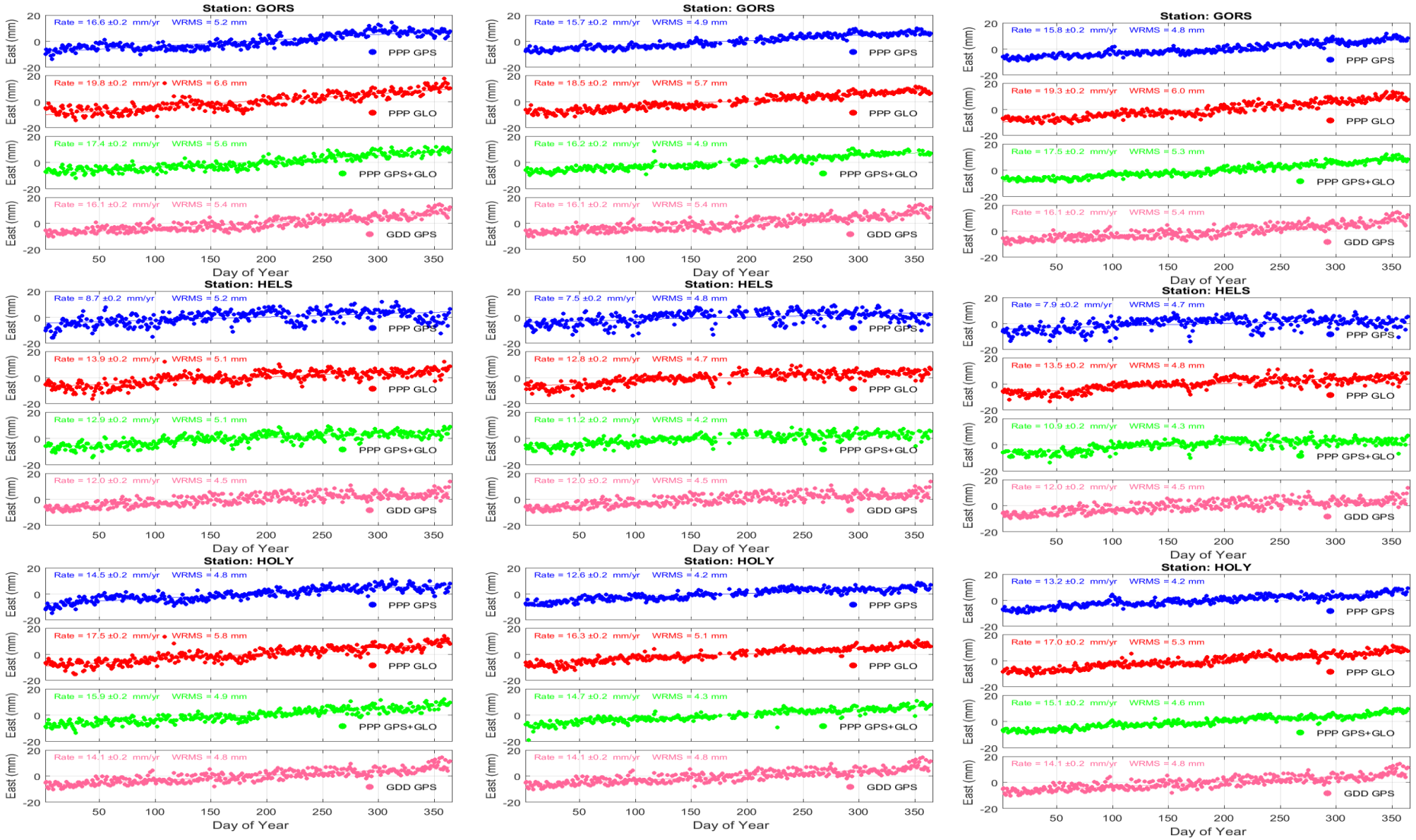


Figure G- 7 Coordinate time series and station rate estimation for the East component using EMX (left), ESA (middle) and GFZ (right) precise products for all PPP scenarios as well as GDD GPS

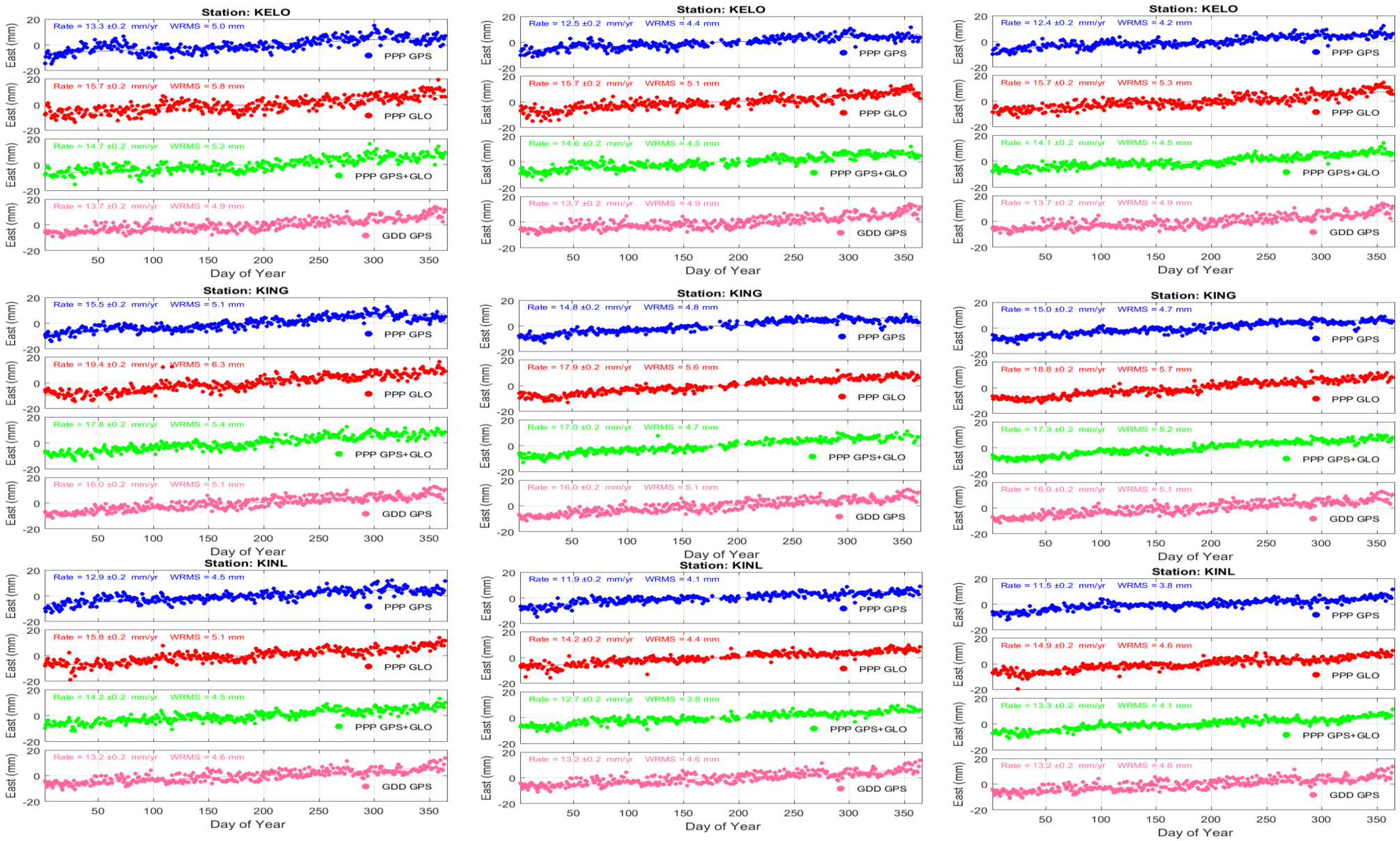


Figure G- 8 Coordinate time series and station rate estimation for the East component using EMX (left), ESA (middle) and GFZ (right) precise products for all PPP scenarios as well as GDD GPS

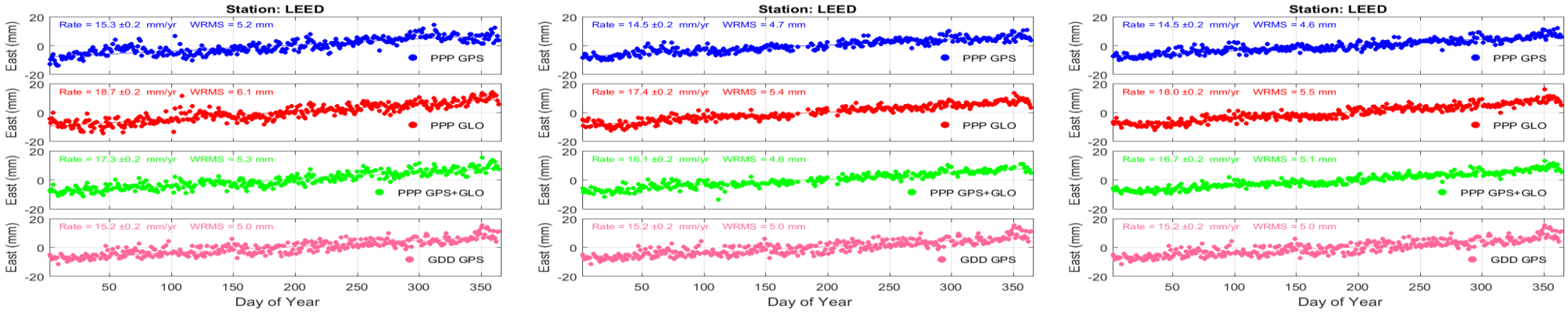


Figure G-9 Coordinate time series and station rate estimation for the North component using EMX (left), ESA (middle) and GFZ (right) precise products for all PPP scenarios as well as GDD GPS

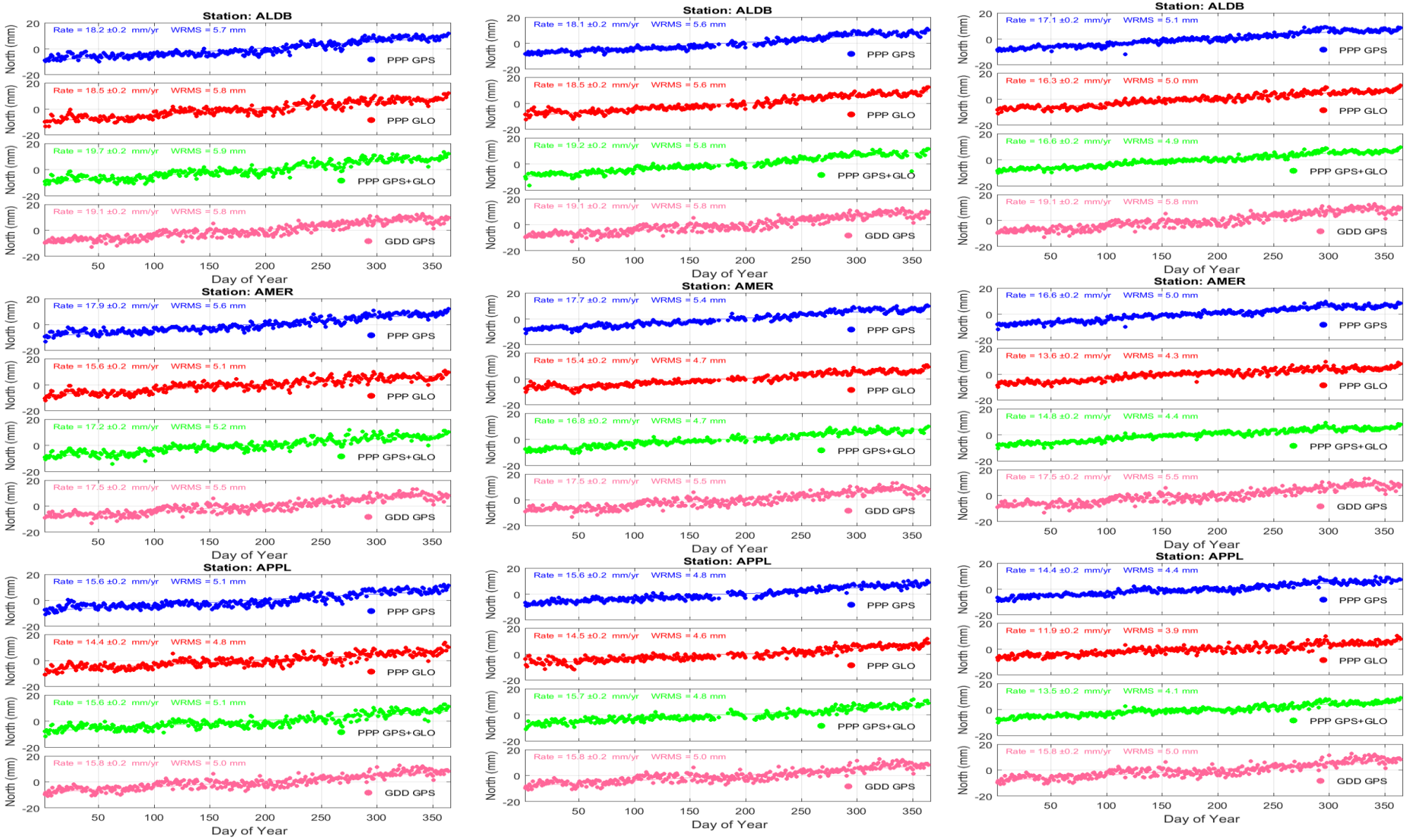


Figure G- 10 Coordinate time series and station rate estimation for the North component using EMX (left), ESA (middle) and GFZ (right) precise products for all PPP scenarios as well as GDD GPS

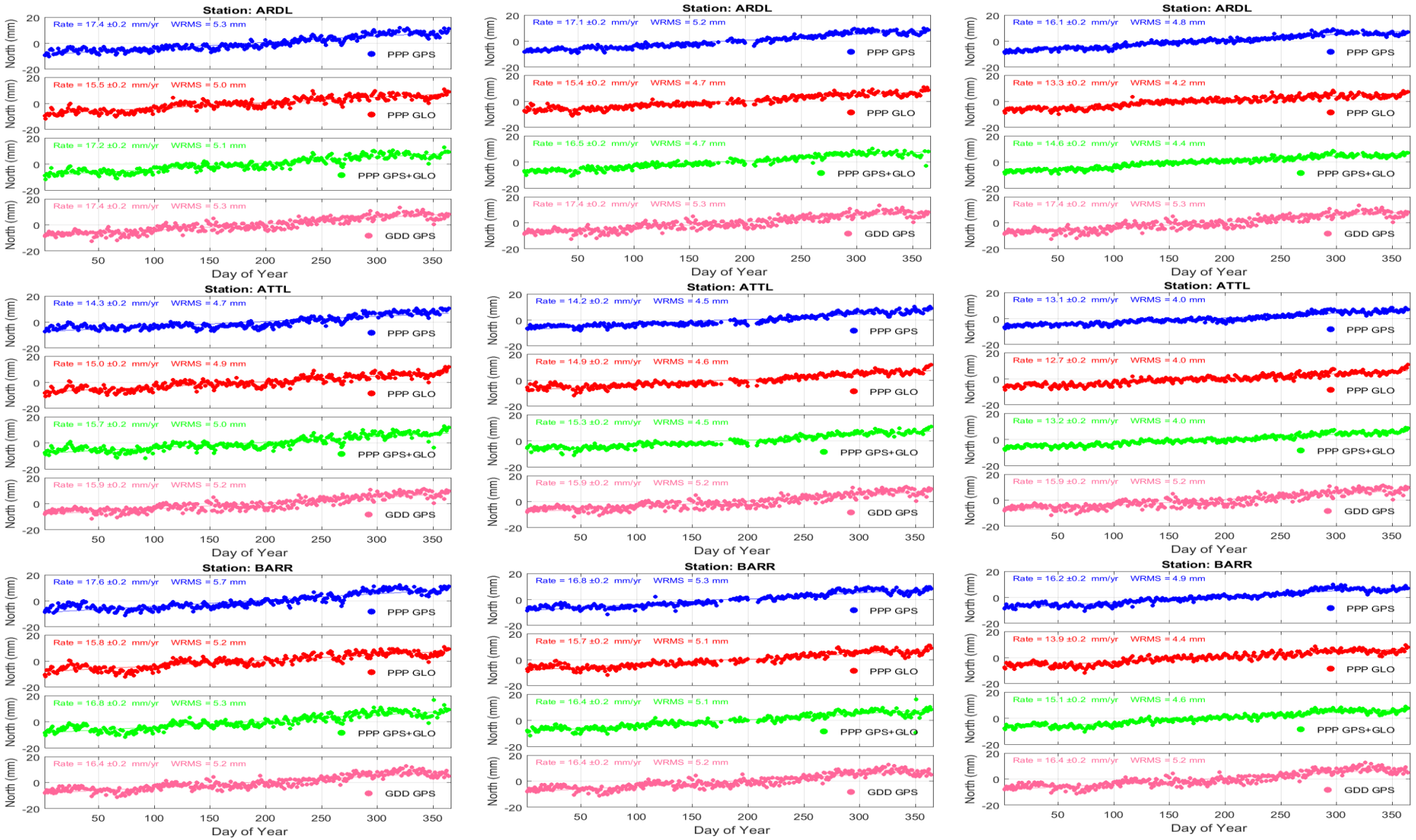


Figure G- 11 Coordinate time series and station rate estimation for the North component using EMX (left), ESA (middle) and GFZ (right) precise products for all PPP scenarios as well as GDD GPS

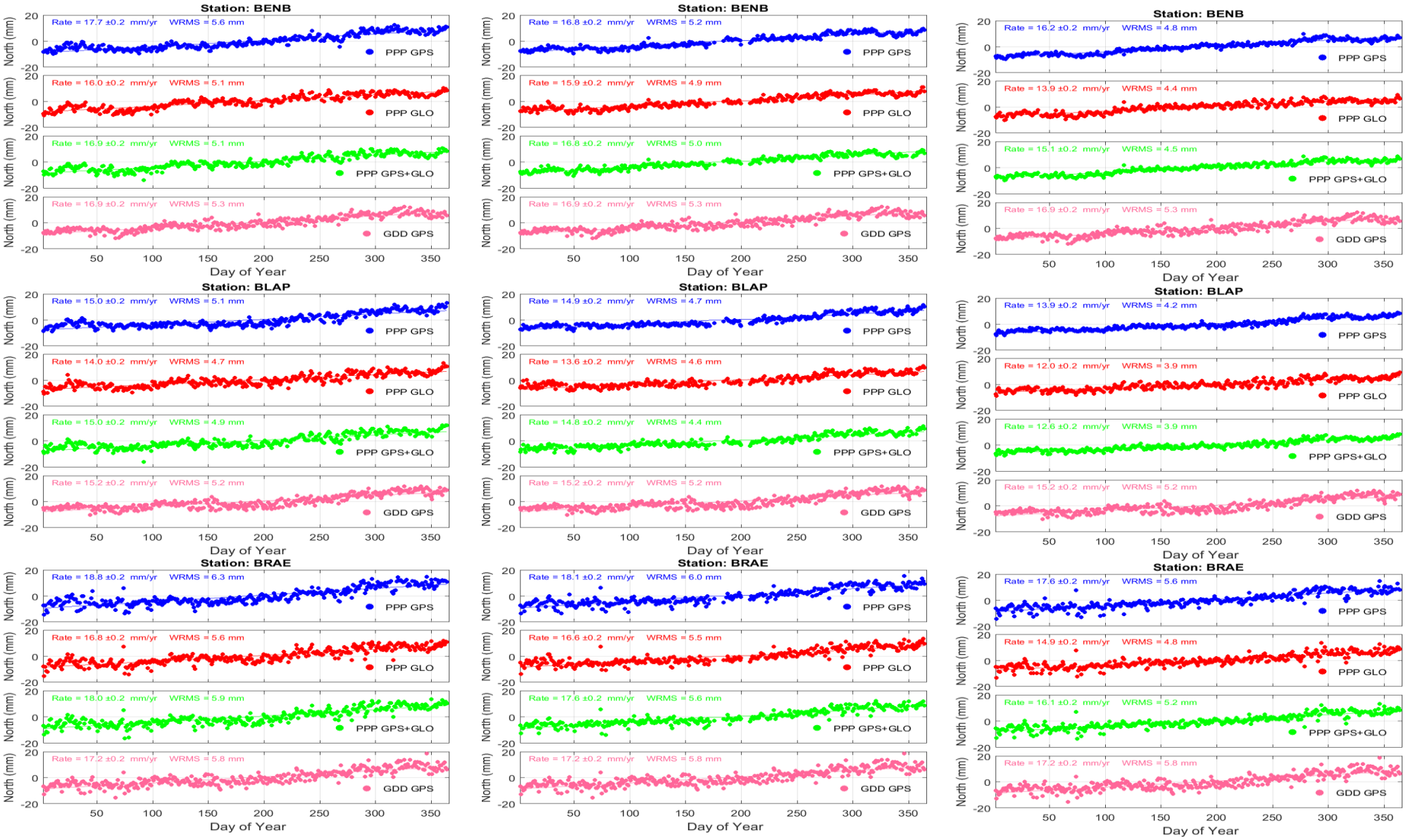


Figure G- 12 Coordinate time series and station rate estimation for the North component using EMX (left), ESA (middle) and GFZ (right) precise products for all PPP scenarios as well as GDD GPS

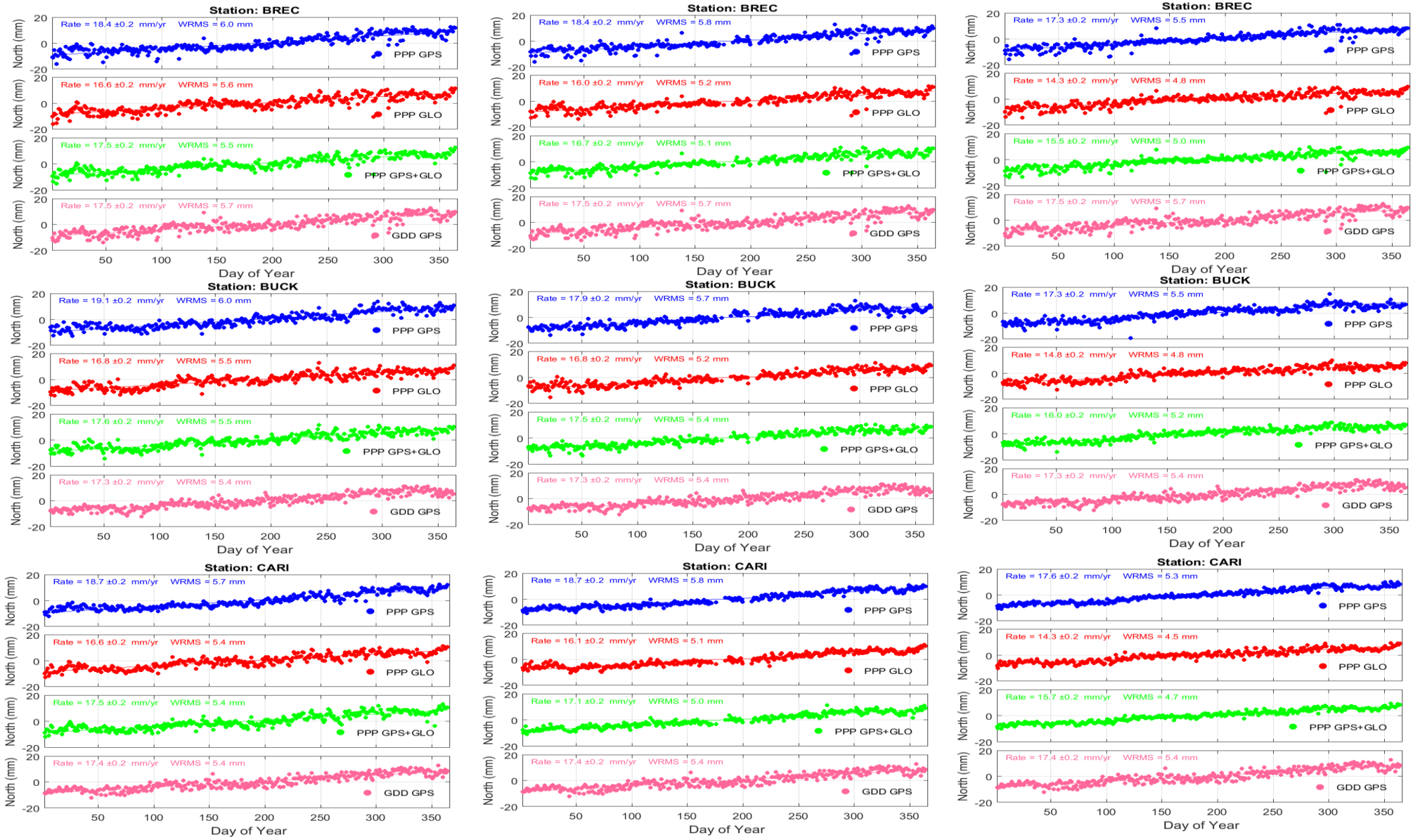


Figure G- 13 Coordinate time series and station rate estimation for the North component using EMX (left), ESA (middle) and GFZ (right) precise products for all PPP scenarios as well as GDD GPS

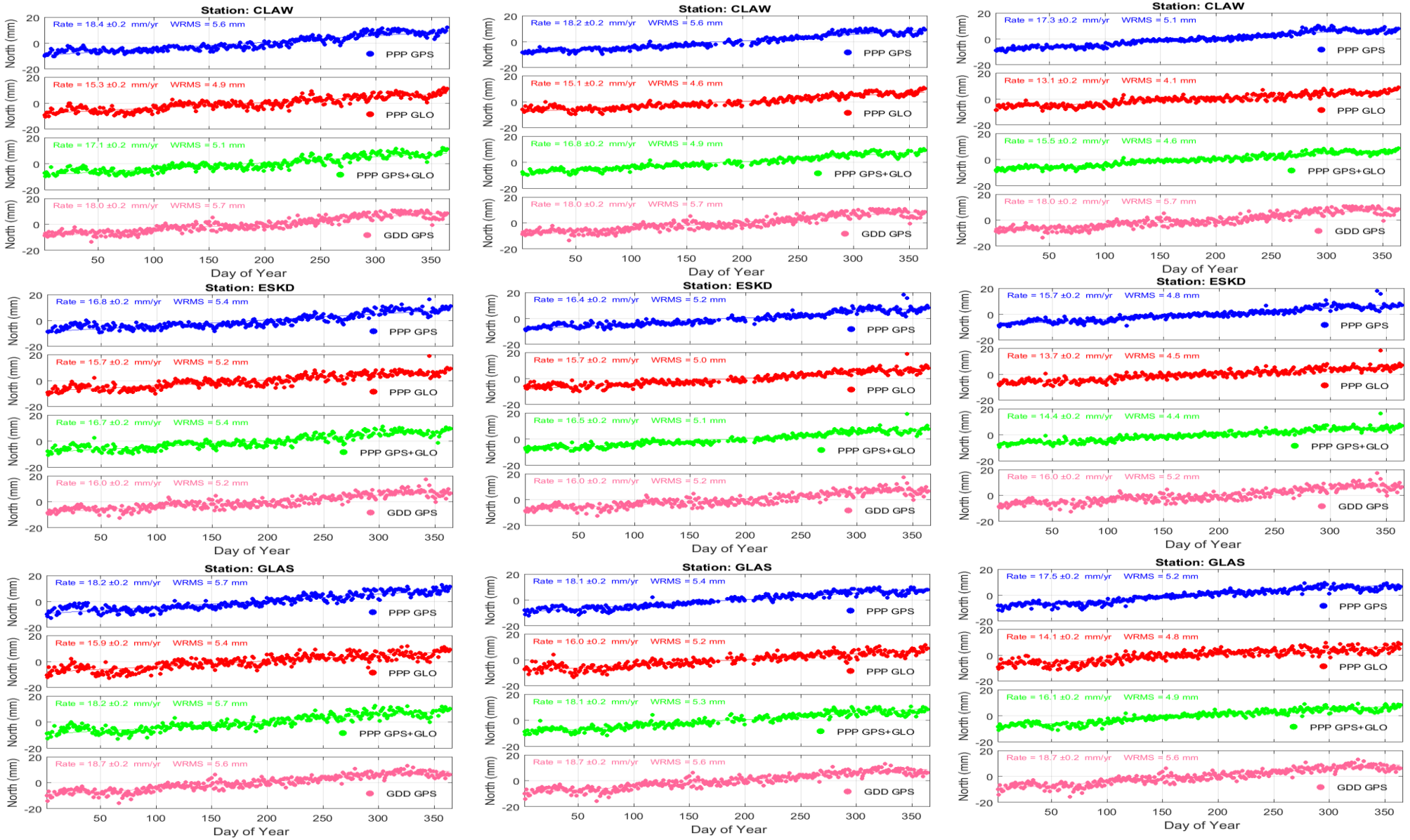


Figure G- 14 Coordinate time series and station rate estimation for the North component using EMX (left), ESA (middle) and GFZ (right) precise products for all PPP scenarios as well as GDD GPS

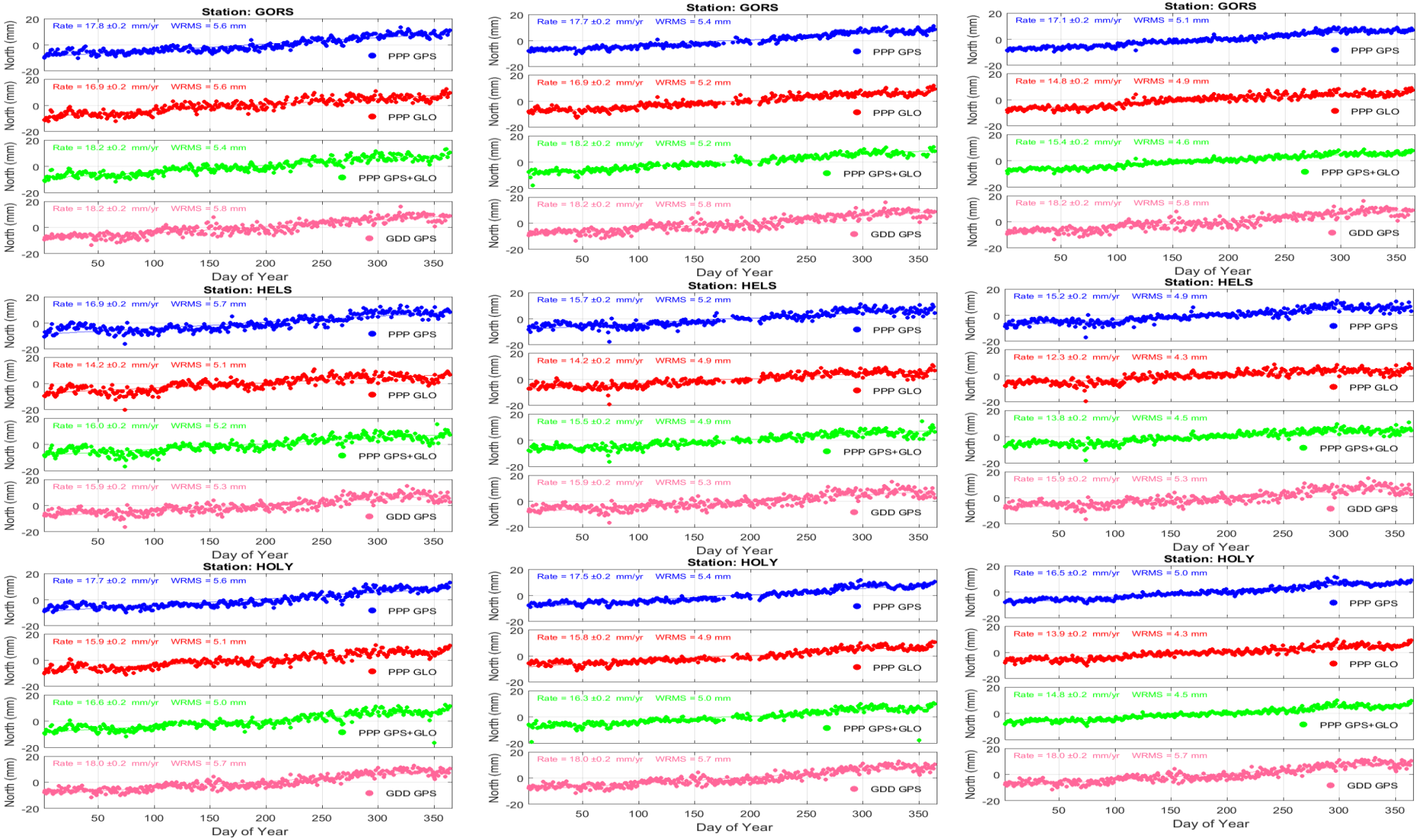


Figure G- 15 Coordinate time series and station rate estimation for the North component using EMX (left), ESA (middle) and GFZ (right) precise products for all PPP scenarios as well as GDD GPS

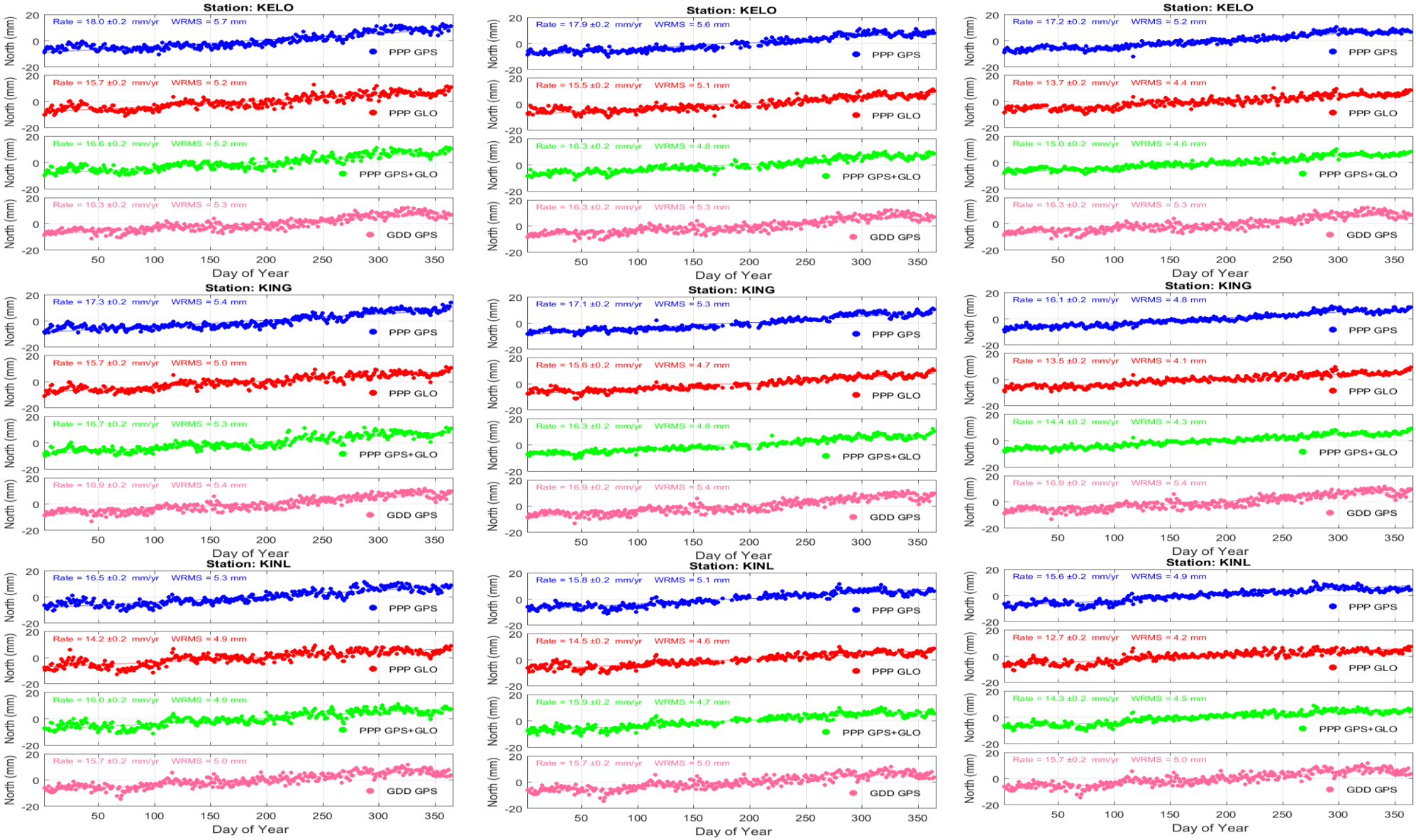


Figure G- 16 Coordinate time series and station rate estimation for the North component using EMX (left), ESA (middle) and GFZ (right) precise products for all PPP scenarios as well as GDD GPS

